ESCOLA DE DOUTORAMENTO
INTERNACIONAL DA USC

Alejandro
Lamas Pérez

Tese de doutoramento

Novel supramolecular designs of cyclic peptides that contain γ- or δ-amino acids

Santiago de Compostela, 2022

Programa de Doutoramento en Ciencia e Tecnoloxía Química

TESE DE DOUTORAMENTO

NOVEL SUPRAMOLECULAR DESIGNS OF CYCLIC PEPTIDES THAT CONTAIN γ- OR δ-AMINO ACIDS

Alejandro Lamas Pérez

ESCOLA DE DOUTORAMENTO INTERNACIONAL DA UNIVERSIDADE DE SANTIAGO DE COMPOSTELA

PROGRAMA DE DOUTORAMENTO EN CIENCIA E TECNOLOXÍA QUÍMICA

SANTIAGO DE COMPOSTELA

2022

USC
UNIVERSIDADE
DE SANTIAGO
DE COMPOSTELA

D. **Alejandro Lamas Pérez**

Título da tese: **Novel supramolecular designs of cyclic peptides that contain γ- or δ-amino acids**

Presento a miña tese, seguindo o procedemento axeitado ao Regulamento, e declaro que:

1) A tese abarca os resultados da elaboración do meu traballo.
2) De ser o caso, na tese faise referencia ás colaboracións que tivo este traballo.
3) Confirmo que a tese non incorre en ningún tipo de plaxio doutros autores nin de traballos presentados por min para a obtención doutros títulos.
4) A tese é a versión definitiva presentada para a súa defensa e coincide a versión impresa coa presentada en formato electrónico

E comprométome a presentar o Compromiso Documental de Supervisión no caso de que o orixinal non estea na Escola.

En Santiago de Compostela, 17 de Febreiro de 2022

USC
UNIVERSIDADE
DE SANTIAGO
DE COMPOSTELA

AUTORIZACIÓN DO DIRECTOR/TITOR DA TESE

[Novel supramolecular designs of cyclic peptides that contain γ- or δ-amino acids]

D. Juan Ramón Granja Guillán

D. Manuel Amorín López

INFORMA/N:

Que a presente tese, correspóndese co traballo realizado por D. Alejandro Lamas Pérez baixo a nosa dirección/titorización e autorizamos a súa presentación, considerando que reúne os requisitos esixidos no Regulamento de Estudos de Doutoramento da USC, e que como director desta non incorre nas causas de abstención establecidas na Lei 40/2015.

De acordo co indicado no Regulamento de Estudos de Doutoramento, declara tamén que a presente tese de doutoramento é idónea para ser defendida en base á modalidade de Monográfica con reprodución de publicacións, nos que a participación do doutorando foi decisiva para a súa elaboración e as publicacións se axustan ao Plan de Investigación.

En Santiago de Compostela, 17 de Febreiro de 2022

USC
UNIVERSIDADE
DE SANTIAGO
DE COMPOSTELA

AGRADECIMIENTOS

En primer lugar, me gustaría agradecer a mis directores Juan R. Granja y Manuel Amorín por acogerme en su grupo a pesar de venir de un grupo de investigación con una temática diferente. Gracias por hacer más llevadero este viaje y ayudarme para que este trabajo saliera adelante, por todos los buenos consejos e ideas que fomentaron mi aprendizaje y crecimiento como científico y, sobre todo, por el trato personal cercano.

Me gustaría agradecer al Prof. Neal Devaraj la oportunidad de realizar una estancia predoctoral en su grupo de investigación para poder ampliar mi formación y conocimiento. En especial a Roberto Brea quien hizo que mi estancia en San Diego fuera inolvidable, por toda la ayuda prestada en el dentro y fuera del laboratorio, aunque en algún momento me quedara de "piedra".

A las instituciones que han financiado este trabajo. Al Ministerio de Economía, Industria y Competitividad por la concesión de una beca predoctoral, así como al resto de instituciones que han financiado los proyectos del grupo en los que estuve involucrado.

A los Prof. Juan Casado y Teo Navarrete por las facilidades para que pudiera sacar el máximo provecho de las estancias exprés en Málaga y por toda la ayuda en la interpretación de de los espectros Raman. Además, me gustaría agradecer a los miembros del SCAI que me ayudaron con las medidas de mis muestras.

A Rebeca García Fandiño y a Javier Montenegro que han seguido mi trabajo desde cerca. A Javier, por su entusiasmo contagioso y motivación constante. Rebeca, porque una gran parte de este trabajo también te pertenece.

Quería agradecer a todos los servicios de apoyo a la investigación de la USC y técnicos del CiQUS. En especial a Mencha, por los espectros de RMN tan importantes en esta memoria. También a Arcadio pai, sin duda, sin ti este trabajo no sería posible, por la herencia y por hacer que todos los equipos sigan funcionando. También quisiera expresar mi agradecimiento a Manuel Marcos del CACTI por el análisis y procesamiento de datos de espectrometría de masas.

A todos mis compañeros de laboratorio, los JG/JM. Gracias por acoger a ese chaval de Mouriño y hacerme la transición más fácil. Gracias por todas las vivencias, las horas compartidas y que todo fuera mucho más alegre y divertido. El camino es largo, pero con un grupo humano como este todo es mucho más fácil.

También, a mis antiguos compañeros del laboratorio del Prof. Mouriño donde di mis primeros pasos como investigador que forjaron mis orígenes.

A otros miembros del CiQUS con los que he compartido gran parte de estos años.

A mis padres que son el mayor ejemplo de esfuerzo y sacrificio. Gracias por apoyarme en todas las decisiones y por siempre sacrificaros para buscar lo mejor para vuestros hijos. Todo

lo que consiga es por y para vosotros. A mi abuelo que, aunque no puedas verme terminar, sé que estarás orgullos.

Por último, a la persona que me aguanta a diario (que no es poco y lo que te queda), mi mayor apoyo y mi mayor crítica. Simplemente, gracias.

USC
UNIVERSIDADE
DE SANTIAGO
DE COMPOSTELA

INDEX

ABBREVIATIONS 13
RESUMO 17
INTRODUCTION 25
CARBON NANOTUBES 25
INORGANIC NANOTUBES 27
SELF-ASSEMBLED NANOTUBES 28
SUPRAMOLECULAR CHEMISTRY AND MOLECULAR SELF-ASSEMBLY 28
ORGANIC NANOTUBES 30
PEPTIDE NANOTUBES 36
Linear peptide nanotubes *36*
D,L,α-Cyclic peptide nanotubes *39*
Novel designs of cyclic peptide nanotubes: non-natural residues *43*
Cyclic peptide nanotubes: β-amino acids *43*
Cyclic peptide nanotubes: γ-amino acids *45*
Cyclic peptide nanotubes: Other designs *52*
APPLICATIONS OF SELF-ASSEMBLED CYCLIC PEPTIDES 53
Selective Membrane Transporters *53*
Biomedical applications *55*
Biosensors *57*
Artificial photosystems *57*
Electronic devices *58*
Nanomaterials *59*
OBJECTIVES 65
CHAPTER 1 69
SELF-ASSEMBLING STUDIES OF α,δ-CYCLIC PEPTIDE 71
DESIGN OF DIMERIC MODELS 71
HOMODIMER FORMATION STUDIES 73
HETERODIMER FORMATION STUDIES 78
SELF-ASSEMBLING STUDIES OF α,γ-CYCLIC PEPTIDE 86
PARALLEL INTERACTION BETWEEN PEPTIDES WITH THE SAME QUIRALITY 86
Synthesis *87*
Structural Studies: α-γ parallel interaction *90*
PARALLEL INTERACTION BETWEEN PEPTIDES WITH DIFFERENT QUIRALITY 92
Synthesis *93*
Structural Studies: γ-γ parallel interaction *94*
CHAPTER 2 101
α,δ-CYCLIC PEPTIDE NANOTUBES: 1ST GENERATION 101
DESIGN 101

USC UNIVERSIDADE DE SANTIAGO DE COMPOSTELA

SYNTHESIS 102
NANOTUBE CHARACTERIZATION 108
α,δ-CYCLIC PEPTIDE NANOTUBES: 2ND GENERATION 112
DESIGN REVISION 112
SYNTHESIS 113
NANOTUBE CHARACTERIZATION 114
FULLERENE ENCAPSULATION 116
SINGLE-WALLED CARBON NANOTUBES ENCAPSULATION (SWCNT) 119
α,δ-CYCLIC PEPTIDE NANOTUBES: 3RD GENERATION 123
NANOTUBES WITH BIGGER DIAMETER 123
SYNTHESIS 124
NANOTUBE CHARACTERIZATION 125
CHAPTER 3 129
SUPRAMOLECULAR CAPSULES 129
METAL COORDINATION CAGES 129
SUPRAMOLECULAR CAPSULES 133
α,δ-CYCLIC PEPTIDE BASED CAPSULES 135
DESIGN 136
COMPUTATIONAL STUDIES 137
1ST SYNTHETIC STRATEGY 138
2ND SYNTHETIC STRATEGY 141
3RD SYNTHETIC STRATEGY 143
CONCLUSIONS 151
EXPERIMENTAL SECTION 155
GENERAL REMARKS 155
SOLID PHASE SYNTHESIS 157
CHAPTER 1 159
SYNTHESIS AND CHARACTERIZATION 159
SUPERCRITICAL FLUID CHROMATOGRAPHY ANALYSIS 166
MASS SPECTROMETRY DIMER IDENTIFICATION: 167
NMR HETERODIMER FORMATION STUDIES 171
CHAPTER 2 175
SYNTHESIS AND CHARACTERIZATION 175
THIOFLAVIN T FLUORESCENCE EMISSION ASSAYS: 178
FULLERENE C_{60} SOLUBILIZATION IN THE PRESENCE OF CYCLIC PEPTIDE: 178
PREPARATION OF SINGLE-WALLED CARBON NANOTUBES DISPERSIONS: 178
ATOMIC FORCE MICROSCPY (AFM): 178
SCANNING TRANSMISSION ELECTRON MICROSCOPY (STEM): 178
CHAPTER 3 179
SYNTHESIS AND CHARACTERIZATION 179
SELECTED SPECTRA 191

LIST OF PUBLICATIONS.....203

USC
UNIVERSIDADE
DE SANTIAGO
DE COMPOSTELA

USC
UNIVERSIDADE
DE SANTIAGO
DE COMPOSTELA

ABBREVIATIONS

$[\alpha]_D$	Optical specific rotation
^{13}C NMR	Carbon Nuclear Magnetic Resonance
^{1}H NMR	Proton Nuclear Magnetic Resonance
2-CTC	2-Chlorotrytil chloride resin
γ-Aca	*cis*-3-Aminocycloalkanecarboxylic acid
γ-Ace	*cis*-4-Amino-cyclopent-2-ene-carboxylic acid
γ-Ach	*cis*-3-Aminocyclohexanecarboxylic acid
γ-Acp	*cis*-3-Aminocyclopentanecarboxylic acid
γ-Aga	Glucuronic acid
γ-Ahf	4-Amino-3-hydroxytetrahydrofuran-2-carboxylic acid
δ	Chemical shift
δ-Ach	*trans*-4-Aminocyclohexanecarboxylic acid
λ_{exc}	Excitation wavelength
ν	Wavenumber
Aa	Amino acid
Abs	Absorbance
AFM	Atomic Force Microscopy
Ala	Alanine
All	Allyl
aq	Aqueous solution
Arg	Arginine
BINAP	(*R*)-(+)-2,2´-*Bis*(diphenylphosphino)-1,1´-binaphthalene
Bn	Benzyl
BNNTs	Boron Nitride Nanotubes
Boc	*tert*-Butoxycarbonyl
br	Broad signal
cac	Critical Aggregation Concentration
CD	Circular Dichroism
CDs	Cyclodextrins
CNTs	Carbon Nanotubes
COSY	Correlation Spectroscopy
CP	Cyclic Peptide
CuAAC	Copper-catalyzed Azide-Alkyne Cycloaddition
D	Doublet
D	Dimer

USC UNIVERSIDADE DE SANTIAGO DE COMPOSTELA

Dd	Doublet of doublets
Ddp	Dodecapeptide
DEPT	Distortionless Enhancement by Polarization Transfer
DIEA	*N,N*-Diisopropylethylamine
DKT	Diketopiperazine
DMAP	4-Dimethylaminopyridine
DMF	Dimethylformamide
DMSO	Dimethyl sulfoxide
DNA	Deoxyribonucleic acid
dp	Dipeptide
DPAs	Diphenylamine[n]arenes
dt	Doublet of triplets
e.e	Enantiomeric Excess
EDC·HCl	1-Ethyl-3-(3-dimethylaminopropyl)carbodiimide
EM	Electron Microscopy
equiv	Equivalent
ESI	Electrospray Ionization
EtOAc	Ethyl Acetate
F	Phenylalanine
FFAAs	Fluorinated Furanoid Sugar Amino Acids
Fmoc	Fluorenylmethyloxycarbonyl
FTIR	Fourier Transform Infrared Spectroscopy
Glu	Glutamic acid
HBC	Hexa-peri-benzocoronene
HFIP	1,1,1,3,3,3-Hexafluoro-2-propanol
His	Histidine
HOBt	1-Hydroxybenzotriazole
HPLC	High Performance Liquid Chromatography
HRMS	High Resolution Mass Spectrometry
INs	Inorganic Nanotubes
J	Coupling constant
K_a	Association constant
LC	Liquid Crystal
Leu	Leucine
Lys	Lysine
m	Multiplet
m/z	Mass-to-charge ratio

USC UNIVERSIDADE DE SANTIAGO DE COMPOSTELA

MALDI	Matrix-Assisted Laser Desorption/Ionization
Me	Methyl
MeOH	Methanol
MS	Mass Spectrometry
N-HATU	1-[Bis(dimethylamino)methylene]-1H-1,2,3-triazolo[4,5-b]pyridinium 3-oxide hexafluorophosphate
N-HBTU	3-[*Bis*(dimethylamino)methyliumyl]-3H-benzotriazol-1-oxide hexafluorophosphate
N-TBTU	2-(1H-Benzotriazole-1-yl)-1,1,3,3-tetramethyluronium tetrafluoroborate
NMM	N-Methylmorpholine
NMR	Nuclear Magnetic Resonance
nOe	Nuclear Overhauser effect
NOESY	Nuclear Overhauser Effect Spectroscopy
Ns	2-Nitrobenzenesulfonyl
NT	Nanotube
op	octapeptide
OPVs	Organic Photovoltaics
PAM	Phenylacetylene Macrocycle
Pbf	2,2,4,6,7-Pentamethyldihydrobenzofuran-5-sulfonyl
PEG	Polyethylene glycol
Ph	Phenyl
PNTs	Peptide Nanotubes
ppm	Part per million
PXRD	Powder X-Ray Diffraction
PyAOP	(7-Azabenzotriazol-1-yloxy)tripyrrolidinophosphonium hexafluorophosphate
q	Quadruplet
R_f	Retention Factor
rt	Room temperature
s	Singlet
SAA	Sugar Amino Acid
SANS	Small-Angle Neutron Scattering
sat	Saturated solution
SCPNs	Self-assembled Cyclic Peptide Nanotubes
SFC	Supercritical Fluid Chromatography
SLPs	Surfactant-Like Peptides
SPPS	Solid-Phase Peptide Synthesis

USC UNIVERSIDADE DE SANTIAGO DE COMPOSTELA

STEM	Scanning Transmission Electron Microscopy
SubPc	Subphthalocyanine
SWCNT	Single-Walled Carbon Nanotube
t	Triplet
^{t}Bu	*tert*-Butyl
TEG	Triethylene glycol
TEM	Transmission Electron Microscopy
TFA	Trifluoroacetic Acid
THF	Tetrahydrofuran
ThT	Thioflavin T
TIS	Triisopropylsilane
TLC	Thin Layer Chromatography
TMSS	*Tetrakis*(trimethylsilyl)silane
TMV	Tobacco Mosaic Virus
TOCSY	Total Correlation Spectroscopy
TOF	Time-Of-Flight Detector
tp	Tetrapeptide
TRIS	2-Amino-2-(hydroxymethyl)propane-1,3-diol
trp	Tripeptide
Tyr	Tyrosine
UV-vis	Ultraviolet-vis spectroscopy
Val	Valine
Z or Cbz	Benzyloxycarbonyl

USC UNIVERSIDADE DE SANTIAGO DE COMPOSTELA

RESUMO

O nacemento da nanotecnoloxía incentivou o interese da comunidade científica de cara ao desenvolvemento de novos materiais de escala nanométrica. A Química posúe as ferramentas sintéticas axeitadas para cumprir esta difícil tarefa. Ao longo dos anos, os químicos idearon enxeñosas metodoloxías que permitisen a ligazón de diferentes átomos ou moléculas entre si con gran selectividade e eficiencia. No entanto, a Química sintética clásica presenta moitas limitacións na preparación de moléculas de maior complexidade e tamaño cunha disposición tridimensional ben definida a través da formación de ligazóns covalentes. Neste contexto, xurde unha nova disciplina neste ámbito científico, a Química Supramolecular, que comprende o estudo das interaccións intra- e intermoleculares débiles de carácter non covalente. Este novo ámbito estende ás alternativas sintéticas posto que facilita a construción de estruturas máis complexas mediante o auto-recoñecemento e organización de compoñentes quimicamente sinxelos polo medio de interacción débiles; como as ligazóns de hidróxeno, as interacción aromáticas tipo π ou as forzas de van der Waals entre unidades de baixa polaridade. O conxunto de tódalas interaccións determinará a xeometría tridimensional e as propiedades físicas dos nanomateriais resultantes.

Entre o elevado número de topoloxías accesibles mediante a estratexia supramolecular, as construcións tubulares son especialmente relevantes dadas as súas extraordinarias propiedades derivadas da súa disposición monodimensional. Estes materiais, chamados nanotubos, posúen dúas contornas separadas, a cavidade interna e a superficie externa, que determinarán as súas propiedades macroscópicas. O control estrito de ámbalas dúas contornas favorece o desenvolvemento de materiais para o confinamento ou tránsito selectivo de moléculas a través do seu poro interno nunhas condicións ou medio determinados. Estes procesos presentan implicacións moi relevantes para a súa explotación en diferentes aplicacións como, por exemplo, contedores moleculares para a encapsulamento de substancias, soporte para catálisis en espazos illados ou transportadores de substancias a través de membranas lipídicas.

Amosada a relevancia das estruturas tubulares, nas últimas décadas desenvolvéronse diversas aproximacións sintéticas supramoleculares para a súa preparación inspiradas en modelos biolóxicos. Unha das estratexias máis recoñecidas, aínda que non se observa na Natureza, consiste na agrupación de subunidades cíclicas planas unha enriba doutra. Esta aproximación ofrece certas vantaxes en comparación con outras propostas sintéticas, xa que permite controlar o diámetro da cavidade en relación ao tamaño do macrociclo modelo. Ademais, a restrición conformacional das subunidades posibilita a funcionalización de ambas as dúas caras do tubo. Neste marco, a variedade e maleabilidade estrutural dos péptidos convérteos nunha plataforma atractiva para o desenvolvemento de novos nanomateriais. En 1993, o grupo do Prof. Ghadiri demonstrou que os péptidos cíclicos (CPs) formados por aminoácidos de quiralidade alternante presentan a capacidade de ensamblarse en arquitecturas con forma tubular. Nos sistemas resultantes, os grupos amino e carbonilo do enlace amida proxéctanse perpendicularmente ao plano do anel posibilitando a interacción entre diferentes as moléculas cíclicas mediante o establecemento de enlaces de hidróxeno. Ademais, as cadeas

laterais dos residuos oriéntanse cara ao exterior do macrociclo; esta disposición favorece o axuste das propiedades externas dos sistemas finais. Con todo, o uso exclusivo de α-aminoácidos ten certas limitacións como a expansión do anel, pois a capacidade para autoensamblarse depende do número de aminoácidos da secuenica; ou a modificación das propiedades internas, xa que, na configuración formadora de nanotubos, o sustituyente na posición α (Hα) oriéntase paralelamente ao eixo do nanotubo.

Co obxectivo de modular as propiedades internas dos nanotubos preparados a partir de péptidos cíclicos, o noso grupo de investigación estudou a incorporación do isómero *cis* de γ-aminoácidos cíclicos (γ-Aca). A combinación destes residuos artificiais con α-aminoácidos da quiralidade adecuada deu lugar a unha nova familia de péptidos cíclicos: os α,γ-CPs. O uso destes residuos cíclicos dota ao sistema resultante dunha rixidez adicional promovendo a formación da estrutura plana necesaria para o agrupamento dos monómeros. Esta característica estrutural deu acceso a macrociclos de maiores dimensión que mantiñan a capacidade de ensamblarse e formar nanotubos. Ademais na arquitectura tubular, estes residuos artificiais dispoñen un grupo metileno orientado caro ao volume interno proporcionando nanotubos con cavidades parcialmente hidrófobas. Outras das características estruturais dos α,γ-CPs e a constitución de dúas caras diferenciadas no anel: os grupos amino e carbonilo dos α-aminoácidos sitúanse na mesma cara do anel (cara α), mentres que estes grupos dos residuos do aminoácidos artificial cíclico quedan expostos na cara oposta (cara γ). Esta característica modula a fortaleza das interacción que gobernan o proceso de autoensamblaxe, dado que está demostrado que a estabilidade das especies supramoleculares formadas a través da cara α son máis estables que as formadas pola cara γ.

Estes estudos realizáronse empregando α,γ-CPs nos que unha das caras está selectivamente bloqueada impedindo o establecemento de enlaces de hidróxeno mediante a substitución dos protóns amídicos por grupos alquilo. De este modo, os péptidos resultantes teñen limitado o ensamblaxe a constitución de formas diméricas. Nos últimos anos, demostrouse que estes grupos obstrutivos da formación da formadores de nanotubos poden desempeñar outras funcións. A presencia dun grupo funcional axeitado para Química tipo click (cicloadición 1,3-dipolares, reacción de formación de hidrazonas, etc.) permite a ancoraxe de dunha tapa molecular na entrada da cavidade do dímero conducindo a cápsulas supramoleculares.

En base a estes precedentes, o obxectivo xeral desta Tese consiste na incorporación dun novo residuo na secuencia dun péptido cíclico coa capacidade de ensamblarse para a formación de dímeros ou nanotubos. Os sistemas supramoleculares resultantes presentarían cavidades internas con propiedades hidrófobas gracias a inclusión dos novos aminoácidos artificiais. Para este propósito, consideramos que o ácido 4-aminociclohexano carboxílico (δ-Ach) sería o candidato máis apropiado, xa que, na configuración tipo cadeira do ciclohexano, os grupos amino e carbonilo do aminoácido ocupan posicións ecuatoriais o que favorecería a estrutura plana do CP necesaria para a formación de nanotubos. Nos sistemas supramoleculares resultantes, proxectaríanse dous grupos metilenos cara ao interior da cavidade. Este tipo de materiais son especialmente relevantes no deseño de novos sistemas de transporte de fármacos ou axentes de diagnóstico.

USC DE SANTIAGO DE COMPOSTELA

No primero capítulo desta memoria abórdase o deseño e a síntese de modelos diméricos de péptidos cíclicos que inclúen δ-Ach na súa secuencia para o estudo das súas propiedades supramoleculares. O isómero *trans* do δ-Ach é necesario para que o péptido poida adoptar a estrutura plana necesaria para o agrupamento vertical dos monómeros. Non obstante, o ángulo descrito entre os grupos amino e ácido carboxílico de este resitduo impide a construción de péptidos cíclicos compostos exclusivamente por este aminoácidos. Nesta situación, o deseño máis sinxelo consistiu en inserir un residuo de δ-Ach entre cada α-aminoácidos constituíndo unha nova familia de péptidos cíclicos: os α,δ-CPs. Este residuo actuará como un elongador ríxido dando lugar a péptidos cíclicos de maior diámetro coa capacidade de formar nanotubos. Con estas pautas estruturais preparáronse tres péptidos de diferentes dimensións (un octámero, un dodecámero e un hexadecámero). Estes péptidos presentaban unha das súas caras, cara *D* ou cara *L*, selectivamente bloqueadas mediante N-metilación o que facilitou o estudo do proceso de autoensamblaxe mediante técnicas Resonancia Magnética Nuclear (RMN). Estes estudos estruturais revelaron que o dodecámero e o hexadecámero proporcionaban os complexos supramoleculares correspondentes en disolución. Pola contra, o octámero permanecía como monómero. Este resultados foron confirmados mediante espectrometría de masas (MS).

Os modelos diméricos iniciais, por limitacións do deseño, poden unicamente ensamblarse a través dunha lámina β antiparalela pola interacción entre as caras de igual quiralidade. Mais, a mestura dos péptidos, un co patrón de metilación correspondente á cara *L* e outro á cara *D*, posibilitaría a interacción entre eles a través da lámina β paralela. Polo tanto, o estudo da mestura de ámbolos dous péptidos permitiría determinar a estabilidade relativas das dúas interaccións posíbeis. Con este propósito, preparáronse os enantiómeros correspondentes e analizouse a mestura deles mediante RMN. Estes estudos evidenciaron que interacción paralela é máis estable que a interacción antiparalela. A maiores, observouse que os octámeros presentaban a capacidade de autoensamblarse en estruturas diméricas por medio da formación da lámina paralela en baixas constantes de asociación.

En base a estes resultados, decidimos ampliar os estudos estruturais aos α,γ-CPs que, ata a data actual, considerábase que a especies formadas a través da interacción antiparalela eran máis estables que as formadas a través da lámina paralela. En orixe, estimouse que a interacción antiparalela sería máis estable debido a diferencia no patrón dos grupos doadores (NH) e receptores (carbonilo) de enlaces de hidróxeno entre a cara α e a cara γ. Sorprendentemente, tras o estudo de diferentes mesturas de péptidos cíclicos que alternaban α- e γ-aminoácidos na súa secuencia, descubriuse que a interacción α-γ paralela proporcionaba especies supremoleculares coas maiores constantes de asociación. Tamén detectouse a especie dimérica derivada da interacción paralela entre as caras γ de dous péptidos cíclicos. . Nos péptidos cíclicos usados para este estudo, se modificou a estereoisomería e/ou o patrón de N-metilación para que a mestura de dous péptidos dese lugar a interacción desexada.

USC UNIVERSIDADE DE SANTIAGO DE COMPOSTELA

Nas probas realizadas, as interaccións están dirixidas polo esqueleto peptídico, mais a diferencia de enerxía entre as posíbeis configuracións no é demasiado grande polo que pódese controlar a formación selectiva dunha especie supramolecular mediante a precisa elección dos α-aminoácidos. De modo que, as interaccións atractivas ou repulsivas entre as cadeas laterais

de dúas subunidades favorecerán a formación preferente dunha das estruturas de láminas β. Os resultados deste capítulo implican un cambio no paradigma con respecto aos deseños de péptidos cíclicos e deberán considerarse de cara a futuros deseños de especies diméricas ou nanotubos preparados a partir de estas macromoléculas.

No segundo capítulo, en base aos resultados experimentais anteriores, deseñouse un dodecámero cíclico precursor de nanotubos (non presentaba grupos N-metilo). Este novo α,δ-CP contiña α-aminoácidos polares para favorecer a súa solubilidade en medio acuoso. Ademais, estes residuos proporcionaron control sobre o proceso de autoensamblaxe mediante a aplicación de estímulos externos. Neste caso concreto, gracias á presencia de dous residuos de histidina, a formación de nanotubos desencadeouse tras a neutralización do pH do medio. As propiedades supramoleculares testáronse en disolución mediante espectroscopia de fluorescencia en presencia dunha sonda planzarizable, a tioflavina T. Estes experimentos indicaron que o novo deseño de α,δ-CP daba lugar a nanotubos en disolucións acuosas a pH básico ou neutro. Os nanotubos resultantes caracterizáronse mediante diferentes técnicas de microscopía: observouse o crecemento de nanotubos individuais a través do microscopio de forza atómica (AFM) e o microscopio electrónico de transmisión de barrido (STEM).

Unha vez confirmada a capacidade do péptido para a formación de nanotubos, centrámonos no estudo das propiedades da súa cavidade interna. Como xa se indicou anteriormente, a incorporación do residuo de δ-Ach modificarías as propiedades do poro debido a disposición de dous grupos metileno orientados cara a faciana interna do cilindro, polo que presentaría propiedades fundamentalmente hidrófobas. Adicionalmente, a súa rixidez estrutural daría lugar a cavidades de maior tamaño. En conxunto, os α,δ-Cps sería perfectos candidatos para o confinamento de moléculas apolares de alto peso molecular. Con este obxectivo en mente, decidimos evaluar a solubilización de moléculas de fullereno C_{60} en medio acuoso na presencia do dodecámero proposto. A análise mediante espectroscopia de absorción ultravioleta-visible (UV-vis) mostrou que disolucións acuosas do péptido a pH neutro tiñan a capacidade de solubilizar estas molécula fullereno. Razoamos que a solubilización explícase en base ás propiedades hidrófobas da cavidade interna do nanotubo ensamblado, xa que o fullereno non é soluble en auga. O estudo das disolucións acuosas de fullereno en presencia do péptido cíclico confirmou que a arquitectura tubular se mantiña tras a encapsulamento.

Nunha segunda aproximación para avaliar as propiedades internas dos nanotubos dedicimos estudar o encapsulamento de nanotubos de carbono de parede simple (SWCNT, *Single-Walled Carbon Nanotubes*) que tamén son insolubles en medio acuoso. Para esta finalidade, decantámonos pola espectroscopia de Raman debido a alta intensidade dos sinais relativos ao SWCNT. Significativamente, disolucións acuosas do péptido cíclico a pH ácido amosaron maior capacidade para o encapsulamento deste alótropo do carbono. Adicionalmente, o estudo destas disolucións de SWCNT en presencia do péptido cíclico mediante técnicas de espectroscopia Raman quiral (ROA, *Raman Optical Activity*) revelaron que existía unha quiralidade neta no sistema. Suxerimos que, dado que a cavidade interna é aquiral, estes sinais débense a transferencia de quiralidade do sistema peptídico ao nanotubo de carbono. Isto é, como a cavidade interna presenta un centro de simetría C_3 se favorece a interacción con

nanotubos de carbono aquirais. Para sair de dúbidas, preparouse o enantiómero do péptido cíclico e estudouse o encapsulamente mediante dicroísmo circular (CD, *Circular Dichroism*) Desafortunadamente, estes estudos non aportaron información estrutural adicional. Finalmente, en relación con estes resultados, decidimos sintetizar α,δ-CPs hexadecaméricos precursores de nanotubos. Debido ao seu maior diámetro interno favoreceríase o encapsulamento dos nanotubos de carbono. Seguindo a mesma metodoloxía, avaliouse a capacidade de ensamblaxe destes péptidos mediante espectrofluorometría en presencia de ThT, porén, naqueles capaces de auotoensamblarse, non se observou o devandito encapsulamento.

No terceiro capítulo de esta Tese doutoral, propuxémonos explorar as posibilidades de deseño dos α,δ-CPs para a construción de cápsulas supramoleculares. De este modo, poderíamos explotar as propiedades de encapsulamento da cavidade interna, estudadas no capítulo segundo, e engadir un efecto director adicional a través dunha tapa molecular. Recentemente, no noso grupo de investigación desenvolvemos diferentes estratexias sintéticas que permitisen a ligazón covalente dun péptido cíclico cunha macromolécula que actuase como cobertura. Entre os diferente exemplos, pódese destacar a construción de nanotubos tipo Venturi mediante a reacción de cicloadición 1,3-dipolar entre dúas subunidades peptídicas de diferente tamaño. Ademais, prepararónse cápsulas supramoleculares a partir de α,γ-CPs mediante a ancoraxe dunha unidade de porfirina mediante unha reacción de condensación entre un aldehído (funcionalidade presente na profirina) e unha hidrazida (funcionalidade introducida como grupo N-alquilo). A posterior ensamblaxe de dúas subunidades deu lugar ás cápsulas supramoleculares.

Seguindo a última estratexia, deseñouse un dodecámero que incorporaba tres resdiuos de δ-Ach N-funcionalizados cun grupo hidrazida. Dado o maior diámetro e a xeometría C_3 do α,δ-CP proposto, seleccionouse como tapa molecular unha molécula de subftalocianina (SubPc). Esta molécula pode ser modificada nas súas posicións periféricas para a inserción dun grupo aldehido que permita a posterior reacción de condensación. A distancia entre estas posicións parece axeitada para estabilización da tapa molecular enriba do dodecámero. Para evaluar a viabilidade do deseño, realizáronse estudos computacionais semiempíricos (PM7) que demostraron que tanto a introdución da SubPc como a formación da especie dimérica resultaban estables. Estes estudos mostraron que o volume interno das cápsulas era moi amplo, pois no seu interior caben ata tres moléculas de fullereno.

Unha vez exploradas as capacidades do sistema, comezamos coa síntese dos péptidos cíclicos. Neste caso, decantámonos polla síntese de péptidos en disolución xa que ofrece maior selectividade e require de menor cantidade de reactivos en cada unha das reaccións. Desafortunadamente, as primeiras estratexias propostas deron lugar a reacción secundarias que impediron a obtención do péptido cíclico desexado. En primeiro lugar, a principal limitación atopouse na introdución do grupo hidrazida nun intermedio peptídico lineal que conduciu á formación de dicetopiperazinas como produtos secundarios. Este subprodutos de reaccións diminuían considerablemente os rendementos das reaccións de acoplamento. Como alternativa propúxose a introducción deste grupo hidrazida na derradeira etapa de síntesis, unha vez ciclado o péptido. Non obstante, o tratamento ácido previo para a eliminación dos grupos protectores

deu lugar a descomposición do péptido. Entón, redeseñamos a estratexia sintética para evitar a formación de produtos non desexados durante o crecemento do péptido lineal. Tras varias probas na procura dos grupos protectores ortogonais máis adecuados, logramos obter o péptido cíclico desexado. Así a todo, ata hoxe non probamos a reacción de condensación entre a tapa molecular e o péptido preparado para a formación das cápsulas moleculares.

En conclusión, ao longo desta Tese avaliouse a capacidade de novos deseños de péptidos cíclicos que conteñen δ-residuos cíclicos para ensamblarse en diferentes estruturas tubulares e as súas propiedades para futuras aplicacións como novos nanobiomateriais. En primeiro lugar, realizouse un estudo exhaustivo das súas propiedades supramoleculares, demostrando que estes péptidos ensámblanse preferentemente mediante unha estrutura de folla β paralela. Ademais, a comparación cos seus predecesores, os α,γ-CP, deu lugar a resultados inesperados que poñen en dúbida os supostos preliminares sobre a estabilidade destas interaccións neste tipo de sistemas. Sorprendentemente, atopamos que, mesmo nestes sistemas, a disposición paralela impulsada polas interaccións entre o esqueleto peptídico das subunidades é máis estable que o aliñamento antiparalelo. Isto suxire un cambio de paradigma respecto dos deseños que deberían considerarse para futuras aplicacións de nanotubos construídos a partir de este tipo de péptidos cíclicos. Na segunda parte desta Tese, confirmouse a capacidade de formar nanotubos mediante o uso de diferentes técnicas de espectroscopia e microscopía. Un deseño adecuado permitiu o control das propiedades de autoensamblaxe mediante a variación do pH do medio debido a presencia de grupos imidazol nas cadeas laterais dos α-aminoácidos. Alternativamente, a disposición de dous grupos metileno do ciclohexilo do δ-Ach cara ao interior da cavidade do nanotubo xera un ambiente apolar. Estas propiedades hidrófobas en combinación co seu amplo diámetro interno implementáronse eficazmente para a encapsulación de fullereno C_{60} e nanotubos de carbono de parede simple. Estes resultados conduciron a novos polímeros supramoleculares con propiedades de ensamblaxe que poderían ser axeitados para o desenvolvemento de plataformas eficientes para o transporte e libreación de fármacos. Ademais, as novas estruturas híbridas descritas no segundo capítulo poderían ter aplicacións en transistores de efecto de campo, nanodispositivos magnéticos ou de almacenamento de datos, láseres a nanoescala, entre outros. Finalmente, no último capítulo consideramos a construción de cápsulas supramoleculares a partir de α,δ- CPs mediante a ancoraxe dunha tapa molecular de subphthalocianina. Demostramos a estabilidade do sistema mediante estudos computacionais tipo PM7, así como a xeración dunha cavidade de gran volume. Tras diferentes intentos de síntese, logramos preparar o péptido cíclico deseñado que permitiría chegar á cápsula supramolecular desexada. Con todo, ata a data non tentamos a incorporación da tapa de SubPc sobre o péptido.

USC UNIVERSIDADE DE SANTIAGO DE COMPOSTELA

INTRODUCTION

USC
UNIVERSIDADE
DE SANTIAGO
DE COMPOSTELA

USC
UNIVERSIDADE
DE SANTIAGO
DE COMPOSTELA

INTRODUCTION

Nanometer-sized structures have gained a lot of attention during the last decades with the birth of nanotechnology.[1] Nanotechnology involves the development of synthetic and characterization methods to build nanometer-sized systems and the study of its properties to reach novel functional materials. The art of miniaturization will provide nanodevices with unique properties that can be tuned by adjusting the size, composition and shape of the entities.[2]

Chemistry (of course) plays an important role in this miniaturization game. There are two ways to construct a nanomaterial: 1) The *top-down* manufacturing method which consist of sculpt a larger piece of material to the desire structure. 2) The *bottom-up* approach that involves the synthesis of the target product atom-by-atom or molecule-by-molecule.[3] In the latter, chemists are specialist in the development of synthetic methodologies to create new forms of matter simply bonding different atoms or molecules in a selective and efficient manner.

The evolution of chemistry allowed the preparation of sub-100 nanometer systems with different shapes, morphologies, and composition.[4] In particular, nanotubes are especially relevant materials because they show unique properties as, for instance, well-defined one-dimensional organization enabling the creation of two separated environments: the inner pore and the outer surface.[5] These attributes make them suitable candidates for the development of novel nanomaterials.

CARBON NANOTUBES

Between the different tubular structures with potential nanotechnological applications, carbon nanotubes (CNTs) shine for their extraordinary geometric, mechanical, thermal, electronic and chemical properties. CNTs were discovered in 1991 by Iijima who detected the formation of graphitic helical microtubules when attempting to prepare fullerenes by a variation of the arc-discharge evaporation method. High-Resolution Electron Microscopy analysis of material deposited at the negative end of the electrode revealed the formation of these cylindrical carbon structures. Each needle –ranging from 4 to 30 nm in diameter– consisted of several coaxial graphitic tubes (between 2 and 20) made up of helically enrolled sheets of carbon hexagons (Figure 1).[6]

CNTs are classified into two main categories attending to the number of concentric rolled-graphene layers that compose them (Figure 1). The first class includes Multi-Walled Carbon Nanotubes (MWCNTs) consisting of multiple layers of wounded graphene into

---

[1] In this essay Prof. Whitesides discussed about the impact of nanotechnology: George M. Whitesides, *Small* **2005**, *2*, 172 – 179.
[2] C. A Mirkin, *Small*, **2005**, 1, 14 – 16.
[3] For detailed information see: A. Dowling *et al. Nanoscience and nanotechnologies: opportunities and uncertainties*, A Report by The Royal Society & The Royal Academy of Engineering: London, **2004**.
[4] L. A. Kolahalam, I. V. K. Viswanath, B. S. Diwakar, B. Govindh, V. Reddy, Y. L. N. Murthy, *Materials Today: Proceedings* **2019**, *18*, 2182 – 2190.
[5] C. Martin, P. Kohli, *Nature Reviews Drug Discov.* **2003**, *2*, 29 – 37.
[6] S. Iijima, *Nature*, **1991**, *354*, 56 – 58.

cylinders (from 2 up to around 50).[6,7,8] A single graphitic sheet wrapped into a seamless tube provides the second category, Single-Walled Carbon Nanotubes (SWCNTs).[9]

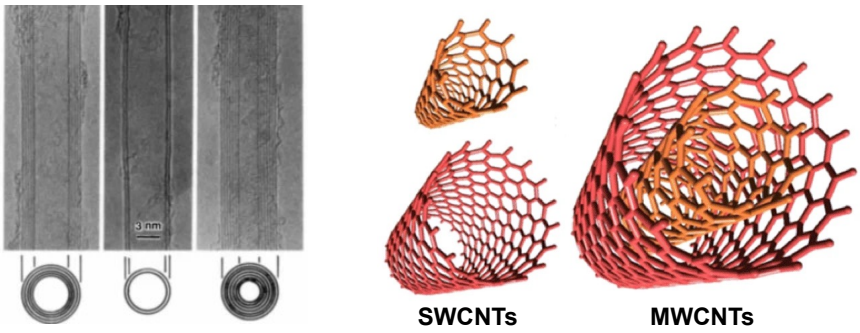


Figure 1. EM micrographs of CNTs taken by Ijima (left). Reproduced with permission from Springer Nature: Ref. 6. Copyright © 1991, Nature Publishing Group. On the right, classification of carbon nanotubes with respect to the number of coaxial tubes. Adapted with permission from Springer Nature: Viviana Negri *et al*. *Top. Curr. Chem*. **2020**, *378*, 15. Copyright © 2020, Springer Nature Switzerland AG.

The structure of each single nanotube is described by (*n, m*) vector that assigns its diameter and chirality. The number of layers and the benzene ring disposition with respect to the cylinder axis (chirality) will determine the nanotubes electronic properties. According to this, they would present metal –armchair SWCNTs– or semiconducting –zigzag or chiral SWCNTs– behavior.[10,11] In comparison with MWCNTs, SWCNTs exhibit more valuable electrical and optical properties, but unlikely, CNTs tend to aggregate in the solid state causing a mixing of different nanotube structures limiting its manipulation.[12]

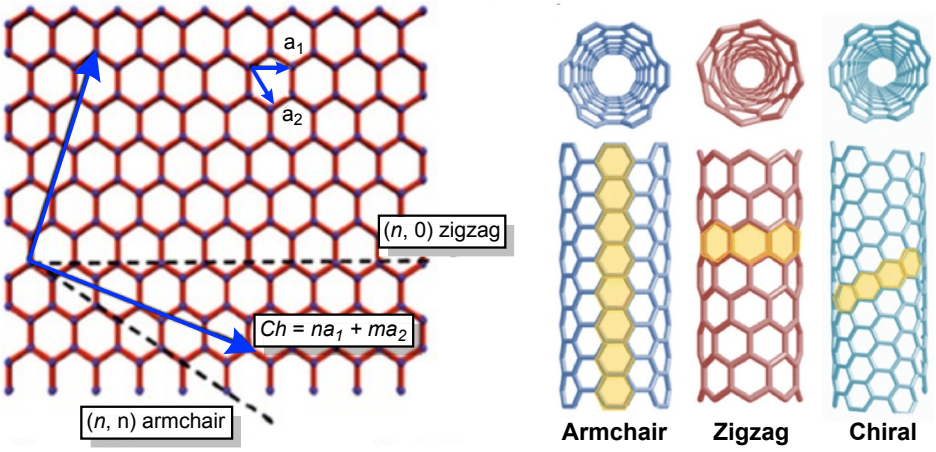


Figure 2. Representation of the chiral vector (C_h) which is defined by the unitary vectors a_1 and a_2 on a graphene sheet (left). Adapted with permission from Elsevier: R. Ghasempour, Hamid Narei, CNT Basics and Characteristics. In *Carbon Nanotube-Reinforced Polymers*, Elsevier, **2018**; 1-24. Copyright © 2018 Elsevier Inc. On the right, possible carbon nanotubular structures in relation to the rolling direction. Adapted with permission from Springer Nature: *Top. Curr. Chem*. **2020**, *378*, 15. Copyright © 2020, Springer Nature Switzerland AG.

USC UNIVERSIDADE DE SANTIAGO DE COMPOSTELA

[7] A. Green, M. Hersam, *ACS Nano*, **2011**, *5*, 1459 – 1467.
[8] T. Ch. Hirschmann, P. T. Araujo, H. Muramatsu, X. Zhang, K. Nielsch, Y. A. Kim, M. S. Dresselhaus, *ACS Nano*, **2013**, *7*, 2381 – 2387.
[9] S. Iijima, T. Ichihashi, *Nature*, **1993**, *363*, 603 – 605.
[10] R. Saito, M. Fujita, G. Dresselhaus, M. S. Dresselhaus, *Appl. Phys. Lett.* **1992**, *60*, 2204 – 2206.
[11] S. G. Louie, *Top. Appl. Phys.* **2001**, *80* (*Carbon Nanotubes*), 113 – 145.
[12] L. J. Carlson, T. D. Krauss, *Acc. Chem. Res.* **2008**, *41*, 235 – 243.

Based on the magnificent properties of CNTs, researchers have exploited them for use in nanotechnological applications.[13] According to its hollow structure with a nanometer-scale diameter, one of the first applications explored was its used as nanoporous materials for gas storage.[14] In view of the ability of these materials to confine molecules within their inner cavity, they were also efficiently used as a solid support for catalysis for heterogeneous catalysis,[15] as well the encapsulation of single-molecule magnets might drive to data storage devices.[16] In addition, due to their extraordinary mechanical strength (greater than steel) they were employed in the fabrication of nanocomposite materials useful in a wide range of technological applications.[17] Semiconducting SWCNTs are especially attractive by virtue of their low scattering and bandgap. In this sense, they have been used in different fields such as the construction of electronic devices[18] and nanobiomedicine for the regeneration of neuronal tissue and modulation of the neuronal electrical activity.[19]

INORGANIC NANOTUBES

The discovery of carbon nanotubes has attracted the interest of scientist in the development of novel nanotube-type structures. In general, compounds that present a graphite-like layered morphology are prone to provide fullerene-analogue structures. Transition metal –tungsten (W) or molybdenum (Mo)– dichalcogenides –sulfides (S) or selenides (Se)– present a layered architecture with hexagonal symmetry close to graphite (Figure 3).[20] This class of compounds have been shown to supply inorganic nanotubes (IN) similar to the carbon counterparts (Figure 3).[21,22] However, dichalcogenides-based nanotubes possess a less regular structure due to the presence of some amorphous material in the exterior.[23]

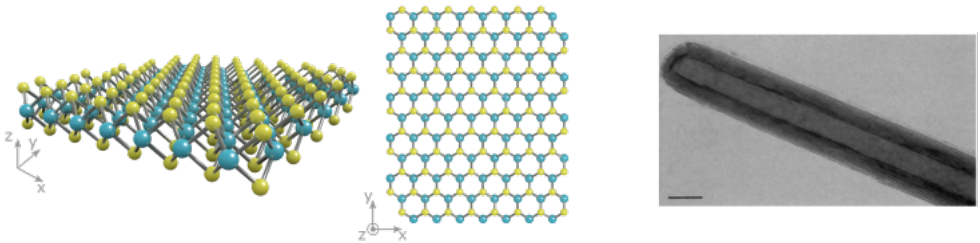


Figure 3. On the left, representation of the crystal structure of Molybdenum Sulfide (MoS_2). On on the right, TEM micrograph of a WS_2 inorganic nanotube (Scale bar= 10 nm). Reproduced with permission from Springer Nature: Ref. 21. Copyright © 1992, Nature Publishing Group.

[13] M. F. L. De Volder, S. H. Tawfick, R. H. Baughman, A. J. Hart, *Science*, **2013**, *339*, 535 – 539
[14] A. C. Dillon, K. M. Jones, T. A. Bekkedahl, C. H. Kiang, D. S. Bettune, M. J. Heben, *Nature*, **1997**, *386*, 377 – 379.
[15] S. A. Miners, G. A. Rance, A. N. Khlobystov, *Chem. Soc. Rev*. **2016**, *45*, 4727 – 4746.
[16] M. C. Giménez-López, F. Moro, A. La Torre, J. Gómez-García, P. D. Brown, J. van Slageren, A. N. Khlobystov, *Nat. Commun.* **2011**, *2*, 407.
[17] For further information about applications see **a)** G. Mittal, V. Dhand, K. Y. Rhee, S.-J. Park, W. R. Lee, *J. Ind. Eng. Chem*. **2015**, *21*, 11–25. **b)** M. Ates, A. A. Eker, B. Eker, *J. Adhes. Sci. Technol*. **2017**, *31*, 1977 – 1997.
[18] L.-M. Peng, Z. Zhang, C. Qiu, *Nat. Electron*. **2019**, *2*, 499 – 505.
[19] R. Rauti, M. Musto, S. Bosi, M. Prato, L. Ballerini, *Carbon* **2019**, *143*, 430 – 446.
[20] M. Serra, R. Arenal, R. Tenne, *Nanoscale*, **2019**,*11*, 8073 – 8090.
[21] R. Tenne, L. Margulis, M. Genut, G. Hodes, *Nature*, **1992**, *360*, 444 – 446.
[22] Y. Feldman, E. Wasserman, D. J. Srolovitz, R. Tenne, *Science*, **1995**, *267*, 222 – 225.
[23] J. L. Musfeldt, Y. Iwasa, R. Tenne, *Physic Today*, **2020**, *73*, 42 – 48.

These nanomaterials exhibit excellent tribological properties and its application as solid lubricators has been extensively studied.[24] Moreover, they present a rare combination of mechanically properties: high strength and flexibility. This finding, together with their optoelectronic properties, expands the possibilities of these inorganic products which were found to be useful for the construction of novel materials.[25]

Theorical studies have suggested that boron nitride (BN) can be considered as a non-carbon analogue of graphite because both present a very similar crystal structure.[26] The group of Zettl has reported the synthesis of the first boron nitride-based nanotubes (BNNTs).[27] In contrast to carbon nanotubes, BN nanotubes display semiconducting –they are considered as insulators– behavior which is independent of the tube diameter, chirality and layers.[28] Due to the similarity to carbon nanotubes in many respects they represent a powerful source of potential applications. In this context, some relevant properties of BNNTs are their high hydrophobicity, high oxidation and heat resistance, and radiation absorption. Among these properties highlights its excellent hydrogen storage capacity, which has been shown to be 0. 85% wt greater than that measured for carbon nanotubes.[29]

Following to Mo or W dichalcogenides and boron nitrides nanotubes, the interest in inorganic nanotubes immensely growth. Although they share some geometrical similarities, INs distinguish themselves by important peculiarities. For this reason, efforts have been devoted to carry out theoretical calculations that allowed to predict the structure and properties of such nanotubes.[30] In the last decades, the synthesis of a vast number of inorganic nanotubes have been reported and their potential applications have been studied.[20,31]

SELF-ASSEMBLED NANOTUBES

SUPRAMOLECULAR CHEMISTRY AND MOLECULAR SELF-ASSEMBLY

Until this point, *top-down* approaches are the standard synthetic methodologies to provide carbon and inorganic nanotubes. Although the processes to achieve smaller molecules in a selective manner has improved during the last years,[20,25,29,32] the *bottom-up* strategy offers better control of the resulting assemblies. Chemists have been using the covalent bond as conventional resource to efficiently connect atoms or molecules together. However, the increase in structural complexity limits the use of the strong covalent connections to build well-define nanoscale

[24] L. Rapport, N. Fleischer, R. Tenne, *J. Mater. Chem*. **2005**, *15*, 1782 – 1788.
[25] B. Višić, L. S. Panchakarla, R. Tenne, *J. Am. Chem. Soc*. **2017**, *139*, 12865 – 12878.
[26] C. Zhi, Y. Bando, C. Tang, D. Golberg, *Mater. Sci. Eng. R Rep*. **2010**, *70*, 92 – 111.
[27] N. G. Chopra, R. J. Luyken, K. Cherrey, V. H. Crespi, M. L. Cohen, S. G. Louie, A. Zettl, *Science*, **1995**, *269*, 966 – 967.
[28] Y Miyamoto, A. Rubio, S. G. Louie, M. L. Cohen, *Phys. Rev. B*. **1994**, *50*, 18360 – 18366.
[29] S. Kalay, Z. Yilmaz, O. Sen, M. Emanet, E. Kazanc, M. Çulha, *Beilstein J. Nanotechnol.* **2015**, *6*, 84 – 102.
[30] A. L. Ivanovskii, *Russ. Chem. Rev*. **2002**, *71*, 175 – 194.
[31] Y. Zhu, Y. Feng, S. Chen, M. Dinga, J. Yao, *J. Mater. Chem. A*, **2020**, *8*, 25626 – 25648.
[32] R. Rao, C. L. Pint, A. E. Islam, R. S. Weatherup, S. Hofmann, E. R. Meshot, F. Wu, C. Zhou, N. Dee, P. B. Amama, J. Carpena-Núñez, W. Shi, D. L. Plata, E S. Penev, B. I. Yakobson, P. B. Balbuena, C. Bichara, D. N. Futaba, S. Noda, H. Shin, K. S. Kim, B. Simard, F. Mirri, M. Pasquali, F. Fornasiero, E. I. Kauppinen, M. Arnold, B. A. Cola, P. Nikolaev, S. Arepalli, H.-M. Cheng, D. N. Zakharov, E. A. Stach, J. Zhang, F. Wei, M. Terrones, D. B. Geohegan, B. Maruyama, S. Maruyama, Y. Li, W. W. Adams, A. J. Hart, *ACS Nano* **2018**, *12*, 11756 – 11784.

architectures. In this context, supramolecular chemistry emerges as a useful tool towards the preparation of complex structures that can perform specific function in relation to their tridimensional framework.[33]

Despite the concept of supramolecular chemistry was introduced long time ago, it was not until the late 60s when it gained more attention. In the pioneering works of Cram,[34] Lehn[35] and Pedersen,[36] supramolecular forces were the main actors in the specific recognition function that these receptors display, *i.e.*, the receptors were designed and synthetized for their ability to interact concretely with a particular specie. The understanding of the thermodynamic basis together with the individual interactions that govern the recognition processes, supramolecular chemistry evolved towards non-covalent synthesis as it allowed the preparation of specific complex structures in a reversible manner under conditions of thermodynamic equilibrium.[37] For this purpose, molecular self-assembly became the most important phenomena.

Molecular self-assembly can be define –from a chemical point of view– as the self-organization of simple components by reversible weak interactions –hydrogen bonds, electrostatic interactions, van der Waals forces or π-π stacking, between others– to give rise to more complex structures that can be controlled through the design of their components (Figure 4). These interactions will determine the physical properties of the aggregates as their solubility or their organization on different surfaces. Attending to the energy of the system, self-assembly can be classified into two main types: the static self-assembly and the dynamic self-assembly (out-of-equilibrium systems).[38] Herein, we will focus on the static self-assembly which involves systems that are at local or global equilibrium and do not dissipate energy. In these systems, the entropic factor rules the energetic balance as molecular self-assembly involves the organization of disperse subunits.

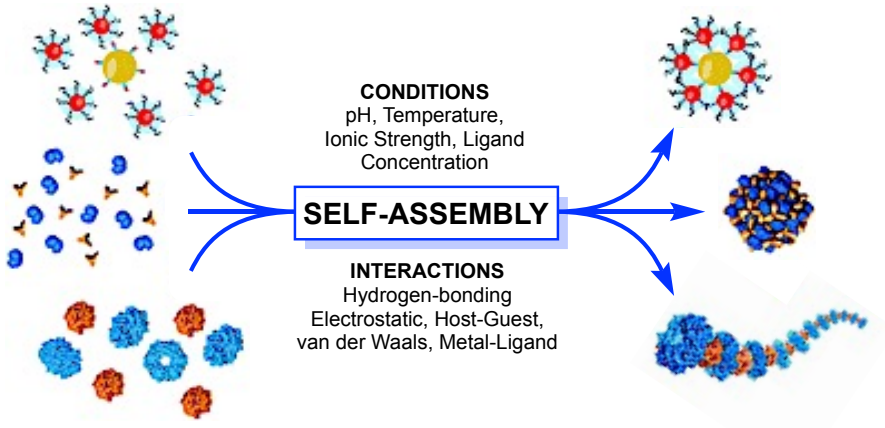


Figure 4. Schematic representation of molecular self-assembly. Adapted with from Royal Society of Chemistry: Ref. 37.

USC
UNIVERSIDADE DE SANTIAGO DE COMPOSTELA

[33] J.-M. Lehn, *Angew. Chem. Int. Ed*. **2013**, *52*, 2836 – 2850.
[34] D. J. Cram, *Angew. Chem. Int. Ed*. **1988**, *27*, 1009 – 1112.
[35] J.-M. Lehn, *Angew. Chem. Int. Ed*. **1988**, *27*, 89 – 112.
[36] C. Pedersen, *Angew. Chem. Int. Ed*. **1988**, *27*, 1021 – 1027.
[37] E. Piccinini, D. Pallarola, F. Battaglinic, O. Azzaroni, *Mol. Syst. Des. Eng*. **2016**, *1*, 155 – 162.
[38] G. M Whitesides, B. Grzybowski, *Science*, **2002**, *295*, 2418 – 2421.

The supramolecular approach based on the molecular self-assembly of smaller units has allowed to access to a plethora of topologies such as spheres,[39] cubes,[40] barrels[41], nanoflowers,[42] and others. Among all the possible morphologies that can be afforded, this Thesis is focused on self-assembled nanotube architectures.

ORGANIC NANOTUBES

Nature has been exploiting the non-covalent forces to carried out biological processes as biorecognition and molecular organization for billions of years. Inspired on the natural machinery, many elegant pathways have been implemented to construct one-dimensional tubular structures by programming weak interactions between carefully designed monomers. The supramolecular recipe would provide better control over the dimensions of the cylindrical architectures –length and diameter– and yields. In Figure 5 are depicted the most common approaches to access to these promising nanomaterials.

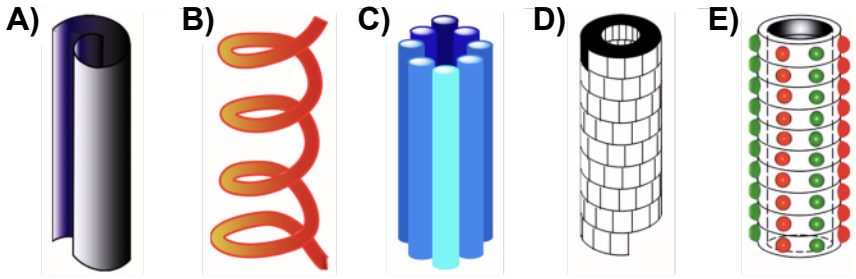


Figure 5. Representation of the different strategies followed to afford self-assembled organic nanotubes: A) Wrap sheet-like molecules around. B) Engineer molecules that fold into helixes leaving a wide internal cavity. C) Group of rod-shaped molecules in a molecular barrel. D) Association of wedge-shaped molecules. E) Stack of cyclic molecules on top of each other.

The first strategy for the construction of tubular systems consists of rolling-up a preformed film into a cylinder. This process is analogous to the folding of a graphite sheet or other inorganic 2D materials to give rise to the nanotubular architectures.[6,21] Schnur and colleagues used this approach for the preparation of phospholipid-based nanotubes.[43] The correct engineering of the amphiphile monomers, the geometry and curvature of the polar head as well as the shape and length of the non-polar tails, allowed tuning the internal and external properties of the assemblies (Figure 6A). This approach led to large cylindrical structures, up to 200 nm, a task that would be really complicated by other methods.[44] Supported by the lipid model proposed by Schnur,[40] Aida *et al.* have reported a new family of graphite-like nanotubes based on the self-assembly of amphiphilic hexa-*peri*-benzocoronene (HBC) derivatives bearing two triethylenglycol (TEG) moieties on one side and dodecyl side chains on the other (Figure 6B).[45]

---

[39] Q.-F. Sun, J. Iwasa, D. Ogawa, Y. Ishido, S. Sato, T. Ozeki, Y. Sei, K. Yamaguchi, M. Fujita, *Science*, **2010**, *328*, 1144 – 1147.
[40] W. J. Ramsay, F. T. Szczypiński, H. Weissman, T. K. Ronson, M. M. J. Smulders, B. Rybtchinski, J. R. Nitschke, *Angew. Chem. Int. Ed.* **2015**, *54*, 5636 – 5640.
[41] W.-Y. Yang, J.-H. Ahn, Y.-S. Yoo, N.-K. Oh, M. Lee, *Nat. Mater.* **2005**, *4*, 399 – 402.
[42] Y. Wang, H. D. Tran, L. Liao, X. Duan, R. B. Kaner, *J. Am. Chem. Soc.* **2010**, *132*, 10365 – 10373.
[43] P. Yager, R. R. Price, J. M. Schnur, P. E. Schoen, A. Singh, D. G. Rhodes, *Chem. Phys. Lipids* **1988**, *46*, 171 – 179.
[44] J. M. Schnur, *Science*, **1993**, *262*, 1669 – 1676.
[45] Jonathan P. Hill, W. Jin, A. Kosaka, T. Fukushima, H. Ichihara, T. Shimomura, K. Ito, T. Hashizume, N. Ishii, T. Aida, *Science* **2004**, *304*, 1481 – 1483.

This approach provided nanotubes tens of hundreds of μm in length with a 14 nm wide inner cavity, larger than those observed in carbon nanotubes. The wall is 3 nanometers thick and consists of helical arrays of π-stacked HBC molecules whose outer and inner surfaces are coated with hydrophilic triethylene glycol chains. In addition, the incorporation of a chiral group at the TEG chain the HBC-derivatives self-assembled into one-handed helical chirality nanotubes.[46] These nanotubes, due to the presence of an ordered graphite-like motif, are redox active and showed remarkable semiconducting behavior upon oxidation.

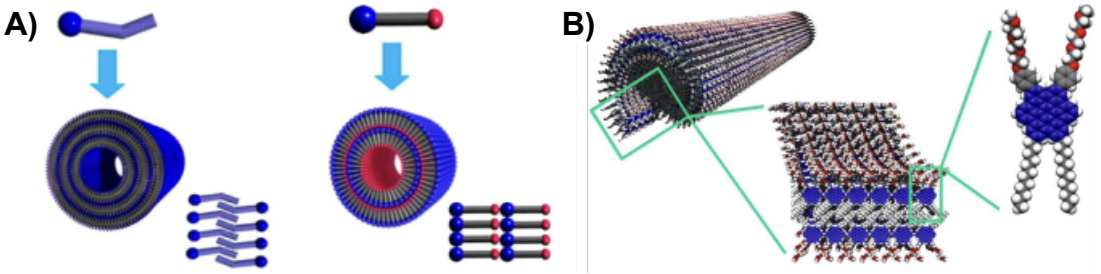


Figure 6. Nanotubes arising from the folding of supramolecular sheets based on A) amphiphilic lipids (adapted with permission from American Chemical Society: T. Shimizu *et al*. *Langmuir* **2016**, *32*, 12242. Copyright © 2016, American Chemical Society) and B) HBC-derivatives. Adapted from Ref. 46.

There are many natural molecules that coil into helical structures.[47] Among them, several extended oligomers have an internal cavity large enough to form a nanotube-like assembly. The natural antibiotic Gramicidin A is a polypeptide that packs together in the form of β-helices, larger than α-helices, forming a hydrophilic hollow suitable for the transit of ions.[48] The formation of these channels in bacteria membranes prevents its ionic balance leading to apoptosis.[49] Based on the in-solution folding of biopolymers into well-define structures, Moore *et al.* have described an aromatic hydrocarbon chain that spontaneously acquires a stable helical conformation with a large cavity.[50] The helical structures were yielded by the solvophobic-driven folding together with stabilizing π-π stacking interactions of *meta*-phenylacetylene monomers (Figure 7A). This class of aromatic compounds that present a strong tendency to adopt a specific compact conformation are known as foldamers.[51] It is possible to tune the internal and external properties of the assemblies by modifying the positions X and R1 positions of the benzene ring represented in Figure 7A, respectively. In addition, other connectors can be used. For instance, aromatic amide oligomers were shown to fold into helical structures which are further stabilize by hydrogen-bonding forces due to the presence of amide groups. .[52] These hollow assemblies have the ability to encapsulate different substances inside the internal void. Zheng's group has published a new series of pyridine/oxadiazole-based helical foldamers that generate ion channels with high selectivity for sodium and potassium cations.[53]

[46] W. Jin, T. Fukushima, M. Niki, A. Kosaka, N. Ishii, T. Aida, *Proc. Natl. Acad. Sci. U.S.A*. **2005**, *102*, 10801 – 10806.
[47] T. P. Begley, H.-W. Liu, *Comprehensive Natural Products III*. Elsevier, San Diego **2020**.
[48] D. A. Kelkar, A. Chattopadhyay, *Biochim. Biophys. Acta* **2007**, *1768*, 2011 – 2025.
[49] J. M. David, A. K. Rajasekaran, *J. Kidney Cancer VHL* **2015**; *2*, 15 – 24.
[50] J. C. Nelson, J. G. Savent, J. S. Moore, P. G. Wolynes, *Science* **1997**, *277*, 1793 – 1796.
[51] For more information about synthetic foldamers see: **a)** G Guichard, I. Huc *Chem. Commun.* **2011**, *47*, 5933 – 5941. **b)** D. Hill, M. J. Mo, R. B. Prince, T. S. Hughes, J. S. Moore, *Chem. Rev*. **2001**, *101*, 3893 – 4011.
[52] Y. Ferrand, I. Huc, *Acc. Chem. Res*. **2018**, *51*, 970 – 977.
[53] F. Cheng, J. Shen, N. Li, A. Roy, R. Ye, C. Ren, H. Zeng, *Angew. Chem. Int. Ed*. **2020**, *59*, 1440 – 1444.

Another class of foldamers are amphiphilic foldamers derived from cholic acid which, in non-polar solvents, are arranged in helical structure with hydrophilic internal cavities.[54]

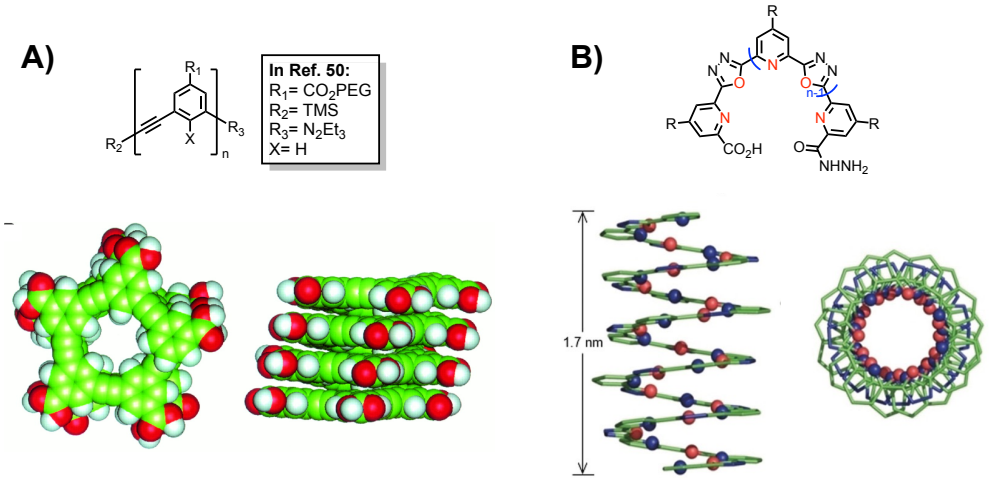


Figure 7. A) Chemical structure of *meta*-phenylacetylene monomer and representation of the helical conformation of an octadecameric chain (n= 18). Adapted from Ref. 50. B) Molecular design and side- and top-view of the helical foldamer based on pyridine/oxadiazole. Adapted with permission from John Wiley and Sons: Ref. 53. Cpyright© 2020 Wiley-VCH Verlag GmbH & Co. KGaA, Weinheim.

Another alternative for the supramolecular preparation of this hollow motifs relies on the assembly of rod-like subunits into barrel frameworks. This approach mimics those pore-forming proteins that insert into membranes as a β-barrel where the staves of the barrel are assembled as α-helical bundles or β-sheets. Some natural examples are the α-hemolysin,[55] porins[56] or the potassium channel.[57] This model of membrane-pipe formation has been exploited by Matile's group constructing the barrel staves from *p*-oligophenyl rods decorated at positions 2 and 5 with small peptide sequences (Figure 8A). The peptide side chains are alternately pointing inwards and outwards of the barrel and the repulsive forces generated between those groups will dictate the size of the ring.[58] In a similar approach, Myongsoo Lee and colleagues have prepared supramolecular barrels based on the non-covalent interaction of amphiphilic rigid-flexible macrocycles.[59] The macrocycles were composed of hexa-*p*-phenylene rods connected by a poly(ethyleneoxide) chain. In-solution assembly of this rods have led to barrel-like tubular structures.

[54] Y. Zhao, Z. Zhong, *J. Am. Chem. Soc*. **2005**, *127*, 17894 – 17901.
[55] L. Song, M. R. Hobaugh, C. Shustak, S. Cheley, H. Bayley, J. E. Gouaux, *Science*, **1996**, *274*, 1859 – 1866.
[56] S. Cowan, T. Schirmer, G. Rummel, M. Steiert, R. Ghosh, R. A. Pauptit, J. N. Jansonius, J. P. Rosenbusch, *Nature*, **1992**, *358*, 727 – 733.
[57] D. A. Doyle, J. M. Cabral, R. A. Pfuetzner, A. Kuo, J. M. Gulbis, S. L. Cohen, B. T. Chait, R. MacKinnon, *Science*, **1998**, *280*, 69 – 77.
[58] N. Sakai, J. Mareda, S. Matile, *Acc. Chem. Res*. **2008**, *41*, 1354 – 1365.
[59] W.-Y. Yang, J.-H. Ahn, Y.-S. Yoo, N.-K. Oh, M. Lee, *Nat. Mater*. **2005**, *4*, 399 – 402.

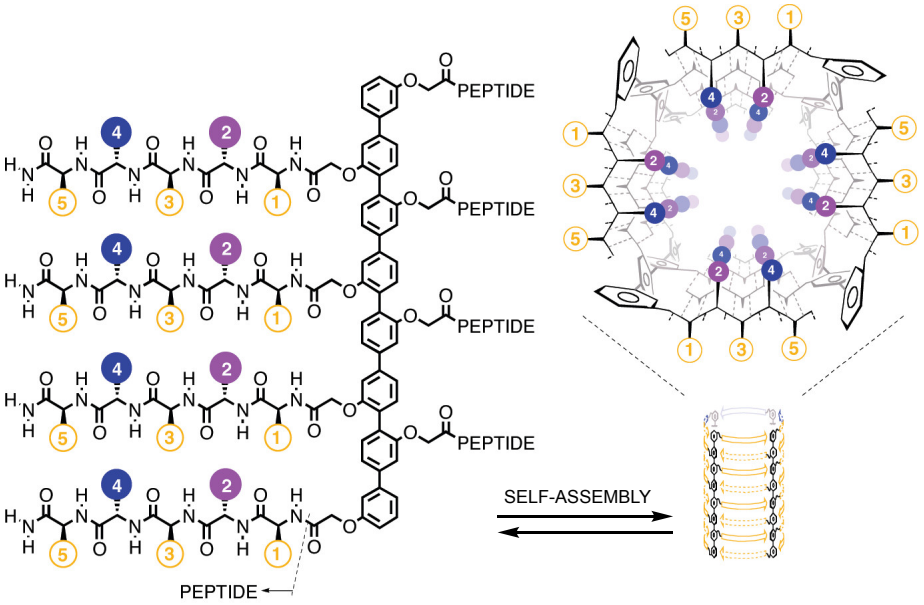


Figure 8. Self-assembly of *p*-oligohenyl rod-like subunits into a barrel structure. Reproduced with permission from American Chemical Society: Ref. 58. Copyright © 2008, American Chemical Society.

A noteworthy feature of DNA is the precise control that provides over the bottom-up approach for the synthesis of more complex structures.[60] Single-stranded DNA has been configured to self-assemble into rigid tile-like geometry (Figure 9A).[61] The non-covalent interaction between the lattices has driven to DNA-tubes with programmable circumferences. Coordination chemistry has afforded control over the tube length, Fujita *et al.* have shown that the complexation of oligo(3,5-pyridine) ligands with end-capped Pd(II) cores in the presence of rod-like guests has led to hollow coordination prism (Figure 9B). The length of the nanotube depends directly on the number of pyridines of the ligand.[62]

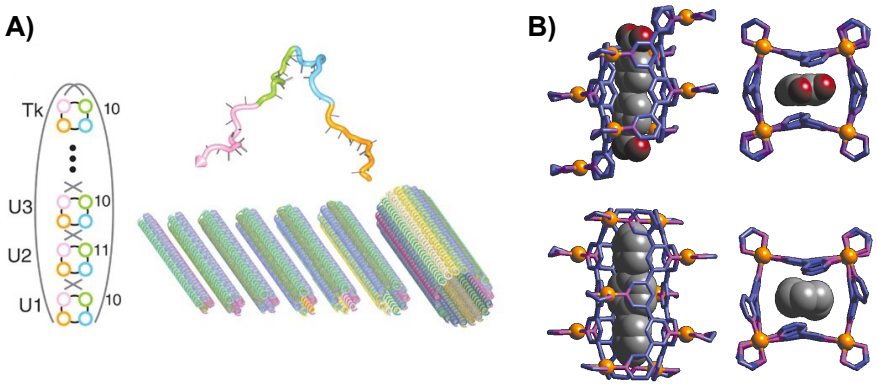


Figure 9. A) Representation of programmed single-stranded DNA tubes. Adapted with permission from American Association for the Advancement of Science. Copyright © 2008, The American Association for the Advancement of Science B) Crystal structure of nanotubes using the coordination approach reported by Fujita. Reproduced with permission from Royal Society of Chemistry: Ref. 62.

USC
UNIVERSIDADE
DE SANTIAGO
DE COMPOSTELA

[60] **a)** N. C. Seeman, H. F. Sleiman, *Nat. Rev. Mater.* **2017**, *3*, 17068. **b)** P. W. K. Rothemund, *Nature* **2006**, *440*, 297 – 302.
[61] P. Yin, R. F. Hariadi, S. Sahu, H. M. T. Choi, S. H. Park, T. H. LaBean, J. H. Reif, *Science*, **2008**, *321*, 824 – 826.
[62] M. Aoyagi, S. Tashiro, M. Tominaga, K. Biradha and M. Fujita, *Chem. Commun*. **2002**, *2*, 2036 – 2037.

In search of new strategies for supramolecular construction of nanotubes, a more complex approach relies on the assembly of wedge-shaped molecules into disks, rosettes or helices that will provide the final tubular structure. This approximation mirrors the tobacco mosaic virus (TMV) coat protein self-assembly process. Early synthetic efforts have been made in Percec's group by preparing nanotubes derived from the hexagonal packing of wedge-shaped amphiphilic dendrimers, where the polar group are pointing outwards and the non-polar groups are heading to the internal channel (Figure 10A).[63] Similarly, Fenniri and colleagues have prepare complementary cytosine- and guanine-modified monomers that arrange in a supermacrocycle –as a rosette– which self-assemble into stable nanotubular architectures.[64] The group of David González-Rodríguez have designed a covalently linked GC dinucleobase monomers that give rise to a tubular structure through an orthogonal multistep pathway involving self-assembling cooperative effects of different hierarchy.[65] A cyclic tetramer formed by the complementary Watson-Crick G:C connections and, a subsequently polymerization process guided by π-π and H-bonding interactions led to the desired supramolecular assembly. The group of Myongsoo Lee has developed another elegant example, they have constructed nanotubes that contract and expand in response to heat from V-bended aromatic subunits. These monomers self-assemble into hexameric macrocycles that spontaneously stack giving rise to chiral nanotubes (Figure 10B). [66] In addition, more complex systems based-on *p*-sulfonatocalix[4]arene have also been shown to assemble into helical tubular structures upon the addition of pyridine N-oxide and lanthanide ions.[67]

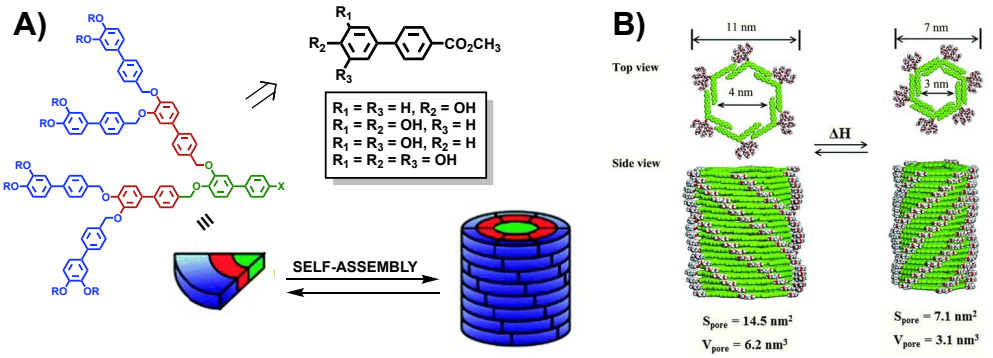


Figure 10. Supramolecular nanotubes constructed from the self-assembly of disks motifs prepared using: A) amphiphilic wedge-shaped dendrimers (adapted with permission from Royal Society of Chemistry: Ref. 63) and B) amphiphilic V-bended aromatic molecules. Reproduced with permission from The American Association for the Advancement of Science: Ref. 66. Copyright © 2012, American Association for the Advancement of Science.

The latest model for the construction of nanometer-sized tubes is based on the stacking of planar cyclic molecules. Although not represented in biological models, this approach has

[63] H.-J. Sun, S. Zhang, V. Percec, *Chem. Soc. Rev*. **2015**, 44, 3900 – 3923.
[64] G. Borzsonyi, R. L. Beingessner, T. Yamazaki, J.-Y. Cho, A. J. Myles, M. Malac, R. Egerton, M. Kawasaki, K. Ishizuka, A. Kovalenko, H. Fenniri, *J. Am. Chem. Soc*. **2010**, *132*, 15136 – 15139.
[65] V. Vázquez-González, M. J. Mayoral, R. Chamorro, M. M. R. M. Hendrix, I. K. Voets, D. González-Rodríguez, *J. Am. Chem. Soc*. **2019**, *141*, 41, 16432 – 16438.
[66] Z. Huang, S.-K. Kang, M. Banno, T. Yamaguchi, D. Lee, C. Seok, E. Yashima, M. Lee, Science, **2012**, *337*, 1521 – 1526.
[67] G. W. Orr, L. J. Barbour, J. L. Atwood, *Science*, **1999**, *285*, 1049 – 1051.

certain advantages over the other designs: It is possible to program the diameter of the tube in relation to the size of the macrocyclic monolayers. In addition, the conformational restriction of the planar structures allows a simple modification of both sides –internal and external– of the tube. In general, *à la carte* tubular materials can be prepared by means of this procedure. There are several publications in the literature in which this strategy has been used, Harada et al. have proposed a combined supramolecular/covalent strategy to create a nanotube through crosslinking of adjacent cyclodextrins (CDs) in a polyrotaxane system. (Figure 11A).[68] Stoddart and coworkers have prepared the cyclic variant of (1→4)α-linked oligosaccharides leading to CD analogues. X-Ray analysis of octameric cyclic oligosaccharide has shown the formation of cylindrical shape molecules with C_4 symmetry in the solid state.[69]

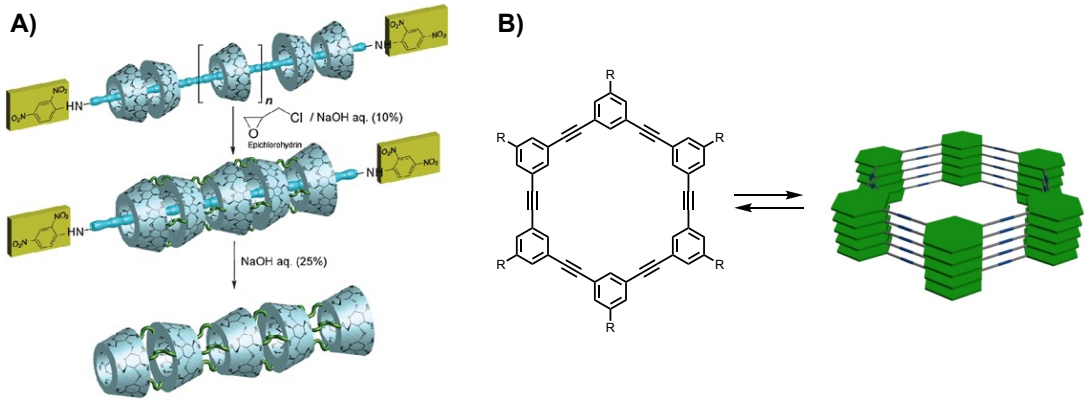


Figure 11. Nanotubular structures based on the stacking of macrocyclic subunits. A) Polymeric nanotube constructed by covalent binding of neighboring cyclodextrins in a rotaxane structure. Reproduced with permission from Chemical Society of Chemistry: Ref. 68b B) π-π Stacking of shape-persistent PAMs. Adapted with permission from Springer Nature: Ref. 74. Copyright © 2020, The Author(s).

Shape-persistent phenylacetylene macrocycles (PAMs) –similar to previously mentioned foldamers– have also presented the ability to stack into tubular structures (Figure 1B).[70] Phenolic derivatives of symmetric PAMs interacts through hexagonal two-dimensional hydrogen bond network resulting in extended tubular porous crystal structures.[71] Similar shape-persistent macrocycles with extraannular polyalkyl substituents have led to solvent-dependent aggregation PAMs as the self-assembly is controlled by non-specific interactions.[72] However, this approximation is strongly conditioned by the electronic nature of the aromatic backbone leading to weak π-π interactions depending on the solvent polarity. Gong *et al.* have prepared a new class of PAM monomers decorated with peripheric amide side chains.[73] The dominant H-bonding nature of the amide groups reinforced macrocycles stacking leading to similar self-assembling properties in many different solvents. Moreover, they have introduced

[68] **a)** A. Harada, J. Li, M. Kamachi, *Nature*, **1993**, *364*, 516 – 518. **b)** A. Harada, Y. Takashimaa, H. Yamaguchi, *Chem. Soc. Rev*. **2009**, *38*, 875 – 882.
[69] P. R. Ashton, C. L. Brown, S. Menzer, S. A. Nepogodiev, J. F. Stoddart, D. J. Williams, *Chem. Eur. J.* **1996**, *2*, 580 – 591.
[70] J. Zhang, J. Moore, *J. Am. Chem. Soc*. **1994**, *116*, 2655 – 2656.
[71] D. Venkatamaran, S. Lee, J. Zhang, J. S. Moore, *Nature*, **1994**, *371*, 591 – 593.
[72] S. Höger, K. Bonrad, A. Mourran, U. Beginn, M. Möller, *J. Am. Chem. Soc*. **2001**, *123*, 5651 – 5659.
[73] Y. Zhong, Y. Yang, Y. Shen, W. Xu, Q. Wang, A. L. Connor X. Zhou, L. He, X. C. Zeng, Z. Shao, Z.-L. Lu, B. Gong, *J. Am. Chem. Soc*. **2017**, *139*, 15950 – 15957.

endo-annular substituents yielding the internal functionalization of the tubular assemblies. More recently, it has been reported that non-planar diphenylamine[n]arenes (DPAs) exhibit intrinsic π–π stacking interactions providing hollow columns with the ability to capture ethene/ethene molecules inside the assembled channels.[74]

PEPTIDE NANOTUBES

In the previous lines several cylindrical motifs have been described from CNTs and INs to many self-assembling strategies with organic compounds. Despite powerful physical properties or elegant designs, many of the above nanomaterials present some limitations. For instance, carbon nanotubes display low solubility and tendency to aggregate in most common solvents, poor biocompatibility and difficulties in controlling their dimensions. On the other hand, due to the limitations in forming specific covalent bonds, some monomer designs of self-assembled nanotubes require tedious synthetic procedures. In this context, self-assembled peptide nanotubes arise as good alternative. The wide structural variety and mouldability capacity together with their biocompatibility and ease of synthesis make them ideal scaffolds for the construction of nanobiomaterials. Many platforms have been described for the constitution of peptide nanotubes (PNTs).[75]

Linear peptide nanotubes

Small dipeptides bearing hydrophobic lateral chains were shown to self-organize into tubular-like architectures in the solid state. The analysis of the crystal structure of phenylalanine-phenylalanine (FF) dipeptide –core structural motif of β-amiloyd protein– allowed Görbitz to identify channel structures with hydrophilic cavities (Figure 12A).[76] Gazit's group, based on these results and their previous studies on this amyloid fibril key structural feature,[77] stablished the self-assembly properties in solution of the FF dipeptide. They found that, after the addition of water to a hexafluoroisopropanol (HFIP) solution of this dipeptide at high concentrations (100 mg/mL), the appropriate conditions were generated to promote discrete and stiff nanotubes.[78] Although other dipeptides were also shown to provide tubular structures,[76] the FF structural motif present the most promising properties and it has been deeply studied for potential applications. In a similar vein, some other oligopeptide sequences derived from β-amyloid were also shown to form nanotubes.[75,79]

Peptide sequences that organize into cylindrical β-helix as previously mentioned Gramicidin A (Figure 12B) were also shown to produce interesting channel materials. In this scenario, DeSantis and colleagues first purposed a synthetic sequence that can drive to β-helix assemblies.[80] Some years ago, the group of Lorenzi has published for first time the atomic resolution X-ray crystal structure of a polypeptide with *D,L*-alternating amino acids that folds

USC UNIVERSIDADE DE SANTIAGO DE COMPOSTELA

[74] L. Mao, Y. Hu, Q. Tu, W.-L. Jiang, X.-L. Zhao, W. Wang, D. Yuan, J. Wen, X. Shi, *Nat. Commun*. **2020,** *11*, 5806.
[75] For further information about PNTs see: I. W. Hamley, *Angew. Chem. Int. Ed*. **2014**, *53*, 6866 – 6881.
[76] C. H. Görbitz, *Chem. Eur. J*. **2001**, *7*, 5153 – 5159.
[77] E. Gazit, *FASEB J*. **2002**, *16*, 77 – 83.
[78] M. Reches, E. Gazit, *Science*, **2003**, *300*, 625 – 627.
[79] T. Li, X.-M. Lu, M.-R. Zhang, K. Hu, Z. Li, *Bioact. Mater*. **2022**, doi:10.1016/j.bioactmat.2021.09.029
[80] F. Ascoli, G. DeAngelis, F. DelBianco, P. DeSantis, *Biopolymers* **1975**, *14*, 1109 – 1114.

into an antiparallel double-stranded β-helix.[81] This family of synthetic peptides composed of linear *D,L* enantiomeric sequences were shown to insert into lipid membranes with ion transport activity.[82] More recently, a hybrid *D,L*-Oligopeptide-PEG [poly(ethylene glycol)] conjugate was also reported to self-assembly into well-define cylindrical nanoparticles with enhanced resistance to phagocytosis and increased ability to repel proteins.[83]

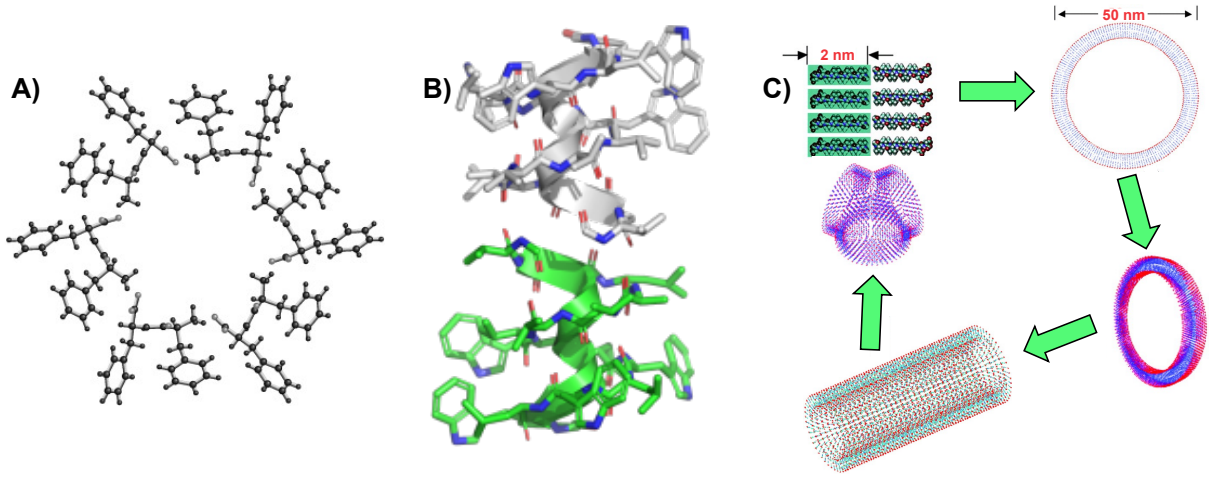


Figure 12. Linear peptide-based nanotubes: A) Top view representation of FF dipeptide-based channel. Reproduced with permission from John Wiley and Sons: Ref. 76. Cpyright © 2001 WILEY-VCH Verlag GmbH, Weinheim, Fed. Rep. of Germany B) Crystal structure of Gramicidin A that compacts into a ß-helix structure (PDB: 1MAG) and C) Surfactant-like peptide-based nanotubes. Reproduced with permission from National Academy of Sciences: Ref. 85. Copyright © 2002, The National Academy of Sciences.

Surfactant-like peptides (SLPs) are a family of amphiphilic peptides composed by two sequence domains: a polar head comprising one or two charged residues; and a longer hydrophobic tail composed of hydrophobic and neutral amino acids.[84] Zhang and colleagues, inspired by the work of Schnur with lipid molecules,[44] start to study the scope of this class of peptides. They have observed the formation of a dense network of nanotubes and nanovesicles having diameters ranging from 30 to 50 nm with a helical twist (Figure 12C).[85] Perutz and coworkers has demonstrated the generation of nanotubes from polyglutamine-rich peptides. They argued that the number of consecutive glutamines in the polypeptide sequence plays a key role in the constitution of a β-helix structure.[86] With this type of building blocks it was possible to control the supramolecular properties of the system by small modifications in the design of the SLPs, such as the position or substitution of amino acids in the peptide sequence, as well as its length.[84] For instance, varying the geometry or number of carbons of residue side chain in the hydrophobic core of bola-amphiphile peptides –a class of SLPs with a charged

USC UNIVERSIDADE DE SANTIAGO DE COMPOSTELA

[81] E. Benedetti, B. DiBlasio, C. Pedone, G. P. Lorenzi, L. Tomasic, V. Gramlich, *Nature,* **1979**, *282*, 630.
[82] P. De Santis, A. Palleschi, M. Savino, A. Scipioni, B. Sesta, A. Verdini. *Biophys. Chem*. **1985**, *21*, 211 – 215.
[83] P. Punzi, S. De Santis, C. Giordano, M. Diociaiuti, F. Novelli, G. Masci, A. Scipioni, *Macromol. Chem. Phys*. **2015**, *216*, 439 – 449.
[84] J. Li, J. Wang, Y. Zhao, P. Zhou, J. Carter, Z. Li, T. A. Waigh, J. R. Lu, H. Xu, *Coord. Chem. Rev.* **2020**, *421*, 213418.
[85] S. Vauthey, S. Santoso, H. Gong, N. Watson, S. Zhang, *Proc. Natl. Acad. Sci. U.S.A*. **2002**, *99*, 5355 – 5360.
[86] M. F. Perutz, J. T. Finch, J. Berriman, A. Lesk, *Proc. Natl. Acad. Sci. U.S.A*. **2002**, *99*, 5591 – 5595.

residue at either end of the molecule– resulted in nanotubular architectures with different diameters.[87]

Other alternatives involve the mutation of natural peptides which provide further understanding of the relationship between the molecular structure and the assembly process. For example, Lareontide is an octapeptide employed for acromegaly treatment which forms hydrogels. Derivatives of this peptide were shown to provide sequence-dependent nanotubes.[88]

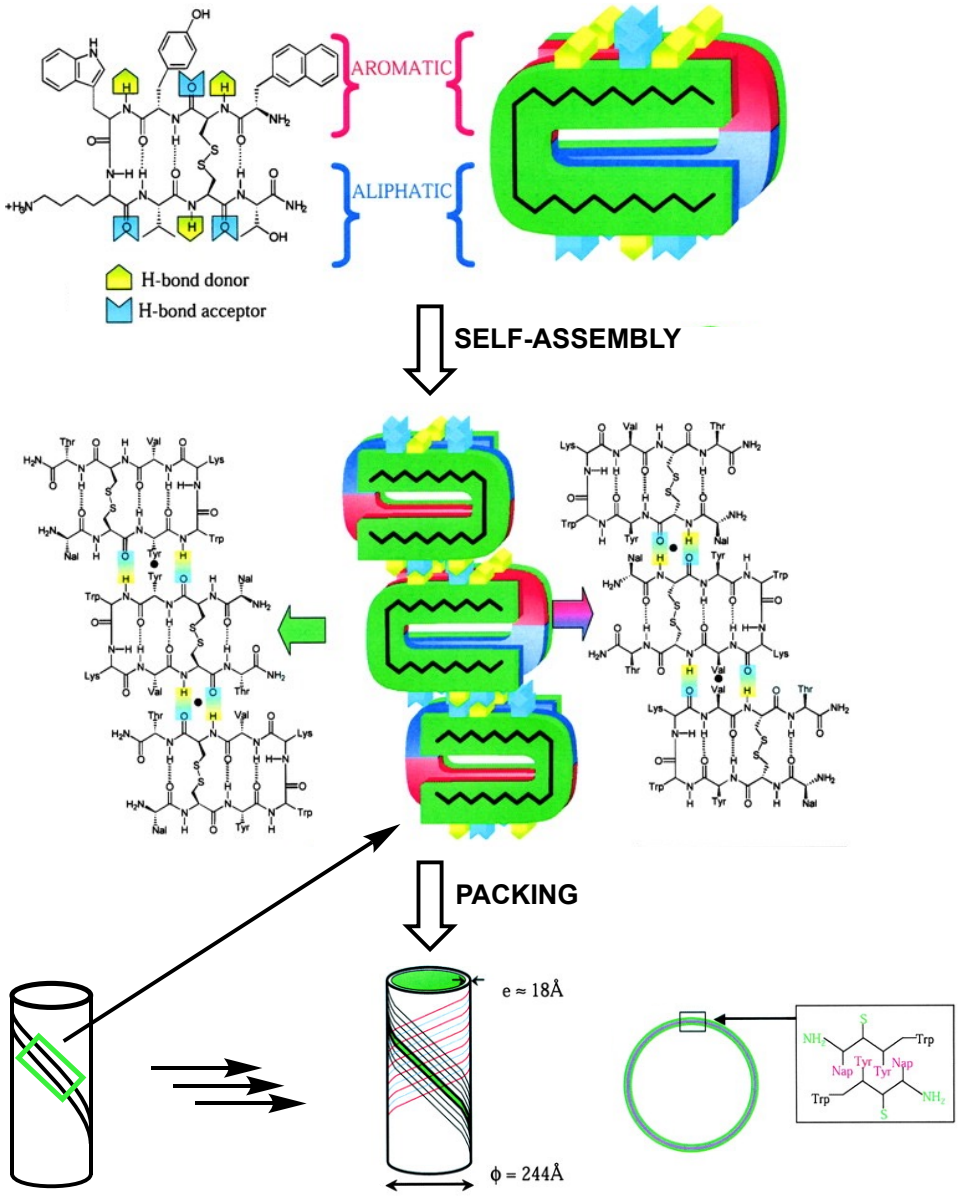


Figure 13. Schematic representation of the different hierarchical levels in the self-assembly process of Lanreotide octapeptide to form nanotubes in water. Adapted with permission from National Academy of Sciences: Copyright © 2003, The National Academy of Sciences.

USC
DE SANTIAGO
DE COMPOSTELA

[87] Y. Zhao, W. Yang, D. Wang, J. Wang, Z. Li, X. Hu, S. King, S. Rogers, J. R. Lu, H. Xu, *Small* **2018**, *14*, 1703216.
[88] C. Valèry, M. Paternostre, B. Robert, T. Gulik-Krzywicki, T. Narayanan, J.-C. Dedieu, G. Keller, M.-L. Torres, R. Cherif-Cheikh, P. Calvo, F. Artzner, *Proc. Natl. Acad. Sci. U.S.A.* **2003**, *100*, 10258 – 10262.

D,L,α-Cyclic peptide nanotubes

Self-assembled cyclic peptide-based nanotubes (SCPNs) consist of the stacking of several cyclic peptide (CPs) subunits supported by hydrogen bond interactions between peptide skeletons. The monomers possess an even number of amino acids of alternating chirality so that the peptide adopts a pleated structure. In this conformation, the side chains are oriented outwards occupying pseudo-equatorial positions, while the amide functions are arranged perpendicular to the plane of the ring. Therefore, hydrogen bonds can be established between the donor (NH) and acceptor (CO) groups of neighboring CPs on both sides of the disc structure (Figure 14).

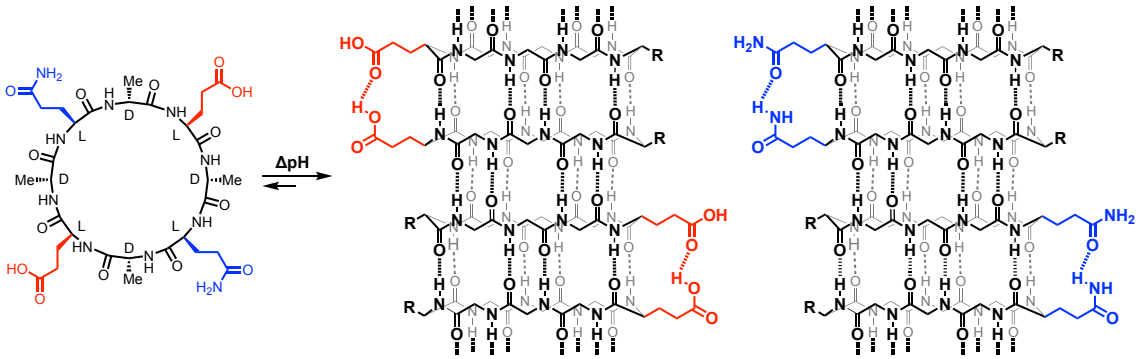


Figure 14. Chemical structure and nanotube representations of the first reported self-assembled cyclic peptide nanotubes. In nanotube representation some lateral chains were excluded for clearness.

The pioneering work in this field corresponds to the group of DeSantis who has published a theoretical study derived from the aforementioned β-helix structures where the structure of cyclic peptides formed by an even number of alternating chirality residues was analyzed.[89] In this study they postulated the formation of a flat β-sheet structure where the amide groups point in opposite directions along the symmetry axis allowing hydrogen bonding interactions due to the complementarity of the donor/acceptor groups. The first experimental approaches to corroborate this hypothesis were carried out by the group of Lorenzi, but the results were inconclusive as the studied cyclic peptides were insoluble in most of the common solvents.[90] A few years later, the same group developed a crystallographic study of two cyclic hexapeptides that demonstrated the adoption of a planar conformation. However, no evidence of nanotube formation was seen due to the strong interaction of solvent molecules with the peptides.[91] In 1993, Ghadiri and colleagues have reported, for the first time, evidence of the formation *D,L*-α-CP-based nanotube.[92] For this purpose, they prepared a rationally design cyclic octapeptide, *c*-(*L*-Gln-*D*-Ala-*L*-Glu-*D*-Ala-)$_2$, whose solubilization properties varied in relation to pH (Figure 14). Controlled acidification of an alkaline solution of the peptide provided microcrystalline aggregates which were characterized by electron microscopy (TEM), electron

USC UNIVERSIDADE DE SANTIAGO DE COMPOSTELA

[89] P. DeSantis, S. Morosetti, R. Rizzo, *Macromolecules*, **1974**, *7*, 52 – 58.
[90] L. Tomasic, G. P. Lorenzi, *Helv. Chim. Acta*, **1987**, *70*, 1012 – 1016.
[91] V. Pavone, E. Benedetti, B. Di Blasio, A. Lombardi, C. Pedone, L. Tomasich, G. P. Lorenzi, *Biopolymers*, **1989**, *28*, 215 – 223.
[92] M. R. Ghadiri, J. R. Granja, R. A. Milligan, D. E. McRee, N. Khazanovich, *Nature*, **1993**, *366*, 324 – 327.

diffraction and infrared spectroscopy (FTIR). These studies revealed that the crystals were constituted by bundles of parallel oriented nanotubes consisting of stacked cyclic peptides.

The choice of sequence is a key structural factor because amino acid side chains contribute during the self-assembly process. At basic pH electrostatic repulsions between the negatively charged glutamates restrict the aggregation while promote the solubility. In contrast, as the pH decreases, the protonation of the side chain substituents allows the establishment of hydrogen bond links between protonated carboxylic functions (Figure 14). Thus, nanotube formation relies on the hydrogen bond network of the peptide backbone plus the contribution of the lateral chains. Moreover, these side chains' forces can also be involved in intertubular connections.[92] The same structural postulates were used to construct nanotubes with larger internal cavity diameters.[93] A cyclic dodecamer was shown to provide nanotubes having a 13 Å van der Waals pore diameter, greater than those observed in CP octamers (7-8 Å). Therefore, the diameter directly depends on the number of residues of the ring.

In order to evaluate the scope of these design principles, four neutral cyclic octapeptides with different nonpolar residues were prepared.[94] It was hypothesized that intertubular van der Waals interactions would have a dominant effect on solid-state nanotubular arrangements. For this reason, the effects of increasing hydrophobic contact surface were analyzed. The studied peptides showed a remarkable stability that can be attributed to the cooperative nature of the non-covalent interactions along the crystal lattice. Moreover, it was found that the length of the nanotube is proportional to the number of hydrophobic contacts, and that the external properties of these assemblies depend on the substitution of the amino acid side chains. These results were subsequently applied by Undén's group to construct heterodimeric nanotubes –alternation of two enantiomers in a SCPN architecture– using amino acids with bulky side chains, such as *tert*-leucine.[95] However, in none of these publications a suitable crystal for atomic resolution by X-ray diffraction was obtained. Recently, the group of Chalmers was able to obtain X-ray diffraction quality crystals for atomic resolution of *D,L*-α-cyclic peptide nanotubes.[96] An important aspect of this work was the formation of nanotubes that are stacked through continuous parallel and antiparallel β-sheet registers. This arrangement shift was produced between two peptides with similar amino acid sequence in which the nonpolar residues differed. These results further support the assumptions that packing geometry in the solid state can be controlled by interactions between adjacent nanotube side chains.

Previously to overcome the lack of X-ray structural information, these supramolecular systems were analyzed at the atomic level using dimeric models. In these systems, the hydrogen bond donor groups (NH) of amino acids of the same quirality were selectively methylated. This homochiral alkylation pattern was selected because the respective NH functions are pointing to the same face of the cyclic peptide. Therefore, hydrogen bonding interactions can only be

USC UNIVERSIDADE DE SANTIAGO DE COMPOSTELA

[93] N. Khazanovich, J. R. Granja, D. E. McRee, R. A. Milligan, M. R. Ghadiri, *J. Am. Chem. Soc*. **1994**, *116*, 6011 – 6012.
[94] J. D. Hartgerink, J. R. Granja, R. A. Milligan, and M. R. Ghadiri, *J. Am. Chem. Soc*. **1996**, *118*, 43 – 50.
[95] K. Rosenthal-Aizman, G. Svensson, and A. Undén, *J. Am. Chem. Soc*. **2004**, *126*, 3372 – 3373.
[96] M. R. Silk, J. Newman, J. C. Ratcliffe, J. F. White, T. Caradoc-Davies, J. R. Price, S. Perrier, P. E. Thompson, D. K. Chalmers, *Chem. Commun*. **2017**, *53*, 6613 – 6616,

established on one side of the ring and, consequently, the corresponding CPs are restricted to assemble into dimeric structures. These dimers were soluble in organic solvents allowing the in-solution study of the thermodynamic basis of the self-assembling process. The first experiments using dimeric models were carried out in the group of Lorenzi, they studied a partial methylated cyclic hexaleucine –*c*-(*D*-Leu-*L*-^{Me}*N*-Leu-)$_3$– using FTIR and Nuclear Magnetic Resonance (NMR) techniques.[97] They observed the ability of this cyclic peptide to self-assembled into dimers establishing six hydrogen bonds between both subunits. They were also able to resolve the crystal structure that evidenced the formation of an antiparallel β-sheet register. One year later, the group of Ghadiri reported a detailed thermodynamic study of the dimerization process.[98] For this purpose, they analyzed by ^{1}H-NMR the cyclic octapeptide *c*-(*L*-Phe-*D*-^{Me}*N*-Ala-)$_4$ finding two species in solution which were attributed to the dynamic equilibrium between the monomeric and dimeric counterparts. The presence of the dimer was justified by the expected downfield shift of the phenylalanine (Phe) NH signals as consequence of their participation in a hydrogen bond network. These results were confirmed by bidimensional NMR experiments (ROESY). The self-assembling process was found to be solvent- and concentration-dependent with association constants around 10^3-10^4 M^{-1}. X-Ray analysis of the solid-state structure corroborated the cylindrical dimeric assembly –deduced from the previous experiments– formed by the stacking of two flat cyclic peptide subunits into an antiparallel β-sheet.

With the same dimeric model mentioned above, they planned to evaluate the thermodynamic preference for the antiparallel vs parallel β-sheet arrangements.[99] For this reason, they prepared a second cyclic octapeptide –*c*-(*D*-Phe-*L*-^{Me}*N*-Ala-)$_4$– which present the opposite quirality, thus both models are enantiomers. As consequence of the design features, a single methylated peptide can only interact with itself providing the antiparallel homodimer. In the same way, the association of two enantiomeric subunits drives exclusively to the heterodimeric parallel β-sheet ensemble (Figure 15). The ^{1}H NMR spectrum of the enantiomeric mixture revealed the formation of both dimeric species and the relative intensity of the ^{1}H NMR resonances permitted to calculate that the antiparallel arrangement is 0.8 kcal/mol more stable than the parallel β-sheet structure. Dimerization studies of a third cyclic octapeptide with different hydrophobic contacts determined the lack of energetic contribution for the formation of both dimers derived from cross-strand side chains interactions. Therefore, the relative stability of the antiparallel vs parallel arrangement was settled by the backbone-backbone hydrogen bonds.

USC UNIVERSIDADE DE SANTIAGO DE COMPOSTELA

[97] X. Sun, G. P. Lorenzi, *Helv. Chim. Acta*, **1994**, *77*, 1520 – 1526.
[98] M. R. Ghadiri, K. Kobayashi, J. R. Granja, R. K. Chadha, D. E. Mcree, *Angew. Chem. Int. Ed*. **1995**, *34*, 93 – 95.
[99] K. Kobayashi, J. R. Granja, M. R. Ghadiri, *Angew. Chem. Int. Ed*. **1995**, *34*, 95 – 98.

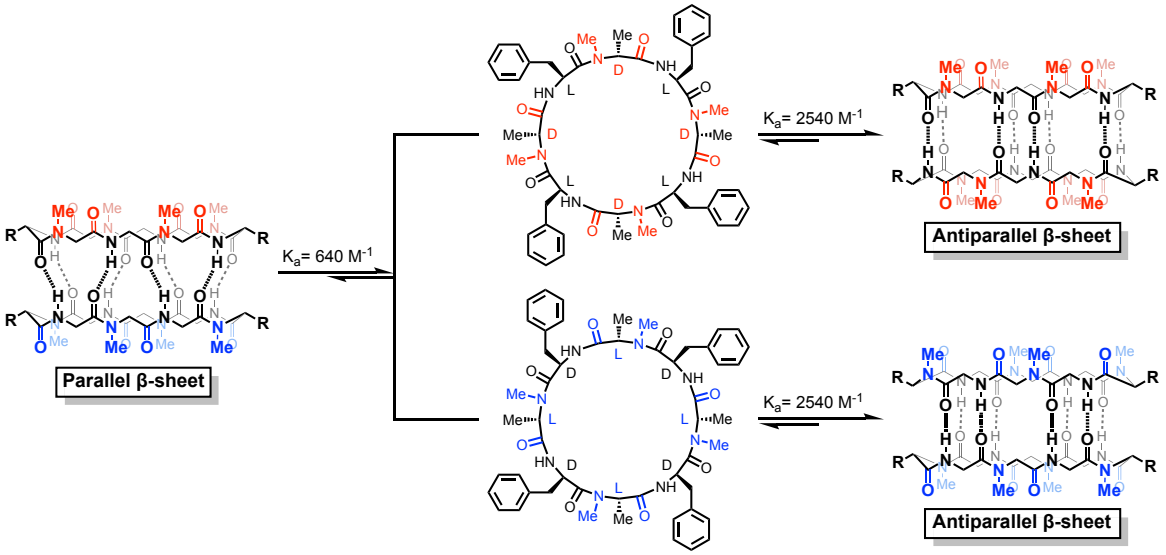


Figure 15. Models utilized for the study of the thermodynamics of the self-assembling process and the resulting dimeric species.

In 1998, Ghadiri's group published a comprehensive study in which they assessed the influence of the ring size, the identity of N-alkyl groups and the amino acid composition on the self-assembling process of dimeric species.[100] These studies revealed that larger cyclic peptides (decamers and dodecamers) did not give rise to the corresponding supramolecular species. In addition, the data collected suggested that the number, location and substitution of the N-alkyl groups (R≠ Me) also affect the dimerization process, although no clear relationship was observed. This influence may be due to possible destabilizing steric repulsions. The influence of this N-alkyl groups may be caused by possible destabilizing steric repulsions.

In 2005, Biesalski and coworkers proposed an alternative way to adjust the nanotube surroundings by linking synthetic polymers.[101] For this purpose, they used the peptide nanotube as a template which was decorated with polymerization initiator groups. Subsequent polymerization reaction produced a hybrid material with a peptide core and a polymeric outer surface. A grafting to approach was described by Börner's group.[102] In this strategy, a pre-synthesized poly(n-butyl acrylate) polymer, functionalized at its end with a carboxylate group, was coupled to a cyclic peptide containing two opposite lysine residues giving rise to a coil-ring-coil conjugate. In both examples, the self-assembly properties were not altered by the presence of the polymeric chains. More recently, the group of Prof. Perrier and Prof. Jolliffe developed a new strategy for the efficient conjugation up to four polymeric arms to a cyclic peptide backbone via cooper catalyzed azide-alkyne cycloaddition (CuAAC) chemistry.[103] Click chemistry is ideal because the chemical groups involved in the reaction are orthogonal to

[100] T. D. Clark, J. M. Buriak, K. Kobayashi, M. P. Isler, D. E. McRee, M. R. Ghadiri, *J. Am. Chem. Soc*. **1998**, *120*, 8949 – 8962.
[101] J. Couet, J. D. Jeyaprakash S. Samuel, A. Kopyshev, S. Santer, M. Biesalski, *Angew. Chem. Int. Ed*. **2005**, *44*, 3297 – 3301.
[102] M. G. J. ten Cate, N. Severin, H. G. Börner, *Macromolecules*, **2006**, *39*, 7831 – 7838.
[103] **a)** R. Chapman, K. A. Jolliffe, S. Perrier, *Aus. J. Chem*. **2010**, *63*, 1169 – 1172. **b)** R. Chapman, K. A. Jolliffe, S. Perrier, *Polym. Chem*. **2011**, 2, 1956 – 1963

the polymerization as well as the peptide synthesis conditions. Structural studies of these conjugates revealed that increasing the size of the polymer reduces the length of the resulting nanotube.[104] This is, therefore, one of the first approximations to control the length of CP nanotubes. Furthermore, it was observed that the polymer shells the peptide core from the solvent preventing the cleavage of hydrogen bonds, as well as that the polymers sterically stabilize these hybrid assemblies by preventing lateral aggregation which is a common structural feature of unconjugated CPs.[105] Model cyclic peptide-polymer conjugates bearing complementary dyes that undergo a Förster resonance energy transfer (FRET) in close proximity allowed the study of the dynamic behavior of these supramolecular materials in several conditions.[106] This approach proved that cyclic peptide nanotubes is not a kinetically trapped system, but instead the subunits are in continuous exchange. An important aspect of this work is the investigation of the dynamic recombination in mammalian cells *in vitro*, the combination of FRET effect and confocal microscopy provided essential structural information in complex biological environments.

Novel designs of cyclic peptide nanotubes: non-natural residues

Nature has created a sophisticated machinery in which proteins and peptides are the natural agents in charge of carrying out many biological tasks. Secondary structure can be defined as the spatial arrangement of local peptide domain that influences its biological function (structure-function relationship). This unique ability to adopt a well-defined organization is dictated by the specific amino acid sequence of a local segment of a protein or peptide. As mentioned above, it presents great benefit to design customized materials that can play distinct roles. However, despite the great advances in this area, naturally occurring α-amino acids limit the scope of peptide-like materials.[107] In mid 1990's, several groups have turned their attention towards this situation and started to evaluate the construction of different systems containing synthetic amino acid derivatives.[108]

Cyclic peptide nanotubes have a very restricted conformation, as they must adopt a flat disk-shape conformation in order to grow the cylinder. In this case, solely use of α-residues presents certain drawbacks such as the limitation of the ring diameter[100] or that the internal properties of the assembly cannot be modified because the proton in α-position points parallel to the nanotube axis. In this context, a lot of efforts have been devoted to developing novel designs that afford better control over the internal and external properties.[109]

Cyclic peptide nanotubes: β-amino acids

β-Peptides were shown to be promising polymeric backbones due to its propensity to acquired secondary structural conformations with enhaced stability that are difficult to achieve

USC UNIVERSIDADE DE SANTIAGO DE COMPOSTELA

[104] R. Chapman, M. L. Koh, G. G. Warr, K. A. Jolliffe, S. Perrier, *Chem. Sci*. **2013**, *4*, 2581 – 2589.
[105] M. L. Koh, P. A. FitzGerald, G. G. Warr, K. A. Jolliffe, S. Perrier, *Chem. Eur. J*. **2016**, *22*, 18419 – 18428.
[106] J. Y. Rho, J. C. Brendel, L. R. MacFarlane, E. D. H. Mansfield, R. Peltier, S. Rogers, M. Hartlieb, S. Perrier, *Adv. Funct. Mater*. **2018**, *28*, 1704569.
[107] S. H. Gellman, *Acc. Chem. Res*. **1998**, *31*, 173 – 180.
[108] W. S. Horne, S. H. Gellman, *Acc. Chem. Res*. **2008**, *41*, 1399 – 1408.
[109] N. Rodríguez-Vázquez, M. Amorín, J. R. Granja, *Org. Biomol. Chem*. **2017**, *15*, 4490 – 4505.

with the natural α-residues counterparts.[110] Notably, Seebach's group reported that linear homooligomers comprised of non-cyclic β-amino acids led to extended helical structures.[111] In the same direction, Gellman and coworkers described helical conformations adopted by polyamides containing *trans*-2-amino-cyclohexanecarboxylic acids.[112] These unnatural peptide-mimetic oligomers were more stable to enzymatic hydrolysis and they provided rational control over the secondary structure. These findings promoted the development of novel supramolecular systems. For instance, helical β-peptide helical foldamers comprised of *trans*-(*1S,2S*)-2-aminocyclopentanecarboxylic acid gave rise to highly homogeneous, well-defined, and unprecedented three-dimensional (3D) shapes upon self-assembly in aqueous solutions.[113] The morphologies of the 3D assemblies can be controlled just by tuning the experimental conditions. Similarly, the inclusion of *trans*-(*1S,2S*)-2-aminocyclopentanecarboxylic acid at the outer positions of a sequence of coiled-coil helical oligomers provided new α,β-peptides with improved conformational stability.[114] In addition, the presence of the β-residues provided novel interaction sites leading to the formation of fibrillar nanostructures not observed in the model composed of α-amino acids.

In 1997, the group of Seebach has reported the first cyclic peptides based exclusively on β-amino acids. The cyclic β-tetrapeptides were made of different combinations of 3-aminobutanoic acid isomers (Figure 16A). Although the resulting oligomers turned out to be insoluble, they were adequate to assess the structure by X-Ray Powder Diffraction (PXRD) which revealed that they adopt flat ring-shaped conformation and stack on top of each other through hydrogen bonding interactions. In contrast to the α-residue counterparts, all hydrogen bond donor groups (NH) point towards the same face of the ring, while the acceptor groups (CO) towards the opposite direction due to the presence of an extra methylene group between the amino and carbonyl groups. As consequence of this distribution, a macrodipolar moment was generated along the nanotube axis. In addition, peptide subunits can only interact with each other through a parallel β-sheet (Figure 16A).[115]

[110] P. S. P. Wanga, A. Schepartz, *Chem. Commun*. **2016**, *52*, 7420 – 7432.
[111] D. Seebach, M. Overhand, F. N. M. Kühnle, B. Martinoni, *Helv. Chim. Acta*, **1996**, *79*, 913 – 941.
[112] D. H. Apella, L. A. Christianson, D. A. Klein, D. R. Powell, X. Huang, J. L. Barchi Jr, S. H. Gellman, *Nature*, **1997**, *387*, 381 – 384.
[113] S. Kwon, A. Jeon, S. H. Yoo, I. S. Chung, S.-S. Lee, *Angew. Chem. Int. Ed*. **2010**, *49*, 8232 – 8236
[114] M. Szefczyk, N. Szulc, M. Gąsior-Głogowska, A. Modrak-Wójcik, A. Bzowska, W. Majstrzyk, M. Taube, M. Kozak, T. Gotszalk, W. Rudzińska-Szostak, Ł. Berlicki, *Nanoscale* **2021**, *13*, 4000 – 4015.
[115] D. Seebach, J. L. Matthews, A. Meden, T. Wessels, C. Baerlocher, L. B. McCusker, *Helv. Chim. Acta*, **1997**, 80, *173* – 182.

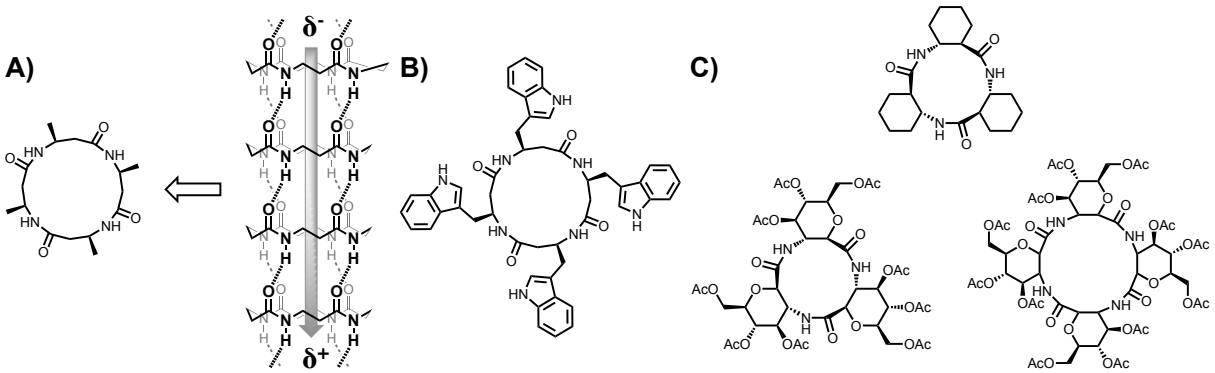


Figure 16. Cyclic ß-peptides sequences synthetized by A) Seebach's group, B) Ghadiri's group and C) Kimura's group.

The group of Ghadiri developed cyclic β-peptides capable to assemble within lipidic membranes. The designed peptide consisted of homoquiral hydrophobic amino acids in which the lateral chains occupy equatorial positions on the exterior of the peptide ring reinforcing hydrophobic interactions with the membranes. These systems exhibited remarkable ion-transport activities (Figure 16B). [116]

Following this precedents, Kimura and colleagues studied cyclic trimers containing the β-amino acid *trans*-2-aminocyclohexylcarboxylic acid. The conformational study using spectroscopic (FTIR and NMR) and microscopy (TEM) techniques, as well as computational calculations showed that these cyclic trimers have a C_3-simmetric conformation in which the amide groups are disposed vertically and parallel to the cyclic interaction enabling the formation of rod-like structures. [117] The solubility issues of peptides constructed with cyclohexane-derived amino acids led this group to introduce sugar amino acids (SAAs). Indeed, the incorporation the SAAs improved the solubility enabling a more exhaustive analysis of the conformational characteristics of these structures (Figure 16C).[118]

Cyclic peptide nanotubes: γ-amino acids

As the potential of cyclic peptide-based nanotubes were set up, new designs emerged to modify their properties and adapt them to new applications. However, the patterns seen up to this point do not offer the capability to modify the internal characteristics of the target material. In this context, our research group has developed a new family of cyclic peptides incorporating the *cis* isomer of cyclic γ-amino acids (*cis* 3-aminocycloalcanecarboxylic acid, γ-Aca). For such purpose, we have considered the structural requirements necessary for the formation of the nanotubes: the cyclic peptide must adopt a planar structure where the NH and CO groups are oriented vertically with respect to the ring axis for the establishment of a hydrogen bonding network. Hence, the simplest design consisted of replacing natural α-amino acids with *cis*

USC UNIVERSIDADE DE SANTIAGO DE COMPOSTELA

[116] T. D. Clark, L. K. Buehler, M. R. Ghadiri, *J. Am. Chem. Soc*. **1998**, *120*, 651 – 656.
[117] F. Fujimura, M. Fukuda, J. Sugiyama, T. Moritaa, S. Kimura, *Org. Biomol. Chem*. **2006**, *4*, 1896 – 1901.
[118] F. Fujimura, T., Tomoyuki Morita, S. Kimura, *Biomacromolecules*, **2006**, *7*, 2394 – 2400.

γ-residues of appropriate chirality.[119] Figure 17 shows the equivalences, in terms of quirality, established between the γ-residues and the α-amino acids.

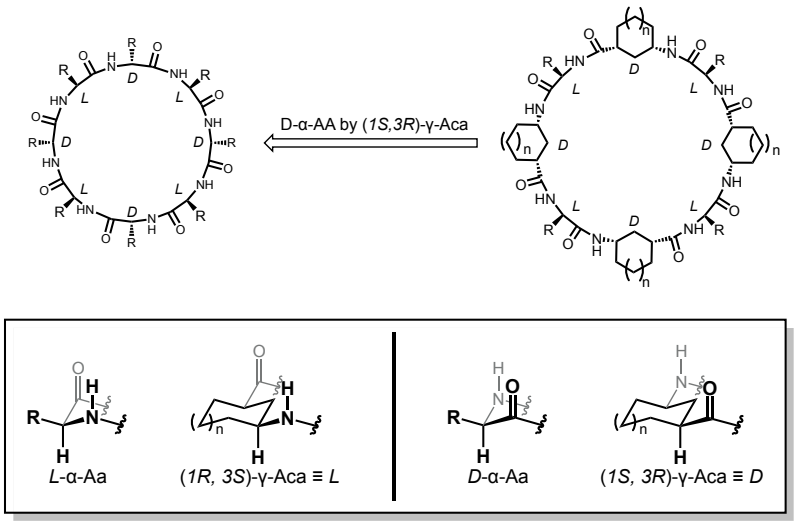


Figure 17. Strategy followed for designing α,γ-CPs and the chirality equivalence of the γ-Acas in accordance with α-Aa terms.

This novel design provides unique structural features that make them potential candidates for pursuing new applications. The incorporation of the cycloalkanes amino acids supplies with an extra rigidity to the ring promoting the formation of the necessary planar conformation. The entropic penalty is therefore reduced increasing the value of the association constants. For this reason, it would be possible to construct macrocycles of bigger dimensions, as this additional stiffness would prevent peptide folding. Moreover, the methylene at C2 position points towards the internal cavity conferring slightly hydrophobic properties. This broadens the spectrum of possible applications; if a functional group is incorporated at this position, it would be possible to tune the internal properties of the assembly.

Another structural feature derived from the use of γ-amino acids, such as α,γ-CPs, is the appearance of two differentiated faces. In both types of amino acids, there is an odd number of atoms between the amino and carbonyl and consequently, both NH and CO groups of each residue are arranged towards the same face of the ring. Thus, the NH and CO of α-amino acids are pointing towards the same direction (α-face, highlighted in red in Figure 18), while all the NH and CO of the γ-Acas are directed to the opposite side (γ-face, highlighted in blue in Figure 18). For geometrical limitations, it has been predicted that the stacking between subunits can only occur through interaction between amino acids of the same type, *i.e.,* the same faces of the ring. Therefore, α-amino acids will only hydrogen-bond with α-amino acids and γ-residues with γ-residues. In the α, γ-CPs systems, the inter-cyclic peptide interplay is restricted to an antiparallel β-sheet (Figure 18).

USC UNIVERSIDADE DE SANTIAGO DE COMPOSTELA

[119] M. Amorín, L. Castedo, J. R. Granja, *J. Am. Chem. Soc*. **2003**, *125*, 2844 – 2845.

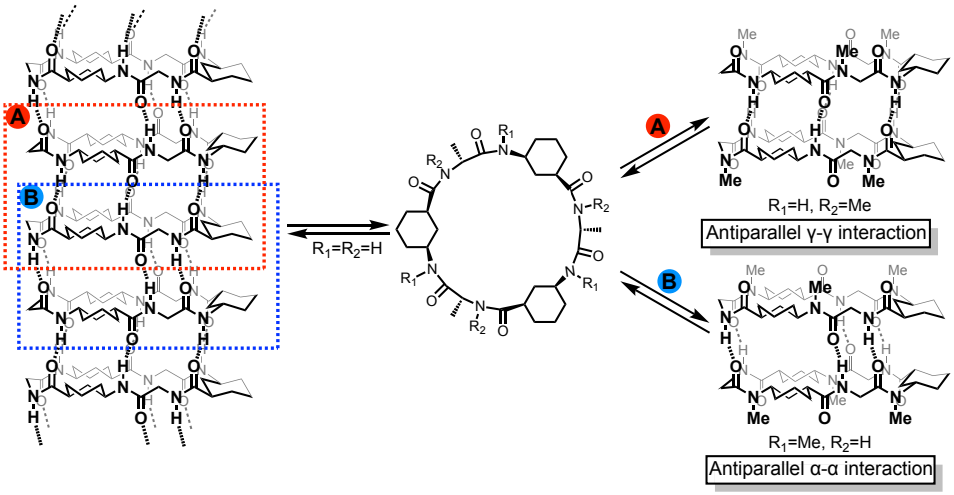


Figure 18. Structure of α,γ-CPs which drives to nanotubes This nanotubes can self-assembled through two different pathways: Path A (highlighted in red) shows the interaction between α-Aas and Path B (in blue) represent the connection between γ-residues.

Our group studied the thermodynamics parameters that governs the interaction process of each independent face. For this purpose, we employed dimeric models which include *cis*-3-aminocyclohexanecarboxylic acid (γ-Ach). For this task, we have prepared two cyclic hexapeptides –*c*-{[*D*-Phe-(*1R,3S*)-^{Me}*N*-γ-Ach-]$_3$} and *c*-{[(*1R,3S*)-^{Me}*N*-γ-Ach-^{Me}*N*-*L*-Ala-]$_3$}– in which type of residues (α or γ) was selectively N-methylated. In this way, it was possible to calculate the association constants of the dimerization process by NMR analysis. It was found that the dimer formed through α-α interaction is more stable, K_a values greater than 10^5 M^{-1}, than the γ-γ interaction ensemble which showed K_a around 10^2 M^{-1}. The crystallographic structure of *c*-{[*D*-Phe-(*1R,3S*)-^{Me}*N*-γ-Ach-]$_3$} which dimerize through α face could be resolved confirming the formation of an antiparallel β-sheet structure. The presence of chloroform molecules inside the cavity proved the hydrophobicity of the lumen (Figure 19A).[119] However, further solid-state studies of dimerization via α face revealed the amphipathic behavior of the inner volume. Depending on the crystallization conditions, chloroform or water molecules (Figure 19B) could be inserted within the hollow structure.[120] Computational studies performed by our group confirmed the good fit of the trichloromethyl motif within the internal cavity of the dimers, but these calculations also suggested that aqueous solutions have a destabilizing effect on the structure. However, organochloride molecules could be used to leads to improve nanotube stabilization in water, thus enabling control over their length.[121] Moreover, in a work in collaboration with the group of Pietro Metrangolo, it was shown that α,γ-cyclic hexapeptides bearing three *meta*-pyridyl moieties was shown to provide dimeric structures capable to confine Xe gas inside the inner volume with unexpected selectivity, thus displacing the chloroform molecules during the crystallization process.[122]

USC UNIVERSIDADE DE SANTIAGO DE COMPOSTELA

[120] M. Amorín, V. Villaverde, L. Castedo, J. R. Granja, *J. Drug. Del. Sci. Tech*. **2005**, *15*, 87 – 92.
[121] R. García-Fandiño, J. R. Granja, *J. Phys. Chem. C* **2013**, *117*, 10143 – 10162.
[122] A. Pizzi, H. L. Ozores, M. Calvelo, R. García-Fandiño, M Amorín, N. Demitri, G. Terraneo, S. Bracco, A. Comotti, P. Sozzani, C. X. Bezuidenhout, P. Metrangolo, Juan R. Granja, *Angew. Chem. Int. Ed. 58*, 14472 – 14476.

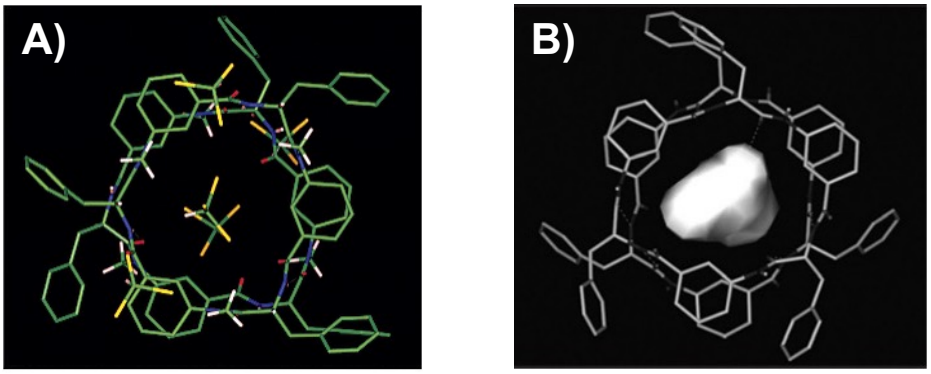


Figure 19. Crystal structures of the supramolecular dimer formed by *c*-[*D*-Phe-(*1R,3S*)-^{Me}*N*-γ-Ach-]$_3$ containing A) a chloroform or B) four delocalized water molecules inside the cavity.

Cycles of other sizes have been also investigated. Tetramers only dimerized through α-α interaction.[123] Octamers were also studied; it was found that the dimer with N-methylated γ-residues showed greater thermodynamic stability with association constants larger than 10^6 M^{-1}.[124] Computational studies revealed that the interaction energies of both self-assembly patterns are very similar.[125] However, the dimerization energies, which also considers the deformation energies, strongly indicated that the α-interaction is more stable due to differences in the deformation energy of the monomers. So that, the α-N-methylated cyclic peptide acquires a conformation that might hampers the dimerization process most probably as consequence of steric repulsions between methyl and carbonyl groups.

Simultaneously, the group according to the same structural concepts has introduced a new cyclic γ-residue, 3-aminocyclopentanecarboxylic acid (γ-Acp).[126, 127] Compared to the six-membered ring counterpart, γ-Acp presents, in addition to a larger flexibility, a wider angle formed by the plane between amino and carbonyl functionalities, 140º vs. 120º of γ-Ach.[127] This angle difference supported the idea of creating cyclic peptides that form nanotubes with bigger diameters. In these systems, it was also observed that the α-interaction showed higher stability than interactions through the other face. Notably, equimolar mixture of a γ-Acp-based cyclic peptide and other containing γ-Ach –both peptides of the same quirality– gave rise to the heterodimeric specie preferentially (Figure 20).[126] NMR analysis of peptide mixture furnished the first proof, as a new set of signals emerged which did not correspond to any of the possible homodimers. NOE cross-peak between the γ-Acp and γ-Ach signals represented a clear indication of heterodimer formation that was also confirmed in solid state by Single Crystal X-Ray Crystallography. The self-assembling process was shown to be independent of side chain cross interactions being guided by CPs skeleton. This heterodimeric preference is unclear yet, but it is attribute to a better packing of the cycloalkane rings which is translated to an improved alignment of the hydrogen bonding partners. Later, studies working with cyclic

USC UNIVERSIDADE DE SANTIAGO DE COMPOSTELA

[123] M. Amorín, R. J. Brea, L. Castedo, J. R. Granja, *Org. Lett*. **2005**, *7*, 4681 – 4684.
[124] M. Amorín, L. Castedo, J. R. Granja, *Chem. Eur. J*. **2005**, *11*, 6543 – 6551.
[125] R. García-Fandiño, L. Castedo, J. R. Granja, S. A. Vázquez, *J. Phys. Chem. B*, **2010**, *114*, 4973 – 4983.
[126] R. J. Brea, M. Amorín, L. Castedo, J. R. Granja, *Angew. Chem. Int. Ed*. **2005**, *44*, 5710 – 5713.
[127] R. J. Brea, L. Castedo, J. R. Granja, *Chem. Commun*. **2007**, *31*, 3267 – 3269.

octapeptides confirmed that the heterodimeric structure between Acp- and Ach-based CPs were also more stable than the corresponding homodimers.[128]

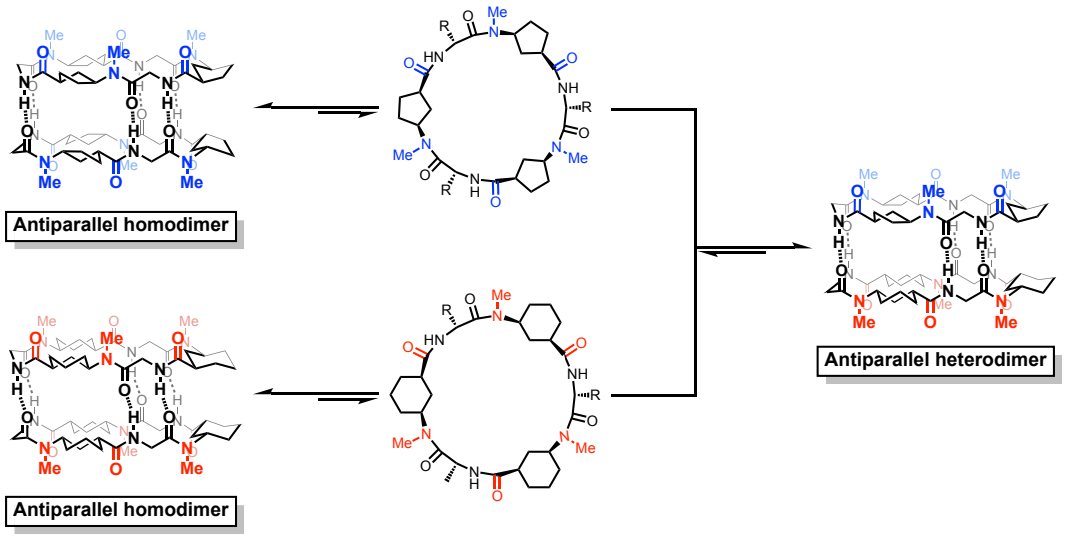


Figure 20. Schematic representation of the three possible dimeric systems in equilibrium with their monomeric counterparts. The heterodimeric systems have shown more stability in comparison with the homodimeric analogs.

These results motivated our group to expand the scope of possible synthetic amino acids. For this purpose, the unsaturated version of γ-Acp, *cis*-4-aminocyclopent-2-enecarboxylic acid (γ-Ace), was tested because it displays wider angles in the plane formed by the two amino acid functionalities.[129] Nevertheless, this new residue proved not to be too stable for peptide synthesis due to its tendency to epimerization. Also, the study of the assemblies revealed very low association constants, plus the synthetic complexity, it was decided not to continue along this path.

So far, all proposed peptide sequences were composed of alternating α,γ-amino acids. Our research group has worked on other designs containing α- and γ-amino acids in a 3:1 ratio (3α,γ-CPs) that enabled both the ring size and symmetry control.[130] In the new designs it was shown that the dimeric structures possess an ellipse shape. In addition, the alteration of the N-methylation pattern provide access to helical supramolecular structures. Deng and coworkers have reported the first cyclic peptide made exclusively of γ-residues.[131] This peptide consisted of a γ-Ach tetramer of alternating chirality in which the *D*-configuration enantiomers had a hydroxyl group at C5 position. This modification helped to increase the solubility of the aggregates by anchoring polyethylene glycol chains.

The great advantage of the cyclic γ-amino acids is the inward orientation of the C2 position into the cavity whose functionalization would allow to modify of the internal properties of the ensembles. With this aim, our research group has described the synthesis of a C2-hydroxy

USC UNIVERSIDADE DE SANTIAGO DE COMPOSTELA

[128] R. J. Brea, M. J. Pérez-Alvite, M. Panciera, M. Mosquera, L. Castedo, J. R. Granja, *Chem. Asian J.* **2011**, *6*, 110 – 121.
[129] C. Reiriz, L. Castedo, J. R. Granja, J. *Pept. Sci*. **2008**, *14*, 241 – 249.
[130] M. Amorín, L. Castedo, J. R. Granja, *Chem. Eur. J*. **2008**, *4*, 2100 – 2111.
[131] L. Li, H. Zhan, P. Duan, J. Liao, J. Quan, Y. Hu, Z. Chen, J. Zhu, M. Liu, Y.-D. Wu, J. Deng, *Adv. Funct. Mater*. **2012**, *22*, 3051 – 3056.

modified γ-amino acid, 4-amino-3-hydroxytetrahydrofuran-2-carboxylic acid (γ-Ahf), and its introduction in cyclic peptides.[132] The first structural study was performed using *c*-[*D*-Leu-γ-Ahf-*D*-Tyr(Me)-^{Me}*N*-*L*-γ-Acp-] (Figure 21). The synthesis of this peptide was carried out with benzyl-protected hydroxyl group. Self-assembling studies showed that, when the protecting group was present, the cyclic peptide did not dimerize. In contrast, the unprotected tetramer showed higher association constants than those mentioned earlier. So, this is indicative that the presence of the hydroxyl group exerts stabilizing interactions between subunits. Furthermore, computational studies helped to determine the most stable rotoisomer: the eclipsed conformation.

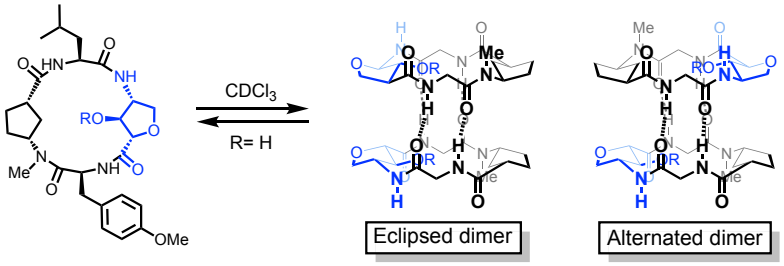


Figure 21. Chemical structure of the studied cyclic peptide and representation of the expected dimer registers after self-assembly of peptide subunits which differ in the relative orientation of the γ-Ahf.

Cyclic tetramers containing γ-Ahf have a very small cavity to be useful in any practical application. To explore the possibilities offered by this functionality, longer peptides were synthesized.[133,134] The first cyclic peptide, *c*-[(*D*-Leu-γ-Ahf-*D*-Tyr(Me)-^{Me}*N*-*L*-Acp-)$_2$], was shown to adopt a folded conformation as a result of establishing intra-hydrogen bond between the amide proton and the carbonyl group of the γ-Ahf (Figure 22, on the left).[133] In a subsequent study, the crystallographic structure revealed that this cyclic peptide folds into a V-shaped conformation. This structure further self-assembles to give rise to a tetrahedral aggregate capable of recognizing biologically relevant anions.[134] The use of N-methylated γ-Ahf residue provided a cyclic peptide –*c*-[(*D*-Leu-^{Me}*N*-γ-Ahf-*D*-Tyr(Me)-^{Me}*N*-*L*-Acp-)]$_2$– that afford a dimeric structure avoiding this folding process.[133] Different behaviors were observed depending on whether the hydroxyl group was protected or free. When it was protected, the presence of dimers with high association constants was observed in deuterochloroform. However, when it was "naked", it was necessary to decrease the temperature or increase the solvent polarity –addition of small amounts of MeOH or water– to detect the formation of these structures (Figure 22, on the right). Most likely to satisfy the donor and acceptor properties of the hydroxy function projected into the cavity.

USC UNIVERSIDADE DE SANTIAGO DE COMPOSTELA

[132] C. Reiriz, M. Amorín, R. García-Fandiño, L. Castedo, J. R. Granja, *Org. Biomol. Chem*. **2009**, *7*, 4358 – 4361.
[133] N. Rodríguez-Vázquez, R. García-Fandiño, M. Amorín, J. R. Granja, *Chem. Sci*. **2016**, *7*, 183 – 187.
[134] N. Rodríguez-Vázquez, M. Amorín, I. Alfonso, J. R. Granja, *Angew.Chem. Int. Ed*. **2016**, *55*,4504 – 4508.

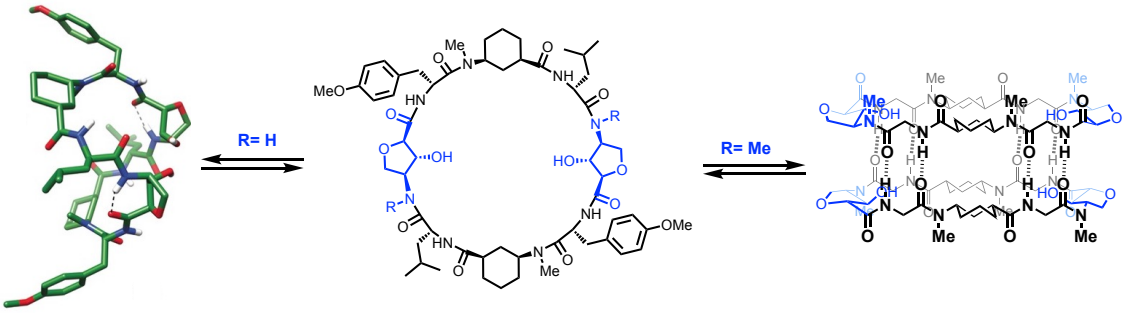


Figure 22. Structure of the octamers containing γ-Ahf (highlighted in blue) and the corresponding supramolecular structures afforded depending on the N-methylation pattern.

Other designs have also been proposed for the modification of the internal properties. For example, our group has described the incorporation of a SAA, 1-amino-glucuronic acid (γ-Aga), into pure γ-derivatives framework (Figure 23A).[135] The γ-Aga's oxygen in β-position points into the hollow core. In addition, modification of the sugar peripheric functional groups would increase the solubility of these systems in polar media. Interestingly, this cyclic peptide only led to a single dimeric specie: the alternated rotoisomer in which the γ-Ach motif is paired with the γ-Aga. In this conformation, γ-Aga derivates are interdigitated between subunits, presumably to avoid the repulsions between the oxygen lone pairs. Dhavale and colleagues have also proposed the synthesis of a fluorinated SAA-derived α,γ-CP for lumen properties modification.[136] In this work, they prepared a α,γ-cyclic tetrapeptide and a hexapeptide containing a Fluorinated Furanoid Sugar Amino Acid (FFSAA) with the fluoride targeting towards the inner volume (Figure 23B). The conformational analysis of the tetramer and hexamer revealed a *C2* and *C3* symmetric flat oval- and triangular- β-sheet-like structures, respectively, which appear to self-assemble into nanotubes.

The group of Ting Xu have also contributed to this research line, they have replaced an α-Aa by an aromatic γ-derivative in a sequence of *D,L*-α-CP (Figure 23C).[137] Thereby, they achieved the preparation of nanotubes with hydrophobic cavities, since the methyl group in β-position is directed towards the inner cavity. However, the incorporation of this artificial amino acid causes the decrease of the nanotube diameter. Computational studies indicated that the incorporation of a second residue would not be feasible as it would induce the distortion of the planar conformation necessary for nanotube formation.

USC UNIVERSIDADE DE SANTIAGO DE COMPOSTELA

[135] A. Guerra, R. J. Brea, M. Amorín, L. Castedo, J. R. Granja, *Org. Biomol. Chem*., **2012**, *10*, 8762 – 8766.
[136] S. S. Burade, T. Saha, N. Bhuma, N. Kumbhar, A. Kotmale, P. R. Rajamohanan, R. G. Gonnade, P. Talukdar, D D. Dhavale, *Org. Lett*. **2017**, *19*, 5948 – 5951.
[137] R.Hourani, C.Zhang, R. van der Weegen, L. Ruiz, C. Li, S. Keten, B. A. Helms, T. Xu, *J. Am. Chem. Soc*. **2011**, *133*, 15296 – 15299.

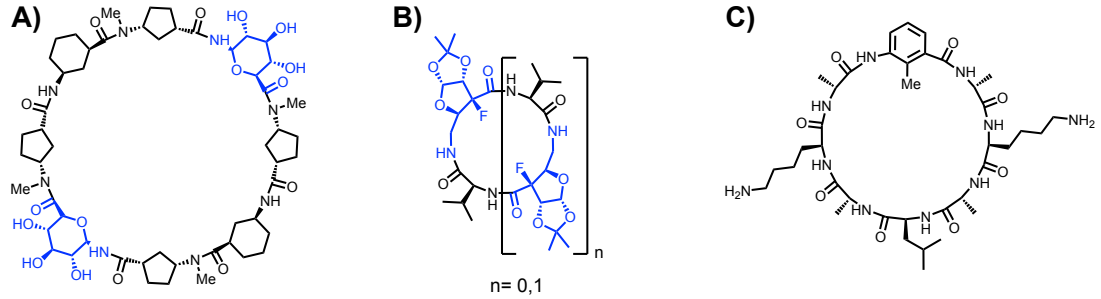


Figure 23. Chemical structure of cyclic peptides containing diverse γ-residues: A) γ-Aga, B) FFSAA and C) aromatic γ-derivative.

Cyclic peptide nanotubes: Other designs

Besides the examples described so far, researchers have been seeking for cyclic peptides upgrades with enhanced properties. On this background, in 2001, Dory's group described the first nanotubes prepared from δ-CPs.[138] They prepared a cyclic hexaglycine isostere from a trimer of *trans* α,β-unsaturated δ-residues. The resulting structures resemble those formed by β-peptides in which the tubes aggregate in a parallel fashion generating a strong macrodipolar moment along the tube (Figure 24A).

Another breakthrough design was proposed by Ghadiri's group, they have studied the incorporation of 1,2,3-triazole-ε-amino into the peptide backbone with the aim of modifying the internal properties of the nanotube. The crystal structure showed that a tetramer based on a pseudopeptidic α,ε-macrocycle had the ability to self-assemble into nanotubes by the stacking of the peptide rings in a parallel arrangement. In this structure, the triazole heterocycles were disposed perpendicular to the ring coating the interior of the nanotube with heteroaromatic residues rich in π-electrons (Figure 24B).[139] Chattopadhyay and colleagues have also included triazole units into a macrocyclic peptide sequence.[140] They reported the preparation of a sugar-based peptide mimetic that consist of a hybrid 1,4-triazole/amide linked macrocycle. These macromolecules exhibited supramolecular behavior similar to those *D,L*-cyclic peptides leading to tubular structures in which the triazole units act as amide isosteres. The most remarkable feature of these scaffolds is that the nanotube formation occurs through simultaneous cross-strand antiparallel/parallel stacking between the triazole moieties and the NH and CO amide groups, respectively.

USC UNIVERSIDADE DE SANTIAGO DE COMPOSTELA

[138] D. Gauthier, P. Baillargeon, M. Drouin, Y. L. Dory, *Angew. Chem. Int. Ed*. **2001**, *40*, 4635 –4638.
[139] W. S. Horne, C. D. Stout, M. R. Ghadiri, *J. Am. Chem. Soc*. **2003**, *125*, 9372 – 9376.
[140] A. Ghorai, A. Gayen, G. Kulsi, E. Padmanaban, A. Laskar, B. Achari, C. Mukhopadhyay, P. Chattopadhyay. *Org. Lett*. **2011**, *13*, 5512 – 5515.

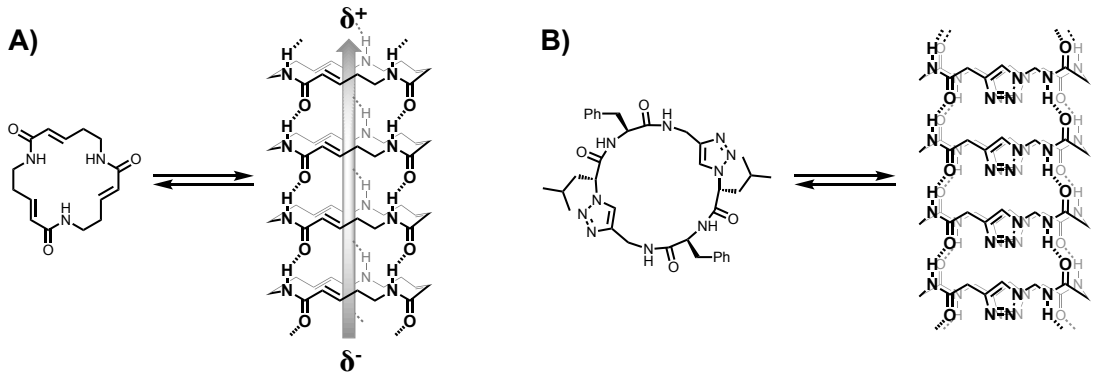


Figure 24. Representation of chemical structures and self-assembling of cyclic peptides comprise of A) δ-Aas and B) α,ε-Aas.

APPLICATIONS OF SELF-ASSEMBLED CYCLIC PEPTIDES

In this introduction, we have discussed the attractive properties of tubular nanoscale structures. Concretely, we have focused on self-assembling cyclic peptides. These molecular scaffolds allow a great control over their composition, size, and shape so that, in addition to those biological applications inspired by their natural equivalents, it becomes feasible to adapt them for use in different fields such as optics, electronics, catalysis, separation technologies, molecular transport and sensing among others.[141]

Selective Membrane Transporters

Cyclic peptides made of α-amino acids have a hydrophilic internal cavity and the external cavity is susceptible to modification by selecting the appropriate sequence. Ghadiri and colleagues have demonstrated that *c*-[*D*-Leu-*L*-Gln-(*D*-Leu-*L*-Trp)$_3$- -] peptide –rich in hydrophobic residues– can insert into phospholipid membranes forming channels. This peptide displayed remarkable Na^+ and K^+ ion transport activity. In contrast, other cyclic peptides with hydrophilic sequences showed no transport behavior.[142] Moreover, these systems are size selective because only those molecules with a smaller size than the nanotube diameter may cross through the peptide channel. Cyclic decamers of larger diameter exhibited efficient transport of small molecules such as glucose[143] or glutamic acid,[144] whereas the octamer mentioned above did not allow the passage of these molecules. Cyclic β^3-peptides have also been tested as membrane ion transporters showing similar activity values to the *D,L*-α-CP counterparts.[117]

USC UNIVERSIDADE DE SANTIAGO DE COMPOSTELA

[141] For more information about CP nanotubes applications see: R. J. Brea, C. Reiriz, J. R. Granja, *Chem. Soc. Rev*. **2010**, *39*, 1448 – 1456.
[142] M. R. Ghadiri, J. R. Granja, L. K. Buehler, *Nature*, **1994**, *369*, 301 – 304.
[143] J. R. Granja, M. R. Ghadiri, J. *Am. Chem. Soc*. **1994**, *116*, 10785 – 10786.
[144] J. Sánchez-Quesada, H. S. Kim, M. R. Ghadiri, *Angew. Chem. Int. Ed*. **2001**, *40*, 2503 – 2506.

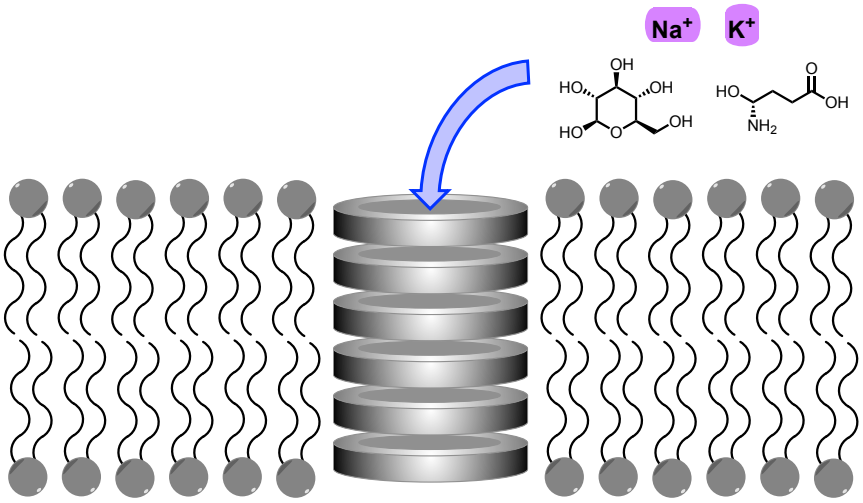


Figure 25. Schematic representation of a cyclic peptide nanotube embedded within a lipid bilayer. It was shown that the pore can be tuned to transport different species across the membrane such as alkali ions (Ref.), glucose (Ref.115) or glutamic acid (Ref.).

Some years later, our group showed that self-assembling α,γ-CPs also form functional membrane transporters. Channels formed by *c*-[*L*-Gln-*D*-γ-Ach-(*L*-Trp-*D*-γ-Ach)$_3$-] showed special selectivity for alkali metals.[145] This class of peptides can be decorated to improve their transport properties. In this sense, the introduction of the γ-Ahf residue would allow the functionalization of the internal cavity. So far, these functionalized systems are not yet achieved. Although, the previously introduced *c*-[(*D*-Leu-γ-Ahf-*D*-Tyr(Me)-^{Me}*N*-*L*-Acp-)$_2$-] peptide acquired a V-shape giving rise to a hexameric cluster have shown very promising tansport properties.[134] This system recognizes biologically relevant anions such as carbonate, chloride or nitrate facilitating their transport across membranes. This transport ability was not the result of the formation of membrane channels, but of the tetrahedral cluster. A new strategy for the development of ionophores molecules has also been developed based on a hydrophobic α,γ-CPs decorated with three pyridine motifs.[146] This cyclic peptide self-assembled into dimeric structures in which the *tris*-pyridine cap acted as ion recognition unit. These molecules were shown to drive ions across lipid bilayers with high potency and efficacy. This is a remarkable example of a dimeric structure that has the capacity to carry simultaneously both type of ions.

USC UNIVERSIDADE DE SANTIAGO DE COMPOSTELA

[145] R. García-Fandiño, M. Amorín, L. Castedo, J. R. Granja, *Chem. Sci*. **2012**, *3*, 3280 – 3285.
[146] A. Fuertes, M. Amorín, J. R. Granja, *Chem. Commun*. **2019**, *56*, 46 – 49.

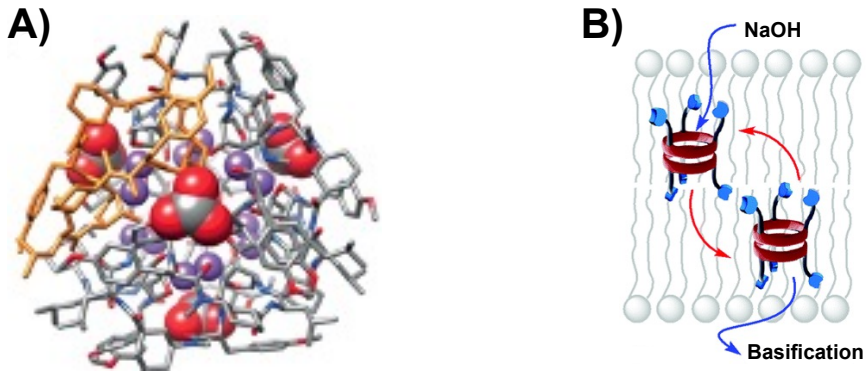


Figure 26. Novel formulations of transmembrane ion transporters based on cyclic peptides: A) supramolecular hexameric cluster in the presence of carbonate anions. B) Symport ionophore molecules based on dimeric structure with three pendant pyridine motifs.

Biomedical applications

The increase in drug-resistant bacteria triggered the demand for the development of new antibiotics with new modes of action.[147,148] Cyclic peptides are proteolytically stable and they can rapidly embed into lipid bilayers if decorated with non-polar substituents. These properties make them perfect candidates for the development of new antimicrobial agents similar to those natural antimicrobial peptides. The use of membrane active cyclic peptides limits the development of bacterial resistance because no specific metabolite route is targeted. The strategy relies on targeting the membrane of bacteria that present different properties than the mammalian membrane. Compared to mammalian cells, bacterial membranes present a net negative charge, so it is possible to design peptides to selectively interacts with them. Amphipathic *D,L*-α-CPs –with two differenced regions: hydrophilic and hydrophobic– displayed great antibacterial activity against a broad spectrum of bacteria including methicillin-resistant *Staphylococcus aureus* (MRSA).[149,150] The discovery of a new family of peptides (the mannopeptimycin) with high antibacterial activity prompted the application of α-*D,L*-CPs to this end.[151] The main structural identification is a saccharide motif attached to the peptide core. This finding motivated Ghadiri's group to study the antibacterial activity of cyclic glycopeptides.[152] Monosaccharide incorporation into peptide nanotube sequences increased its solubility and reduced the cytotoxicity without affecting antibacterial activity. In addition, the type and position of the sugar was observed to modulate membrane selectivity. The proposed mechanism of action of these amphiphilic nanotubes involves the interaction and accumulation of a bunch of CPs in the bacterial membrane disposing the hydrophobic region embedded in

[147] J. M. Blair, M. A. Webber, A. J. Baylay, D. O. Ogbolu, L. J. Piddock, *Nat. Rev. Microbiol*. **2015**, *13*,42 – 51.
[148] L. L. Ling, T. Schneider, A. J. Peoples, A. L. Spoering, I. Engels, B. P. Conlon, A. Mueller, T. F. Schäberle, D. E. Hughes, S. Epstein, M. Jones, L. Lazarides, V. A. Steadman, D. R. Cohen, C. R. Felix, K. A. Fetterman, W. P. Millett, A. G. Nitti, A. M. Zullo, C. Chen, K. Lewis, *Nature* **2015**, *517*,455 – 459.
[149] S. Fernández-Lopez, H.-S. Kim, E. C. Choi, M. Delgado, J. R. Granja, A. Khasanov, K. Kraehenbuehl, G. Long, D. A. Weinberger, K. M. Wilcoxen, M. R. Ghadiri, *Nature*, **2001**, *412*, 452 – 455.
[150] J. T. Fletcher, J. A. Finlay, M. E. Callow, J. A. Callow, M. R. Ghadiri, *Chem. Eur. J*. **2007**, *13*, 4008 – 4013.
[151] H. He, R. T. Williamson, B. Shen, E. I. Graziani, H. Y. Yang, S. M. Sakya, P.J. Petersen, G. T. Carter, *J. Am. Chem. Soc*. **2002**, *124*, 9729 – 9736.
[152] L. Motiei, S. Rahimipour, D. A. Thayer, C.-H. Wong, M. R. Ghadiri, *Chem Commun*. **2009**, 3693 – 3695.

the lipid bilayer.[153] Self-assembly would lead to the formation of longer nanotubes resulting in an increase of bacteria permeability. Consequently, it would lose its ionic balance causing cell death. To improve the properties of these agents, in our group we developed a new methodology for the preparation of a cyclic peptide platforms using orthogonal click reactions that allows simple and efficient incorporation of different hydrophilic or hydrophobic groups.[154] The special aspect of this work is the reduced number of hydrophobic residues in the peptide sequence that provided materials with improved solubility in aqueous medium as it restricts the formation of larger aggregates.

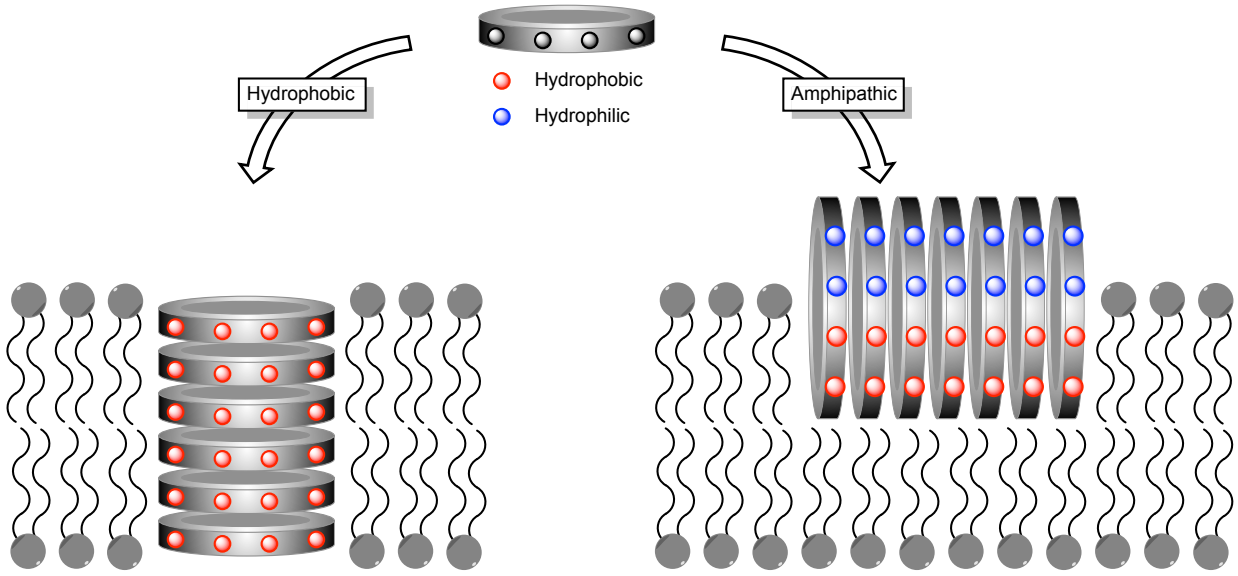


Figure 27. Schematic representation of cyclic peptide insertion in lipid bilayer depending on the nature of the amino acids' side chains. Nanotubes made only of hydrophobic residues lead to transmembrane channel, while amphipathic nanotubes inserts laterally with the hydrophobic residues facing the membrane.

In view of the ability of cyclic peptides to interact with lipid bilayers, these materials could be used in the field of medicinal chemistry as drug transporters. In 2014, the first approach based on a peptide-polymer conjugate was reported.[155] In this publication, the authors linked a polymer loaded with RAPTA-C, a ruthenium-based anticancer drug, to a hydrophobic cyclic peptide. This hybrid aggregate exhibited 10-fold higher anticancer activity than the isolated drug. In the same year, following a similar pathway, a cyclic peptide was externally modified with a polyethylene glycol (PEG) chain and the anticancer drug doxorubicin (DOX).[156] These nanometric dispersions, compared to free DOX, showed *in vitro* higher cytotoxic activity, higher uptake and altered intracellular distribution. In our group, taking advantage of the internal functionalization provided by the introduction of a γ-Ahf residue we have developed a

USC UNIVERSIDADE DE SANTIAGO

[153] B. Claro, E. González-Freire, M. Calvelo, L. J. Bessa, E. Goormaghtigh, M. Amorín, J. R. Granja, R. García-Fandiño, M. Bastos, *Colloids Surf. B*. **2020**, *196*, 111349.
[154] E. González-Freire, F. Novelli, A. Pérez-Estévez, R. Seoane, M. Amorín, J. R. Granja, *Chem. Eur. J.* **2021**, *27*, 3029 – 3038.
[155] B. M. Blunden, R. Chapman, M. Danial, H. Lu, K. A. Jolliffe, S. Perrier, M. H. Stenzel, *Chem. Eur. J.* **2014**, *20*, 12745 – 12749.
[156] Y. Wang, S. Yi, L. Sun, Y. Huang, S. C. Lenaghan, M. Zhang, *J. Biomed. Nanotechnol*. **2014**, *10*, 445 – 454.

macro peptide-*cis*-platinum complex.[157] The γ-Ahf hydroxyl group that points to the internal cavity was transformed into a carboxylic acid function that enabled the coordination of *cis*-platinum derivatives. The CP-Pt(II) complex showed lower activity than the free *cis*-platinum derivative, but it was observed that it retained activity in resistant cell lines as well as being less toxic in healthy cell lines.

Biosensors

The control over the dimensions and composition of these assemblies has enabled the construction of diffusion-based dynamic ion sensors. Hydrophobic cyclic octamers deposited on self-assembled monolayers (SAMs) of organosulfurs on gold films have resulted in a size-selective diffusion system to probe redox species.[158] Redox activity was monitored by cyclic voltammetry. Only the ionic species smaller size than pore diameter were able to cross the lumen and showed redox activity (Figure 28A).

In our group, multicomponent networks have been designed that exhibit a controlled fluorescence signal by taking advantage of the greater stability of α,γ-CPs based heterodimers. The heterodimer is composed of an Acp-containing CP bearing a dapoxyl molecule linked via hydrogen bonding to another pyrene-derivatized Ach-based CP. This system makes use of excimer or fluorescence resonance energy transfer (FRET) effects to study the self-assembly process by following the formation of different supramolecular aggregates that display specific output signals (Figure 28B).[159] Similar patterns were obtained with octapeptides derived with pyrene/perylene.[160]

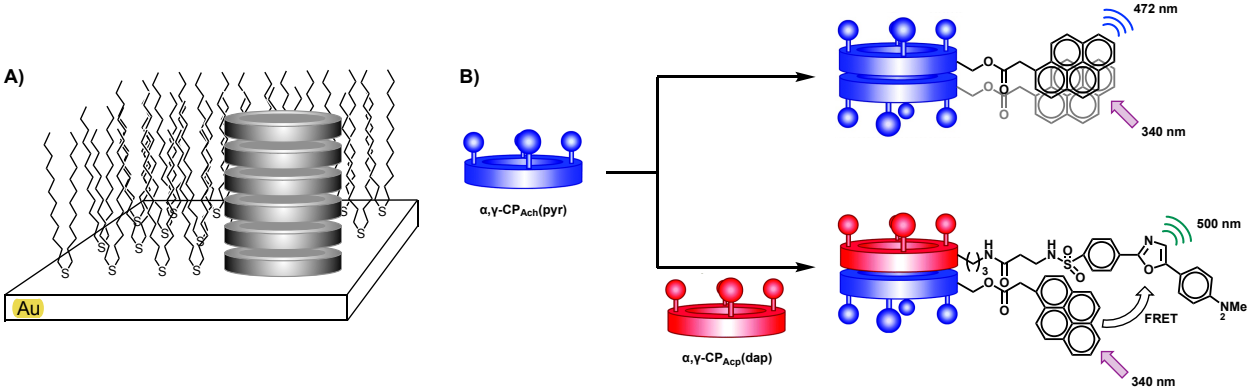


Figure 28. A) Dynamic ion sensor based on the deposition of hydrophobic cyclic peptides on organosulfur coated gold surface. B) Homo- and heterodimeric equilibria that can be used as biosensors due to their fluorescence properties.

Artificial photosystems

Taking advantage of the same heterodimerization strategy facilitated by the combination of α,γ-CPs, a bio-inspired light harvesting/light conversion system have been developed in our

USC UNIVERSIDADE DE SANTIAGO DE COMPOSTELA

[157] N. Rodríguez-Vázquez, R. García-Fandiño, M. J. Aldegunde, J. Brea, M. I. Loza, M. Amorín, J. R. Granja, *Org. Lett.* **2017**, *19*, 2560 – 2563.
[158] K. Motesharei, M. R. Ghadiri, *J. Am. Chem. Soc.* **1998**, *119*, 11306 – 11312.
[159] R. J. Brea, M. E. Vázquez, M. Mosquera, L. Castedo, J. R. Granja, *J. Am. Chem. Soc.* **2007**, *129*, 1653 – 1657.
[160] R. J. Brea, M. J. Pérez-Alvite, M. Panciera, M. Mosquera, L. Castedo, J. R. Granja, *Chem. Asian J.* **2011**, *6*, 110 – 121.

group.[161] To this end, one of the peptide subunits bears an electron-donating motif, π-extended tetrathiafulvalene (exTTF), while the other subunit of the heterodimer carried attached a photoactive electron-accepting molecule, a fullerene derivative. Upon photoexcitation of these heterodimeric platforms, electron transfer processes occurred through spatial interactions that confirmed their practical utility as efficient artificial photosystems. In addition, a new design has been presented in which a Zn porphyrin was used as electron donor unit. The highlight of this design is the attractive interaction between the molecules involved in the electron transfer process (the fullerene and the porphyrin), which stabilizes the heterodimeric structure increasing the efficiency of the assembly (Figure 29).[162]

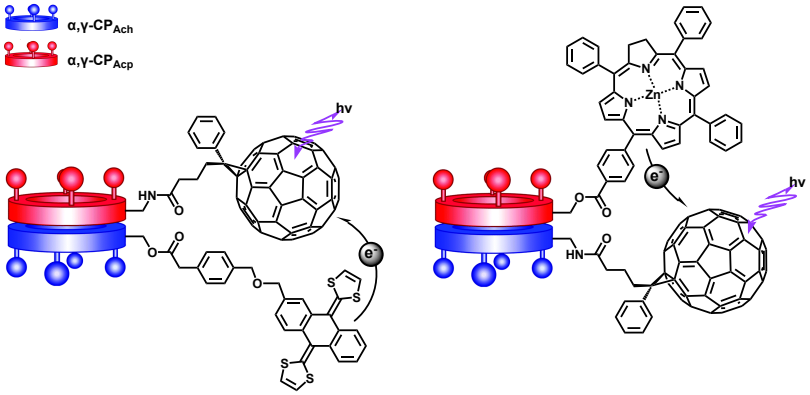


Figure 29. Electron transfer supramolecular devices using the heterodimer strategy. On the right, α,γ-CP heterodimer with a subunit decorated with a fullerene molecule and another with a electro-donating exTTF motif. On the left, a similar system in which the exTTF was replaced by a Zn porphyrin.

Electronic devices

As discussed above, one of the main applications of nanotubes is their use as electronic nanowires owing their privileged one-dimensional structure. In this sense, nanotubes based on cyclic peptides emerge as a suitable option due to the possibility to control their dimensions: length and diameter. Ghadiri's group prepared a series of N-methylated *D,L*-α-peptides containing 1,4,5,8-naphthalenetetracarboxylic acid diimide (NDI).[163] The anchoring of these aromatic groups allowed the study of the self-assembly process by fluorescence spectroscopy observing that the peptide self-assembly acted as a template to direct the stacking and charge transfer between the NDI motifs. Following the same design concept, they prepared a cyclic peptide that had four anchored NDI molecules. Redox-activated self-assembly in aqueous solution resulted in nanotubes of hundreds of nanometers that exhibit extended charge delocalized states (Figure 30).[164] This strategy has provided a solid basis for the fabrication of supramolecular materials with potential optical and electronic properties. Following a similar

USC UNIVERSIDADE DE SANTIAGO DE COMPOSTELA

[161] R. J. Brea, L. Castedo, J. R. Granja, M. A. Herranz, L. Sánchez, N. Martín, W. Seitz, D. M. Guldi, *Proc. Natl. Acad. Sci. U.S.A*. **2007**, *104*, 5291 – 5294.
[162] G. Aragay, B. Ventura, A. Guerra, I. Pintre, C. Chiorboli, R. García-Fandiño, L. Flamigni, J. R. Granja, P. Ballester, *Chem. Eur. J*. **2014**, *20*, 3427 – 3438.
[163] W. S. Horne, N. Ashkenasy, M. R. Ghadiri, *Chem. Eur. J*. **2005**, *11*, 1137 – 1144.
[164] N. Ashkenasy, W. S. Horne, M. R. Ghadiri, *Small*, **2006**, *2*, 99 – 102.

pattern, our group published a new design with potential electronic properties.[165] In this case, an α,γ-CP was used that had covalently attached a fullerene molecule. The deposited nanotube on a solid support displayed the fullerene molecules in an alternating fashion to both sides of the CP aggregate (180º orientation) leading to the formation of two parallel buckyball-based nanowires separated by insulating material (Figure 30).

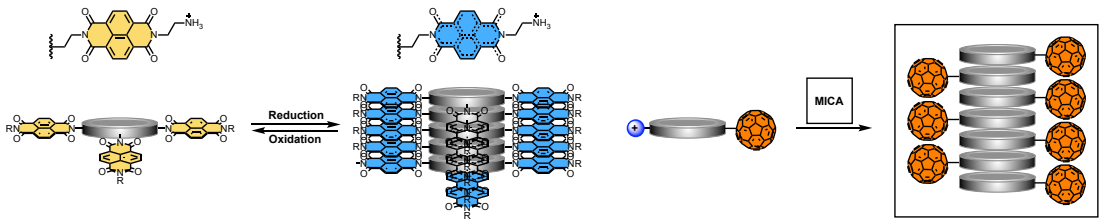


Figure 30. Electronic devices fabricated with cyclic peptide nanotubes: On the right, redox-promoted self-assembly leading to a nanotube with extended charge delocalized states. On the left, formation of buckyball parallel nanowires after mica deposition.

Alternatively, Kimura's group published the synthesis of a cyclic β-tripeptide functionalized with three terpyridines (tpy).[166] These ligands promoted Cu(II) metal ions coordination at the periphery of the peptide backbone producing a macrodipolar structure featuring a π-electronic system. These platforms might be useful in the field of organic electronics. Later, the same group reported a similar approach for the fabrication an electronic device comprised of a cyclic β-peptide bearing a TTF molecule at its side chain.[167] The electronic properties of the TTF-derivative tripeptide were studied by current-sensing Atomic Force Microscopy (AFM) revealing a current-voltage profile typical of a p-semiconductor.

Nanomaterials

The development of new nanomaterials has been a major area of implementation for cyclic peptides. As seen so far, most of cyclic peptide applications involve the modification of their external surface accessible through the amino acid side chains. In this sense, the coating of SCPNs with polymeric chains emerges as a promising strategy for the fabrication of nanomaterials that can be welcomed in multiple technological fields. This apporach offered the possibility to prepare a wide variety of structures with programmable properties due to the large availability of polymers. Among the different examples, it should be highlighted the Janus[168] polymer-peptide nanotube that has two contrary functionalities.[169] This peptide-polymer hybrids were shown to form pore in phospholipid bilayers. Xu and colleagues have exploited the external chemical modeling using polymers to fabricate porous nanomaterials with vertically aligned channels. In this demonstration, they combined cyclic peptides with low-molecular-weight polymers, and they subsequently deposited these conjugates in a block

USC UNIVERSIDADE DE SANTIAGO DE COMPOSTELA

[165] C. Reiriz, R. J. Brea, R. Arranz, J. L. Carrascosa, A. Garibotti, B. Manning, J. M. Valpuesta, R. Eritja, L. Castedo, J. R. Granja, *J. Am. Chem. Soc*. **2009**, *131*, 11335 – 11337.
[166] F. Fujimura, S. Kimura, *Org. Lett*. **2007**, *9*, 793 – 796.
[167] H. Uji, H. Kim, T. Imai, S. Mitani, J. Sugiyama, S. Kimura, *Biopolymers*, **2016**, *106*, 275 – 282.
[168] They called Janus to this peptide-polymer hybrid in reference to the Roman God that is represented with two faces.
[169] M. Danial, C. My-Nhi Tran, P. G. Young, S. Perrier, K.A. Jolliffe, *Nat. Commun*. **2013**, *4*, 2780 – 2793.

copolymer.[170] The tethered polymers promoted solubilization of the polymer-peptide hybrids in the block copolymer microdomains and guided self-assembly in confined spaces. A different strategy was used to obtain porous materials functionalized with carboxylate groups.[171] In this example, cyclic peptides were used as a template to produce carboxylated polymeric pores. These peptides were decorated with norborene units linked by an ester bond which upon self-assembly and polymerization was hydrolyzed giving rise to these robust polymeric pores.

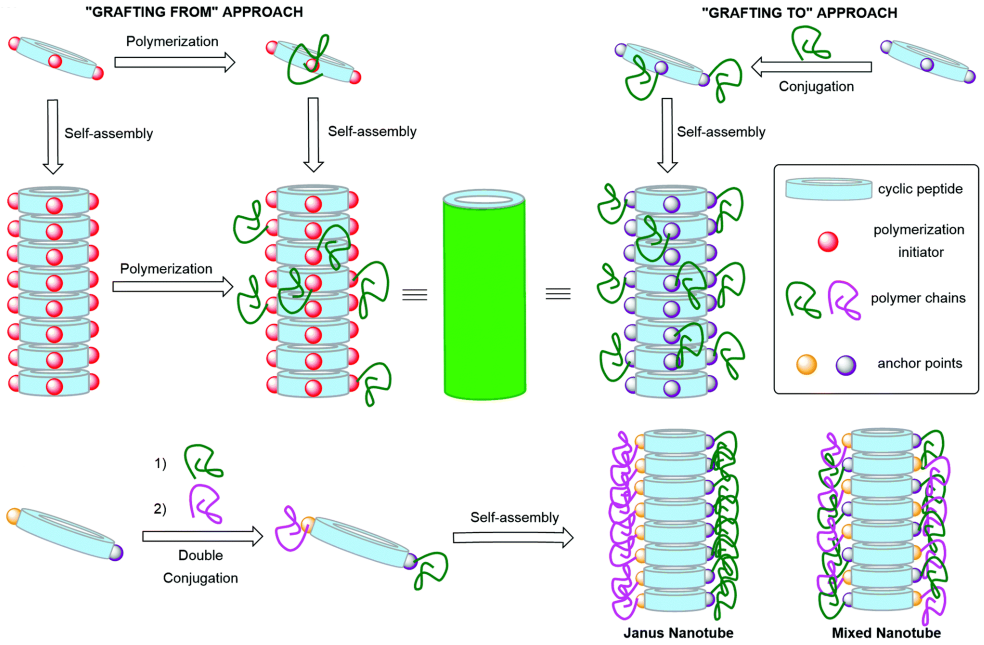


Figure 31. Schematic representation of diverse strategies used for obtaining CP-polymer hybrid materials.

In recent years, in our group we have successfully harnessed the outward modification of SCPNs with small aromatic molecules such as pyrene, which has allowed us to prepare a wide range of nanomaterials.[172–174] For example, this strategy allowed the preparation of dual composites that combine two of the main types of nanotubes: SWCNTs and SCPNs.[172] In this strategy, the pyrene motif engages the carbon nanotubes through π-type interactions stabilizing their dispersion in water. The resulting hybrid structures possess the properties of both components. The same strategy was used to align silver nanoclusters along the nanotube axis (Figure 32).[173] These materials would also have applications as electronic devices due to the excellent conductivity properties of carbon nanotubes and the aligned metal clusters. On the other hand, rationally design octapeptides were shown to yield stimuli-responsive hierarchal tubular assemblies in confined spaces.[174] The tethered pyrene motif contributes to the

USC UNIVERSIDADE DE SANTIAGO DE COMPOSTELA

[170] T. Xu, N.Zhao, F. Ren, R. Hourani, M. T. Lee, J. Y. Shu, S. Mao, B. A. Helms, *ACS Nano*, **2011**, *5*, 1376 – 1384.
[171] M. Potnuru, N. Madhavan, *Polym. Chem*. **2016**, *7*, 31 – 35.
[172] J. Montenegro, C. Vázquez-Vázquez, A. Kalinin, K. E. Geckeler, J. R. Granja, *J. Am. Chem. Soc*. **2014**, *136*, 2484 – 2491
[173] M. Cuerva, R. García-Fandiño, C. Vázquez-Vázquez, M. A. López-Quintela, J. Montenegro, J. R. Granja, *ACS Nano* **2015**, *9*, 10834 – 10843.
[174] A. Méndez-Ardoy, J. R. Granja J. Montenegro, *Nanoscale Horiz*. **2018**, *3*, 391 – 396.

stabilization of the hydrogen-bonded nanotubes via π-π interactions. These supramolecular systems exhibited dynamic behavior that may have important implications in the field of synthetic biology.

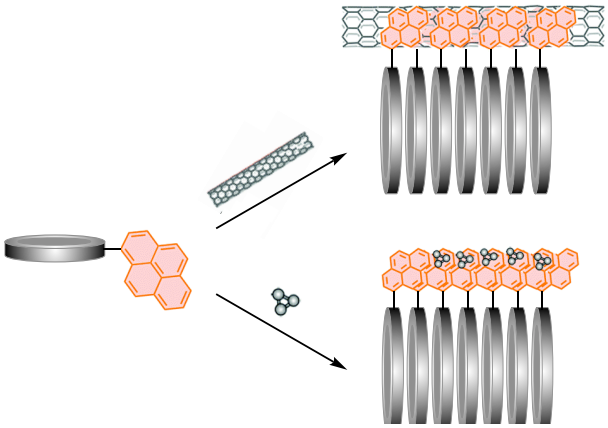


Figure 32. Peptide nanotubes supramolecular hybrids: CP/SWCNT and CP/metal clusters.

Our group has also developed novel biomaterials using α,γ-CPs. For instance, a dimer-forming peptide was decorated with three mesogenic dendron moieties to modulate the self-organization of the architecture into liquid crystal phase.[175] In this system, the amide groups self-assemble in a β-sheet fashion, while the inclusion of three dendron units drives the formation of a columnar mesophase (Figure 33). Furthermore, two α,γ-components of different diameter and orthogonal assembly properties were covalently linked by click chemistry.[176] In this work, a cyclic tetramer was N-decorated with an azide function and a cyclic octamer was N-functionalized with an alkyne group, subsequent copper catalyzed azide-alkyne cycloaddition (CuAAC) reaction provided a covalent dimer. The combination of the covalent dimer with other complementary cyclic peptides provided Venturi-like nanotubes with controlled dimensions (Figure 33).

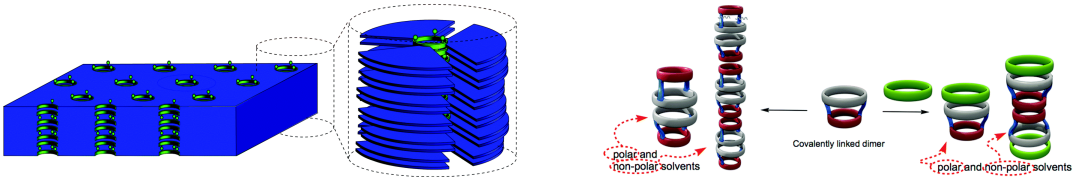


Figure 33. Model for the formation of porous liquid crystals using dimer-forming cyclic peptides decorated with mesogenic dendrons and Venturi-like nanotubes which allows nanotube length control.

USC
UNIVERSIDADE
DE SANTIAGO
DE COMPOSTELA

[175] M. Amorín, A. Pérez, J. Barberá, H. L. Ozores, J. L. Serrano, J. R. Granja, T. Sierra, *Chem. Commun*. **2014**, *50*, 688 – 690.

[176] A. Fuertes, H. L. Ozores, M Amorín, J. R. Granja, *Nanoscale*, **2017**, *9*, 748 – 753.

USC
UNIVERSIDADE
DE SANTIAGO
DE COMPOSTELA

OBJECTIVES

USC
UNIVERSIDADE
DE SANTIAGO
DE COMPOSTELA

USC
UNIVERSIDADE
DE SANTIAGO
DE COMPOSTELA

OBJECTIVES

The general objective of this doctoral thesis is the preparation and study of a new class of self-assembling cyclic peptides for the construction of nanotubular systems with a hydrophobic internal cavity. For this purpose, we propose the use of a new cyclic amino acid with very special properties, rigidity and linear shape. In the Introduction, it has been shown that materials derived from cyclic peptides are very versatile due to its structural variety and mouldability which allows the construction of a wide range of structures with applications in many different fields. In addition to the natural α-amino acids, the incorporation of non-natural residues enhances the potential of these biomaterials. In this regard, the use of γ- or δ-residues provided fascinating results with respect to the control of the self-assembly properties of the resulting cyclic peptides.

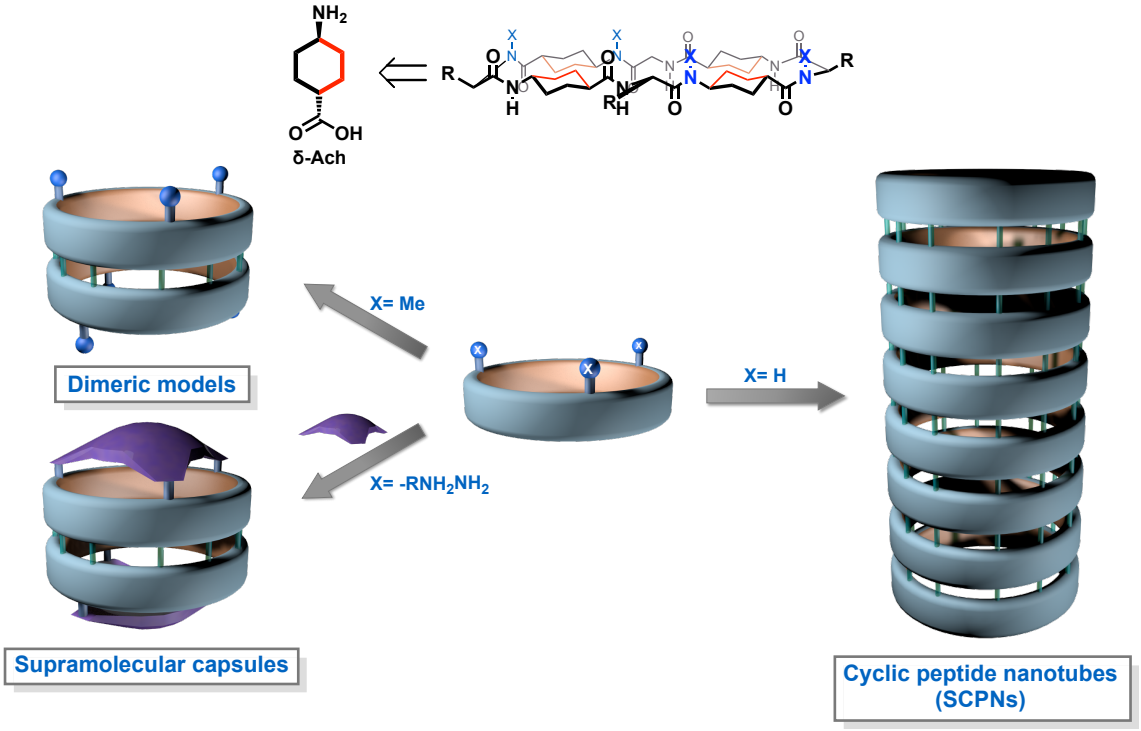


Figure 34. Chemical structure of δ-Ach and proposed cyclic peptide design (up). Below, schematic representation of the different supramolecular structures that can be prepared based of this type of materials.

Based on this, the first objective of this work is the evaluation of the relative stability of the parallel and antiparallel β-sheet registers of cyclic peptides that contain 4-aminocyclohexanecarboxylic acid (δ-Ach, Figure 34). The introduction of this novel residue in a cyclic peptide sequence would increase the hydrophobic character of the inner cavity of the self-assembled nanotubes due to the disposition of two methylene groups projected towards the lumen of the resulting supramolecular structure. However, the structural rigidity of this residue –the amino and carbonyl groups are oriented in opposite directions (180° angle) occupying equatorial positions in the chair conformation of the cyclohexane– prevents the synthesis of cyclic peptides made exclusively of δ-Ach. For this reason, it will be combined with α-amino acids, so it would act as a rigid elongator allowing the preparation of nanotubular

constructions with larger dimensions. This residue has a different conformational behavior regarding the relative orientation of the NH and carbonyl groups of the amide bonds compared to α-amino acids. For this reason, we will address the differences in stability between parallel and antiparallel stacking.

To elucidate these differences, we will work with α,δ-CP dimeric constructs. Hence, N-methylated cyclic peptides comprising δ-Ach in combination with α-amino acids will be prepared (α,δ-CPs, Figure 34, left up). These supramolecular dimers will be used as models for the study of the supramolecular interactions of the system. Moreover, as detailed in the Introduction, cyclic peptides composed only by β- or δ-amino acids can only stack through the parallel β-sheet. However, in the newly systems that combine α-amino acids with δ-residues both the parallel and the antiparallel packing are possible. Consequently, a precisely design of CPs of this constitution would allow to assess the relative stability of both types of interactions. To this end, we will employ different techniques that allow the identification of the self-assembled species, such as Nuclear Magnetic Resonance, Mass Spectrometry or Fourier-Transform Infrared Spectroscopy. Furthermore, the same methodology can be employed for subsequent comparison with α,γ-CP models, although several studies indicated that differences in the NH and carbonyl groups on both faces of these cyclic peptides would favor the antiparallel structure.

After these structural studies we will address the next objective of this doctoral thesis: the construction of nanotubes based on α,δ-CPs (α,δ-SCPNs, Figure 34 right) and their encapsulation properties. Here, we will consider the introduction of polar α-amino in the cyclic peptide sequence to afford water-soluble assemblies and their implication in nanotube formation. In this way, a biocompatible tubular system with a hydrophobic pore would be obtained due to the presence of the novel δ-residues. This hypothesis will be tested by encapsulating non-polar substances in the presence of the α,δ-SCPNs. Accordingly, these compounds will be hosted in the internal volume of the nanotube to avoid the contact with the solvent.

The selective N-methylation of one face of a cyclic peptide to restrict the association of different subunit to the formation of self-assembled dimeric species might be used in the construction of new and large supramolecular capsules. To this end, the incorporation of functional groups suitable for click chemistry reactions (azide-alkyne cycloaddition, hydrazone formation reactions) instead of the N-methyl motifs should allow the attachment of a C_3 panel that could act as molecular cap to lead to a cyclic peptide-based capsules (Figure 34 left down). In this way, the possible host-guest properties of the peptide could be enhanced with an additional directing effect provided by the molecular cover of the capsule. Therefore, as a last objective we set out to prepare supramolecular capsules based on α,δCPs.

USC UNIVERSIDADE DE SANTIAGO DE COMPOSTELA

CHAPTER 1

USC
UNIVERSIDADE
DE SANTIAGO
DE COMPOSTELA

USC
UNIVERSIDADE
DE SANTIAGO
DE COMPOSTELA

CHAPTER 1

The original cyclic peptide-based nanotubes proposed by Ghadiri[92] consisted of stacking peptide macrocycles composed of an even number of α-amino acids of alternating chirality. This amino acid sequence reverses the dihedral angle of the peptide backbone resulting in a pleated structure that favors β-type hydrogen bonding interactions between macrocyclic subunits. As detailed in the Introduction, the groups involved in the hydrogen-bonding network –the carbonyl (hydrogen-bond acceptor) and NH (hydrogen-bond donor) of the amide function– lie perpendicular to the disk-shaped structure. Due to the fluctuating quirality, these groups will point alternately towards opposite faces of the ring having all the amide groups of the same quirality facing the same direction defining the *D*- and *L*-faces (Figure 35). The interaction between cyclic peptides can lead to two different types of β-sheet arrangements: parallel and antiparallel. In the antiparallel disposition, H-bonding occurs between amino acids of the same quirality, in other words, the cyclic peptide *L*-face interacts with the *L*-face of another subunit and the *D*-face with *D*-face. In contrast, in the parallel array, these interactions are drawn between faces of opposite quirality. It is worth to mention that in the parallel disposition an amino acid interacts with two residues of another subunit, while in the antiparallel β-sheet each amino acid is joined with those residues of the same chirality. In any case, as illustrated in Figure 35, all residues of the same chirality are aligned along the vertical axis of the nanotube.

Several studies have been conducted suggesting the thermodynamic preference for the antiparallel β-sheet structure. The first evidence was observed when cyclic peptide nanotubes were first reported by the group of Ghadiri, the electron diffraction patterns and FTIR measurements pointed to the antiparallel packing of nanotubes.[92] Later, the same group evaluated the relative stability of parallel vs antiparallel β-sheet structure using dimeric models.[99] NMR experiments showed that the antiparallel disposition is more stable than the parallel arrangement, but the relative ratio between them was not too big. Gailer and Feigel performed the first computational study using AM1 semiempirical method.[177] The calculated dimerization energies were almost identical for both conformations. However, in contrast to the experimental results, they found a slightly preference by 0.13 kJ/mol for the parallel β-sheet structure, but such energetic difference is not significant at any rate. More recently, Liu and coworkers, based on a variety of computational approaches, proposed a new self-assembly mechanism that explained the greater stability of the antiparallel organization.[178] They claimed that this energetic difference was mainly attributed to cross-strand side chain van der Waals interactions instead of those between the peptide backbone. Thus, depending on the sequence, the antiparallel stacking through the frame with divergent side-chain orientation was more favorable (Figure 35, inset). Further nanotube formation was based on the stacking of this dimers. Although most of these reports suggested that the antiparallel β-sheet is the most stable, Silk *et al.* reported the crystallization of SCPNs from two CPs with minor structural variations

[177] C. Gailer, M. Feigel, *J. Comput. Aided. Mol. Des*. **1997**, *11*, 273 – 277.
[178] W. Qu, H. Tan, G. Chen, R. Liu, *Int. J. Quantum Chem*. **2010**, *110*, 1648 – 1659.

that exhibit different packing organization.[96] They argued that parallel or antiparallel conformation in the solid state may be dictated by intra- and inter-nanotube interactions.

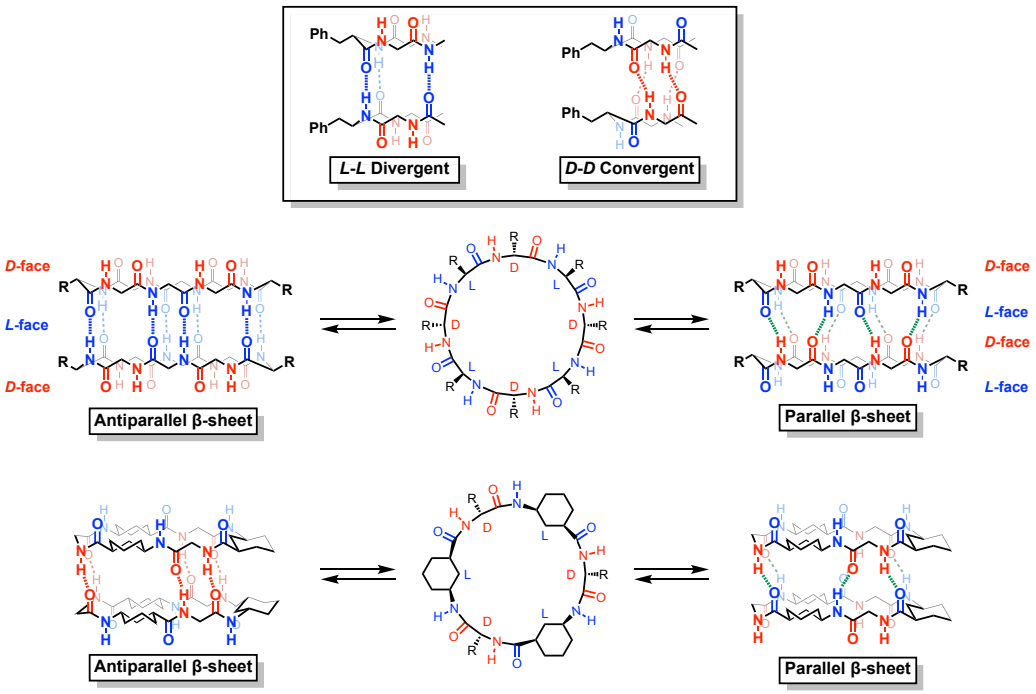


Figure 35. Representation of different stacking assemblies of α-CPs (up) and α,γ-CPs (down). The NH and CO groups are highlighted in red for *D*-amino acids and blue for *L*-amino acids. Moreover, H-bonds of the parallel arrangement are colored in green. In the inset, self-assembly mechanism proposed by Qu *et al.* (Ref. 178).

In the previous section, a new class of cyclic peptides containing γ-amino acids has been introduced. As detailed, different designs have been shown to assemble into hollow tubular structures: prepared with alternating α,γ-amino acids (α,γ-CPs, Figure 35),[119,124,126,127,129,132] three α-amino acids of fluctuating chirality combined with one γ-residue of the corresponding chirality (3α,γ)[130] or solely by γ-amino acids.[131,135] The incorporation of the γ-Ach provides nanotubes with amphipathic cavities due to the projection of one methylene group towards the lumen.[120] In addition, the inner properties can be modulated by using residues bearing different functions at C2 position, such as the γ-SAA derivatives γ-Ahf[132] that has an hydroxyl group at this position. Therefore, it was demonstrated that the use of artificial residues enables the modification of the internal properties.

These designs (*D,L*-α-CPs and α,γ-CPs) includes amino acids that have an odd number of atoms between the amino and carbonyl functionalities. This structural feature causes that –in the pleated structure– the amino and carbonyl groups of the same amino acid are directed towards the same face of the ring. The amide groups arrangement, as mentioned above, drives to different β-sheet structures: antiparallel and parallel. On the other hand, other peptides that can also lead to SCPNs, such as β-[115–118] and δ-peptides,[138] have an even number of atoms between those functional groups. Therefore, the resulting peptides exhibit a different orientation pattern. The NH and CO groups of the same residue are arranged towards opposite sides. For this reason, cyclic peptides' stacking is restricted to the parallel disposition. Consequently, a distinctive feature of the resulting nanotubes is the generation of a macrodipolar moment along the tube

axis. Moreover, the δ-nanotubes proposed by Dory's group consisting of a trimer of α,β-unsaturated lactams were organized as mesogenic phases when dissolved in a nematic liquid crystal (LC) due to the presence of polar (the amides) and apolar (the alkene) regions.[179] Exploiting this arrangement, our group have shown very recently that the incorporation of two consecutive β-Ala units restricts the nanotube formation to the parallel stacking.[180]

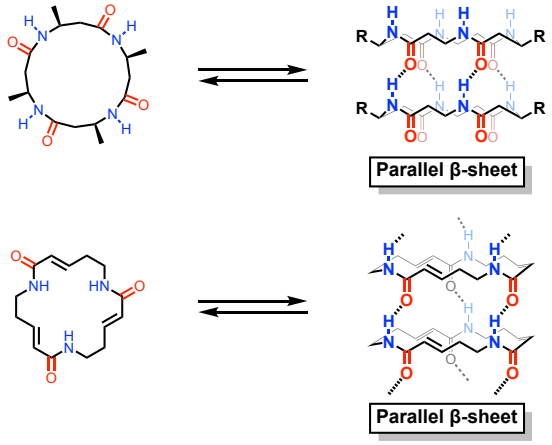


Figure 36. Representation of the parallel stacking of β-CPs (up) and δ-CPs (down). All the NH groups (highlighted in blue) point to the same face of the ring, while the carbonyl groups (in red) to the opposite side.

In view of these precedents, we sought to prepare nanotubes with hydrophobic cavities because these kinds of materials are highly desirable for drug transport or development of diagnostic agents.[181] Moreover, the stability of the resulting supramolecular species is also of great interest: for these assemblies, the most stable packing in the parallel or antiparallel fashion. This knowledge would allow the rational design of novel functional materials based on cyclic peptides. To this end, we envisioned that the constitutional isomer of γ-Ach, 4-aminocyclohexanecarboxylic acid (δ-Ach, Figure 37), would be a suitable candidate for the preparation of tubular structures with inner hydrophobic properties. This novel residue would project two methylene groups into the hollow cylinder increasing its lipophilic properties. With this in mind, we plan to design and synthesize dimeric models of cyclic peptides containing this artificial residue for in-depth study of their supramolecular properties. These studies will also be extended to α,γ-CPs since, unlike α-CPs,[99] this kind of structural studies have not yet been performed.

SELF-ASSEMBLING STUDIES OF α,δ-CYCLIC PEPTIDE

DESIGN OF DIMERIC MODELS

The key structural requirements for nanotube formation are the generation of a monomeric planar structure with the hydrogen-bonding groups arranged perpendicular to its plane. For that purpose, the *trans* isomer of δ-Ach is necessary. However, the 180° angle described between the NH and carbonyl groups –derived from the tendency to occupy equatorial positions–

[179] S. Leclair, P. Baillargeon, R. Skouta, D. Gauthier, Y. Zhao, Y. L. Dory, *Angew. Chem. Int. Ed.* **2004**, *43*, 349 – 353.
[180] F. Novelli, M. Vilela, A. Pazó, M. Amorín, J. R. Granja, *Angew. Chem. Int. Ed.* **2021**, *60*, 18838 – 18844.
[181] W. B. Liechty, D. R. Kryscio, B. V. Slaughter, N. A. Peppas, *Annu. Rev. Chem. Biomol. Eng.* **2010**, *1*, 149 – 173.

precludes the synthesis of cyclic peptides composed exclusively by δ-Ach (Figure 37). Consequently, we anticipate that in order to afford a cyclic monomer it must be combined with α- or γ-amino acids. Hence, this novel residue would act as a rigid elongator leading to SCPNs of larger diameter and internal hydrophobic behavior.

To implement the use of δ-Ach in the construction of nanotubes we carried out a preliminary design. First, to favor the formation of the pleated structure, the straightforward design is the intercalation of one δ-Ach after each α-amino acids in a *D,L*-α-peptide strand (Figure 37). This design will lead to a different H-bonding pattern from those seen so far. Due to the combination of residues with an odd (α-amino acids) and even (δ-Ach) number of atoms, the carbonyl group of the δ-residue will be oriented towards the same face as the carbonyl of the preceding α-amino acid, while the NHs will be pointing in the same direction as the corresponding group of the following amino acid as illustrated in Figure 37. The resulting structures may be assembled in either a parallel or antiparallel fashion. In the antiparallel β-sheet, α-amino acids of the same chirality would interact between them, while the carbonyl group of the consecutive δ-Ach would be connected to the amide proton of the δ-Ach preceding the α-amino acid with equal chirality of the other subunit. Whereas, in the parallel arrangement, the NH and carbonyl groups of the α-amino acid of a given chirality would interact with the carbonyl and amide protons, respectively, of the δ-residues flanking the α-amino acid of the corresponding chirality.

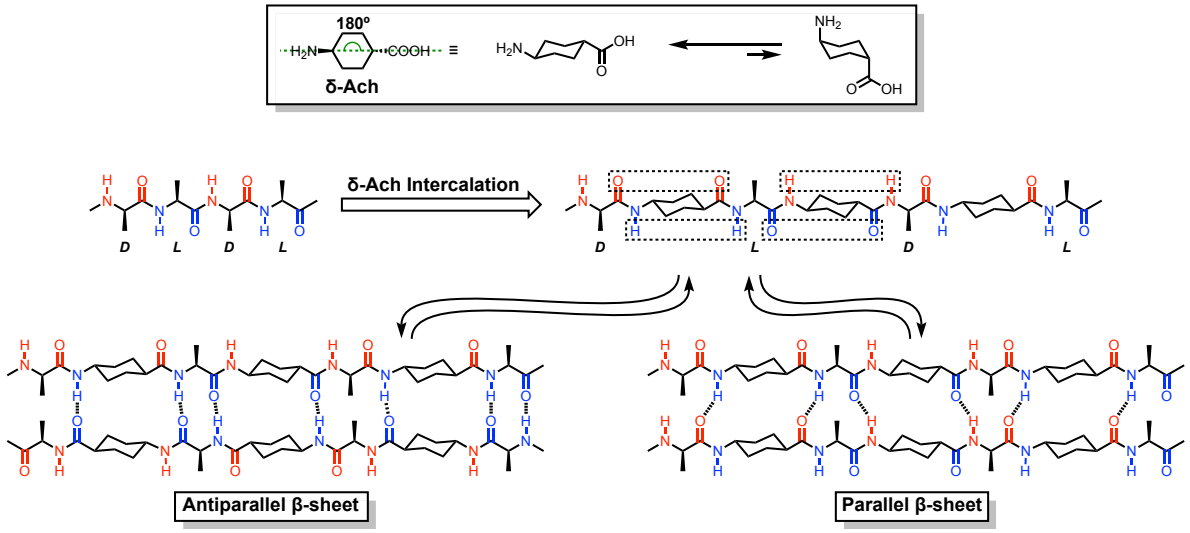
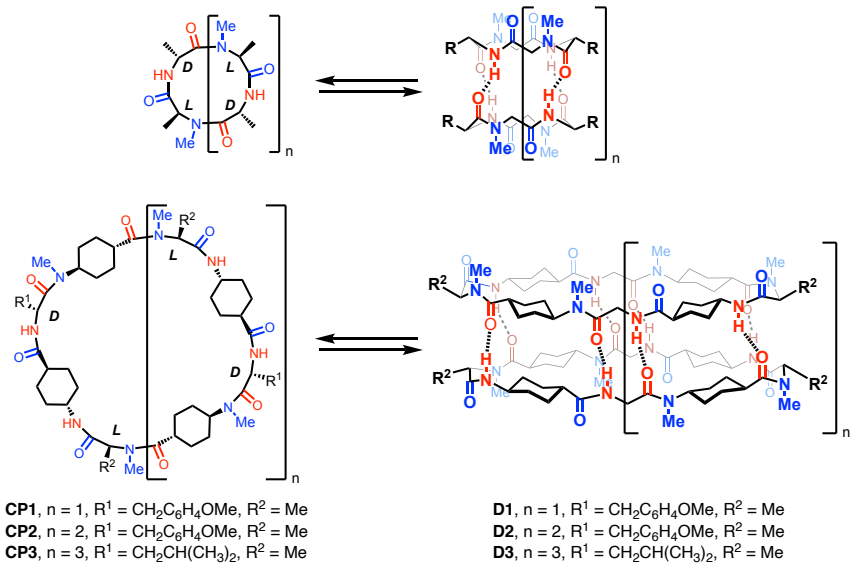


Figure 37. In the inset, structure of δ-Ach and representation of both cyclohexane chair conformations. Below, representation of the possible β-sheet interactions upon intercalation of δ-Ach in a *D,L*-peptide strand. Carbonyl and NH groups are highlighted in blue or red depending on their orientation in a disk-shaped conformation.

The amide bond profile is very important in the design of dimeric models because the N-alkylation pattern must be correctly defined to selectively block only one of the faces. In this scenario, α-amino acids of a determined chirality and those δ-Ach preceding them in the sequence should be N-methylated. Unlike α,γ-counterparts, there will not exist differentiated faces in relation to the type of amino acids involved in the H-bonding network. Considering the structural prerequisites, cyclic peptides incorporating δ-Ach were designed from tetramer, hexamer and octamer templates of *D,L*-α-CPs proposed by Ghadiri giving rise to the

corresponding dimeric models depicted in Scheme 1. The selected α-amino acids for cyclic peptides **CP1** and **CP2** were alanine (Ala) due to its simple N-methylation reaction and tyrosine (Tyr) since its high extinction coefficient would facilitate monitoring the cyclic peptide synthesis and HPLC purification. However, Tyr residues were replaced by leucine (Leu) in **CP3** to avoid undesirable side products during the peptide synthesis. In addition, the proposed α,δ-CPs feature a symmetry center –C_2 in **CP1**, C_3 in **CP2** and C_4 in **CP3**– preventing the formation of several rotodimers which might help to fully characterize them by Nuclear Magnetic Resonance (NMR).



CP1, n = 1, R^1 = $CH_2C_6H_4OMe$, R^2 = Me
CP2, n = 2, R^1 = $CH_2C_6H_4OMe$, R^2 = Me
CP3, n = 3, R^1 = $CH_2CH(CH_3)_2$, R^2 = Me

D1, n = 1, R^1 = $CH_2C_6H_4OMe$, R^2 = Me
D2, n = 2, R^1 = $CH_2C_6H_4OMe$, R^2 = Me
D3, n = 3, R^1 = $CH_2CH(CH_3)_2$, R^2 = Me

Scheme 1. Original *D,L*-α-CPs dimeric models (on top) used to design the novel α,δ-CPs dimers (down) to study its self-assembling properties. In the scheme NH and CO of *D*-amino acids are represented in red as well as those groups of δ-Ach that points to the same face. The same groups of *L*-amino acids are colored in blue.

Computational studies carried out by Martin Calvelo using this initial design endorse our hypothesis.[182] In these studies we confirmed the formation of both β-sheet structures in parallel and antiparallel manner consequence of the stacking of this new cyclic peptide formulation.

HOMODIMER FORMATION STUDIES

In a previous work, Dr. Arcadio Guerra has synthesized and studied **CP1**, **CP2** and **CP3** presenting the structural design discussed above.[183] The peptides were soluble in non-polar organic solvents facilitating the in-solution analysis of the self-assembly process by NMR. The ^{1}H NMR spectra of each sample showed well-defined and sharp signals due to the symmetric structure (Figure 38). The coupling constants of NH signals (J_{NH}) exhibited values higher than 7 Hz, indicating an *all-trans* conformation characteristic of β-sheet structures. The amide protons' chemical shift (δ) of **CP1** was δ 6.48 (NH_{Tyr}) and 6.23 ($NH_{δ\text{-}Ach}$) ppm. In contrast, the same signals of **CP2** and **CP3** showed higher values: δ 8.68 (NH_{Tyr}) and 7.78 ($NH_{δ\text{-}Ach}$) ppm

[182] M. Calvelo, *Computational Methods for the Design and Applications of Self-Assembled Cyclic Peptide Nanotubes*. PhD. Dissertation, Universidade de Santiago de Compostela, Santiago de Compostela, **2021**.

[183] A. Guerra, *Diseño y Síntesis de Ciclopéptidos que Contienen γ- y/o δ-Aminoácidos Cíclicos y Estudio de sus Propiedades de Autoensamblaje: Síntesis De Nuevos Nanotubos Peptídicos*. PhD. Dissertation, Universidade de Santiago de Compostela, Santiago de Compostela, **2017**.

for **CP2** and δ 8.32 (NH_{Leu}) and 7.91 ($NH_{δ\text{-}Ach}$) ppm for **CP3**. The down-field shift in dodecamers and hexadecamers (**CP2** and **CP3**) suggested the participation of these groups in hydrogen-bonding interactions, whereas the octamer (**CP1**) might remain as a monomer in solution.

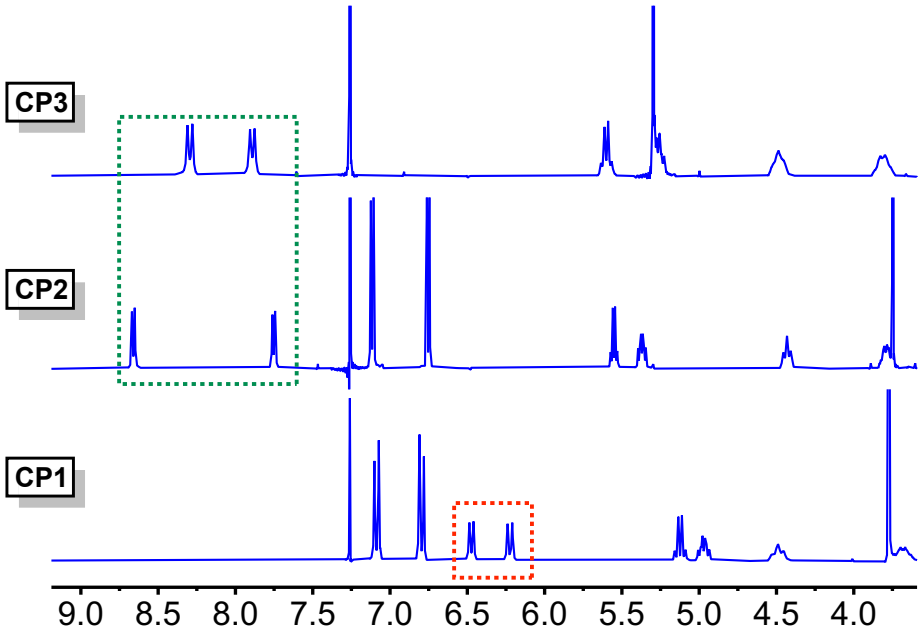


Figure 38. ^{1}H NMR spectrum of cyclic peptides **CP1**, **CP2** and **CP3**. Highlighted in green, signals corresponding to NH protons that are involved in a hydrogen-bonding network. In red, signals corresponding to the NH signals attributed to the monomeric form.

These supramolecular behaviors were confirmed by two-dimensional NMR studies, the cross-peak traces between the NH_{Tyr} protons and the Hδ of ^{Me}N-δ-Ach residue, as well as between the same Hδ proton with Hα of δ-Ach residue confirmed the formation of the dimeric structure (Figure 39). In the case of **CP3**, similar NOE effect was also observed between NH_{Leu} and Hα of δ-Ach with Hδ of ^{Me}N-δ-Ach which also indicated the presence of the self-assembled species.

USC UNIVERSIDADE DE SANTIAGO DE COMPOSTELA

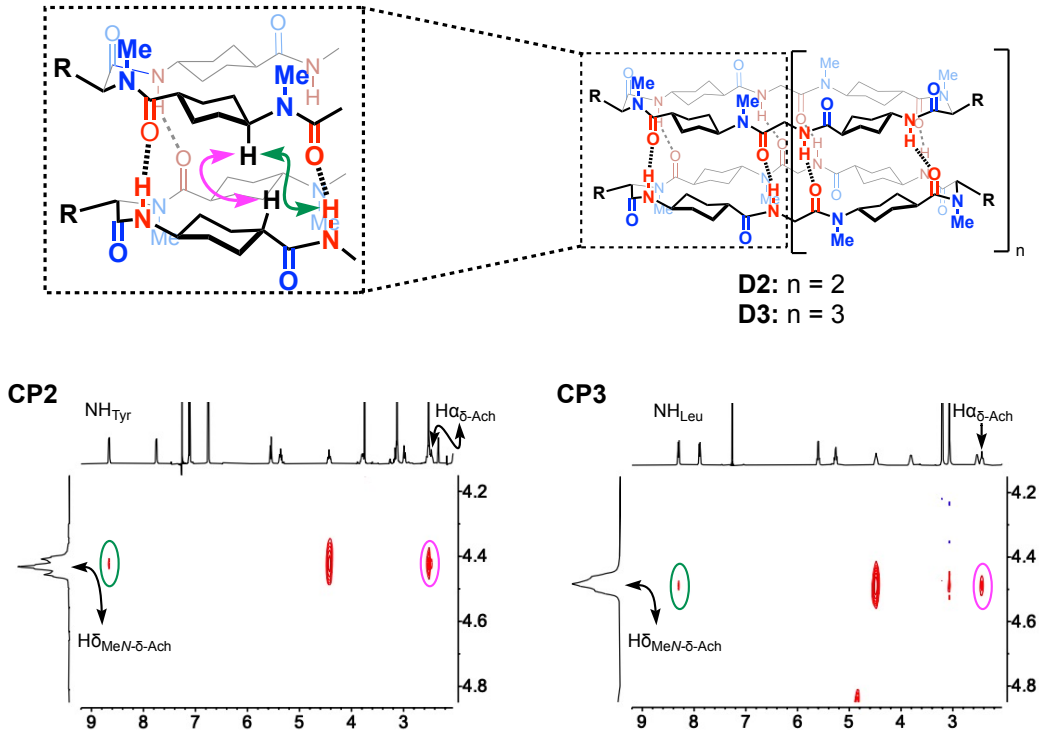


Figure 39. Representation of the supramolecular dimeric structure. Zoom in, nOe cross-peak observed in the NOESY experiments of **CP2** (left) and **CP3** (right) in which the highlighted cross-strand interactions confirmed the formation of the supramolecular system.

In the same work done by Dr. Guerra, peptide self-assembly was also studied by FTIR measurements. Although some publications reported that the presence of a NH stretch mode band around 3310 and 3270 cm^{-1} (also known as amide A band) might suggest the formation of a hydrogen-bonded supramolecular architecture,[184] for these peptides the FTIR data collected was not conclusive. In all cases, an amide A band was detected around this wavenumber, including the octamer which, in NMR experiments, did not show the characteristic features of the constitution of supramolecular assemblies. Further FTIR information collected from the three macrocycles is consistent with the characteristic bands of a peptide β-sheet structure.

In continuation of the experiments performed by Dr. Guerra, we decided to evaluate homodimer formation by electrospray ionization-time-of-flight (ESI-TOF) mass spectrometry. For this purpose, we compared the experimental isotopic distribution with the simulated results for those peaks that could be associated with the dimeric form. In this way, we analyzed peak at 1580.9 m/z of **CP2** that might correspond to the $[M_2H_2]^{2+}$ (dimer with 2 positive charges) or $[MH]^{+}$ (one-charged monomer). We observed that the monomeric and dimeric species coexist because the experimental isotopic distribution coincides with the overlap of the simulated spectra for both species (Figure 40). Moreover, the appearance of a peak at 1054.3 m/z that can only be assigned to $[M_2H_3]^{3+}$ (dimer with 3 charges) also confirmed the presence of the dimeric supramolecular assembly. In comparison with the NMR results, the signal intensity of the peaks

[184] S. Krimm, J. Bandekar, *Adv. Protein Chem.* **1986**, *38*, 18 – 364.

corresponding to the dimeric specie appeared to be very low, most likely due to its lower ionization ability.

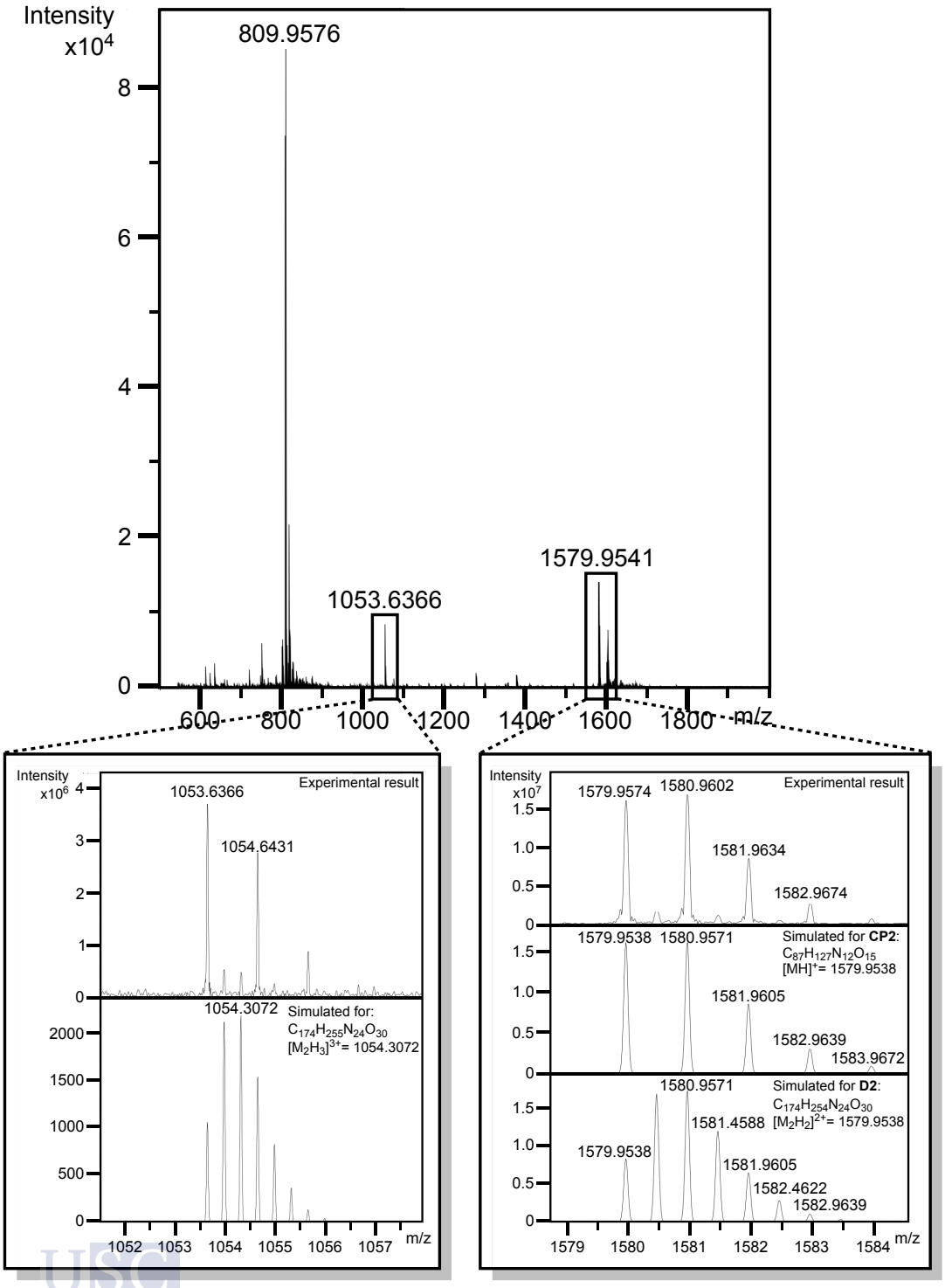


Figure 40. ESI-TOF mass spectrum of **CP2**. In the insets are shown the comparison between the experimental and simulated isotopic distributions of the $[M_2H_3]^{3+}$ peak (1054.6366, left) and $[M_2H_2]^{2+}$ (1579.9541, right).

We employed the same procedure to establish the dimeric structure of **D3** (Figure 41). Here again, the coexistence of the two species was confirmed because the experimental isotopic

distribution of the $[M_2H_2]^{2+}$ peak (1850.3 m/z) represents an average of the simulated isotopic distributions for monomer and dimer. In addition, the $[M_2H_3]^{3+}$ peak (1234.5 m/z) assignable exclusively to **D3** was again identified.

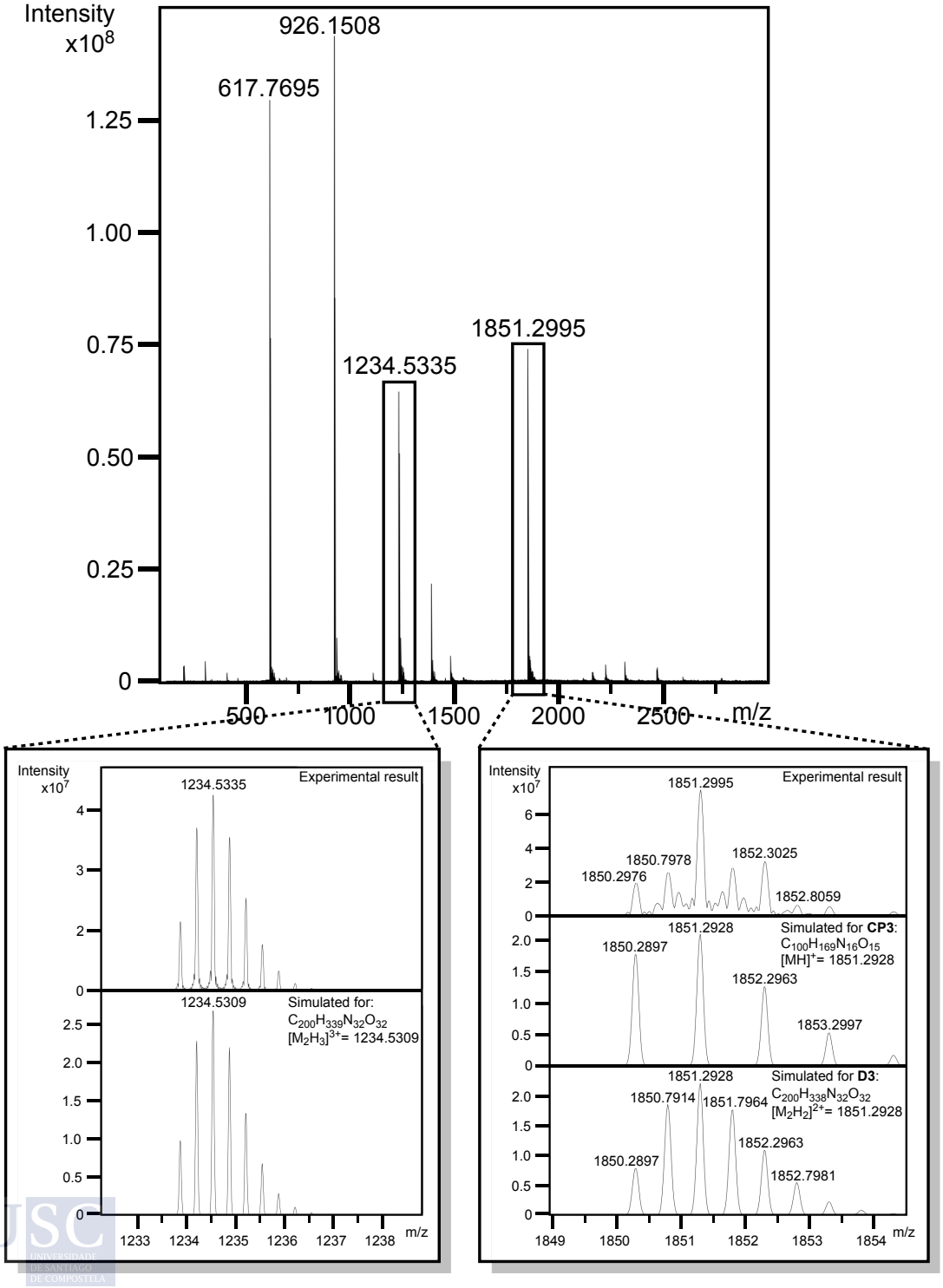


Figure 41. ESI-TOF mass spectrum of **CP3**. In the insets are shown the comparison between the experimental and simulated isotopic distributions of the $[M_2H_3]^{3+}$ peak (1234.5335, left) and $[M_2H_2]^{2+}$ (1851.2995, right).

Finally, the absence of the dimeric form for the octamer (**CP1**) was also validated by MS. Its mass spectrum showed only the $[MH]^+$ and $[MH_2]^{2+}$ signals associated with the monomer. In addition, the ion mass corresponding to the $[M_2H_3]^{3+}$ signal observed in the previous dimeric structures was not detected for **CP1** reflecting the difficulty to form a dimeric structure (Figure 42).

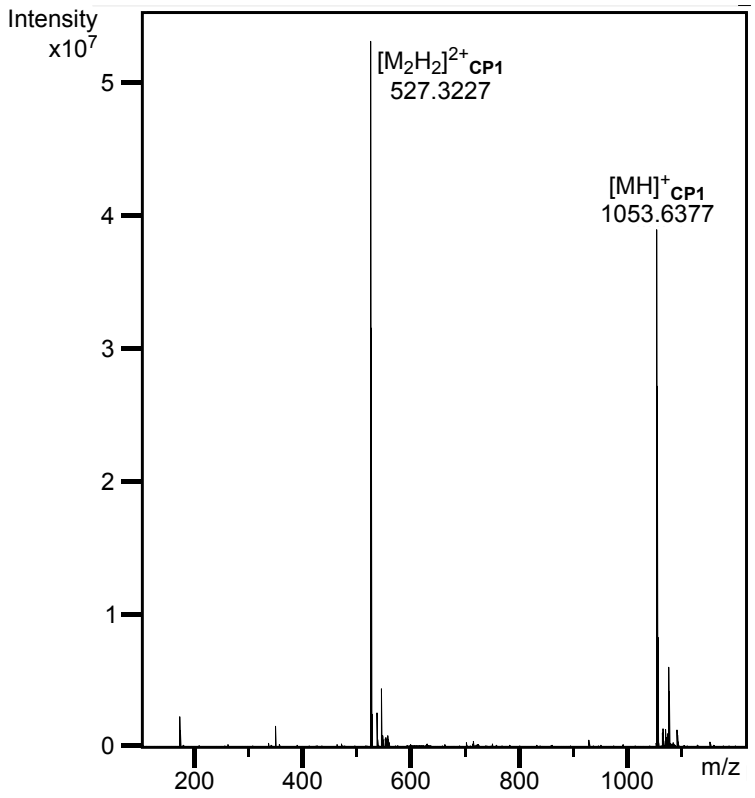
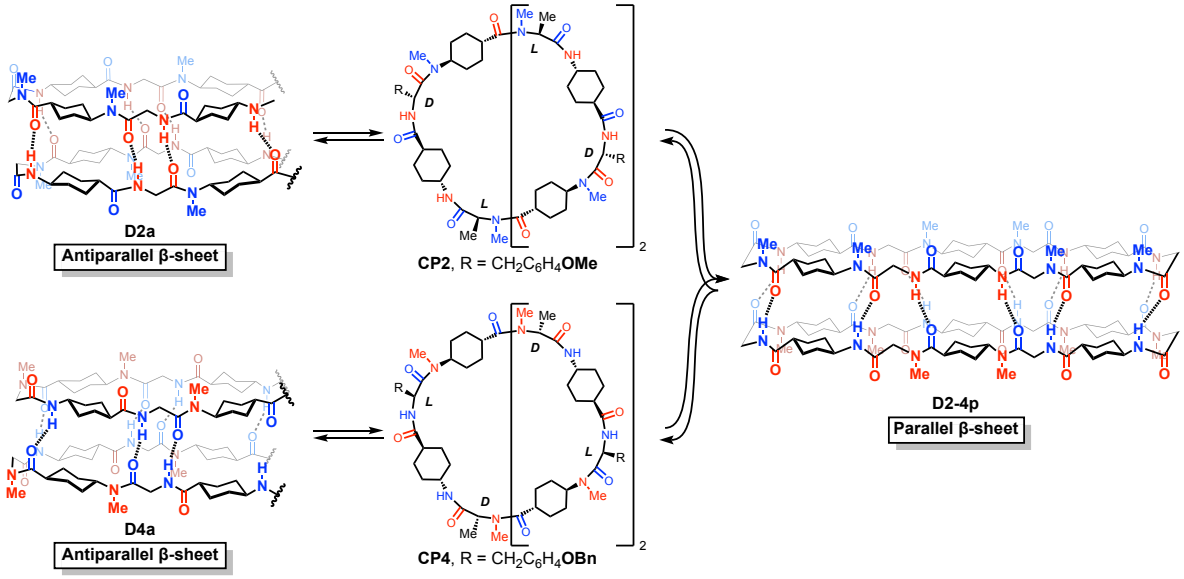


Figure 42. ESI-TOF mass spectrum of **CP1**. In the spectrum peaks corresponding to the monomeric specie are shown.

HETERODIMER FORMATION STUDIES

Once the self-assembly ability of α,δ-CPs was demonstrated, the next step was to study the relative stability of both types of assemblies, the parallel and antiparallel β-sheet structures. However, cyclic N-methylated peptides can only self-associate through an antiparallel arrangement because, to give rise to the parallel alignment, the *D*-face must interact with the *L*-face of the following peptide. Therefore, the N-methylation strategy does not work to study this interaction for one single peptide. In contrast, the enantiomeric specie will have a switched N-methylation pattern from the *D*-face to the *L*-face. Consequently, equimolar mixture of both peptides could provide, in addition to the corresponding antiparallel homodimers, the heterodimeric specie upon interaction of both enantioforms via a parallel β-sheet. For this purpose, the dodecameric model was selected due to its high tendency to produce dimers with high association constants in solution. In relation to these aspects, we prepared **CP4** which is a pseudo-enantiomeric structure of **CP2** (Scheme 2).[183] In contrast to **CP2**, *D*-residues are N-methylated, as well as the δ-Ach residues preceding them in the peptide sequence. Furthermore, the side chain protecting group of the Tyr residues was different for both peptides,

methyl ether for **CP2** and benzyl ether for **CP4**. This switch will facilitate the spectroscopic differentiation. As expected, the in-solution behavior of both peptides is equivalent leading to dimeric species, as demonstrated by the downfield shift of the amide proton signals in the ^{1}H NMR spectrum.



Scheme 2. Structural model of the equilibria between the cyclic dodecamers **CP2** and **CP4** to lead to the corresponding homodimers **D2a** and **D4a** (antiparallel interaction), as well as the heterodimer **D2-4p** (parallel interaction). In the dimeric models, side chains were removed for clarity.

To achieve this goal, Dr. Guerra followed the same strategy developed by Ghadiri to evaluate heterodimer formation.[99] For this purpose, the addition of 0.2 equiv. aliquots of **CP4** (27.3 mM) over a deuterochloroform solution of **CP2** (5.1 mM) was monitored by NMR. As can be seen in Figure 43, the addition of 0.2 equiv. already showed significant changes in the ^{1}H NMR spectra. Therein, a new group of signals appeared between δ 7-9 ppm that did not correspond to either the antiparallel homodimers **D2a**[185] and **D4a** or the monomers **CP2** and **CP4** due to the downfield chemical shift of the amide protons. While the number of equivalents increased, **D2a** and **D4a** NH signals gradually were disappearing and the intensity of the new signals increased. Similar behavior was observed for the Hα signals of ^{Me}N-Ala and Tyr (δ 5.58 and 5.40 ppm) of the antiparallel homodimers which were gradually vanishing meanwhile a new set of signals come up (δ 5.84 and 5.30 ppm) after the successive additions. Finally, after carefully analysis of the equimolar mixture, the coexistence of the three species in solution was appreciated: the two antiparallel homodimers and the parallel heterodimer in a ratio of 20:1 in favor to the parallel β-sheet.

USC UNIVERSIDADE DE SANTIAGO DE COMPOSTELA

[185] For clarity, dimeric species are named as Da (antiparallel) or Dp (parallel) depending on the conformation they establish.

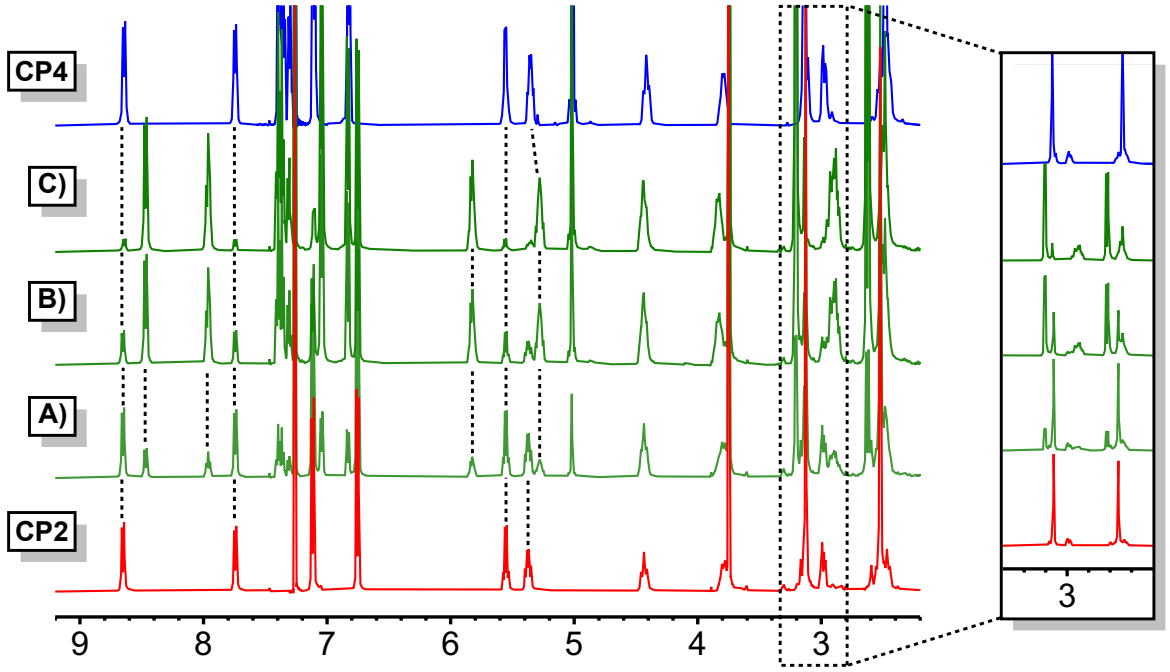


Figure 43. ^{1}H NMR spectra of the additions A) 0.2 equiv, B) 0.6 equiv and C) 1.0 equiv (green spectra) of a solution of **CP4** (27.3 mM, blue spectrum) to a solution of **CP2** (5.1 mM, red spectrum) in $CDCl_3$ to evaluate the formation of the parallel heterodimeric structure.

Further evidence of heterodimer formation was derived from 2D-NMR experiments of the resulting equimolar mixture in which nOe cross peaks between both cyclic peptide subunits were observed. These signals can only be attributed to the heterodimer **D2-4p**, as those between the NH of the Tyr and Hα of ^{Me}N-Ala, as well as between δ-Ach amide proton and Hδ of ^{Me}N-δ-Ach. In addition, additional signals between the side chains of the α-amino acids were also noted as depicted in Figure 44.

USC UNIVERSIDADE DE SANTIAGO DE COMPOSTELA

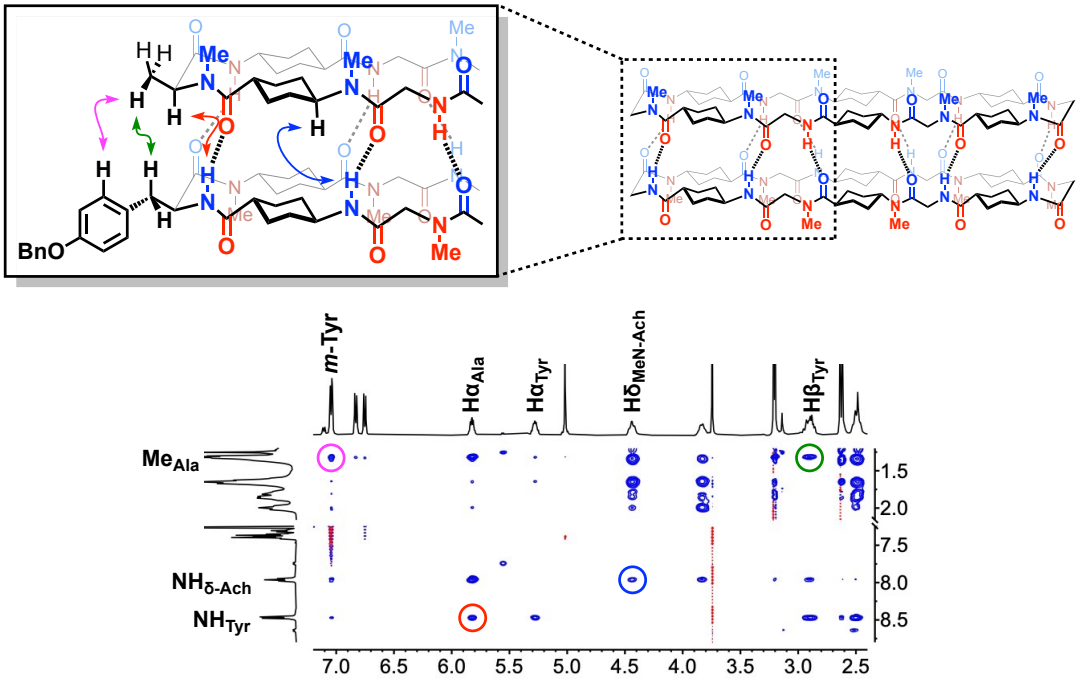


Figure 44. Representation of the supramolecular dimeric structure. Zoom in, nOe cross-peak observed in the NOESY experiment in which the highlighted cross-strand interactions confirmed the formation of the supramolecular system.

To complete these studies, we also demonstrated the formation of the heterodimeric form by ESI-TOF mass spectrometry (Figure 45). The different molecular mass of both cyclic peptides due to the different protecting groups on the Tyr side chains facilitated its mass characterization. In the spectrum we found an ion mass of 1695 m/z with an isotopic distribution differentiated by half unit that correspond to a double-charged component $[M_2H_2]^{2+}$ whose mass matches with the heterodimer. We contrasted this information by comparing the isotopic distribution of this signal with the theoretical isotopic distribution. In addition, we identify the molecular ion of both monomers as consequence of the mass ionization process, as well as residual antiparallel homodimers.

USC UNIVERSIDADE DE SANTIAGO DE COMPOSTELA

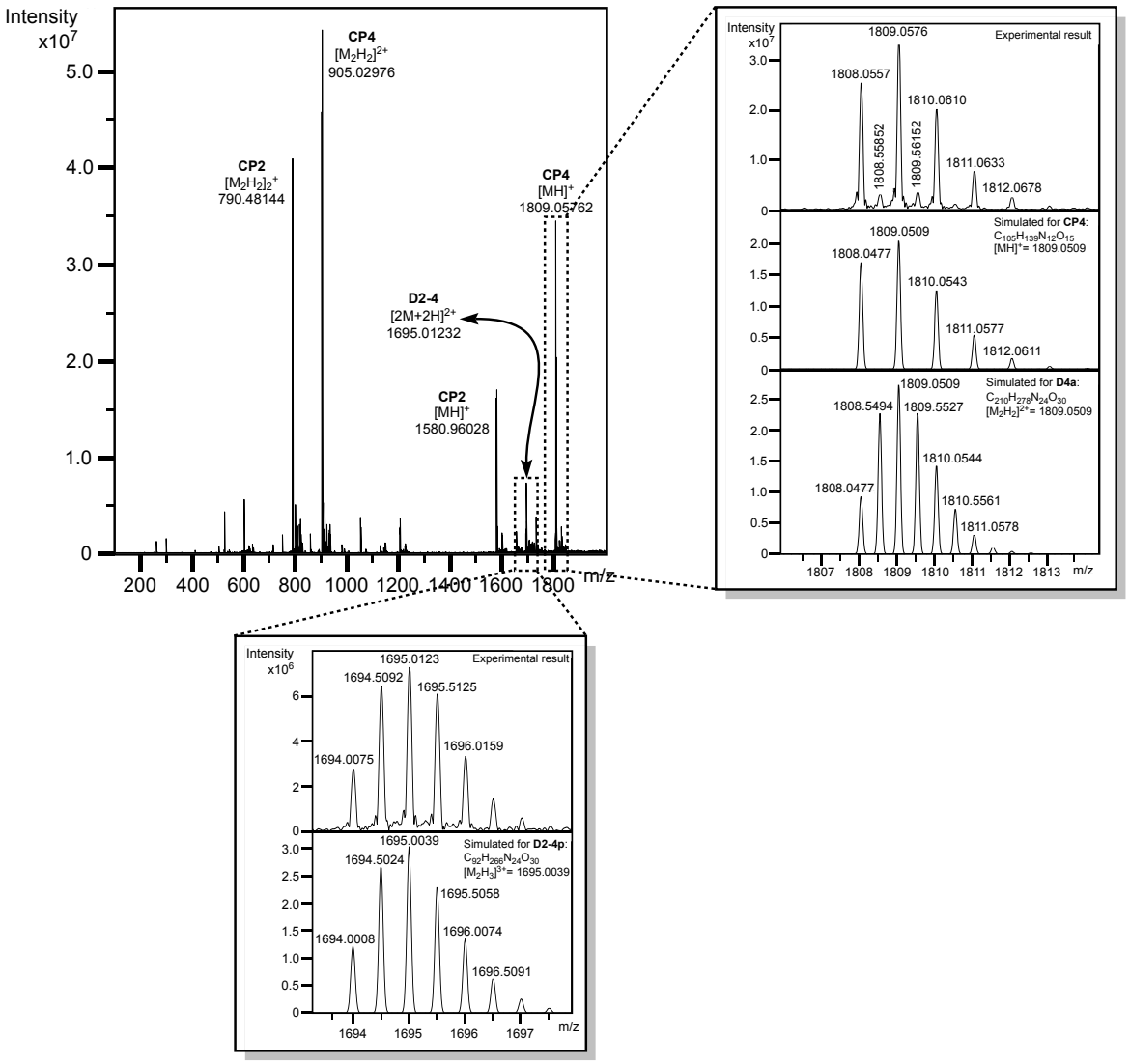


Figure 45. ESI-TOF mass spectrum of equimolar mixture of **CP2** and **CP4**. In the insets are shown the comparison between the experimental and simulated isotopic distributions of the $[M_3H_3]^{3+}$ peak (1695.0123, down) and $[M_2H_2]^{2+}$ (1809.0576, right).

As previously mentioned, DFT calculations using similar α,δ-dimeric systems in which the α-amino acids were Ala residues in order to study the dimerization process considering exclusively the peptide backbone interactions were carried out by Martín Calvelo.[182] In Table 1 the interaction and dimerization energies obtained by using the Counterpoise method are summarized. These calculations indicated that the parallel arrangement (**D2-4p**) interaction energy is more stable by 3.7 kcal·mol^{-1} against the antiparallel homodimeric forms (**D2a or D4a**). Likewise, the dimerization energy which also considers the adequate monomer geometry for the self-assembling process (deformation energy) is still more favorable for parallel conformation by 2.6 kcal·mol^{-1}. To understand better these results, the most relevant geometrical H-bonding parameters were calculates, such as O···N and O···H distances and O···H-N and C=O···H angles. However, the information obtained from these descriptors is not conclusive to justify the greater preference of the parallel structure.

PARALLEL D2-4p		ANTIPARALLEL D2a or D4a	
Interaction Energy	Dimerization Energy	Interaction energy	Dimerization energy
-124.4	-95.0	-120.7	92.4

Table 1. Interaction and dimerization energies (in kcal·mol^{-1}) of the corresponding ß-sheet structures formed upon α,δ-cyclic peptides stacking.

The relative stability of both conformations may also be influenced by the relative position of the protons that are not involved in hydrogen bonding interactions: axial protons of the cyclohexyl moieties, the Hα of α-amino acids and one of the hydrogens of the Ala side chain. As illustrated in Figure 46, in the parallel β-sheet all the axial hydrogen of both peptide subunits are interdigitated and the inter-hydrogen distances are longer than the sum of the van der Waals radii. Whereas, in the antiparallel arrangement, the cyclohexyl axial hydrogens are aligned on top of each other. Moreover, there are a couple of contacts below the sum of the van der Waals radii (~2.4 Å), such as the axial hydrogen located at the Ala side chain (d_2, Figure 46). As consequence, the rings twist to minimize the steric congestions, while, in the parallel arrangement, the better packing of the axial hydrogens permitted the establishment of shorter H-bonds without twisting the CP structure reasoning its greater stability.

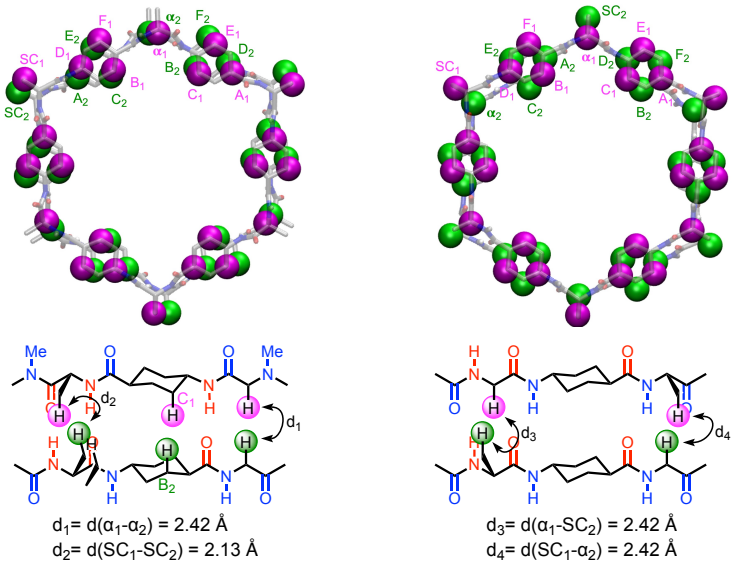
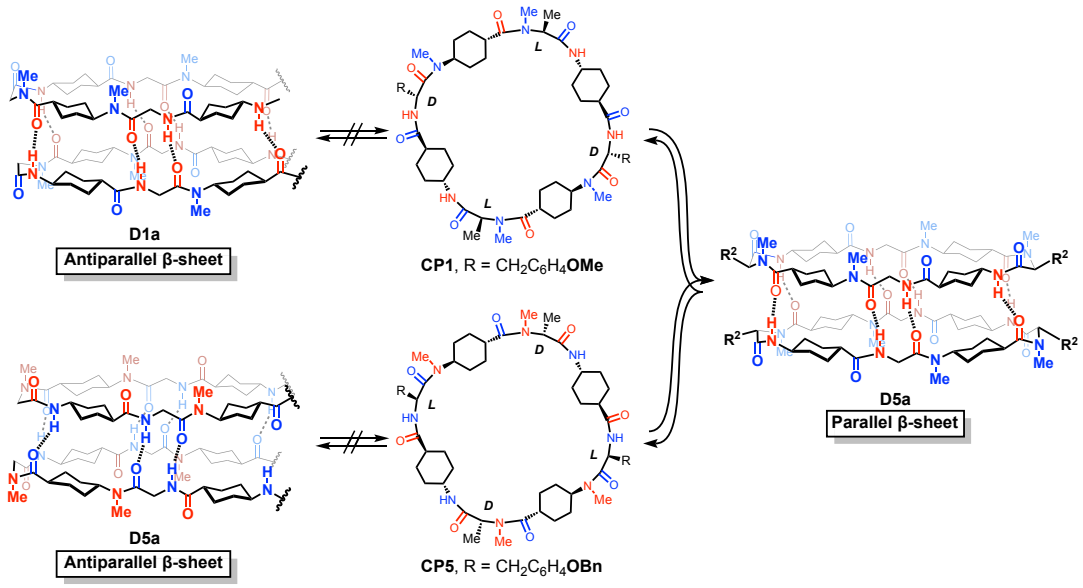


Figure 46. Top(up) and side (bottom) view of the cyclic dodecapeptide dimers in which the axial protons of the cyclohexyl moieties are represented as CPK models and highlighted in colors (pink for the hydrogens of the top CP and green for those corresponding to the bottom CP).

Intrigued by these results we decided to study the parallel interaction of the octameric system which did not give rise to the homodimeric (antiparallel) aggregate. Therefore, as for the dodecamer, **CP5** –a pseudoenantiomer of **CP1**– was prepared (Scheme 3). Although antiparallel dimer was not assembled, we envisaged that the previously observed greater stability of the parallel arrangement would open the possibility of finding some self-assembly properties in cyclic octapeptides.



Scheme 3. Structural model of the equilibria between the cyclic octamers **CP1** and **CP5** to lead to the heterodimer **D1-5p** (parallel interaction) whose corresponding homodimers are not formed. In the dimeric models, side chains were removed for clarity.

Interestingly, after performing NMR titration experiments (Figure 47), different changes of some relevant signals were detected in the spectrum of the mixture. As key features, it was noted the disappearance of the signals corresponding to the amide protons of the monomeric species and the appearance of new broad signals at downfield chemical shift. Also, the signals associated with the Hα of Tyr residue (δ 4.96 ppm) downfield shifted. In addition, a small variation of the signals associated to Hδ ^{Me}N-δ-Ach was also observed. Upon additions, these signals gradually disappeared, and broad bands emerged at downfield chemical shift. This suggested the formation of a supramolecular specie with low association constants that could be associated to the parallel interaction. These alterations are characteristic of β-sheet structures.

USC UNIVERSIDADE DE SANTIAGO DE COMPOSTELA

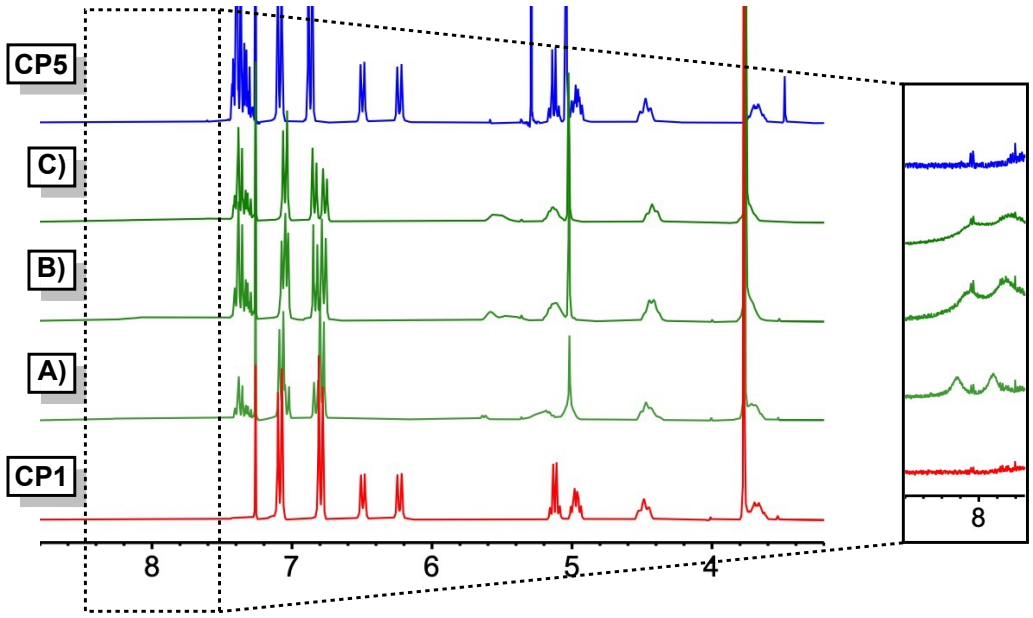


Figure 47. ^{1}H NMR spectra of the additions A) 0.2 equiv, B) 0.6 equiv and C) 1.0 equiv (green spectra) of a solution of **CP5** (83.0 mM, blue spectrum) to a solution of **CP1** (20.6 mM, red spectrum) in $CDCl_3$ to evaluate the formation of the parallel heterodimeric structure. In the inset, zoom in between δ 7.8-8.6 ppm where the broad signals attributed to the heterodimeric specie raised.

Finally, we verified the presence of **D1-5p** by mass spectrometry (Figure 48). As in the previous case, the different protecting groups facilitated the analysis because the two pseudoenantiomeric monomers have different molecular masses: $[MH]^+_{\mathbf{CP1}}$= 1053.6 m/z and $[MH]^+_{\mathbf{CP5}}$= 1205.7. In the spectrum of Figure 48, we were able to identify the molecular ion signals of both subunits plus a peak of mass 1130 Da that we assigned to the double-charged dimeric ion ($[M_2H_2]^{2+}$). This mass matched with the theoretical isotopic distribution. The lower stability of the antiparallel versus the parallel interaction was mainly attributed to the distortion of the ring in the planar conformation due to the rigidity added by the δ-residue hindering the formation of the homodimeric form. In contrast, a good match between axial proton of δ-Ach residues, as previously observed for dodecamers, enabled the constitution of the heterodimer **D1-5p**. Despite the geometry appeared to be adequate to allow the interaction by a parallel arrangement, the association constants were quite low.

USC UNIVERSIDADE DE SANTIAGO DE COMPOSTELA

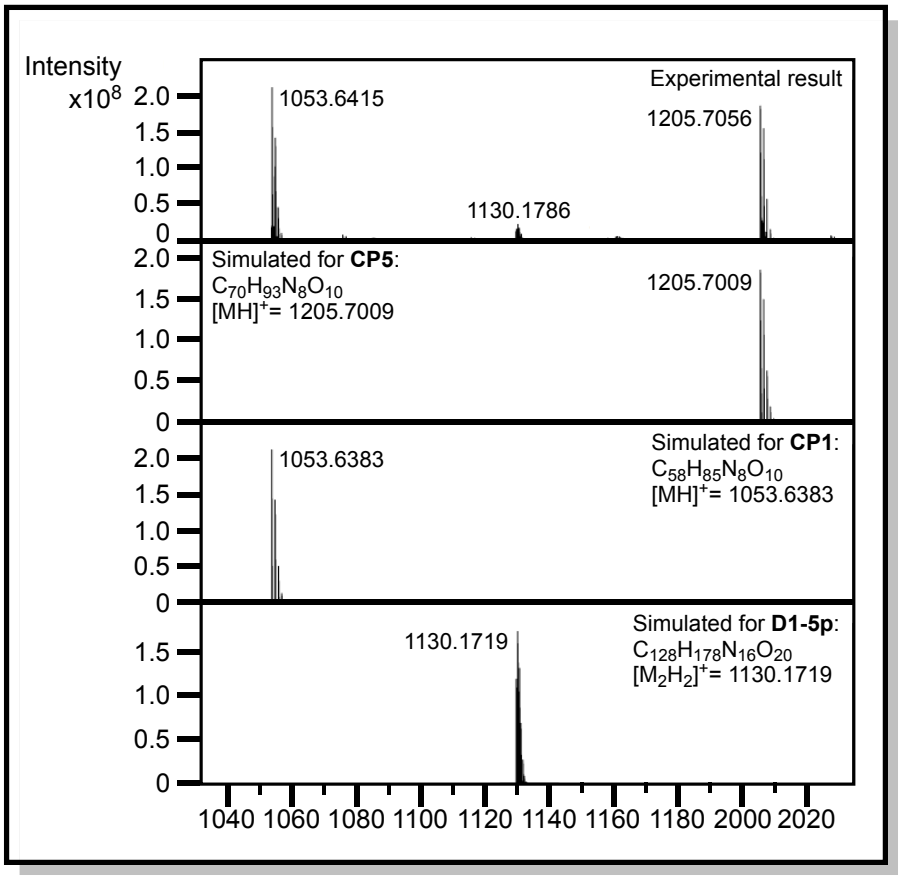


Figure 48. ESI-TOF mass spectrum of the equimolar mixture of **CP1** and **CP5** (upper spectrum). It is also shown the simulated isotopic distributions for molecular mass of **CP5** (1205.7009), **CP1** (1053.6383) and **D1-5p** ($[M_2H_2]^{2+}$= 1130.1719).

In this case, theoretical studies using analogue structures were not conclusive.[182] The calculations suggested that the formation of both dimers (parallel **D1-5p** and antiparallel **D1a** and/or **D5a**) have a similar stability.

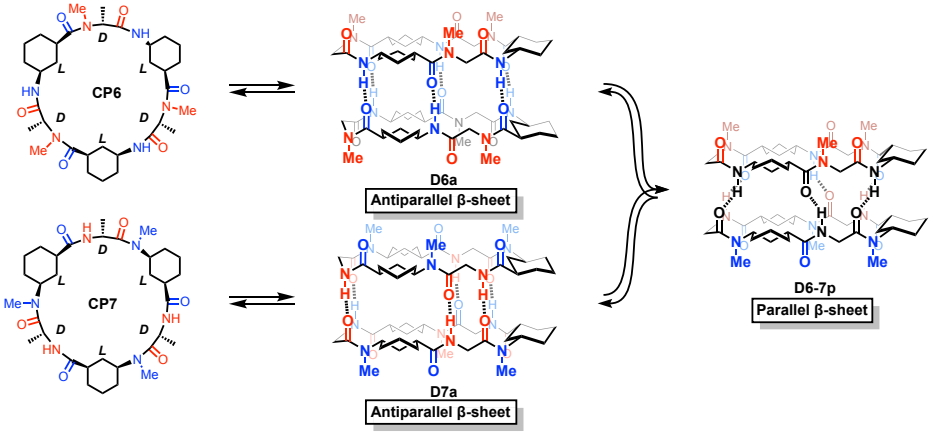
SELF-ASSEMBLING STUDIES OF α,γ-CYCLIC PEPTIDE

In light of the obtained results, we then decided to perform a detailed study of the self-assembly properties of the α,γ-CPs. Originally, the antiparallel β-sheet was considered as the most stable organization. However, no study contemplating the feasibility of the parallel interaction has been conducted for these structures so far.

PARALLEL INTERACTION BETWEEN PEPTIDES WITH THE SAME QUIRALITY

As discussed in the Introduction, cyclic peptides consisting of alternating α,γ-amino acids can be organized through the α-face (α-α interaction) or the γ-face (γ-γ interaction). Considering this, the parallel arrangement could be achieved through the combination of two peptides that contain amino acids of the same chirality with shifted methylation pattern. Therefore, peptides **CP7** which is γ-methylated and **CP6** which have N-alkylated α-amino acids were designed (Scheme 4). To minimize the possible repulsive forces between the side chains, Ala residues were selected as α-Aa for both isomers. These peptides self-assemble by antiparallel β-sheet to give rise to the corresponding homodimers (**D6a** and **D7a**) with different association constants

that we associate with the folding ability of **CP6**.[119] The combination of both subunits would afford the heterodimeric specie through a parallel α-γ interaction providing information about their relative stability.



Scheme 4. Structural model of the equilibria between the cyclic hexamers **CP6** and **CP7** and their corresponding homodimers (**D6a** and **D7a**) and the parallel heterodimer **D6-7p** (parallel interaction). Amino acid side chains were removed for clarity.

Synthesis

Once the design of the systems for the study of the supramolecular properties was established, the next step was the synthesis of both peptides. For this purpose, we decided to employ a convergent synthesis in solution. We chose this synthetic strategy over solid-phase peptide synthesis (SPPS) due to diverse considerations. First, SPPS requires large excess of reagents of amino acids and coupling agents. In these systems, artificial amino acids are used and, as we will show hereafter, they imply synthetic processes that increase the value of these building blocks. In-solution synthesis enables greater control over the number of equivalents, thus reducing the necessary amino acid quantities to be used. In addition, there are three N-methylated amino acids in the structure of each peptide. Secondary amines are less reactive and take longer reaction times. The reactivity decreases as the peptide strand grows. Therefore, using this approach permits to grow the peptide chain from repetitive units and reduce the number of couplings on secondary amines to one per peptide. Another advantage is that N-methylated peptides are more soluble in organic solvents than those non-methylated which facilitates its synthesis in solution. Also, the design incorporates Ala as α-amino acid, so that we would be obliged to carry out the cyclization in solution because this amino acid does not have a side chain that can be anchored to the resin.[186]

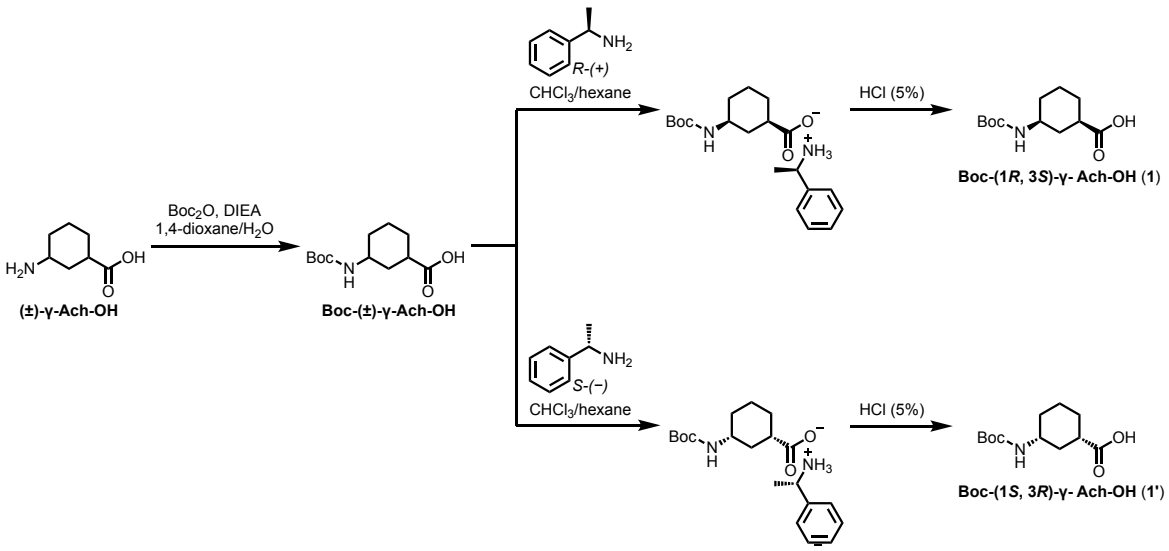
At this point, we defined the N- and C-terminal end protecting groups. In this synthesis we decided to use the *tert*-butoxycarbonyl carbamate group (Boc) for the N-terminal end as it is stable against basic, nucleophilic, and palladium-catalyzed hydrogenolysis conditions. In addition, its suppression under acidic conditions (usually trifluoroacetic acid) needs simple procedures and short reaction times. We include the methyl ester group (OMe) at the C-terminal

[186] On-resin cyclization will be discussed in Chapter 2.

end because of it is orthogonality with the Boc group. Moreover, the protection methods are usually straightforward and the deprotection consists of a simple saponification reaction in the presence of an alkaline hydroxide salt, commonly lithium hydroxide.

Having designed the synthetic protocol, the first step implied the preparation of the corresponding isomers (*D* or *L*) of N-protected γ-Ach. This process consisted of two steps, first protection of commercial 3-aminocyclohexanecarboxylic acid [**(±)-γ-Ach-OH**] and subsequent chiral resolution of the resulting racemic product (Scheme 5). The chosen protecting group (Boc) was introduced by treatment of the commercial amino acid with Boc anhydride in the presence of base (DIEA) providing the racemic intermediate **Boc-(±)-γ-Ach-OH**. Subsequently, the racemic compound was resolved by classic crystallization techniques. For this purpose, a solution of **Boc-(±)-γ-Ach-OH** in a $CHCl_3$/hexane mixture was treated with chiral 1-phenylethanolamine giving rise to two different diastereoisomers. The resulting salts will present different solubility properties in the solvent mixture, so one of the diastereoisomers will selectively crystallize allowing separation by filtration. The first crystallization was carried out in the presence of **(*R*)-(+)-1-phenylethylamine** in a mixture of $CHCl_3$/hexane (3:1) for one week. As shown in Scheme 5, crystallization of the 1*R,*3*S* enantiomer is favored. According to the conversion shown in Figure 17 (Introduction), it would correspond to the *L*-isomer. The crystallized diastereoisomer was filtrated, resuspended in CH_2Cl_2, and the **Boc-γ-Ach-OH** was protonated through washes with an aqueous solution of hydrochloric acid (5% v/v). The enantiomeric enrichment was checked by specific optical rotation measurements. After the first crystallization, a value of [α]= -26º (in MeOH) was obtained that is still far from the values described for the pure enantiomer ([α]= −50º).[124] Therefore, this process was repeated up to 4 times by progressively increasing up to 1 equiv the amount of the chiral amine and the ratio of $CHCl_3$ in the solvent mixture until the hexane was eliminated. After the fourth crystallization, a value of [α]= −48º was registered. At this point, the enantiomeric excess was determined using a more accurate analytical technique. Specifically, we used Supercritical Fluid Chromatography (SFC) with a chiral stationary phase leading to the separation of both enantiomers. The procedure and specifications are detailed in the Experimental Section. Finally, the enantiomeric excess was calculated integrating the area of the signals that correspond to each enantiomer. We determined up to 98% of enantiomeric excess. The other enantiomer was obtained following the same protocol using the amine of opposite chirality: **(*S*)-(−)-1-phenylethylamine**.

USC UNIVERSIDADE DE SANTIAGO DE COMPOSTELA



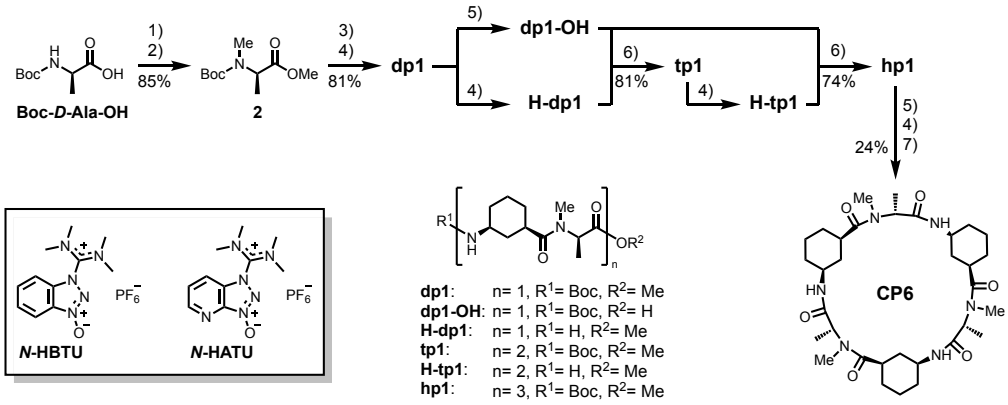
Scheme 5. Synthetic scheme for the enantiopure preparation of both **Boc-γ-Ach-OH** enantiomers.

The next step involved the N-methylation of the α-Aa. This process consisted of two consecutive reactions: N-methylation and C-terminal end protection of carboxylic acid. For the first stage, **Boc-*D*-Ala-OH** was treated with a strong base (NaH) and methyl iodide (MeI) in THF. The use of a strong base led to the amine deprotonation that reacted with the MeI providing the methylated intermediate that was used in the next step without further purification. The last step in the sequence provided the N-methylated alanine methyl ester (**2**, Scheme 6) by treatment of the isolated intermediate with a mild base (Na_2CO_3) and MeI in DMF. In this case, short reaction times were used to avoid Ala α-carbon epimerization.

Once the amino acids required for peptide preparation were obtained, we started the synthesis of the linear hexamers. Thus, we began preparing dipeptide **dp1** (Scheme 6) that was obtained through removal of Boc group from compound **2** and then reacted with **Boc-(*1R,3S*)-γ-Ach-OH** (**1**) using *N*-HATU as coupling reagent in the presence of DIEA in CH_2Cl_2 providing the desired **dp1** in good yields. This dipeptide was used for the preparation of **tp1**. To this end, **dp1** was split into two portions. One portion was treated with a 1:1 mixture of TFA/CH_2Cl_2 giving rise to N-terminal end deprotected dipeptide (**H-dp1**). The other sample was reacted with LiOH in a 3:1 MeOH/H_2O mixture providing carboxylic acid-free dipeptide (**dp1-OH**) which was, then, treated with *N*-HBTU and DIEA in CH_2Cl_2 and the resulting mixture was poured into a solution of **H-dp1** in the same solvent to yield targeted **tp1**. The linear hexamer (**hp1**) was prepared following a similar strategy, the amine group of **tp1** was deprotected by acid treatment and then coupled with **dp1-OH**. As in the synthesis of **tp1**, both deprotected fractions were coupled in the presence of *N*-HBTU and DIEA in CH_2Cl_2 giving rise to desired linear **hp1**. The selection of coupling agents is not a trivial issue. The nitrogen in position 7 of *N*-HATU enhances its reactivity and makes this reagent more suitable for the coupling of secondary amines.[187] Although *N*-HBTU is less reactive, it is more stable in solution, cheaper and, therefore, more appropriate for linking primary amines.

[187] A. El-Faham, F. Albericio, *Chem. Rev*. **2011**, *111*, 6557 – 6602

Finally, the cyclization step was carried out. For this purpose, both termini were sequentially deprotected starting from the carboxylic acid. Lastly, fully unprotected linear hexapeptide was cyclized under high dilution conditions (1 mM) in basic medium using *N*-TBTU as a coupling agent. The high dilution conditions were necessary to favor the intramolecular reaction avoiding the formation of polymeric side products or larger macrocycles. To finish, the reaction crude was purified by HPLC affording **CP6** in an overall yield of 10%. The other cyclic peptide (**CP7)** was previously prepared in our laboratory by Alberto Fuertes.[188]



Scheme 6. Synthetic strategy for the preparation of **CP6**. In the inset, the chemical structures of the coupling reagents used are shown. Conditions: 1) NaH, THF, then MeI; 2) MeI, Na_2CO_3, DMF; 3) TFA/CH_2Cl_2; 4) **Boc-(*1R,3S*)-γ-Ach-OH (1)**, *N*-HATU, DIEA, CH_2Cl_2; 5) LiOH, MeOH/H_2O; 6) *N*-HBTU, DIEA, CH_2Cl_2; 7) *N*-TBTU, DIEA, CH_2Cl_2.

Structural Studies: α-γ parallel interaction

As previously demonstrated, **CP7** self-assembles in deuterochloroform through α-α interaction giving rise to the antiparallel β-sheet. On the other hand, **CP6** dimerizes through the antiparallel γ-γ interaction providing dimer **D6a** with lower association constants. The NMR spectrum is characteristic of an equilibrium process of monomer and dimer exchange exhibiting a broad single signal corresponding to the NH_{Ach} protons whose chemical shift depends on peptide concentration. To analyze the formation of the heterodimer, the same procedure used with the α,δ-CPs was followed, the addition of gradually increasing amounts (0.2 equiv per addition) of a solution in deuterochloroform of **CP6** (29 mM) over a solution of **CP7** (8 mM) was monitored by NMR (Figure 49). The addition of 0.2 equiv already caused changes in the ^{1}H NMR spectrum of the mixture. Novel groups of signals emerged at δ 8.41 (NH_{Ala} of **CP7**), 7.90 ($NH_{\gamma\text{-}Ach}$ **CP6**) and 5.46 ($H\alpha_{Ala}$ of **CP7**) ppm. These signals did not correspond to any of the antiparallel forms or monomers. Therefore, they were attributed to the heterodimeric specie. Addition of higher amounts of **CP6** (up to 1.2 equiv) led to the disappearance of the NH_{Ach} signal corresponding to the original **D6a** homodimer, while the intensity of the new signals increased. In the equimolar mixture, it could be observed that signals attributed to parallel assembly predominate. An important aspect of the new dimer is that the equilibrium is now a

[188] A. Fuertes, *Nuevas Estrategias para el Transporte de Iones y la Encapsulación Selectiva de Ligandos Basadas en α,γ-Ciclopéptidos*. PhD. Dissertation, Universidade of Santiago de Compostela, Santiago de Compostela, **2019**.

slow process at the NMR timescale. A ratio of 20:1 in favor of the heterodimeric form was estimated by integration of the peaks related to each specie.

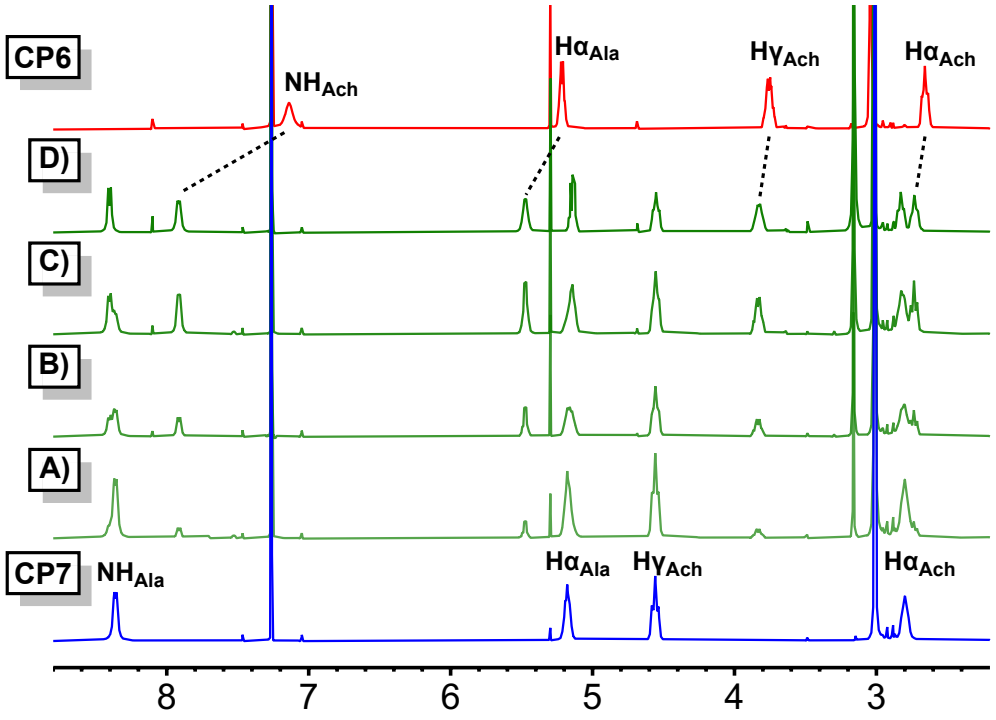


Figure 49. ^{1}H NMR spectra (between 2.2 and 8.8 ppm) of the additions A) 0.2 equiv, B) 0.6 equiv and C) 1.0 equiv (green spectra) of a solution of **CP6** (29.0 mM, red spectrum) over a solution of **CP7** (6.0 mM, red spectrum) in $CDCl_3$ to evaluate the formation of the parallel heterodimeric structure. The dotted lines are used to establish the correlation of protons that correspond to **CP6** in the homodimeric and the formed heterodimeric structures.

To validate the presence of the heterodimeric structure, NOESY spectrum of the final mixture of **CP6** and **CP7** was recorded (Figure 50). In this spectrum the nOe cross-peaks signals between the signal at 8.41 ppm ($NH_{\gamma\text{-Ach}}$ of **CP6**) and the signal at 7.90 ppm ($H\gamma_{MeN\text{-}\gamma\text{-Ach}}$ of **CP7**) as well as NH_{Ala} of **CP6** and $H\alpha_{MeN\text{-}Ala}$ of **CP7** were identified. These NOEs can only be attributed to the heterodimeric form. Therefore, it is confirmed the majority presence of this supramolecular entity in solution.

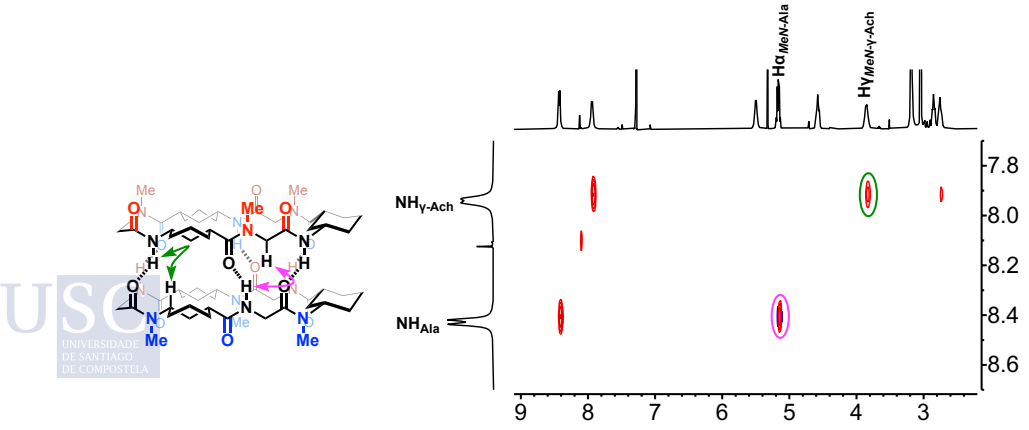


Figure 50. Representation of **D6-7p** structure (above) and NOESY spectrum of the amide area (below). In the spectrum, the highlighted cross-peak signals (green and magenta) confirmed the establishment of the parallel interaction.

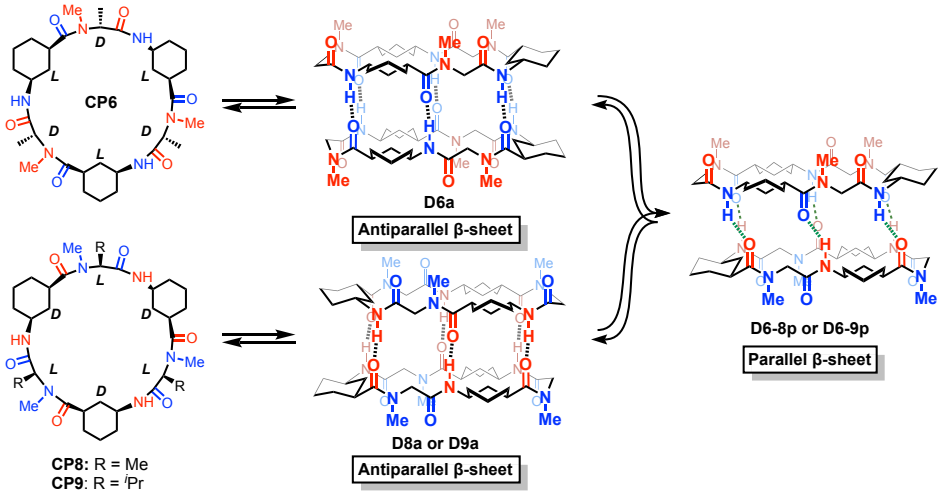
These results with α,γ-CPs challenge preliminary assumptions about this type of structures. Interestingly, these studies provided strong evidence for the higher stability of the parallel arrangement directed by peptide backbone interactions. Once again, the better van der Waals contacts between cyclohexyl moieties could provide additional stability to the parallel dimer. Additionally, these experimental results are supported by DFT theoretical calculations that confirmed the preferred parallel α-γ interaction between **CP6** and **CP7**.[182] Henceforth, the paradigm shifts when designing new tubular materials with this type of cyclic peptides.

PARALLEL INTERACTION BETWEEN PEPTIDES WITH DIFFERENT QUIRALITY

In view of these results, we decided to extend this investigation to other possible combinations of α,γ-CPs. In the previous scenario, only peptides with chiral identical amino acid sequences were examined. Considering the enantiomers of the previously described peptides, the number of possible dimeric disposition increases. Hence, two new parallel sheets could be accessed by combining **CP6** and **CP7** with their respective enantiomers. In the case of **CP6** and its enantiomer (**CP8**), the dimeric structure would be formed through its γ faces, while **CP7** and its enantiomer would give rise to the parallel sheet through the interaction from the α face. Analyzing the possibility of such structures, computational studies revealed that α-α parallel interaction would be very unfavorable with respect to the corresponding antiparallel dimers.[182] However, **CP6** could be favorably paired with its enantiomer through the γ-γ interaction in a parallel fashion as illustrated in Scheme 7. Interestingly, this new dimeric structure (**D6-8p**) would be generated through a new hydrogen bonding pattern. While the dimer composed of a single enantiomer (**D6a**) is paired with the analogous γ-residues of the opposite subunit, in the parallel β-sheet, each γ-residue is linked to the γ-units flanking the α-amino acid. In this case, the hydrogen-bonding pattern is very similar between both parallel and antiparallel dimeric structures. In both assemblies there are 5 atoms between each hydrogen-bonding groups (NH and CO), while in the previous architectures, the 3,3-atom separation in antiparallel α-α interaction (**D7a**) and 5,5-atom separation in γ-γ antiparallel interaction (**D6a**) changes to a 3,5-atom pattern in the parallel β-sheet (**D6-7p**, see Scheme 4). The novel arrangement (**D6-8p**) would lead to tubular systems with partial helicoidal character as the parallel conformation leads to a deviation of the alignment between amino acids of the same nature. Thus, the α-amino acids' side chains are aligned on top γ-residues so that, a nanotube structure following this pattern could present this helicoidal characteristic.

To evaluate this new interaction, we decided to prepare 2 new peptides (**CP8** and **CP9**). **CP8** is the enantiomer of **CP6**. This peptide would allow the study of the interaction through the peptide skeleton exclusively because the inclusion of Ala as α-Aa would avoid inter-side chain destabilizing effects. The main drawback of this strategy is the difficulty to differentiate both enantiomers by NMR. Specially, in this scenario that the self-assembly process is a fast equilibrium that do not allow to distinguish both forms (dimer and monomer). For that, we also prepared a second peptide (**CP9**) of opposite chirality (with respect to **CP6**) in which alanine residues were replaced by valine (Val). This peptide would help to identify all the components of the mixture. The incorporation of an amino acid with a bulkier side chain could favor the

formation of the parallel structure incorporating further van der Waals contacts among CPs. In addition, the different molecular mass would favor the spectroscopic identification.



Scheme 7. Structural model of the equilibria between the cyclic hexamers **CP6** and **CP8** to lead to the heterodimer **D6-8p** (parallel interaction). In the dimeric models, side chains were removed for clarity.

Synthesis

To address the synthesis of these new peptide units, we followed the same protocol used for **CP6**. We proposed a synthetic strategy in solution using Boc/OMe protecting groups that are compatible with both designs. First, the commercially available N-methylated α-amino acids (**H-*^{Me}N*-Ala-OH** and **Boc-*^{Me}N*-Val-OH**) were protected at their C-terminal end. For this purpose, the same synthetic conditions were used for both amino acids. Esterification was carried out by treating the residues with thionyl chloride in methanol. The reaction with **H-*^{Me}N*-Ala-OH** proceeded at room temperature. However, this reaction with **Boc-*^{Me}N*-Val-OH** did not work at room temperature and it was necessary to heat to reflux giving the corresponding methyl ester in quantitative yield confirming its reduced reactivity. During the reaction hydrochloric acid is produced leading to the elimination of the Boc protecting group at the N-terminal end.

In the next step, linear hexamers were grown from the corresponding dipeptides: **Boc-*D*-γ-Ach-*^{Me}N*-Ala-OMe** (**dp2**) and **Boc-*D*-γ-Ach-*^{Me}N*-Val-OMe** (**dp3**). These dipeptides were obtained by coupling each α-amino acid with **Boc-*D*-γ-Ach-OH** (**1'**) using *N*-HATU and DIEA in CH_2Cl_2. To arrive at the linear hexamer, a sequential deprotection and coupling steps, similar to those described for **CP6**, were carried out. First, tetrapeptides **tp2** and **tp3** were obtained by coupling together the respective dipeptides. Each tetrapeptide was attached in the next step to the corresponding dipeptide providing the linear hexamers **hp2** and **hp3**. As in the previous synthesis, for reaction with primary amines the chosen coupling agent was *N*-HBTU. Finally, **hp2** and **hp3** were cyclized with *N*-TBTU and DIEA under high dilution conditions providing the cyclic peptides **CP8** and **CP9**.

Structural Studies: γ-γ parallel interaction

First, we evaluated the combination of **CP6** with its enantiomer **CP8**. As expected, **CP8** exhibited the same behavior as its enantiomer in solution. The ^{1}H NMR spectrum showed a dynamic equilibrium between the monomer (**CP8**) and the dimer (**D8a**) at the NMR time scale. Therefore, **CP8** assembles with itself giving rise to the homodimer **D8a** with ~10^{2} M^{-1} association constants. Next, we proceeded to study the parallel interaction between the two peptides. For this, we followed the same procedure used in the previous experiments. In this case, we added progressively ascending quantities (0.2 equiv per addition) of a solution of **CP8** (30 mM) to another solution of **CP6** (6 mM) in deuterochloroform (Figure 51). In this experiment, upon the additions, a new set of signals that might be associated with the heterodimer were observed. At the amide region, one signal started to grow at 6.92 ppm after the addition of 0.6 equiv of the second enantiomer. This could be related with the formation of a second homodimer whose concentration was around half of the starting cyclic peptide (**CP6**). Further addition of **CP8** did not downfield shift the NH signal but it kept showing the increment of the new signal at 6.94 ppm. The intensity of this signal started to decrease upon addition of further equivalents. Additionally, the signal at 7.06 ppm moved to downfield chemical shift after the addition of 1 equiv of **CP8**. Other signals, as those corresponding to the N-methyl groups, also showed similar behavior. A new signal appeared at 3.01 ppm upon the addition of 0.6 equiv and kept growing until the addition of 1 equiv. The excess of **CP8** caused the displacement to downfield chemical shift of this novel signal. These results suggested that the antiparallel homodimeric forms (**D6a** and **D8a**) and the parallel heterodimer (**D6-8p**) might coexist in solution.

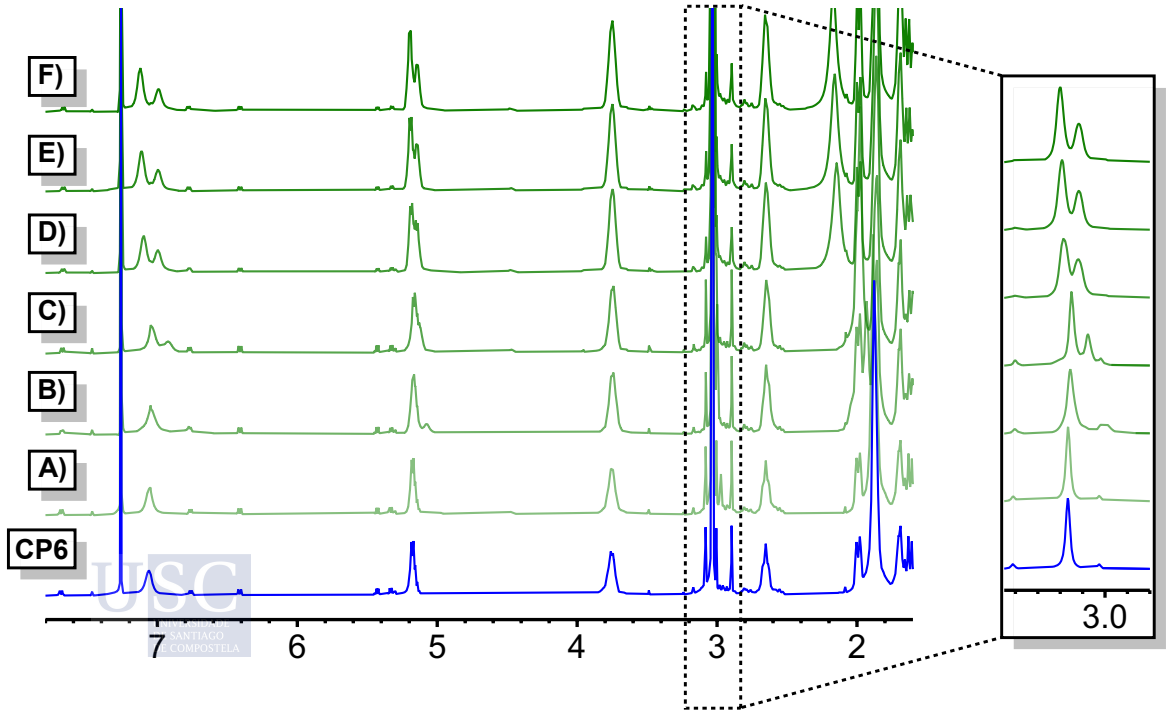


Figure 51. ^{1}H NMR spectra of the additions A) 0.2 equiv, B) 0.6 equiv, C) 1.0 equiv, D) 1.2 equiv, E) 1.4 equiv and F) 1.6 equiv (green spectra) of a solution of **CP8** (30.0 mM, red spectrum) to a solution of **CP6** (6.0 mM, blue spectrum) in $CDCl_3$ to evaluate the formation of the parallel heterodimeric structure.

To identify the signals from each system, we performed 2D-NMR experiments –TOCSY and NOESY– using the final mixture (Figure 52). Being **CP6** and **CP8** enantiomers, the ^{1}H NMR spectra are identical. As we expected, TOCSY indicated that both groups of signals present similar spin systems. The cross-peak traces between the signal at δ 3.74 ppm (Hγ of γ-Ach) and the signals that appear in the aliphatic region (between δ 1.3 and 2.2 ppm) allowed the identification of the corresponding protons of the cyclohexyl moiety of the γ-residue. Specifically, the signals at δ 1.87, 1.69, 1.67 and 1.41 ppm (highlighted in Figure 52) exhibit a nOe effect with the signal at δ 5.21 ppm (Hα of Ala) in the NOESY experiments of the mixture. These signals could only be attributed to the formation of the **D6-8p** heterodimer since in the parallel arrangement the γ-Ach residues lie on top of α-Aa. In contrast, the signal at δ 5.12 ppm did not show any cross-peak signal with the signals from the aliphatic region. These results suggested that both dimers (parallel and antiparallel) coexist in solution and that a dynamic equilibrium occurs at the NMR time scale. The nOe cross-peak signal between both NH_{Ach} δ 7.13 and 6.89 ppm might indicated the interconversion of both supramolecular species confirming the dynamic exchange between the parallel and antiparallel β-sheet structures.

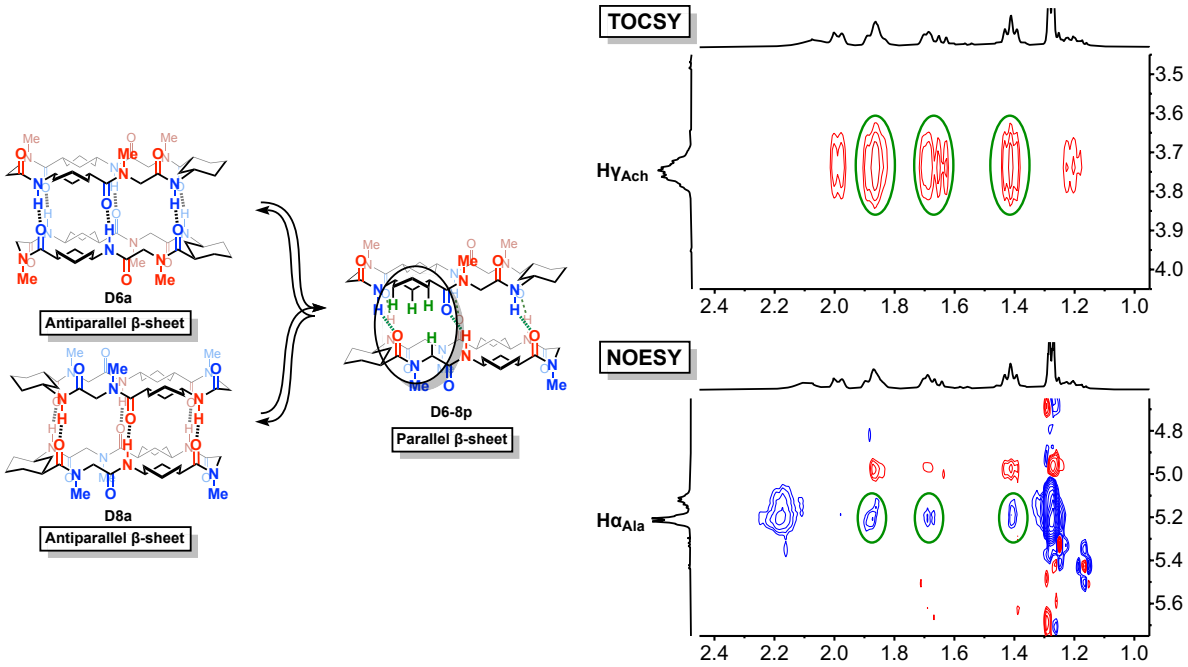


Figure 52. On the left, representation of the possible dimeric models. On the right, TOCSY spectrum (top, identified axial protons are highlighted in green) and NOESY spectrum (bottom, nOe effect between Hα of N-methyl alanine and those axial protons of the cyclohexane motif are also highlighted in green).

Finally, we performed measurements of the sample at lower temperatures. While the temperature of the system decreases, the equilibrium would also slow down. Therefore, it might allow to obtain more defined signals that would provide more evidence. The ^{1}H NMR spectra of the final mixture at -20 ºC and -40 ºC were recorded. In these spectra, it was noted that the NH_{Ach} signals move to downfield chemical shift (δ 7.91 ppm). Moreover, it was possible to detect signals around δ 6.5 ppm that could be attributed to the monomeric specie (non-assembled cyclic peptides). At lower temperatures, the dynamic equilibrium is slower than the NMR time scale, thus both species can be observed. We also noted that the N-methyl alanine

Hα signals overlapped into a single signal group. This fact is also observed in the signals of the N-methyl groups, which no longer appeared split into two singlets. In addition, the new signal at δ 2.17 ppm disappeared. Low-temperature NMR indicated that the formation of two dimers was not clearly established.

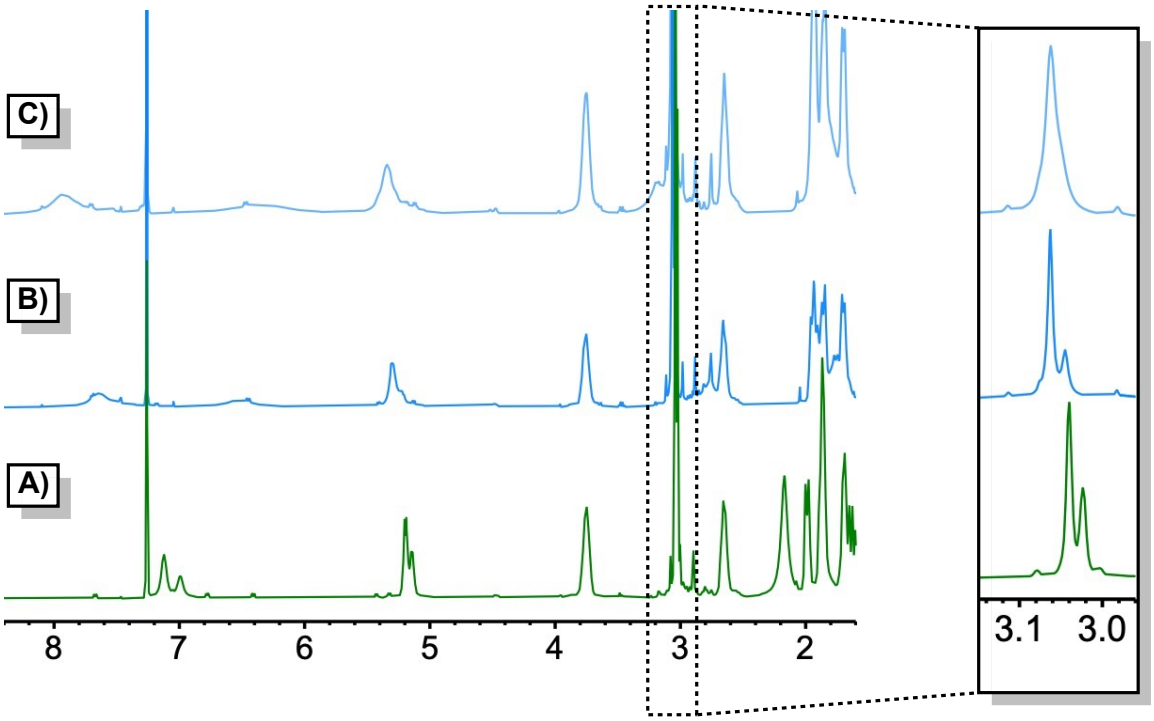


Figure 53. ^{1}H NMR spectra of the equimolar mixture of **CP6** and **CP8** at different temperatures A) 25 °C, B) −20 °C and C) −40 °C.

We next performed the same study but replacing α-amino acids. The use of an α-amino acid with a more voluminous side chain could favor the formation of the parallel heterodimer due to steric constraints between side chains of each subunit. As we have seen in the precedents of this chapter, Silk *et al.* have crystallized two SCPNs that group in parallel or antiparallel fashion introducing slightly modifications in the peptide sequence.[96] They observed that the inclusion of an amino acid with a bulkier side chain led to nanotubes that preferentially stacked in a parallel fashion.

Contrary to our expectations, the NMR spectrum of **CP9** (Figure 54) showed that the NH_{Ach} (δ 7.92 ppm) signal appeared at downfield chemical shift. This signal was not concentration-dependent, *i.e.*, its chemical shift did not vary with the concentration. These results suggested that **D9a** exhibits higher association constants than the Ala derivatives indicating that van der Waals contacts might favor the dimer formation. Therefore, the homodimer **D9a** is more stable than its Ala analogues (**D6a** or **D8a**). As previously observed, the planar structure necessary for supramolecular pairing is distorted in **CP6** and **CP8** due to repulsions between the methyl group located on the amine and the carbonyl of the α-amino acid.[119] Furthermore, it has been observed that the incorporation of Val into peptide sequences

preferentially leads to β-sheet like structures.[189] Hence, the use of Val in **CP9** could favor the establishment of a planar structure favoring γ-interaction as it aids to maintain the planar conformation necessary for peptide stacking.

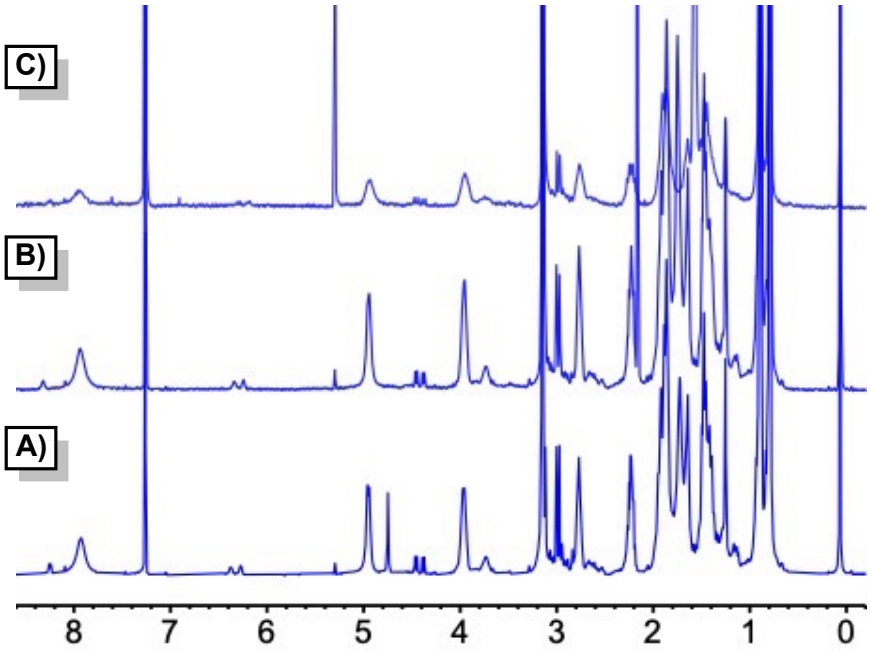


Figure 54. ^{1}H NMR spectra of **CP9** at different concentrations A) 16 mM, B) 6.6 mM and C) 1.5 mM.

We continued with the parallel formation experiment (Figure 55). For this, we followed the same protocol as in the previous studies. Increasing amounts (0.2 equiv) of a 25.6 mM solution of **CP9** were added on top of another solution of **CP6** (8.5 mM) in deuterochloroform. In the equimolar mixture, no change in the original signals of both cyclic peptides was observed. Possibly, the antiparallel dimer **D9a** is more stable, so parallel β-sheet formation is disfavored in this system and, therefore, the corresponding (**D6-9p**) heterodimer is not formed.

USC
UNIVERSIDADE DE SANTIAGO DE COMPOSTELA

[189] C. K. Smith, L. Regan, *Acc. Chem. Res*. **1997**, *30*, 153 – 161.

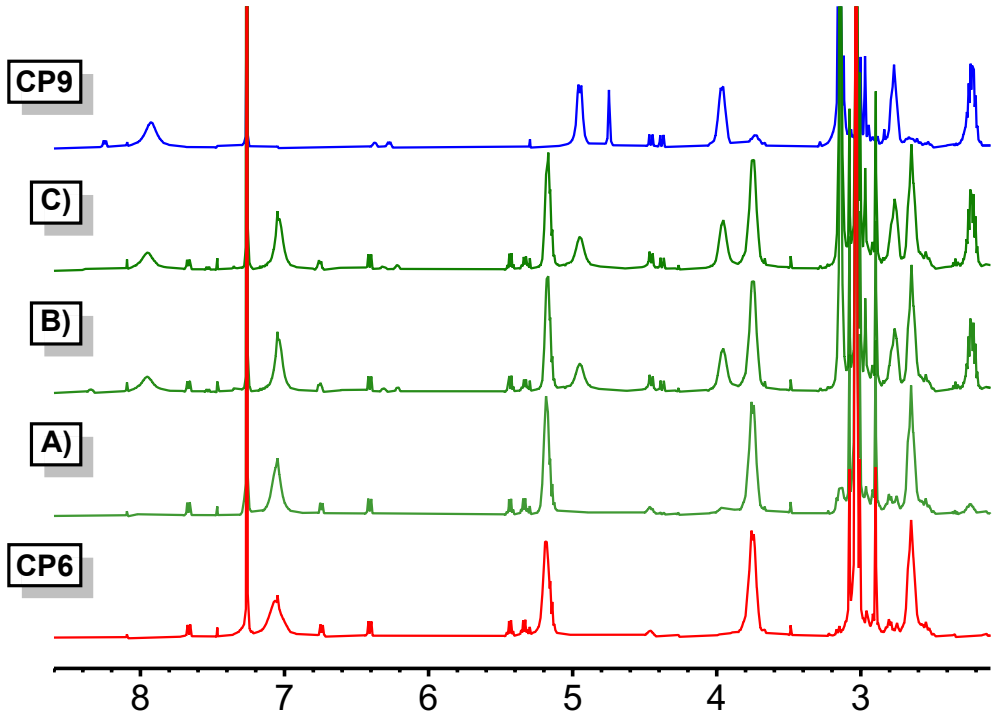


Figure 55. ^{1}H NMR spectra of the additions A) 0.2 equiv, B) 0.6 equiv and C) 1.0 equiv (green spectra) of a solution of **CP9** (25.6 mM, red spectrum) to a solution of **CP6** (8.5 mM, red spectrum) in $CDCl_3$ to evaluate the formation of the parallel heterodimeric structure.

In summary, in this chapter we have performed a structural study to elucidate the stability of parallel and antiparallel interactions between cyclic peptides containing δ- or γ-amino acids. The combination of these artificial residues with α-amino acids provided tubular supramolecular systems in which one (γ-Ach) or two (δ-Ach) methylene groups are oriented towards the interior of the hollow cavity increasing their hydrophobic character. To our knowledge, this is the first structural study performed with α,δ-CPs focusing on their structure and stability. Owing to the novelty of this system, we lacked considerable structural information. These experiments indicated that dodecamers and hexadecamers self-assembled with high association constants, while octamers remained as monomers in solution. Possibly, the structural rigidity of octamers caused by the inclusion of the δ-residue distorted the planar conformation constraining the stacking of the subunits. In contrast to *D,L*-α-CPs, in α,δ-cyclic peptide system the parallel arrangement was shown to be more stable. Computational studies revealed that this difference could be explained by the orientation of the δ-Ach axial hydrogens in the β-sheet structure. In parallel interaction, axial H-H repulsions between subunits are reduced. In addition, a comparison was carried out with α,γ-CPs on which structural studies regarding their stability had not been performed so far. Interestingly, these studies showed that the parallel sheet is more stable when both subunits share the same chirality. Also, the γ-γ parallel and antiparallel interaction present similar stability since equilibrium between both species was observable by NMR. In this case, the stability is influenced by the side chains. The incorporation of amino acids with bulky side chains preferentially forms the antiparallel β-sheet. These results contrast with previous assumptions about these systems and should be accounted for future designs of nanomaterials based on this type of cyclic peptides.

CHAPTER 2

USC
UNIVERSIDADE
DE SANTIAGO
DE COMPOSTELA

USC
UNIVERSIDADE
DE SANTIAGO
DE COMPOSTELA

CHAPTER 2

In the previous chapter, a structural study of α,δ-CPs was performed using dimeric models. These studies confirmed the self-assembly properties of these novel macrocyclic systems. In these models, one of the peptide faces is selectively blocked by N-alkylation restricting the growth of the assembly to the shorter structure: the dimer. Therefore, the elimination of these restricting alkyl group should allow the stacking of the subunits through both faces giving rise to the nanotube architecture. In this context, we decided to extend the study towards this end using α,δ-CPs.

α,δ-CYCLIC PEPTIDE NANOTUBES: 1ST GENERATION

DESIGN

As demonstrated above, the choice of peptide sequence is not trivial. A rational design is necessary to optimize the self-assembling properties. We have seen that both the length of the sequence –number of residues which determines the CP diameter– and the choice of amino acids influence the arrangement of the final structure. In the scenario of nanotube formation, this section is even more important as the polarity of the peptide increases, therefore the solubility of the nanotubes is compromised in low polar solvents. It should be mentioned that SCPNs made of standard non-polar residues are not very soluble in non-polar solvents because the formation of hydrogen bonds in these media is so favored, then nanotubes grow until they come out of the solution.

Based on the previous results (Chapter 1), we opted for the alternation of α-amino acids with δ-residues that leads to the required planar structure in which the hydrogen bonding complementarity is retained. We also noted that macrocycles consisting of 12 and 16 amino acids provided stable supramolecular structures. For this reason, we decided to prepare a 12-residue α,δ-CP because of the easier synthetic feasibility. For the choice of α-amino acids we decanted for polar residues that could help to solubilize the final product in aqueous media. The incorporation of amino acids such as lysine (Lys) and glutamic acid (Glu) residues, in addition to increasing aqueous solubility, would contribute to the ring stacking by establishing salt bridge interactions along the tube. It was also decided to include a hydrophobic amino acid (Leu) that would facilitate the synthetic process improving the solubility in less polar solvents, such as DMF. In addition, this residue would participate in the self-assembly process through hydrophobic effects.[94,190] The last amino acid selected was arginine (Arg) whose guadinium group has a positive charge in a wide pH range and would promote the SCPNs deposition on anionic surfaces that could help in the characterization of the nanotube. Based on these assumptions, it was decided to prepare *c*-[*D*-Lys-δ-Ach-*L*-Leu-δ-Ach-*D*-Glu-δ-Ach-*L*-Glu-δ-Ach-*D*-Arg-δ-Ach-*L*-Lys-δ-Ach-] (**CP10**, Figure 56). In this design, we envisaged that the most stable CP stacking would be that in which the Glu and Lys residues are paired guided by electrostatic attractions. This arrangement would align the Arg side chains along the nanotube

[190] I. Insua, J. Montenegro, *J. Am. Chem. Soc.* **2020**, *142*, 300 – 307.

axis which would facilitate their subsequent deposition. Additionally, on the opposite side would be aligned Leu residues. Computational studies carried out by Martin Calvelo confirmed this structure over other parallel and antiparallel stacking.[182]

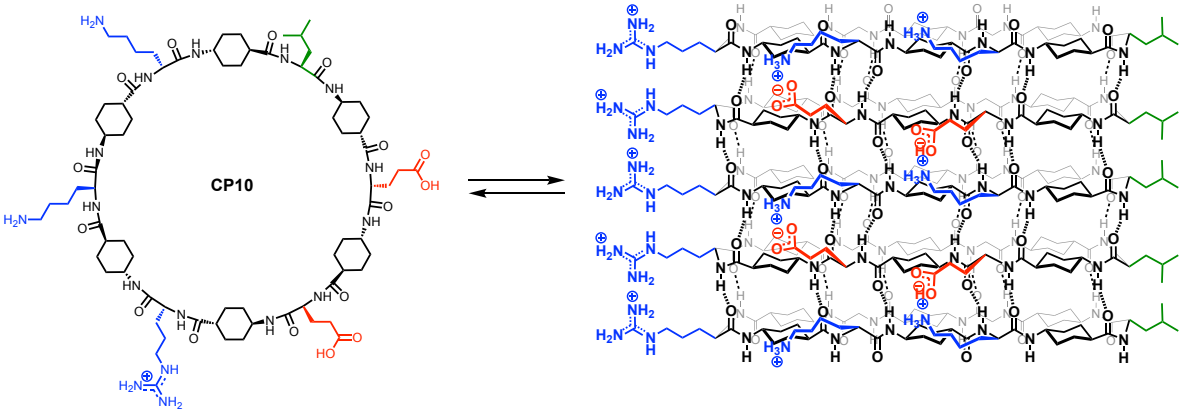


Figure 56. Proposed design for water-soluble nanotube-forming α,δ-cyclic peptide **CP10**.

SYNTHESIS

Once the design was settled down, we proceeded with the synthesis of the peptide. The proposed design (**CP10**) does not have any N-methylated residue, the polarity of the strands increases as the chain grows (higher proportion of amide bonds) and consequently, the solubility of the products is compromised in standard low polar solvents used in solution synthetic procedures. This limitation is especially reflected in the purification processes required after each coupling step. For this reason, we opted for the solid-phase peptide synthetic (SPPS) methodology.[191] This process consists of attaching the first amino acid to a polymeric support which is insoluble under the synthesis conditions. Then, the same two-step sequence is repeated until the fully protected desired peptide is formed. First step, the N-terminal end of the amino acid (or peptide) anchored to the resin is deprotected and then, a subsequent amino acid coupling step is performed in the presence of the appropriate coupling reagents. The synthesis of the peptide grow form the C-terminus to the N-terminus of the peptide. The advantage of this methodology is that a large excess of reagents can be use because the elimitation of reaction side-products and excess of reagents can be easily done through a simple washing and filtration process which avoids tedious intermediate purification stages.

The first residue is usually anchored to the solid support via the carboxylate group at the C-terminal end (Figure 57, Path A). Alternatively, the first amino acid can be attached through its side chain (Figure 57, Path B).[192] The first option constrains the preparation of cyclic peptides, because the resulting linear peptide must be separated from the resin to run in-solution cyclization. Therefore, this approach would entail too many drawbacks, since the cyclization step must take place once the peptide is released having all α-amino acids side chains protected

USC UNIVERSIDADE DE SANTIAGO DE COMPOSTELA

[191] **a)** P. Lloyd-Williams, F. Albericio, E. Giralt, *Tetrahedron*, **1993**, *49*, 11065 – 11133. **b)** R. B. Merrifield, *J. Am. Chem. Soc*. **1993**, *85*, 2149 – 2154.

[192] J. N. Lambert, J. P. Mitchell, K. D. Roberts, The synthesis of cyclic peptides. *J. Chem. Soc. Perkin Trans 1* **2001**, 471 – 484.

to avoid undesired side reactions, in addition to the aforementioned solubility issues. The only exception is the use of oxyme resins that allow the N- to C-cyclization and cleavage in the same step.[193] Unfortunately, this methodology has a number of limitations for the synthesis of long peptides and complex sequences. For this reason, there is a synthetic alternative in which the first amino acid are attached through a residue lateral chain.[193] This will allow to carry out the cyclization on the solid support.[194] Another important consideration is the choice of the protecting groups which will also determine the type of resin used. In general, the N-terminal end is protected as a carbamate because these groups have been shown to give high coupling reaction yields.[195] In solid phase, the fluorenylmethoxycarbonyl (Fmoc) strategy is the usual method of choice.[196] This N-protecting group is stable to many of coupling and deprotection conditions and it is removed using bases or nucleophiles, usually piperidine. For our system, the Fmoc/^{t}Bu strategy would be the most suitable, so that it would involve the use of acid-labile protecting groups on amino acid side chains. These groups are removed during the peptide cleavage step. However, as we will perform the last stage of cyclization on resin, a three-dimensional orthogonal strategy is necessary. For this purpose we opted for the allylic ester which is stable to mild acidic and basic conditions and can be removed by treatment with Pd(0) solutions in presence of nucleophiles.[194]

USC UNIVERSIDADE DE SANTIAGO DE COMPOSTELA

[193] C. Bérubé, A. Borgia, N. Voyer, *Tetrahedron Lett*. **2018**, 59, 4176 – 4179.
[194] S. A. Kates, Nuria A. Solé, C. R. Johnson, D. Hudson, G. Barany, F. Albericio, *Tetrahedron Lett*. **1993**, *34*, 1549 – 1552.
[195] F. Albericio, *Biopolymers* **2000**, *55*, 123 – 139.
[196] **a)** R. Behrendt, P. White, J. Offer, *J. Pept. Sci*. **2016**, *22*, 4 – 27. b) L. A. Carpino, G. Y. Han, *J. Am. Chem. Soc*. **1970**, *92*, 5748 – 5749.

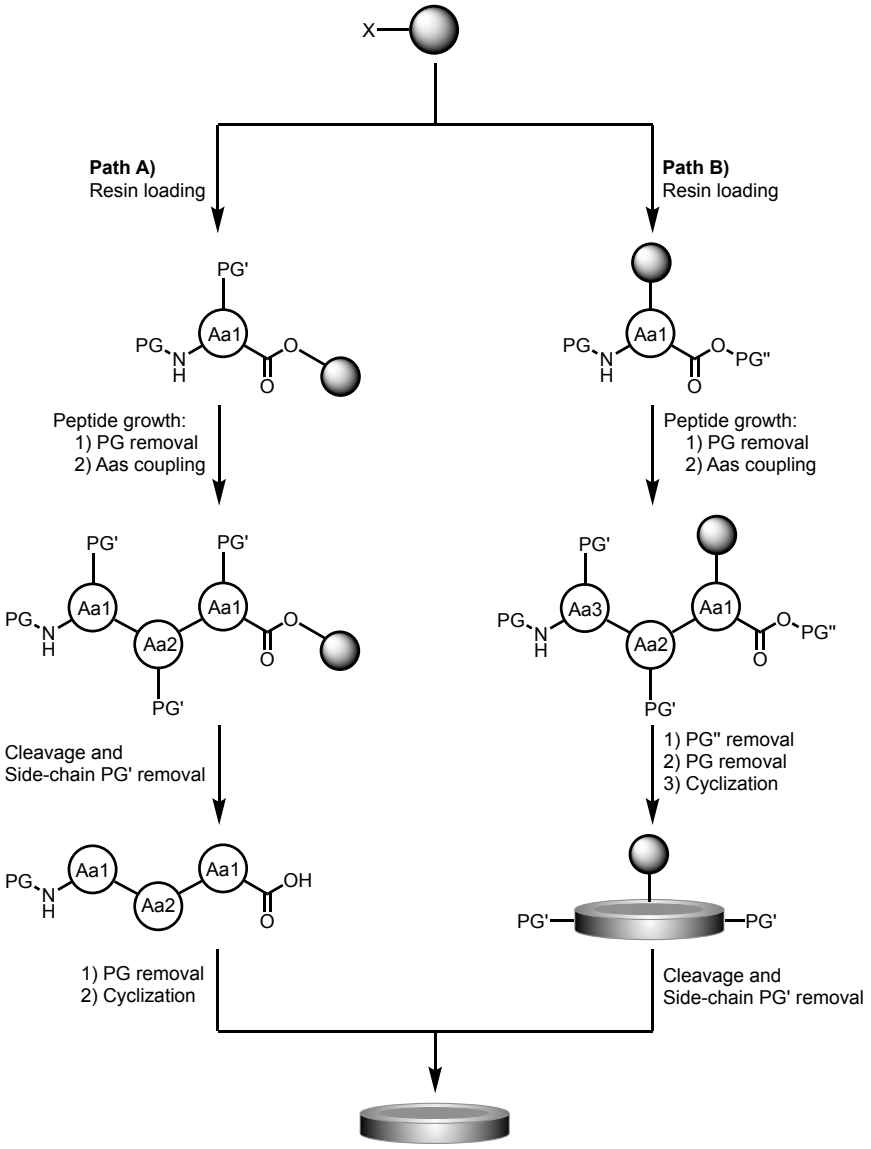
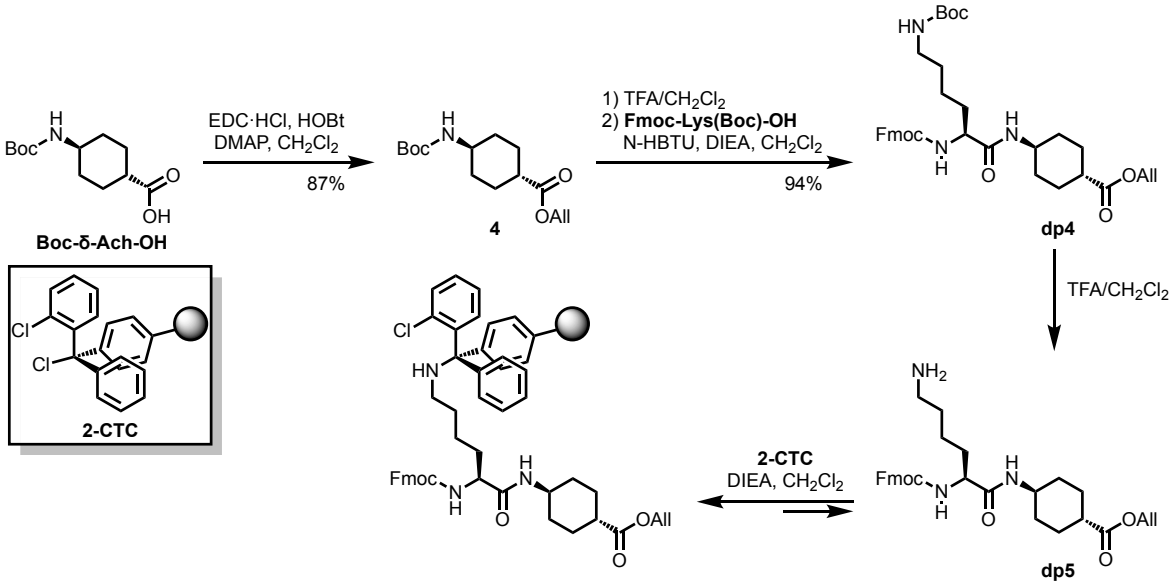


Figure 57. Schematic representation of solid-phase peptide synthesis. Path A) the first amino acid is anchored through the C-terminal group and Path B) the first amino acid is anchored through its lateral chain.

Based on the above considerations, a strong-acid labile solid support was selected: 2-chlorotrytil chloride resin (2-CTC). 2-CTC resin is loaded via a heterolytic cleavage of chloro-trityl bond leading to a stable trityl cation that react with nucleophiles present in the media.[197] In our synthetic plan we look for performing on-resin cyclization from the amino group of an α-residue. For this purpose, we decided to load the resin with dipeptide Fmoc-*L*-Lys-δ-Ach-OAll (**dp5**). This should lead to better yields in the cyclization step. Arguably, the conformational rigidity of the δ-Ach restricts the course of the amide bond formation from this residue making more difficult the nucleophilic attack in the cyclization process. Dipeptide **dp5** was prepared in solution from commercially available **Boc-δ-Ach-OH** (Scheme 8). First, this amino acid was protected by the treatment with allyl alcohol in the presence of EDC·HCl, HOBt

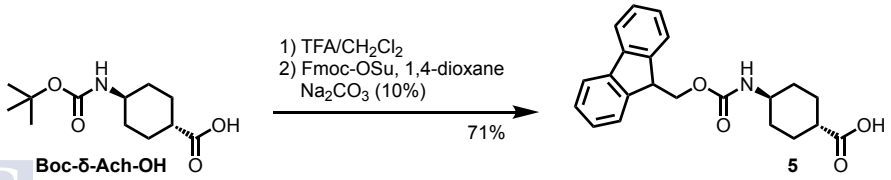
[197] K. Barlos, O. Chatzi, D. Gatos, G. Stravropoulos, *Int. J. Peptide Protein Res*. **1991**, *37*, 513 – 520.

and DMAP to give rise to the corresponding ester **4**. The Boc-group was later removed by stirring **4** in a mixture of TFA/CH_2Cl_2 and subsequently, coupled with **Fmoc-*L*-Lys(Boc)-OH**. For this transformation, *N*-HBTU was used as coupling agent and provided the fully protected dipeptide (**dp4**). Finally, Lys side chain protecting group (Boc) was removed by acid treatment with a TFA/CH_2Cl_2 mixture to provide Fmoc-*L*-Lys-δ-Ach-OAll (**dp5**) in almost quantitative yield. This dipeptide was attached to the swallowed resin under anhydrous conditions in the presence of base (Scheme 8). The resin loading was calculated by using the Fmoc quantification procedure.[198] For this, a weighed small portion of dried resin (~10 mg) was treated with a piperidine/DMF mixture (1:4 v/v) for 30 min to remove the Fmoc protecting group. Then, an aliquot of this solution was diluted and the absorbance of the final sample was recorded at 290 and 301 nm. The loading was calculated using the extinction coefficients for dibenzofulvene adducts reported in literature.[198]



Scheme 8. Preparation of **dp5** from **Boc-δ-Ach-OH** followed by polymeric **2-CTC** resin loading.

On the other hand, Fmoc-δ-Ach-OH (**5**) was prepared for its used in SPPS. For this purpose, **Boc-δ-Ach-OH** was stirred in a TFA/CH_2Cl_2 mixture and subsequently, the resulting ammonium salt was treated with Fmoc-OSu in basic conditions giving rise to Fmoc-protected δ-residue **5** (Scheme 9).

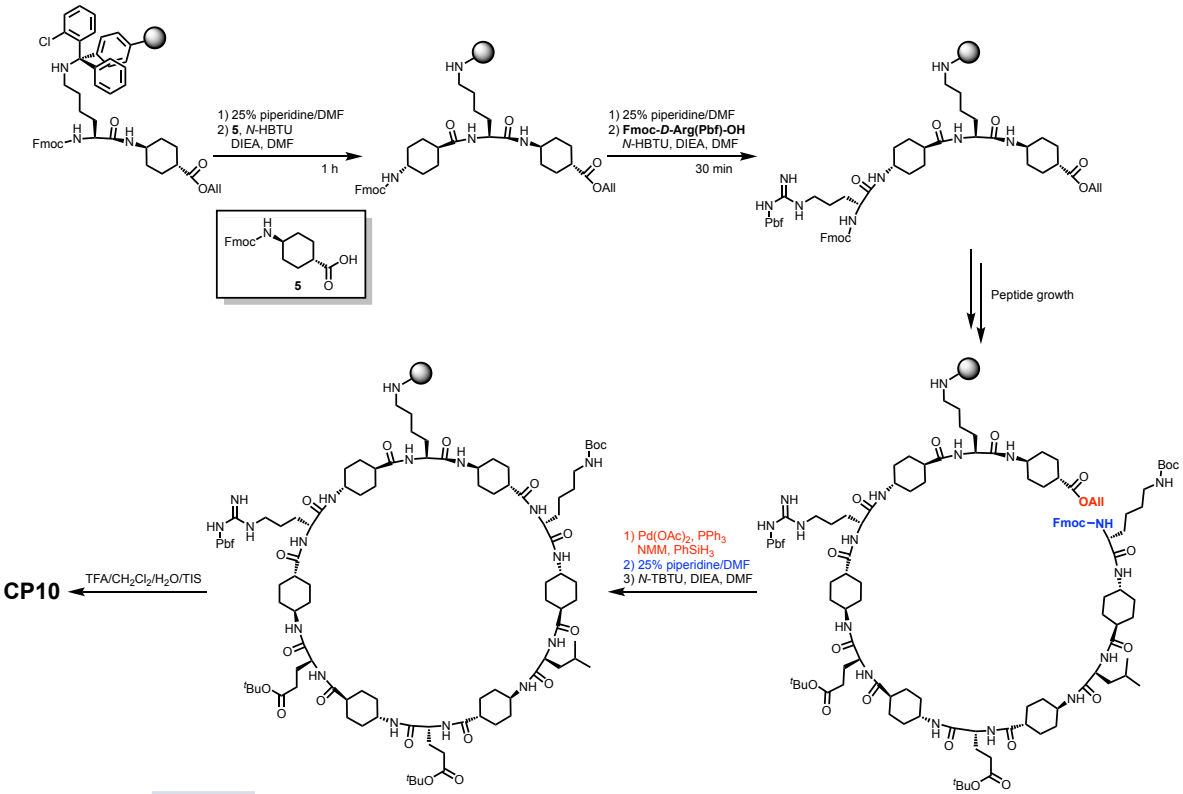


Scheme 9. Preparation of Fmoc-δ-Ach-OH (**5**) for its use in SPPS.

USC UNIVERSIDADE DE SANTIAGO DE COMPOSTELA

[198] J. Meienhofer, M. Waki, E. P. Heimre, T. J. Lambros, R. C. Makofske, C.-D. Chang, *Int. J. Pept. Protein Res.* **1979**, *13*, 35 – 42.

Once **dp5** was anchored to the solid support, the linear peptide was grown following the synthetic strategy represented in Scheme 10. To carry out each coupling stage, Fmoc was removed by treatment with a solution of piperidine in DMF (25% v/v) for 20 min. After this time, the mixture was filtered and thoroughly washed with DMF for three times. Then, the preformed active ester of the corresponding amino acid was added to the resin.[199] For ester activation, a solution of the required amino acid and *N*-HBTU (3.0 equiv) in DMF was treated with DIEA and stirred for 1 min and then poured into the solid-phase reactor containing the swelled resin. For the coupling reaction of the commercially available α-amino acids, 3 equiv were used and the stirring lasted for 30 min. Alternatively, 1.5 equiv of Fmoc-δ-Ach-OH (**5**) and longer reaction time (1 h) were used because we did not worry too much for the epimerization of **5** during long coupling reactions saving time and cost in its preparation. After each coupling, the mixture was filtered and the excess of reagents was removed by several washing/filtration process (3 times) with DMF. These steps were repeated each time until the linear peptide was obtained. During the synthesis, the progress of the reactions was checked by TNBS test.[200] The coupling step was repeated with half of the equiv in case of positive test. Moreover, every four coupled amino acids a small sample of resin was taken, the peptide was released from the solid support and the resulting solution was analyzed by HPLC-MS.



Scheme 10. Solid-phase peptide synthesis strategy for the preparation of **CP10**.

USC UNIVERSIDADE DE SANTIAGO DE COMPOSTELA

[199] S. B.D. Kent, D. Alewood, P. F. Alewood, M. Baca, A. Jones, M. Schnölzer, *Innovation and Perspectives in Solid Phase Synthesis* (R. Epton Ed.) Intercept Ltd., U.K. **1992**.

[200] C. Kay, O. E. Lorthioir, N. J. Parr, M. Congreve, S. C. McKeown, J. J. Scicinski, S. V. Ley, *Biotechnol. Bioeng*. **2000**, *71*, 110 – 118.

For the cyclization, C-terminal and N-terminal protecting groups were removed sequentially in this order. To liberate the carboxylic group, the resin was treated under argon atmosphere with a mixture of PPh_3, $Pd(OAc)_2$, N-methylmorpholine (NMM) and phenylsilane in dry CH_2Cl_2 during 5 h. Then, the mixture was filtered, and the resin was washed twice with a sodium diethyldithiocarbamate solution in DMF (0.5% w/v) for 30 min and 3 times with a solution of DIEA in DMF (10% v/v) for 10 min. Then, a small portion cleavage and checked by HPLC-MS. Afterwards, the N-terminal protecting group was removed by treatment with a solution of piperidine in DMF (25% v/v). In this case, the resin was shaken for 45 min to ensure the complete Fmoc-removal. Finally, the resulting linear peptide was on-resin cyclized using *N*-TBTU as coupling reagent in presence of DIEA in DMF for 12 h. Again, the progress of the reaction was checked by HPLC-MS to confirm the absence of starting linear peptide and the formation of the desired cyclic peptide.[201]

Finally, the cyclic peptide was cleaved from the resin by treatment with a mixture of TFA/CH_2Cl_2/H_2O/TIS (9:5:2.5:2.5:2.5) for 2 h. After this time, the mixture was filtered and the resulting filtrates were precipitated by pouring over chilled diethyl ether. Unfortunately, the obtained precipitate turned out to be insoluble in water. However, it was partially soluble in aqueous mixtures with organic solvents (≥ 1:1 MeOH/H_2O or ACN/H_2O). Due to the high portion of organic solvent required, purification by HPLC proved impossible, instead the crude was purified by washes with cold MeOH. Under this condition we obtained a white solid that was composed mainly by compound **CP10**, as could be inferred by its spectroscopic properties.

CP10 structure was confirmed by several techniques. ^{1}H NMR spectra were recorded using deuterated trifluoroacetic acid (CF_3CO_2D) or DMSO-*d6* (Figure 58A). These spectra showed broad and poorly defined signals because the high aggregation of the system together with the different possible conformations affect to the resolution of the spectra. Still, characteristic groups of signals were identified that are highlighted in Figure 58A. Maldi mass spectrometry allowed to corroborate the obtention of the peptide. In the IR spectrum, intense amide I and amide II bands were detected at 1542 and 1632 cm^{-1} which are attributed to a hydrogen-bonded antiparallel β-sheet structure. The amide A stretch band at 3270 cm^{-1} supported the ring-to-ring piled tubular structure with an average inter-annular distance of 4.75-4.8 Å.[202]

USC UNIVERSIDADE DE SANTIAGO DE COMPOSTELA

[201] For more synthetic details see: Solid phase synthesis (Experimental Section).
[202] H. S. Kim, J. D. Hartgerink, M. R. Ghadiri, *J. Am. Chem. Soc*. **1998**, *120*, 4417 – 4424.

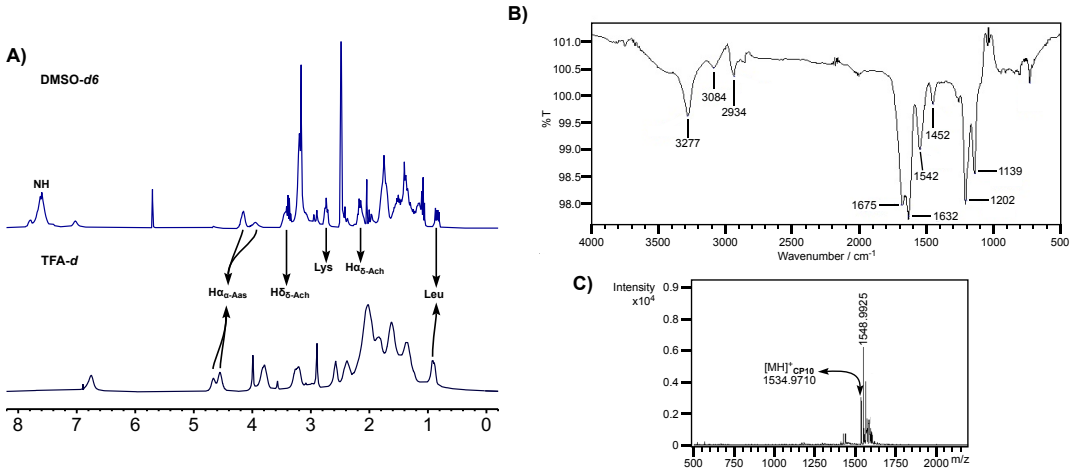


Figure 58. Characterization of **CP10**: A) ^{1}H NMR spectra registered in different solvents [DMSO-*d6* (top) and TFA-*d* (bottom)], B) FTIR spectrum (neat) and C) MALDI-TOF mass spectrum.

NANOTUBE CHARACTERIZATION

Once the peptide was characterized, we studied the self-assembly properties in solution by using fluorescence spectroscopy in the presence of thioflavin T (ThT).[203] ThT is a planarizable probe used for the detection of amyloid aggregates, such as in Alzheimer's disease, whose fluorescence increases after binding to β-sheet structures. For this experiment, the addition of increasing amounts of a stock solution of **CP10** (2 mM) in a MeOH/H_2O (0.5% TFA) over a solution of ThT (20 μM) in the same solvent mixture was monitored (Figure 59). It was observed that the intensity of the emission band (excitation wavelength 420 nm) at 485 nm increased with peptide concentration. These results suggested the in-solution peptide aggregation. To corroborate that these changes are related with the self-assembly process, different control studies were carried out. First, the percentage of TFA (1% TFA) in the sample was increased, whereas, in the second control analysis, the concentration of ThT was changed to 50 μM. Both samples gave similar results, demonstrating that the fluorescent rise is explained by β-sheet structures supramolecular association. On the other hand, the same experiment was performed using a less polar organic co-solvent, such as ACN. Samples of **CP10** (2 mM) in ACN/H_2O containing 0.1% TFA did not produce any modification in emission intensity. With this solvent mixture, it was necessary to add up to 5% TFA to observe fluorescence activity. Presumably, due to the poor solubility of the cyclic peptide in this solvent composition.

USC UNIVERSIDADE DE SANTIAGO DE COMPOSTELA

[203] **a)** R. Khurana, C. Coleman, C. Ionescu-Zanetti, S. A. Carter, V. Krishna, R. K. Grover, R. Roy, S. Singh, *J. Struct. Biol.* **2005**, *151*, 229 – 238. **b)** P. K. Singh, A. K. Mora, S. Nath, *Chem. Commun*. **2015**, *51*, 14042 – 14045.

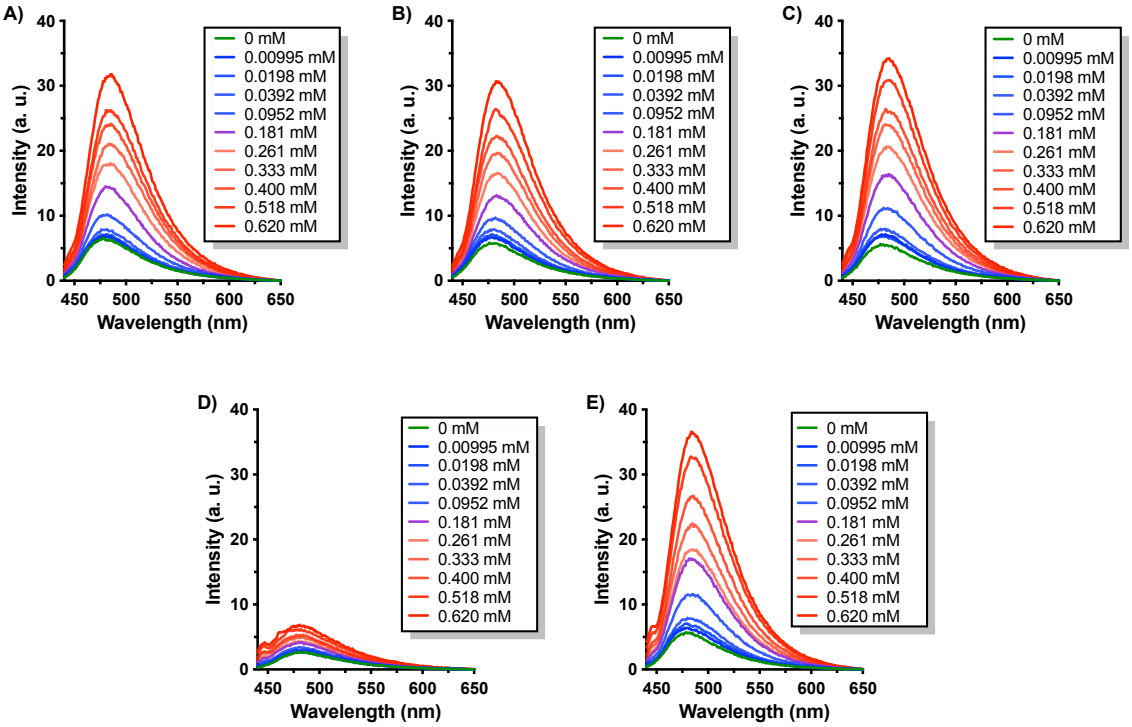


Figure 59. Fluorescence spectra of increasing additions of a 2 mM solution of **CP10** over a ThT solution in A) MeOH/H_2O (0.5% TFA, [ThT]= 20 μM), B) MeOH/H_2O (1% TFA, [ThT]= 20 μM), C) MeOH/H_2O (0.5% TFA, [ThT]= 50 μM), D) ACN/H_2O (0.1% TFA, [ThT]= 20 μM) and D) ACN/H_2O (5% TFA, [ThT]= 20 μM).

The next step involved nanotube imaging. As stated above, in the cyclic peptide sequence, an Arg residue was incorporated whose guanidinium group would promote the adhesion of the nanotube on anionic surfaces by electrostatic forces. Deposition of peptide solutions on mica (anionic solid support) would permit the characterization of the tubular assemblies by Atomic Force Microscopy (AFM). To this end, we first attempted to optimize the deposition conditions on the solid support. Table 2 summarizes the different conditions tested. The general procedure consisted of casting **CP10** samples (20 μL) on mica varying different parameters such as sample concentration, solvent composition or contact time with the surface. After the indicated time, the surface was washed with the solvent mixture employed for deposition and dried under a flow of argon (Ar).

USC UNIVERSIDADE DE SANTIAGO DE COMPOSTELA

ENTRY	[CP10] (mM)	SOLVENT COMPOSITION	DEPOSITION TIME (min)	AFM
1	1	MeOH/H_2O (1% TFA)	15	-
2	1	MeCN/H_2O (1% TFA)	15	Amorphous aggregates
3	1	THF/H_2O (1% TFA)	15	Amorphous aggregates
4	1	MeOH/H_2O (1% TFA)	To dryness	Amorphous aggregates
5	1	MeCN/H_2O (1% TFA)	To dryness	Amorphous aggregates
6	1	THF/H_2O (1% TFA)	To dryness	Amorphous aggregates
7	0.1	MeOH/H_2O (1% TFA)	15	-
8	0.25	MeOH/H_2O (1% TFA)	15	-
9	0.5	MeOH/H_2O (1% TFA)	15	-
10	2	MeOH/H_2O (1% TFA)	15	-
11	0.5	MeOH/H_2O (1% TFA)	30	Nanotubes
12	2	MeOH/H_2O (1% TFA)	30	Nanotubes

Table 2. Summary of the conditions tested for deposition of **CP10** on mica surface to be analyzed by AFM.

We first studied the most suitable solvent mixture. In this scenario, organic co-solvents of different polarity were evaluated. The use of less polar co-solvents (such as ACN or THF) could contribute to the formation of nanotubes through hydrophobic effects between δ-residues, in addition these solvents would reduce the competition for the formation of hydrogen bonds. However, in all the samples analyzed, amorphous aggregates with different heights were observed. Deposition time was also adjusted. For this, samples were left on the solid support until dryness. Under these conditions, no defined structures were detected either. Finally, we performed a screening of concentrations and casting time using MeOH/H_2O (1% TFA) as solvent mixture because it gave the best results in the fluorescence studies. In Figure 60, AFM micrographs taken from the conditions of entries 11 and 12 can be observed. Tubular structures with lengths of about 0.8 μm can be seen in these images. But the height profile of the assemblies (between 1.2-1.8 nm) did not match with the expected sizes for this system.

USC UNIVERSIDADE DE SANTIAGO DE COMPOSTELA

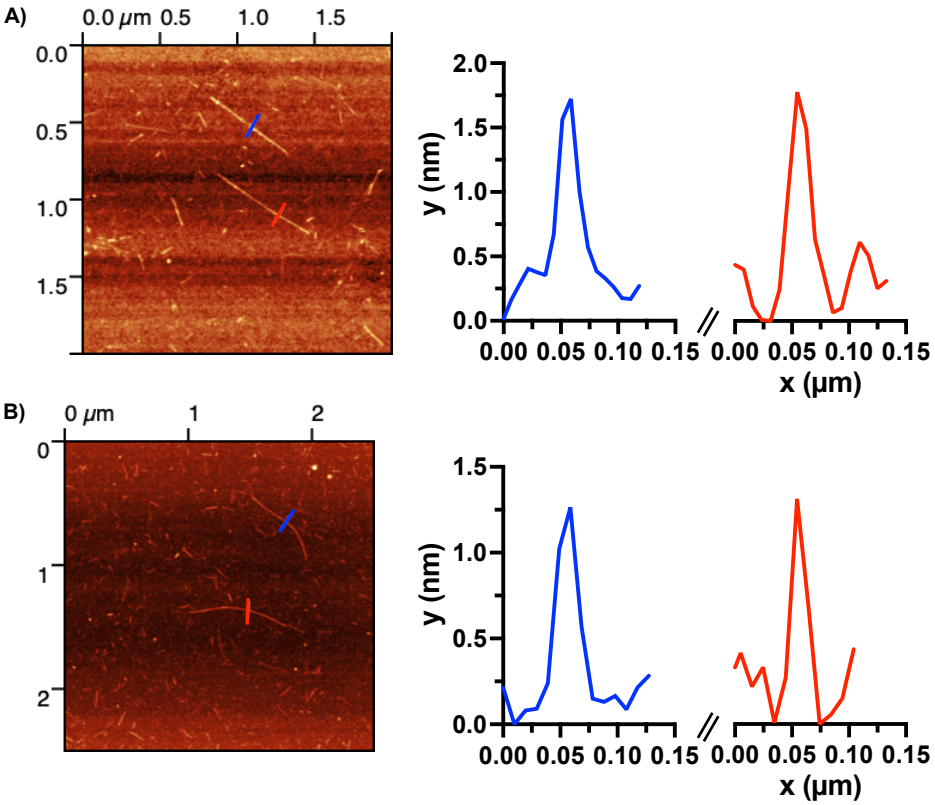


Figure 60. AFM topography micrographs of a **CP10** solution in a MeOH/H_2O mixture (1% TFA) at A) 2 mM and B) 0.5 mM.

In complement to the AFM studies, fluorescence microscopy studies were also conducted. Given the lack of a fluorophore group in the peptide, these studies were carried out in presence of ThT (20 μM). For this purpose, different samples were prepared varying the solvent composition and dropped on a slide. The samples were observed under the microscope in solution or dried on the glass slide. Table 3 summarizes the different conditions evaluated for the characterization of the nanotubes.

USC UNIVERSIDADE DE SANTIAGO DE COMPOSTELA

ENTRY	[CP10] (mM)	SOLVENT COMPOSITION	DEPOSITION TIME (min)	FLUORESCNCE MICROSCOPY
1	1	MeOH/H_2O (1% TFA)	Solution	-
2	1	MeCN/H_2O (1% TFA)	Solution	-
3	1	THF/H_2O (1% TFA)	Solution	-
4	1	MeOH/H_2O (1% TFA)	Dried	-
5	1	MeCN/H_2O (1% TFA)	Dried	-
6	1	THF/H_2O (1% TFA)	Dried	-
7	0.5	MeOH/H_2O (1% TFA)	Solution	Fibrils
8	0.5	MeOH/H_2O (1% TFA)	Dried	Fibrils
9	2	MeOH/H_2O (1% TFA)	Solution	-
10	2	MeOH/H_2O (1% TFA)	Dried	-

Table 3. Summary of the conditions tested for of **CP10** drop-casting on a slide for epifluorescence microscopy analysis.

Unfortunately, no evidence of nanotube formation was detected in most of the samples measured. However, in the conditions of entries 7 and 8 (Figure 61) some fibrillar aggregates were observed that could be attributed to the lateral association of several nanotubes giving rise to bundles.

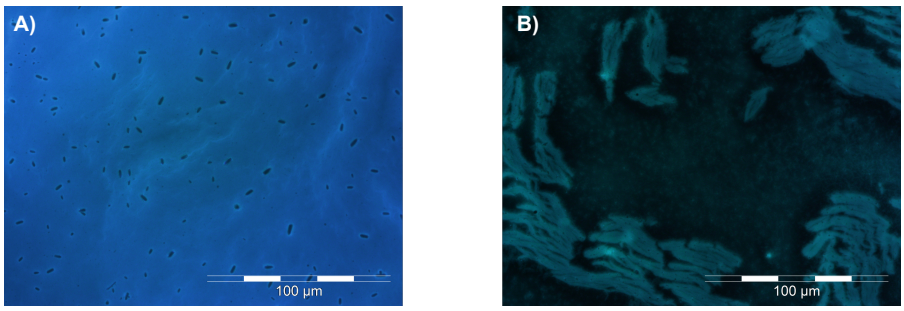


Figure 61. Epifluorescence microscopy images obtained from deposition of a solution of **CP10** in MeOH/H_2O (1% TFA) containing ThT (20 µM) from entries A) 7 and B) 8 (Table 3).

α,δ-CYCLIC PEPTIDE NANOTUBES: 2ND GENERATION

DESIGN REVISION

In light of the obtained results, we decided to make some changes to the peptide structure. In the new sequence, a Lys and a Glu residue were replaced by two histidine (His) amino acids. The incorporation of His would favor the solubility in aqueous media and facilitate its purification and characterization, as previously found for another nanotube forming cyclic peptides.[174] In addition, it would provide some control over the self-assembling properties

(pH modification) under neutral conditions.[204] The novel sequence was *c*-[*D*-His-δ-Ach-*L*-Leu-δ-Ach-*D*-His-δ-Ach-*L*-Glu-δ-Ach-*D*-Arg-δ-Ach-*L*-Lys-δ-Ach-] (**CP11**).

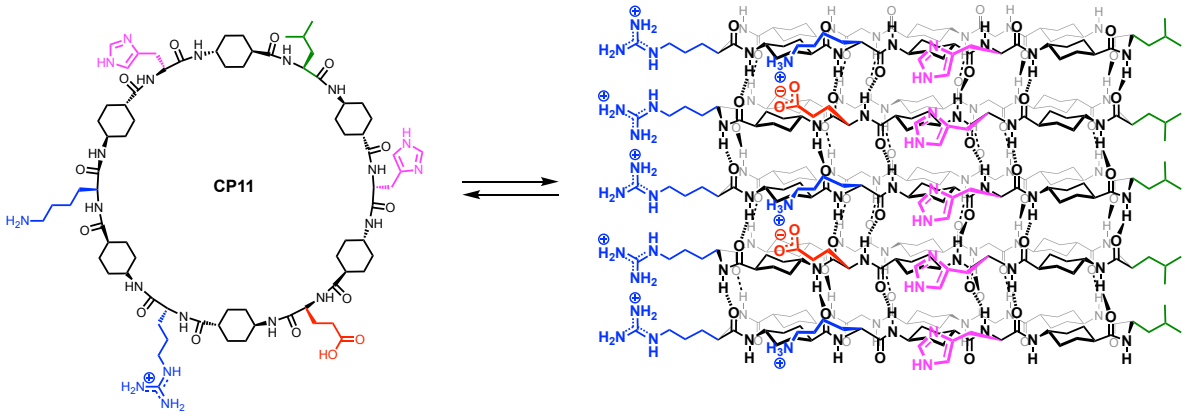


Figure 62. Proposed design modification for water-soluble nanotube-forming α,δ-cyclic peptide **CP11**.

SYNTHESIS

The same solid-phase strategy described above was followed for the synthesis of **CP11**. The peptide was synthesized on 2-CTC polymeric support using the Fmoc/^{t}Bu approach. The resin was loaded with the dipeptide Fmoc-*L*-Lys-δ-Ach-OAll (**dp5**) and the linear peptide was grown manually following the typical deprotection/coupling cycles. Finally, both terminal ends were deprotected and the peptide was cycled on resin prior to its cleavage. After treatment with TFA cocktail, the crude was precipitated on cold Et_2O, dried and purified by HPLC (see Experimental Section for details). During purification, peptide aggregation issues were observed as the ratio of ACN in the solvent mixture increased. To prevent aggregation, hexafluoroisopropanol (HFIP) was added to the mobile phase.[205] HFIP would act as a destabilizing solvent favoring the elution of the product as a monomer. After purification, the collected fractions were freeze-dried providing **CP11** as a white solid.

The peptide structure was confirmed by NMR and ESI-TOF MS (Figure 63). This time, ^{1}H NMR spectrum was recorded in D_2O showing well-defined sharp signals, such as those corresponding to the NH groups, Hα of α-Aas, Hδ of δ-Ach, Hα of δ-Ach and other relative to the side chains of α-residues. In the IR spectrum, the amide I and amide II bands appeared at 1537 and 1627 cm^{-1}, respectively, confirming the β-sheet type structure. The amide A signal was also observed at 3270 cm^{-1} suggesting the tight packing between subunits.

USC UNIVERSIDADE DE SANTIAGO DE COMPOSTELA

[204] Y. Le Duc, M. Michau, A. Gilles, V. Gence, Y.-M. Legrand, A. van der Lee, S. Tingry, M. Barboiu, *Angew. Chem. Int. Ed.* **2011**, *50*, 11366 – 11372.

[205] **a)** P. A. Korevaar, C. J. Newcomb, E. W. Meijer, S. I. Stupp, *J. Am. Chem. Soc.* **2014**, *136*, 8540 – 8543. **b)** K. Sato, W. Ji, L. C. Palmer, B. Weber, M. Barz, S. I. Stupp, *J. Am. Chem. Soc.* **2017**, *139*, 8995 – 9000.

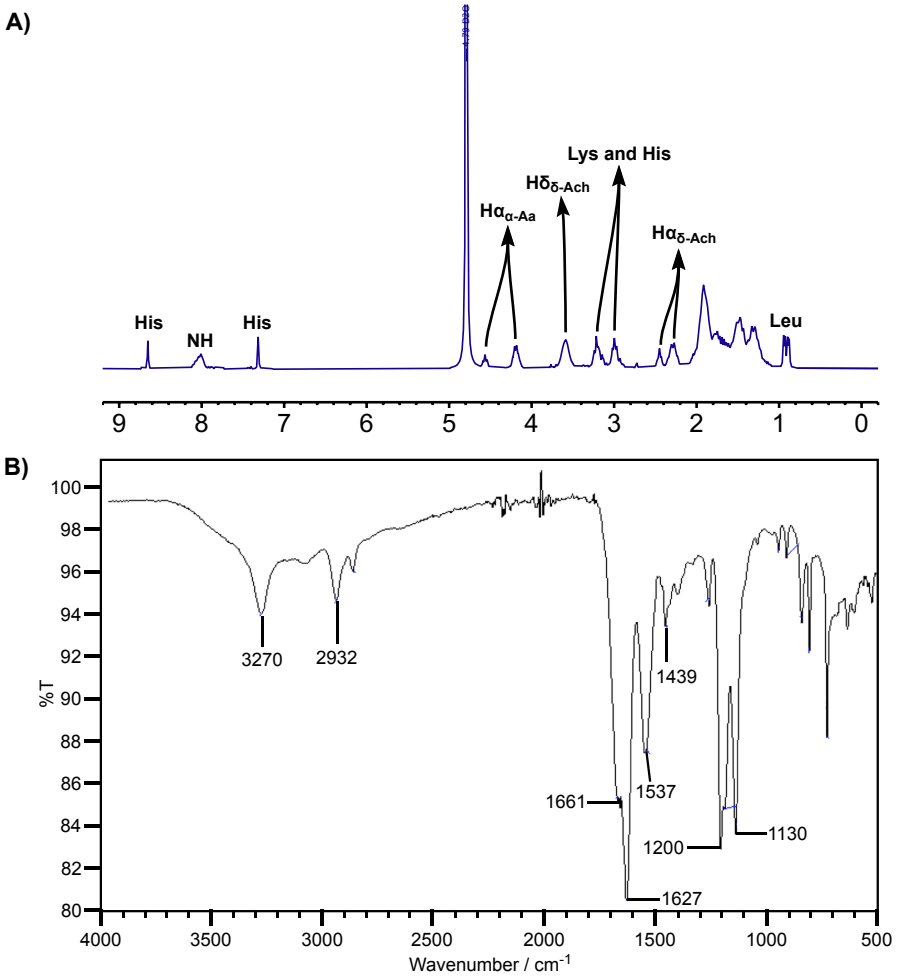


Figure 63. Characterization of **CP11**: A) ^{1}H NMR spectrum (D_2O. 298 K) and B) FTIR spectrum.

NANOTUBE CHARACTERIZATION

Once the peptide structure was confirmed, self-assembling properties were studied by fluorescence spectroscopy in presence of ThT. **CP11** includes pH sensitive residues (His) that could promote nanotube stacking through His-His hydrogen-bonding when the imidazolyl groups are partially deprotonated. For this reason, two aqueous samples at different pH were measured: pH 3.3 and pH 8.1. Addition of increasing amounts of an acidic aqueous solution **CP11** (pH 3.3) over another solution containing ThT (20 μM, pH 3.3) did not produce any variation in the fluorescence spectrum. In contrast, identical experiment using a solution of **CP11** in TRIS buffer (pH 8.1) gave rise to a clear increase in dye emission that confirms the interaction of ThT with the cyclic peptide assemblies. The neutralization of the system led to His deprotonation triggering the supramolecular events. The plot of the ThT emission band at 385 nm against the logarithm of peptide concentration at pH 8.1 gave an estimated critical aggregation concentration (cac) value of 38.9 μM.

USC DE SANTIAGO DE COMPOSTELA

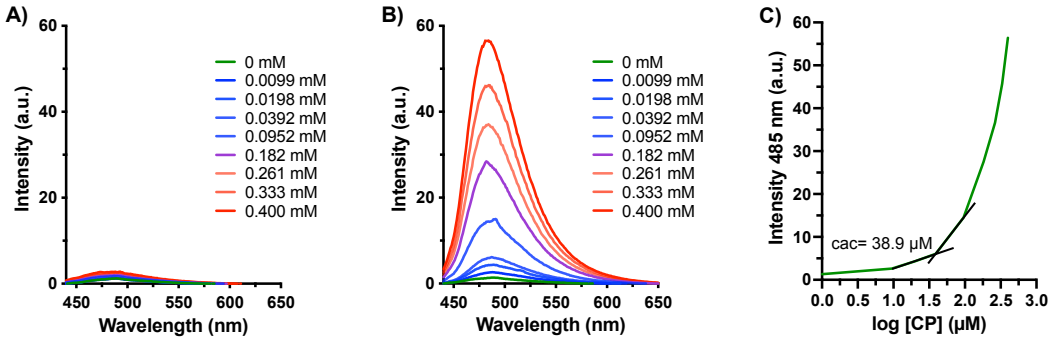


Figure 64. A) and B Fluorescence spectra of increasing additions of a 2 mM solution of **CP10** over a ThT solution in acid pH (A) and TRIS buffer pH 8.1 (B). C) Calculation of critical aggregation concentration.

The next step consisted of the characterization of nanotubes by AFM (Figure 65). For that purpose, an aqueous solution of **CP11** in TRIS buffer (20 µL, 1.0 mM, pH 8.1) was drop casted on mica for a few seconds and then, it was removed under a flow of Ar. AFM micrographs revealed fibrous structures with lengths of a few µm and average heights of 3.6 nm ± 0.3 nm. Analogous images were recorded from solutions in buffer-free water at the same pH values. These results agreed with those expected for a single nanotube composed of the corresponding dodecameric ring. Similar results were obtained in scanning transmission electron microscopy (STEM) experiments. For this, an aqueous solution of **CP11** was deposited on a STEM grid and stained with a solution of uranyl acetate or phosphotungstic acid.

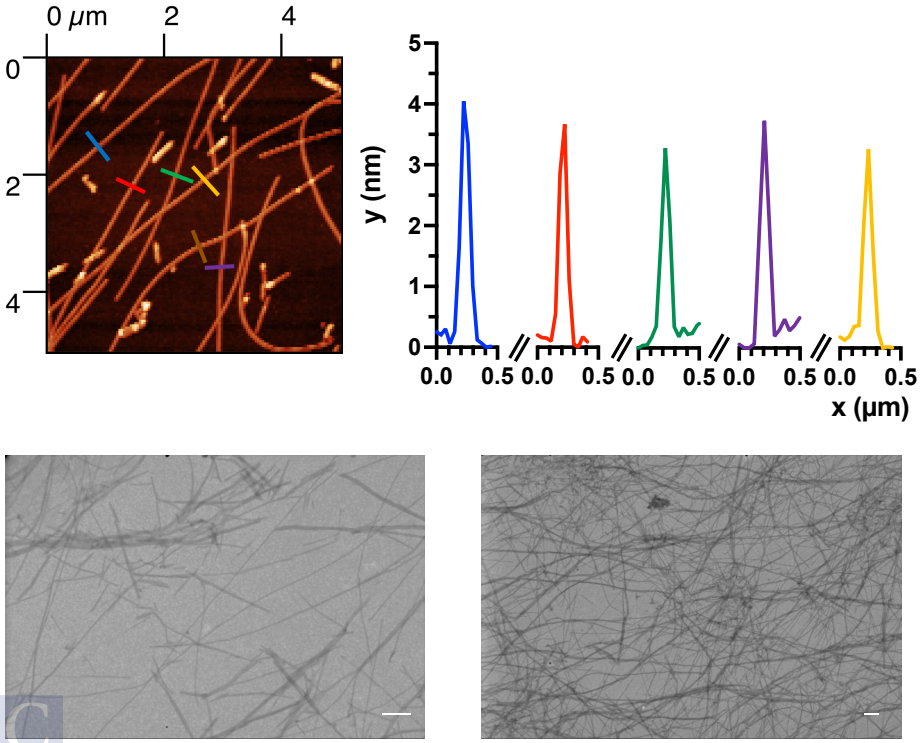


Figure 65. On top, AFM topography micrographs of a **CP11** solution (1 mM) in TRIS buffer (pH 8.1) and nanotubes profiles that afford average heights of 3.6 nm. On the bottom, STEM micrographs of basic solutions (pH 8.1) of **CP11** in water (scale bars 200 nm).

FULLERENE ENCAPSULATION

Computational calculations suggested that the internal hydrophobic properties and diameter size of dodecameric α,δ-SCPNs are favorable for the encapsulation of nanometer-sized hydrophobic molecules, such as C_{60} fullerene. Therefore, we planned to study the encapsulation properties of α,δ-CPs. For this goal, a solution of **CP11** (1.0 mM) in H_2O at pH 8.1 was added over an Eppendorf tube containing C_{60}. The mixture was sonicated, first in an ultrasonic bath and then using a tip horn sonicator. The resulting solution was centrifuged (7500 rpm) to remove the non-solubilized solid affording a brownish solution that was stable for weeks.

Fullerene encapsulation was studied by UV-vis spectroscopy (Figure 66A). The absorption bands (265 and 345 nm) characteristic of buckminsterfullerene dispersed in water were observed in the absorption spectrum.[206] Moreover, a long wavelength band between 400 and 480 nm was also observed. This band was attributed to the interaction between C_{60} molecules, suggesting that the entrapped fullerenes might be aligned inside the nanotube. Therefore, a peapod-like system was proposed as showed in Figure 66D. The UV-vis spectrum was essentially the same with time indicating the stability of the aqueous dispersion. Considering the proposed molar extinction coefficients in aqueous media [30.000-60.000 $M^{-1}\cdot cm^{-1}$ for λ_{max} (360 nm)], it was estimated a fullerene concentration of 70 μM.[207] On the other hand, acidic aqueous solutions (pH 3.5) of **CP11** (1.0 mM) did not show any evidence of fullerene encapsulation. In addition, the acidification of the basic **C_{60}@SCPN11** solution that led to the disassembly of the nanotubes produces the precipitation of the encapsulated fullerene. It is worth to mention that fullerene is not soluble in water under similar conditions, acidic (pH 3.5) or basic (pH 8.1) pH. These results confirmed that the **SCPN11** must be assembled to promote the solubilization of the molecule in aqueous media.

USC UNIVERSIDADE DE SANTIAGO DE COMPOSTELA

[206] X. Chang, P. J. Vikesland, *Environ. Sci. Technol*. **2011**, *45*, 9967 – 9974.
[207] **a)** J. A. Sene, M. V. B. Pinheiro, K. Krambrock, P. J. S. Barbeira, *Talanta*, **2009**, *78*, 1503 – 1507 **b)** S. J. Vance, V. Desai, B. O. Smith, M. W. Kennedy, A. Cooper, *Biophys. Chem*. **2016**, *214 – 215*, 27 – 32.

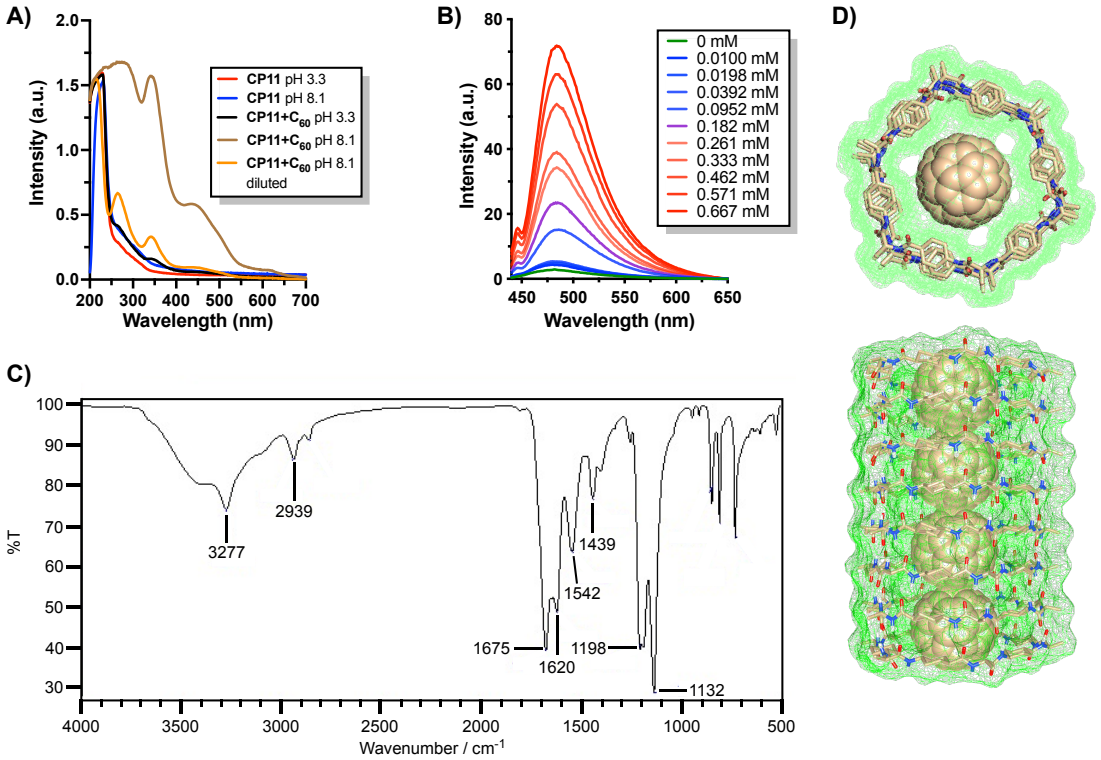


Figure 66. A) UV-vis spectrum from fullerene C_{60} encapsulation studies in presence of **CP11**. B) Fluorescence emission spectrum of additions of a basic (pH 8.1) aqueous solution of **CP11** + C_{60} over a solution of ThT (20 μM). C) FTIR of the **CP11** + C60 (neat, 298 K) and D) side and top views of a computer assisted model of C_{60} encapsulated in the inner cavity of **SCPN11**.

Then, we studied the system properties by fluorescence emission measurements in presence of ThT (Figure 66B). For that, increasing amounts of the basified solution of **C_{60}@SCPN11** were added over a ThT solution (20 μM) in TRIS buffer (pH 8.1). The fluorescence spectrum showed characteristic emission band of the dye at 485 nm that suggest the presence of β-sheet like structure. These results were confirmed by FTIR (Figure 66C), the spectrum revealed intense amide I and amide II signals at 1542 and 1620 cm^{-1}, respectively, and a broad amide A band at 3277 cm^{-1} characteristics of β-sheet structures involved in a hydrogen-bonding network.[184,202]

Finally, fullerene dispersions in presence of **CP11** were characterized by AFM (Figure 67A). The topography micrographs of the basic sample also showed a few μm long horizontal fibrous structures with average heights of 4.2 ± 0.4 nm slightly higher than those observed for the nanotubes obtained with CP alone. This increase in diameter could be a consequence of the greater stiffness of the peapod structure. No spherical 1 nm-sized particles were observed deposited on the tubular assemblies in any case, providing further evidence of C_{60} entrapment inside the internal cavity. Therefore, the ability of the cyclic peptide to maintain a tubular structure after fullerene encapsulation was validated. The same solution was also deposited on a carbon holey grid for STEM analysis (Figure 67B). Images of short fibers of a few μm long that correspond to individual nanotubes were collected. Interestingly, deposition of solutions more than a week old showed the formation of small nanotube bundles in AFM. Heights

between 7-9 nm were detected in these images. This was explained due to the lateral association of two nanotubes. Similar results were observed by STEM.

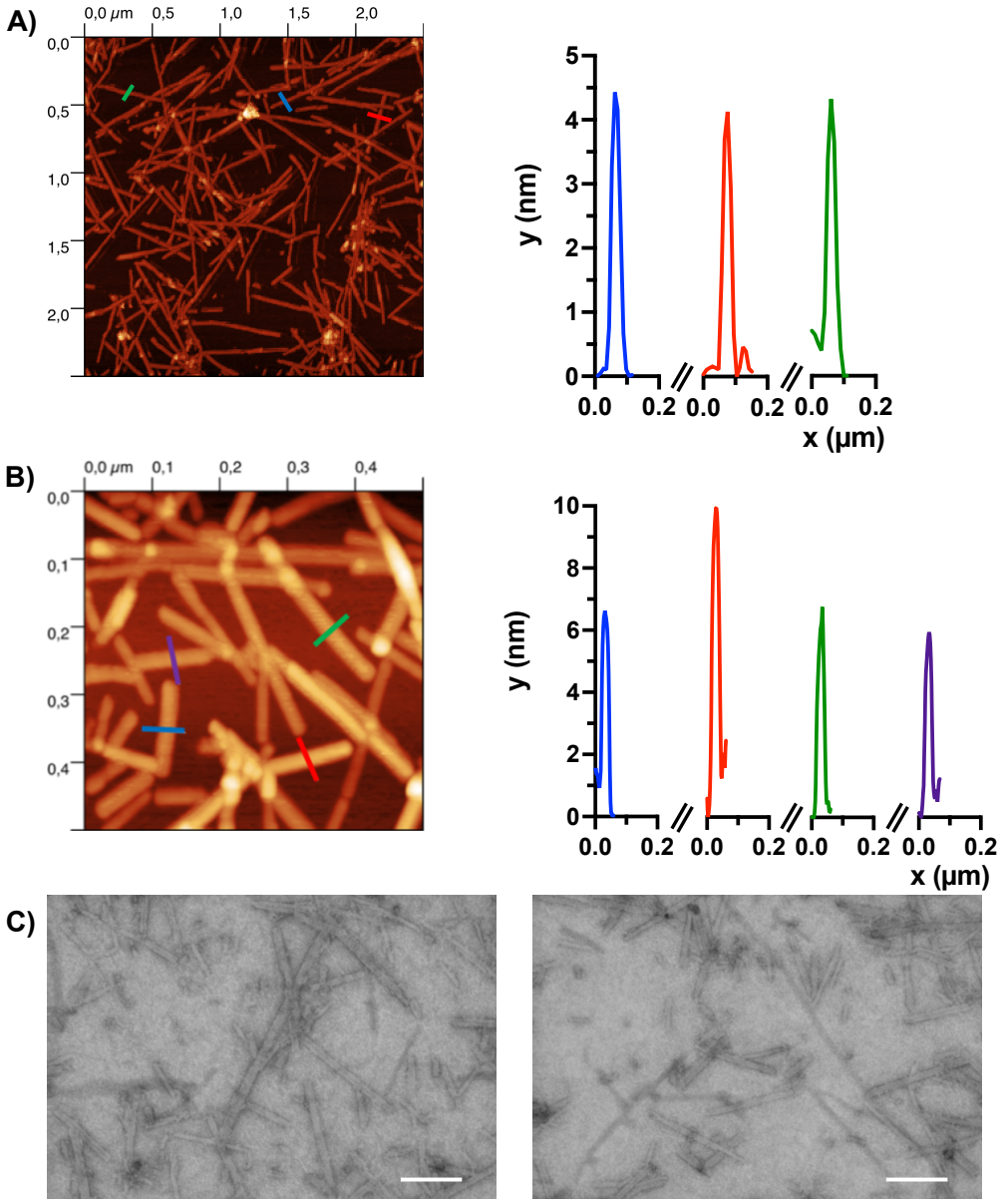


Figure 67. AFM topography micrographs from aqueous solutions of **CP11** and C_{60} deposited over mica (100 mM, pH 8.1) A) fresh sample B) one-week old sample and the corresponding height profiles along the highlighted transects. C) STEM images of an aqueous solution of **CP11** and C_{60} after deposition on a carbon holey grid (scale bars 100 nm).

In view of these results, **SCPN11** was tested for C_{70} solubilization. However, contrary to the theoretical studies, the aqueous solution of the cyclic peptide was not able to dissolve this carbon allotrope after sonication. This unexpected result can be rationalized considering the best Rebek's packing coefficient,[208] on the base of the larger size of this fullerene that must not fit in the nanotube cavity.

[208] S. Mecozzi, J. Rebek Jr, *Chem. Eur. J.* **1998**, *4*, 1016 – 1022.

SINGLE-WALLED CARBON NANOTUBES ENCAPSULATION (SWCNT)

The hydrophobic behavior of the internal cavity was assessed by fullerene encapsulation we considered the possibility to encapsulate SWCNT. Since their discovery, a lot of effort have been devoted to improving the synthetic[209] and purification[210,211] methods to afford samples of carbon nanotubes (CNTs) with high purity and homogeneous structural and electronic properties. However, despite being based on well-known reactions that can be controlled, chemical functionalization implies the modification of the native structure that provides the great properties discussed in the Introduction of this thesis. In this context, supramolecular chemistry arises as a powerful alternative because it would respect its original structure. Some years ago, Prof. Emilio M. Pérez argue about the advantages of threading carbon nanotubes through cyclic molecules.[212] He claimed that SWCNTs supramolecular functionalization, such as π,π-interaction with pyrene moieties,[213] can be lost at later stages due to the inherent labile properties of supramolecular assemblies. In contrast, rotaxane-like structures might present greater stability due to the higher strength of mechanically interlocked molecules.[214] In our case, the use of cyclic peptide whose internal dimensions can be controlled might help to afford individual SWCNT of a given diameter in aqueous media. In addition, the expected hybrid structures might be used for biomedical applications derived from the peptide biocompatibility. Solubilization of carbon nanotubes in presence of cyclic peptides (*D,L*-α-CPs) was already reported by Dieckmann and coworkers using cyclic peptides modified at both terminal ends with thiol groups that close around the CNT upon oxidation.[215] Recently, we reported twin nanotubes made of coupled CNTs and CPs bearing a pyrene moiety.[172] In this system, the CNT is interacting with the aromatic paddle on the outer surface of the SCPN. In this work, we are interested in forming coaxial nanotubes in which the peptide nanotube could display the role of the external insulator while the CNT would play the role of conducting material.

To achieve this goal, a similar procedure used for fullerene encapsulation was followed. A neutral aqueous solution (pH 7.8) of **CP11** (1.0 mM) was added over a SWCNT sample (1.2-1.5 nm). The mixture was sonicated and then centrifugated (14560 rpm) to remove the excess of solid sample affording a grey dispersion. The resulting solution was stable without special conditions at room temperature for months without any observed flocculation. A combination of analytical, spectroscopic and microscopic experiments in collaboration with the group of Juan Casado and Juan Teodomiro López Navarrete were conducted to study the water solubilization of carbon nanotubes in presence of α,δ-CPs. Resonant Raman scattering is a widely used technique to evaluate the electronic and structural properties of carbon nanotubes

[209] F. Yang, X. Wang, M. Li, X. Liu, X. Zhao, D. Zhang, Y. Zhang, J. Yang, Y. Li, *Acc. Chem. Res.* **2016**, *49*, 606 – 615.
[210] T. Tanaka, H. Liu, S. Fujii, H. Kataura, *Phys. Status Solidi RRL* **2011**, *5*, 301 – 306.
[211] X. Tu, M. Zheng, *Nano Res.* **2008**, *1*, 185 – 194.
[212] E. M. Pérez, *Chem. Eur. J*. **2017**, *23*, 12681 – 12689.
[213] D. M. Guldi, G. M. A. Rahman, N. Jux, D. Balbinot, N. Tagmatarchisc, M. Prato, *Chem. Commun*. **2005**, 2038 – 2040.
[214] **a)** S. Mena-Hernando, E. M. Pérez, *Chem. Soc. Rev*. **2019**, *48*, 5016 – 5032. **b)** D. B. Amabilino, J. F. Stoddart, *Chem. Rev*. **1995**, *95*, 2725 – 2828.
[215] A. Ortiz-Acevedo, H. Xie, V. Zorbas, W. M. Sampson, A. B. Dalton, R. H. Baughman, R. K. Draper, I. H. Musselman, G. R. Dieckmann, *J. Am. Chem. Soc*. **2005**, *127*, 9512 – 9517.

(Figure 68).[216] The Raman spectra of carbon nanotubes barely changed after aqueous dispersion in the presence of **SCPN11** indicating that there is no electronic perturbation after supramolecular interaction. This is in good agreement with the non-covalent functionalization of SWCNTs.[217] The major difference was found in the decreased intensity ratio of D-band to G-band (I_D/I_G ratio). This suggested that the solubilized carbon nanotubes have a smaller number of defect sites on their surface.[218] Therefore, **CP11** has a higher affinity for those nanotubes that did not undergo chemical modifications (such as oxidation processes) during their synthesis and manipulation. This result strongly supports that the driving forces are not governed by polarity effects, therefore the most likely supramolecular association would be based on CH-π type interactions between the methylene groups of the δ-Ach and the aromatic rings of the SWCNT. This highlights the increased hydrophobicity of the cyclic peptide after incorporation of the δ-residues. Furthermore, the diameter of the encapsulated nanotubes can be estimated by analyzing the radial breathing mode (RBM) frequency, between 150-300 cm^{-1}, using the following equation:[219,220]

$$\nu_{RBM} = \frac{A}{d} + B$$

The RBM observed frequency 163 cm^{-1} corresponds to SWCNTs with an approximate diameter of 1.48 nm. This result is contrary to findings from the fullerene experiments. The dispersed SWCNT would be expected to have a diameter of around 1 nm. In addition, computational calculations (Chapter 1) show an internal diameter of 13.5 Å nm which is not compatible with entrapment of these molecules inside the peptide inner cavity.

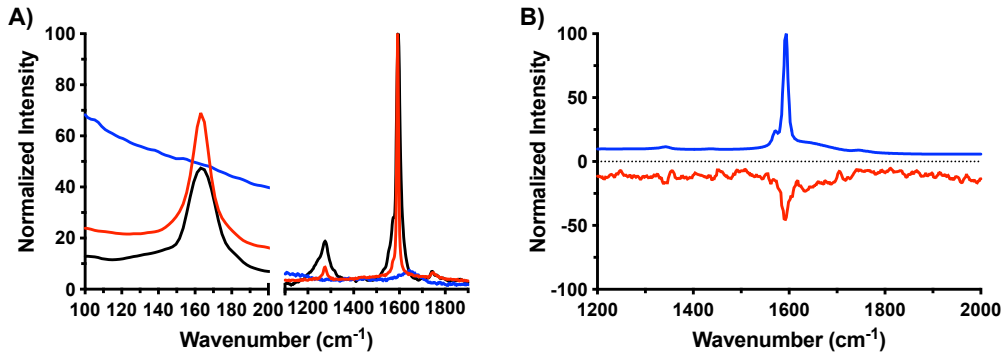


Figure 68. A) In-solution Raman scattering spectrum (λ_{exc}= 1064 nm) of SWCNTs (black), **CP11** (blue) and **CP11** + SWCNT (red) and B) Comparison of Raman spectrum (λ_{exc}= 532 nm, blue) with ROA spectrum (red).

To corroborate that the carbon material was solubilized by action of the α,δ-CPs, controls were run using the same procedure solutions but without the CP. In the absence of CP, we could not disperse CNTs. Raman optical activity spectrum was registered in order to study chirality

USC UNIVERSIDADE DE SANTIAGO

[216] M. S. Dresselhaus, G. Dresselhaus, A. Jorio, A. G. Souza Filho, M. A. Pimenta, R. Saito, *Acc. Chem. Res*. **2002**, *35*, 1070 – 1078.
[217] A. López-Moreno, E. M. Pérez, *Chem. Commun*. **2015**, *51*, 5421 – 5424.
[218] C. Fantini, M. L. Usrey, M. S. Strano, *J. Phys. Chem. C* **2007**, *111*, 17941 – 17946.
[219] In this equation A and B are empirically derived parameters: A= 223.3 cm^{-1} and B= 12.5 cm^{-1}.
[220] S. M. Bachilo, M. S. Strano, C. Kittrell, R. H. Hauge, R. E. Smalley, R. B. Weisman, *Science* **2002**, *298*, 2361 – 2366.

of the system (Figure 68B). Surprisingly, ROA signal was detected which strongly supports the action of the peptide in SWCNT solubilization. This chiral signal could be explained as a result of the transfer of chirality from the CP to the CNT after solubilization. However, it cannot be excluded that the observed chirality might be derived from the carbon material itself. For this reason, it was decided to prepare **CP12** which is the enantiomer of **CP11**. In this scenario, if the ROA spectrum shows the opposite chirality, it means that the chirality is transferred from the peptide. Cyclic peptide **CP12** was prepared following the same procedure as its enantiomer by a Fmoc/^{t}Bu SPPS strategy on 2-CTC resin. Once synthesized, its self-assembling properties were evaluated by spectrofluorescence emission assays in presence of ThT. As expected, **CP12** gave similar results after additions of a basic solution (pH 8.1) of this peptide in HEPES (2 mM) over a ThT (20 μM) in the same media. Finally, long nanotubes with similar diameter (3.5-4.0 nm) were observed after STEM analysis.

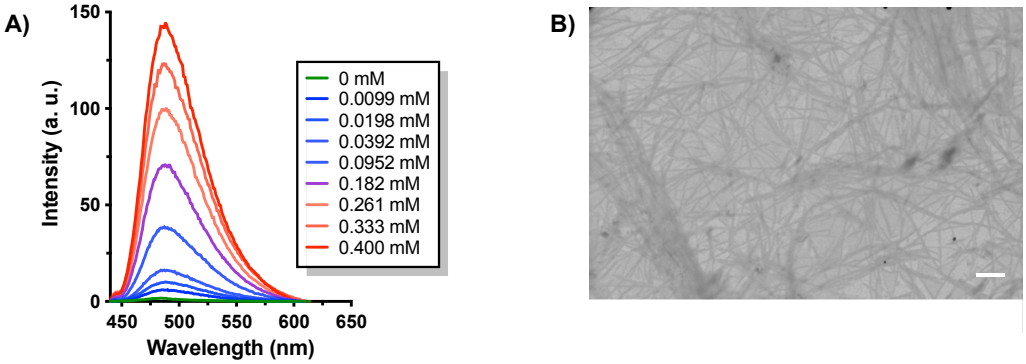


Figure 69. A) Fluorescence emission spectrum of additions of a basic (pH 8.1, TRIS buffer) aqueous solution of **CP12** over a solution of ThT (20 μM). STEM images of an aqueous solution of **CP12** after deposition on a carbon holey grid (scale bars 200 nm).

After confirming the self-assembling properties of the novel peptide, dispersions of SWCNTs using both enantiomers (**CP11** and **CP12**, 250 μM) were prepared following the same sonication and centrifugation procedure under acidic (pH 3.3) and neutral (pH 7.8) aqueous conditions. Surprisingly, greater encapsulation was observed in the samples at acidic pH, perhaps due to the easier threading of a CNT with a single cyclic monomer compared with the preassembled nanotube. To study the effect of the stereochemistry, circular dichroism (CD) was selected because it is sensitive to the absolute configuration as well as to conformational features. Every sample containing SWCNTs was analyzed by CD and was compared with the corresponding cyclic peptide enantiomer in the same conditions (Figure 70). However, a random coil distribution was observed at acidic pH that did not provide any structural information. On the other hand, at pH 8.1 the solution of **CP12** showed a negative and a positive cotton effect at 206 and 218 nm, respectively, that can be associated to the β-sheet structure characteristic of peptide nanotubes. The positive cotton effect at 218 nm was preserved in presence of carbon nanotubes while the negative one showed a much lower intensity.[221] As expected, the same result were obtained with the other enantiomer (**CP11)** but with inversed

[221] R. Chamorro, L. de Juan-Fernández, B. Nieto-Ortega, M. J. Mayoral, S. Casado, L. Ruiz-González, E. M. Pérez, D. González-Rodríguez, *Chem. Sci*. **2018**, *9*, 4176 – 4184.

sign. In any case, these experiments did not give any additional information about chirality of the nanotubes.

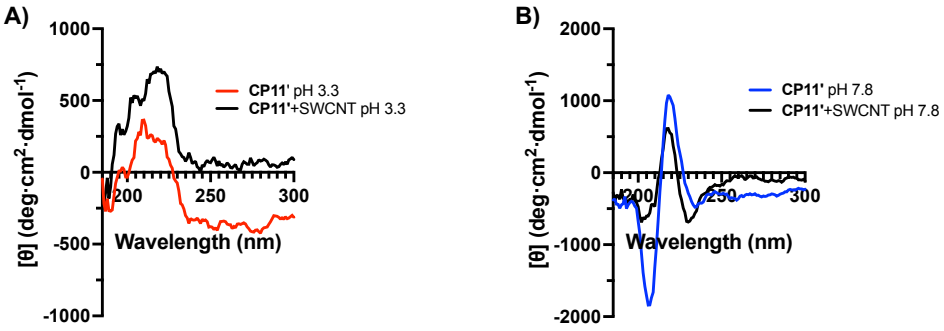


Figure 70. CD spectrum of samples at A) pH 3.3 and B) pH 7.8.

To get more insights, these systems were studied with different microscopic techniques. To acquire SEM images (Figure 71A and B), the samples were deposited on silicon wafer previously lyophilized by treatment with a mixture of H_2O_2/H_2SO_4 (3:1) for 2 h. SEM analysis of the **SWCNT@CP12** samples at pH 3.3 revealed a fibrous network surrounded by of amorphous aggregates. This material might come from the commercial source of carbon nanotubes as demonstrated by comparison with SEM images of a dispersion of SWCNTs in SDS in which similar aggregates were detected. In contrast, SEM pictures of the basic solution (pH 7.8) of CNTs with **CP12** showed a dense nanotube network. In this sample, impurities were not observed. However, control measurements of **CP12** in absence of the carbon material provide similar results. Hence, it was necessary identification a purification method to remove the excess of CPs from those that are interacting with CNTs forming the coaxial couple to favor their microscopy identification. For that purpose, these samples, as in the previous nanotube couple,[172] were dialyzed using a GeBAflex-tube equipped with a dialysis membrane of 3.5 kDa cut off. However, after dialysis we did not find any appreciable difference between both systems.

Exploration of the CP-SWCNT mixtures under AFM was consistent with the SEM studies (Figure 71C and 64D). AFM micrographs were obtained after spin-coating the sample on mica and subsequently dried under a flow of Ar. Dialyzed suspensions at basic pH showed fibrous networks with heights around 4 nm that were essentially attributed to cyclic peptide-based nanotubes. In some sites it was possible to identify tubular structures with heights between 1-2 nm that might correspond to carbon nanotubes. Nevertheless, no clear evidence of CNTs threading was found. The samples at acidic pH provided tubes of lower heights. It was already stablishing that under these conditions the cyclic peptides do not assemble into SCPNs, so these assemblies were associated with bundled of carbon nanotubes as they heights observed did not matched with individualized SWCNTs. Similar results were obtained by STEM, although basic samples were previously dialyzed, they did not provide any further evidence of the entrapment. In contrast, acidic samples revealed individualized nanotubes surrounded by organic units that might correspond with **CP12** added to the surface of the SWCNTs.

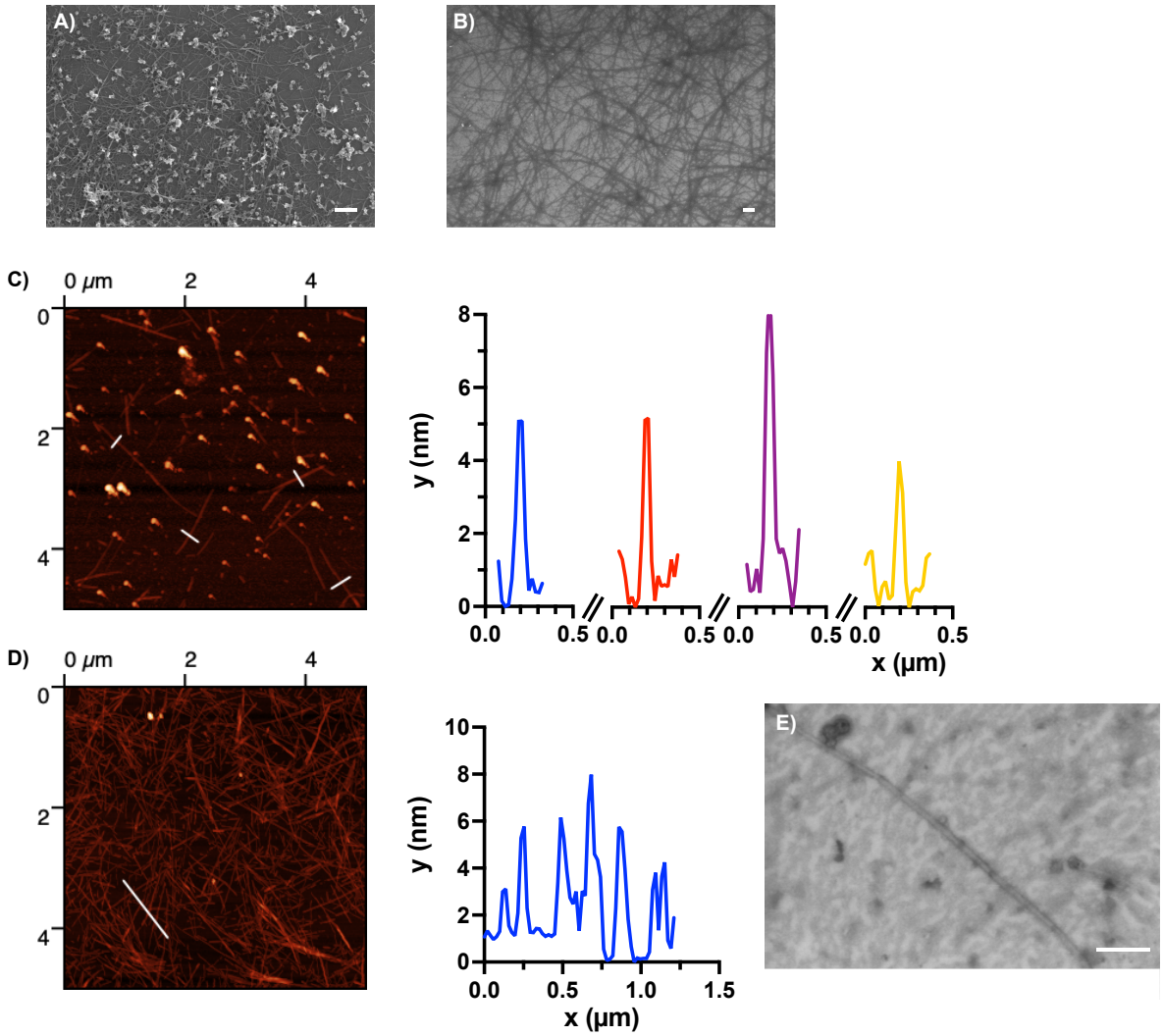


Figure 71. Imaging experiments of samples of **CP12** + SWCNT samples (250 μM): A) SEM image of a sample at pH 3.3 (scale bar= 200 nm), B) SEM image of a sample (250 μM) at pH 7.8 (scale bar= 200 nm), falta de la muestra sola sin CNTs C) AFM topography micrograph of a sample at pH 3.3 and profile of different tubes, D) AFM topography micrograph of a sample at pH 7.8 and profile of different tubes and E) STEM image of a sample at pH 3.3 (scale bar= 100 nm).

Finally, regarding the calculated internal diameter and previous results, we estimated that that nanotubes around 1 nm would be the preferred guest for cyclic peptide nanotubes based on the modeled structure of α,δ-dodecamers. For this reason, the encapsulation of a batch of carbon nanotubes of smaller diameters (0.8-1.2 nm) was also attempted. Unfortunately, solubilization was not observed under any of the conditions tested.

α,δ-CYCLIC PEPTIDE NANOTUBES: 3RD GENERATION

NANOTUBES WITH BIGGER DIAMETER

Considering the results of Chapter 1, cyclic hexadecamers made of α-Aa of alternating chirality and δ-amino acids were shown to self-assemble into dimeric models. These structures will provide nanotubes with bigger diameter while maintaining the hydrophobic properties of the pore changing the internal C_6-simmetry for a C_8 center. Therefore, this larger CP would thread carbon nanotubes more easily than the cyclic dodecamers through the tubular assemblies.

Moreover, it would also facilitate de microscopy differentiation due to the larger diameter of the peptide system.

Based on dodecamers, three novel cyclic peptides were designed (Figure 72). Polar α-amino acids were incorporated to enhanced water solubility. These polar residues might also participate in nanotube formation by providing additional interactions. For instance, Lys and Glu will create salt bridges in adequate conditions, as well His residues, as previously shown, will trigger self-assembling by means of pH neutralization. In these systems, as in previous design, an Arg residue was incorporated to assist nanotube deposition on mica surfaces. In addition, the incorporation of non-polar α-amino acids (Ala or Leu) were also incorporated to simplify the synthetic process. The number and the position of these residues vary in the proposed sequences in order to increase the attractive contacts between side chains. The proposed sequences for the α,δ-hexadecamers are shown in Figure 72.

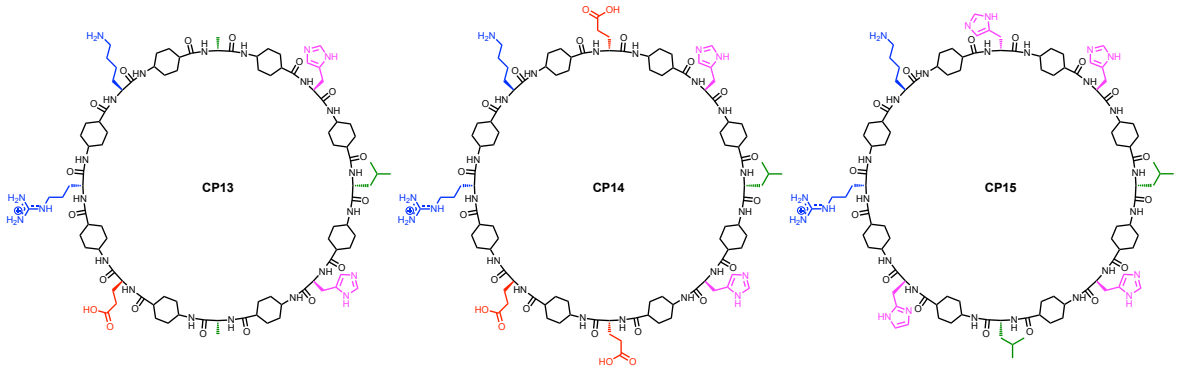


Figure 72. Proposed design for α,δ-cyclic peptide hexadecamers **CP13**, **CP14** and **CP15**.

SYNTHESIS

For the synthesis of this peptides, we followed the same strategy as for the preparation of α,δ-CPs of smaller diameter. The linear peptides were manually grown by solid phase synthesis on 2-CTC resin and cyclized in the same conditions prior to its cleavage. In all-three peptides the resin was loaded with **dp5** through reaction of the Lys lateral chain with the solid support. After cleavage with TFA cocktail, the cyclic peptides were precipitated on cold Et_2O and dried under high vacuum. Although the resulting crudes were soluble in water, HPLC purification was unfeasible due to their aggregation properties that made broad and poorly defined peaks. For this reason, they were purified via washes with chilled MeOH to provide **CP13**, **CP14** and **CP15** as white solids. Peptide structure was confirmed by MALDI MS. In the IR spectrum of the three cyclic peptides were identified amide I, amide II and amide A bands characteristic of β-sheet structures. This information is summarized in Table 4.

USC UNIVERSIDADE DE SANTIAGO DE COMPOSTELA

ENTRY	CYCLIC PEPTIDE	AMIDE I (cm^{-1})	AMIDE II (cm^{-1})	AMIDE A (cm^{-1})
1	**CP13**	1538	1631	3271
2	**CP14**	1541	1630	3272
3	**CP15**	1543	1631	3273

Table 4. Summary of the observed FTIR characteristic bands of the hexadecameric cyclic peptides.

NANOTUBE CHARACTERIZATION

The nanotube formation capabilities of **CP13**, **CP14** and **CP15** were tested in solution by fluorescence assays in presence of the planarizable probe ThT. Since every sequence have a self-assembling pH-triggered motif, they were tested under different pH conditions (Figure 73). Therefore, these peptides were measured at acidic pH 3.1 in citrate buffer and at neutral pH 7.4 in phosphate buffer. Although all the peptide present higher emission at higher pH, the studies revealed that **CP13** and **CP15** did not show especially relevant supramolecular ability to give rise to nanotubes in solutions, as the probe emission in both examined conditions was not very intense. In contrast, the emission spectrum of **CP14** at neutral pH exhibited a huge increase, almost ten times, in the probe emission with the peptide additions. Therefore, it seems that **CP14** give rise to supramolecular architectures through β-sheet-type interactions of monomeric structures. In view of the spectroscopic studies, supramolecular structures of **CP14** were examined by AFM. However, after several attempts of aqueous solutions of **CP14** at different pH (3.5 and 7.4) and concentrations (250 and 250 μM) we did not observe any tubular assemblies; instead, spherical-shaped aggregated were detected which were associated to buffer crystallization on the anionic surface. We believe that new microscopy characterization should be carried out using a non-ionic buffer for sample deposition on mica. Moreover, additional microcopy techniques, *i.e.*, confocal microscope or STEM must be tested.

USC UNIVERSIDADE DE SANTIAGO DE COMPOSTELA

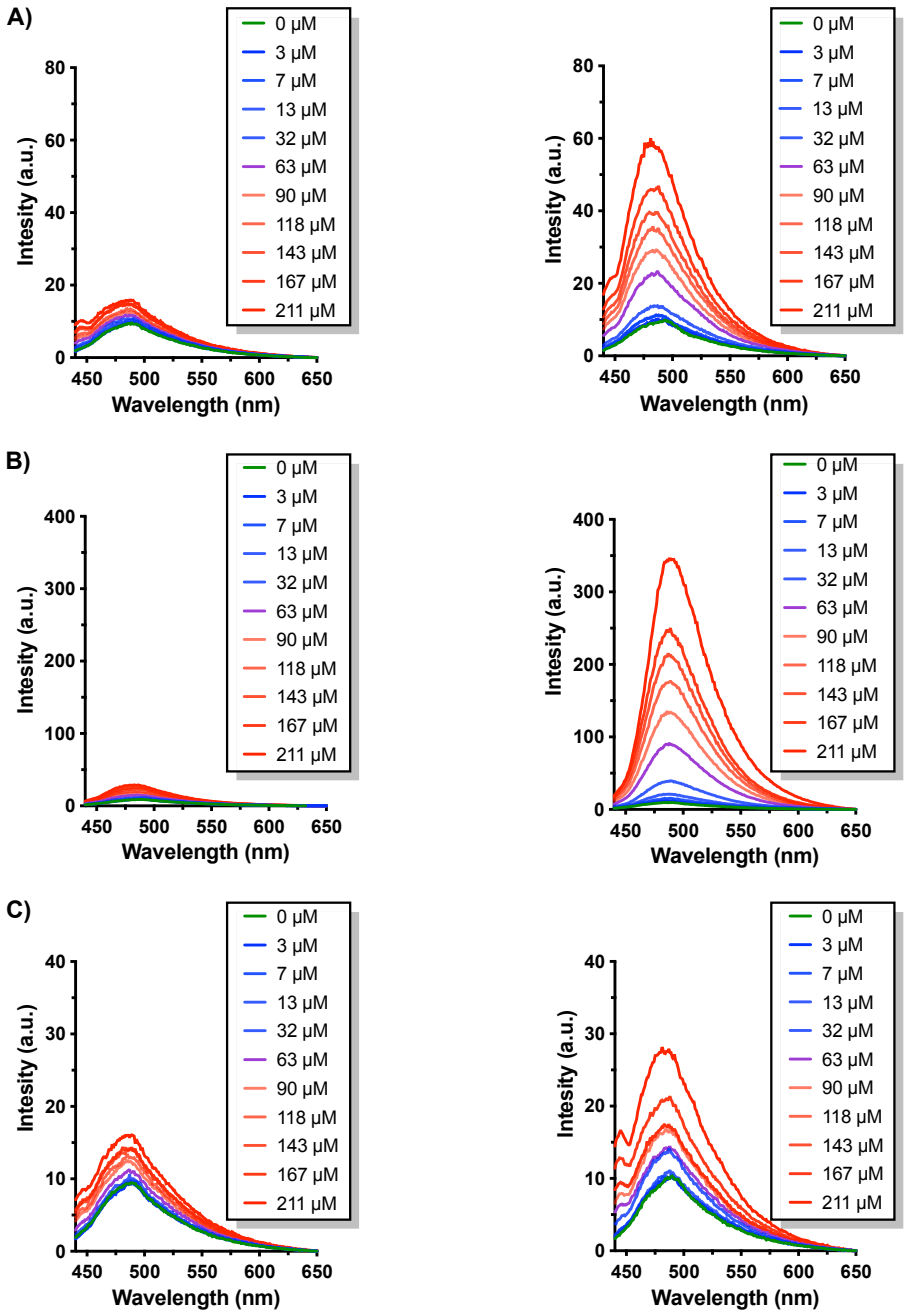


Figure 73. Fluorescence emission spectrum of additions of aqueous solution of A) **CP12** at pH 3.1 (left) and pH 7.4 (right), B) **CP13** at pH 3.1 (left) and pH 7.4 (right) and C) **CP14** at pH 3.1 (left) and pH 7.4 (right).

USC UNIVERSIDADE DE SANTIAGO DE COMPOSTELA

CHAPTER 3

USC
UNIVERSIDADE
DE SANTIAGO
DE COMPOSTELA

USC
UNIVERSIDADE
DE SANTIAGO
DE COMPOSTELA

CHAPTER 3

SUPRAMOLECULAR CAPSULES

With the evolution of supramolecular chemistry in the field of molecular recognition (host-guest chemistry), new hollow three-dimensional structures capable of hosting smaller molecules within their inner volumes were developed. These macromolecules were called molecular containers. The most significant asset of these receptors is the ability to confine the guest molecules protecting them from the surrounding environment. The hosted molecules will behave different inside the containers leading to new conformations and stereochemical relationships that will depend on the characteristics of the cage (shape and formulation).[222] The original molecular containers were developed by Cram's group,[223] their strategy consisted of a condensation reaction between two resorcin[4]arene units in the presence of the target ligand leading to the confinement of the molecule. Since the evolution of the seminal receptors developed by Cram's group known as carcerands or hemicarcerands,[224] other porous molecules –named as organic cages– have been discovered in which the porosity is a function of the internal voids.[225] Despite the great progress in the development of these complexes, their applications are quite limited because the construction of three-dimensional structures using covalent chemistry increases the synthetic cost and restricts the reversibility of the encapsulation as, in some cases, it is necessary to break (at least) one bond to allow the exit of the guest. The use of dynamic covalent chemistry as alternative for the construction of this covalent recipients has mitigated these constraints.[226] In any case, the supramolecular approach emerges as the most suitable alternative for the preparation of nanoscale functional molecular receptors. In these systems, two concepts related with supramolecular chemistry are exploited: molecular self-assembling for the construction of the capsules from simple monomeric components and molecular recognition for guest entrapment. These systems operate under dynamic equilibrium conditions giving access to adaptative containers that allow greater control over the entrance and exit of the guest.

For the non-covalent synthesis of these systems, two main supramolecular forces have been exploited: hydrogen-bond and metal-ligand interactions. The key aspect of these forces is the intrinsic directional behavior that give access to a plethora of well-defined architectures.

METAL COORDINATION CAGES

The use of coordination chemistry in the production of artificial molecular containers represented a major advance over their covalent analogues.[227] The metal cores have defined geometries that depend on the nature of the metal and the selected ligands. Therefore, the

USC UNIVERSIDADE DE SANTIAGO DE COMPOSTELA

[222] P. Ballester, M. Fujita, J. Rebek Jr. *Chem. Soc. Rev*. **2015**, *44*, 392 – 393.
[223] D. J. Cram, S. Karbach, Y. H. Kim, L. Baczynskyj, G. W. Kalleymeyn, *J. Am. Chem. Soc*. **1985**, *107*, 2575 – 2576.
[224] For more information about these systems see: F. Liu, R. C. Helgeson, K. N. Houk, *Acc. Chem. Res*. **2014**, *47*, 2168 − 2176.
[225] T. Hassel, I. Cooper, *Nat. Rev. Mater*. **2016**, *1*, 16053.
[226] F. Beuerle, B. Gole, *Angew. Chem. Int. Ed*. **2018**, *57*, 4850 – 4878.
[227] F. J. Rizzuto, L. K. S. von Krbek and J. R. Nitschke, *Nat. Rev. Chem*. **2019**, *3*, 204 – 222.

correct choice of those components enables the construction of tridimensional structures with programmable morphology in a simple and efficient manner. In 1988, Saalfrank and co-workers serendipitously encountered the first coordination-driven adamantoid-like assembly when attempting the preparation of tetradonor-substituted allenes.[228] Shortly thereafter, Professors Makoto Fujita and Kenneth N. Raymond pioneered the preparation of functional 3D metal-coordination architectures.[229] They also stablished the design principles of the molecular paneling approach to construct and predict the formation of these self-assembled systems.[230] This strategy is based on the geometrical relationship between the chelating ligands and the metals used. In general, rigid aromatic ligands that constitute the edges (molecular walls) are employed in the presence of transition metals that are located at the vertices of the self-assembled cage.

The first coordination cage was described by Fujita's group in 1995,[231] the combination of a Pd(II) complex with a flat triangular ligand [tris-(4-pyridyl)-triazine] led to the formation of a metallooctahedral box (Figure 74). This receptor was shown to be very efficient in the encapsulation of a variety of organic compounds. [232] Simply modifications of the subcomponents led to supramolecular structures with diverse properties. For instance, a different ligand at the metal core gave rise to similar molecular containers with different solubility and crystallinity properties.[233] In addition, this modification was also reported to provide bowl-shaped molecular containers.[234] Another metal ion with planar square geometry such as Pt(II) resulted in more robust (kinetically stable) receptors that were resistant to acidic and basic conditions.[235] As an example of the scope of this approach, the combination of the tris(4-pyridyl)triazine ligand with a sterically hindered ligand, tetramethyl-4,4′-bipyridine drove selectively to in a prism-shaped box capable to encapsulate large aromatic compounds such as pyrene (Figure 74).[236]

[228] R. W. Saalfrank, A. Stark, K. Peters, H. G. von Schnering, *Angew. Chem. Int. Ed*. **1988**, *27*, 851 – 853.
[229] Hiroki Takezawa**,** Makoto Fujita**,** *Bull. Chem. Soc. Jpn*. 2021, *94*, 2351 – 2369.
[230] R. Chakrabarty, P. S. Mukherjee, P. J. Stang, *Chem. Rev*. **2011**, *111*, 6810 – 6918.
[231] M. Fujita, D. Oguro, M. Miyazawa, H. Oka, K. Yamaguchi, K. Ogura, *Nature* **1995**, *378*, 469 – 471.
[232] M. Yoshizawa, M. Tamura, M. Fujita, *J. Am. Chem. Soc*. **2004**, *126*, 6846 – 6847.
[233] T. Kusukawa, M. Fujita, *J. Am. Chem. Soc*. **2002**, *124*, 13576 – 13582.
[234] M. Fujita, S. Y. Yu, T. Kusukawa, H. Funaki, K. Ogura, K. Yamaguchi, *Angew. Chem. Int. Ed*. **1998**, *37*, 2082 – 2085.
[235] F. Ibukuro, T. Kusukawa, M. Fujita, *J. Am. Chem. Soc*. **1998**, *120*, 8561 – 8562.
[236] M. Yoshizawa, J. Nakagawa, K. Kumazawa, M. Nagao, M. Kawano, T. Ozeki, M. Fujita, *Angew. Chem. Int. Ed*. **2005**, *44*, 1810 – 1813.

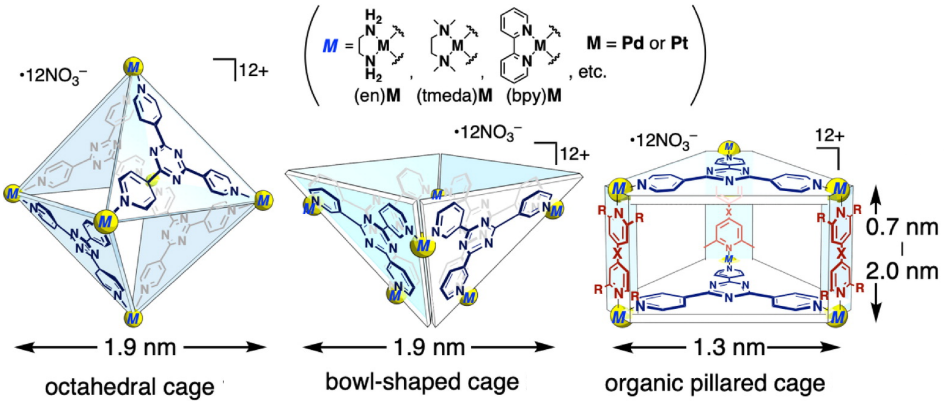


Figure 74. Selection of coordination cages developed by Fujita's group using the molecular paneling approach. Reproduced with permission from Chemical Society of Japan: Ref. 229.

In addition to the polyhedral capsules, Fujita's group have developed other spherical boxes with general formula M_nL_{2n} where M is the Pd(II) metal core and L the pyridine-based ligands (Figure 75).[237] The combination of the same metal cores of square planar geometry with rigid bent organic ligands provided this type of polyhedral structures upon self-assembly. The ligand bend angle will dictate the stoichiometry of the final supramolecular system. Using this approach, they demonstrated the formation of cuboctahedral ($M_{12}L_{24}$)[238] or rhombicuboctahedra ($M_{24}L_{48}$) [239] structures. Recently, they serendipitously found a spherical supramolecular structure that contains 30 Pd(II) ions and 60 bent ligands. [240] This novel supramolecular structure has the symmetry of a tetravalent Goldberg polyhedron, a shape family that has not previously been observed experimentally. Moreover, in the same publication they used graph theory to predict the largest coordination cage described so far, where 48 metal centers are attached to 96 bipyridine ligands derived from 3,4-dimethoxyselenophene. A similar approach was used to prepare a plethora of metal-linked peptide nanostructures using small peptides decorated with pyridine motifs at both terminal ends through a metal-mediated folding and assembly cooperative process.[241] The final architecture depends on the sequence of the peptide that a acquire a specific conformation during metal coordination and simultaneously assembles into a more complex nanostructure. These giant cages were used for a variety of applications, to mention just one, the group of Fujita was able to stabilize the tertiary structure of a protein inside this metal-coordination containers in the presence of organic solvents which prolonged the active half-life of the caged protein while preserving its catalytic activity.[242]

[237] For further information about these systems see: K. Harris, D. Fujita, M. Fujita, *Chem. Commun*. **2013**, *49*, 6703 – 6712.
[238] M. Tominaga, K. Suzuki, M. Kawano, M. Fujita, *Angew. Chem. Int. Ed*. **2004**, *43*, 5621 – 5625.
[239] Q.-F. Sun, J. Iwasa, D. Ogawa, M. Fujita, *Science*, **2010**, *328*, 1144 – 1147.
[240] D. Fujita, S. Sato, N. Mizuno, T. Kumasaka M. Fujita, *Nature*, **2016**, *540*, 563 – 566.
[241] T. Sawada, M. Fujita, *Chem*, **2020**, *6*, 1861 – 1876.
[242] D. Fujita, R. Suzuki, Y. Fujii, M. Yamada, T. Nakama, A. Matsugami, F. Hayashi, J.-K. Weng, M. Yagi-Utsumi, M. Fujita, *Chem*, **2021**, *7*, 2672 – 2683.

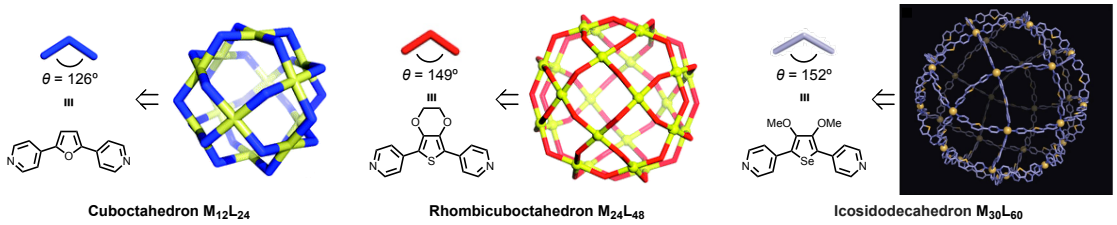


Figure 75. Structure of $M_{12}L_{24}$ (left), $M_{24}L_{28}$ (center) and $M_{30}L_{60}$ metal-coordination supramolecular spheres. Left and center figures were adapted with permission from Royal Society of Chemistry: Ref.: 237. Right figure adapted with permission from The American Association for the Advancement of Science: Ref. 239. Copyright © 2010, The American Association for the Advancement of Science.

At the same time, the group of Prof. Raymond followed the same molecular paneling strategy to prepare coordination frameworks with tetrahedral geometry (M_4L_6).[243] In this case, they employed metal ions with octahedral coordination spheres [Ga(III) or Fe(III)] and aromatic ligands decorated with two catechol units (Figure 76). Since the metal environment is chiral, racemic mixtures of homochiral molecular containers (Δ,Δ,Δ,Δ,Δ or Λ,Λ,Λ,Λ,Λ) were obtained. These receptors have a net negative charge (-12), are soluble in water and have a large hydrophobic cavity that has the ability to recognize protonated amines, phosphines or ferrocene ions with high affinity constants.[244] Moreover, the ability to recognize and stabilize cationic species within the inner volume of the tetrahedral box in addition to its acidic environment provided a useful supramolecular reactor with catalytic properties.[245] Earlier in 1997, Stang and co-workers firstly reported the preparation of a M_6L_4-type chiral metal organic cage with *T* symmetry via self-assembly of tridentate pyridine ligands with [(*R*)-(+)-BINAP]Pd(II)/–Pt(II) bis(triflates).[246]

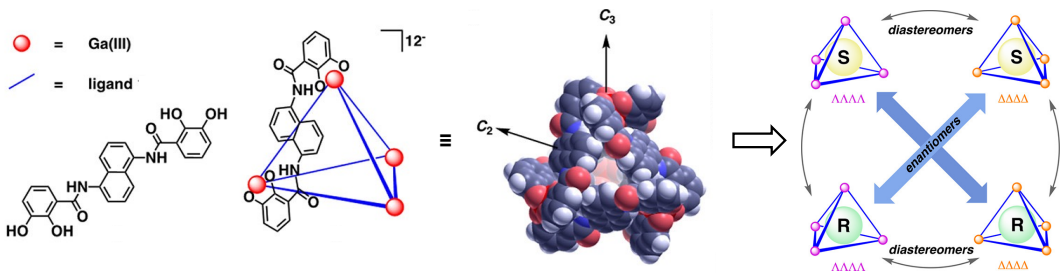


Figure 76. Structure of tetrahedral metal-coordination cages developed in Raymond's groups. Adapted with permission from American Chemical Society: Ref. 245. Copyright © 2018, American Chemical Society

The group of Prof. Nitschke is another major contributor to the field of supramolecular coordination cages. In their designs, they introduced the implementation of dynamic covalent chemistry to obtain new multidentate ligands based on imine bonds (Figure 77A).[247] The combination of linear aromatic diamines with 2-formylpyridines gave rise to new ligands that afforded innovative tetrahedral molecular containers in the presence of Fe(II) ions. These capsules were shown to bind hydrophobic species within the internal cavity driven by a

USC UNIVERSIDADE DE SANTIAGO DE COMPOSTELA

[243] D. L. Caulder, R. E. Powers, T. N. Parac, K. N. Raymond, *Angew. Chem. Int. Ed.* **1998**, *37*, 1840 – 1842.
[244] M. D. Pluth, R. G. Bergman, K. N. Raymond, *J. Am. Chem. Soc.* **2007**, *129*, 11459 – 11467.
[245] C. M. Hong, R. G. Bergman, K. N Raymond, F. D. Toste, *Acc. Chem. Res.* **2018**, *51*, 2447 – 2455.
[246] P. J. Stang, B. Olenyuk, *Organometallics*, **1997**, *16*, 3094 – 3096.
[247] P. Mal, D. Schultz, K. Beyeh, K. Rissanen, J. R. Nitschke, *Angew. Chem. Int. Ed.* **2008**, *47*, 8297 – 8301.

hydrophobic effect as consequence of the lesser net charge of the supramolecular structure surrounded by aromatic hydrophobic walls. This strategy gave access to a wide variety of metal coordination structures.[227] Thus, not only tetrahedral complexes have been developed, but also different geometries have been explored providing structures with larger cavities that allow encapsulation of larger molecules. In addition, the use of porphyrin-walled motifs supplied receptors with another metallic center that affords an extra directing effect for guest encapsulation (Figure 77B).

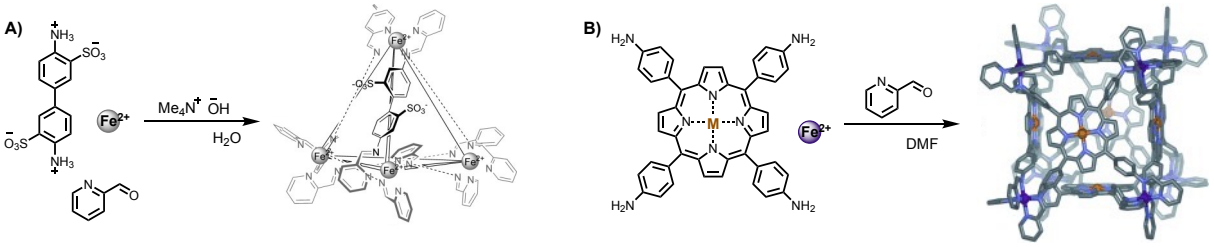


Figure 77. Iron-based coordination cages developed by Nitschke's group using dynamic covalent chemistry: A) Tetrahedral complex (Reproduced with permission from John Wiley and Sons: Ref. 247. Copyright © 2008 WILEY-VCH Verlag GmbH & Co. KGaA, Weinheim) and B) Cubic porphyrin-walled receptor.

The use of metalloporphyrins for the construction of new functional materials is a widely explored field.[248] Their planar geometry with tunable peripheral sites led to different types of coordination boxes. These materials have been used for a wide range of applications as the recognition and purification of fullerene derivatives (Figure 77).[249] An analogue host-guest fullerene-binding coordination cage was successfully used for the regioselective functionalization of C_{60}.[250]

SUPRAMOLECULAR CAPSULES

The first example of molecular containers based on hydrogen bonding forces was developed in collaboration between the groups of Professors Rebek Jr. and J. Mendoza.[251] In this work, two complementary *bis*-glycoluryl subunits were connected giving rise to a tennis ball-like dimeric structure in a reversible manner. Subsequently, they found that these dimers were able to accommodate small hydrocarbons (methane, ethane and ethylene) within its empty cavity.[252] Later, they prepared a larger supramolecular capsule from resorcin[4]arene monomers modified with diazaphthalimide groups. The most significant feature of these systems was that the capsule was obtained exclusively in the presence of the guest molecules and exhibited an extraordinary selectivity.[253] These receptors were used in the recognition of linear alkanes of different lengths (C_6-C_{14}). Longer chain hydrocarbons (> C_{10}) adopted a helical conformation to fit inside the host superstructure that would not exist in the absence of a stabilizing recipient.

USC UNIVERSIDADE DE SANTIAGO DE COMPOSTELA

[248] S. Durot, J. Taesch, V. Heitz, *Chem. Rev*. **2014**, *114*, 8542 – 8578.
[249] W. Brenner, T. K. Ronson, J. R. Nitschke, *J. Am. Chem. Soc*. **2017**, *139*, 75 – 78.
[250] C. Fuertes-Espinosa, C. García-Simón, M. Pujals, M. Garcia-Borràs, L. Gómez, T. Parella, J. Juanhuix, I. Imaz, D. Maspoch, M. Costas, X. Ribas, *Chem*, **2020**, *6*, 169 – 186.
[251] R. Wyler, J. de Mendoza, J. Rebek, Jr. *Angew. Chem. Int. Ed*. **1993**, *32*, 1699 – 1701.
[252] N. Branda, R. Wyler, J. Rebek Jr. *Science*, **1994**, *263*, 1267 – 1268.
[253] For a detailed description of these works see: D. Ajami, J. Rebek Jr. *Acc. Chem. Res*. **2013**, *46*, 990 – 999.

Moreover, the addition of glycoluril motifs led to expanded capsules that allowed to confine longer hydrocarbon chains.

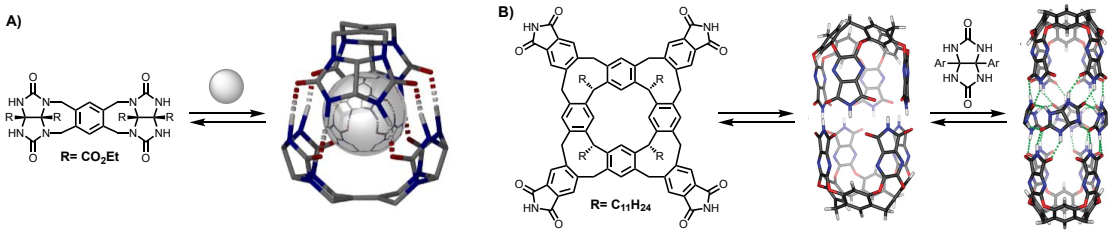


Figure 78. Supramolecular capsules developed by the group of Rebek Jr. through soft templating approach: A) Tennis ball-shaped and B) Cylinder capsules that dimerized in the presence of guest molecules. Adapted with permission from American Chemical Society: Ref. 253. Copyright © 2013, American Chemical Society.

Other convex structures were also studied for the construction of self-assembled capsules. For instance, Atwood and colleagues showed that calix[4]resorcinaren derivatives are capable to self-assemble into stable hexameric complexes in aqueous medium (Figure 79A).[254] This group also reported the first example of internal functionalization using calix[4]arene monomers derived from phenol.[255] These nanocontainers present a hydroxyl group oriented towards the inner volume modulating the interaction with the solvent molecules that act as guest. Another interesting example introduced by Sessler's group is the use of calix[4]pyrroles, the pyrrole rings led to tighter hydrogen bonds dimeric capsules.[256] The calix[4]pyrrole derivatives were exploited by Pablo Ballester and co-workers who were able to control the final supramolecular structure by means of small modifications (Figure 79B). The introduction of aromatic rings with hydrogen-bonding substitutions at *meso* position gave rise to hexameric clusters,[257] similar to those shown by Atwood. On the other hand, urea-subtituted calixpyrrol components led to dimeric supramolecular capsules.[258] These receptors were useful for the encapsulation and stabilization of several guest inside the inner volume.[259]

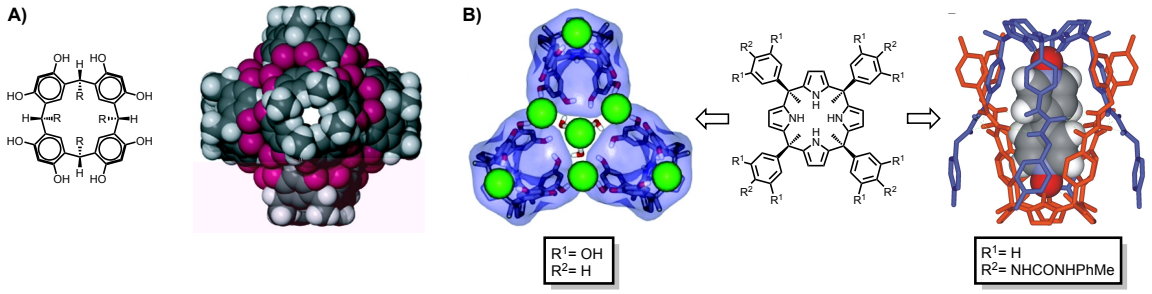


Figure 79. A) Self-assembled hexameric capsules derived from calix[4]resorcinaren monomers (reproduced with permission from National Academy of Sciences: Ref. 255. Copyright © 2002, The National Academy of Sciences) and B) Supramolecular capsules based on calix[4]pyrroles motif: depending on the substituents of the aromatic moiety, different architectures are obtained. Adapted with permission from American Chemical Society: Ref. 257. Copyright © 2007, American Chemical Society.

USC UNIVERSIDADE DE SANTIAGO DE COMPOSTELA

[254] L. R. MacGillivray, J. L. Atwood, *Nature*, **1997**, *389*, 469 – 472.
[255] J. L. Atwood, L. J. Barbour, A. Jerga, *Proc. Natl. Acad. Sci. U. S. A.* **2002**, *99*, 4837 – 4841.
[256] P. Anzenbacher Jr. K. Jursıíková, V. M. Lynch, P. A. Gale, J. L. Sessler, *J. Am. Chem. Soc.* **1999**, *121*, 11020 – 11021.
[257] G. Gil-Ramírez, J. Benet-Buchholz, E. C. Escudero-Adán, P. Ballester, *J. Am. Chem. Soc.* **2007**, *129*, 3820 – 3821.
[258] P. Ballester, G. Gil-Ramírez, *Proc. Natl. Acad. Sci. U. S. A.* **2009**, *106*, 10455 – 10459.
[259] For further information about molecular recognition see: L. Escobar, P. Ballester, *Chem. Rev.* **2021**, *121*, 2445 – 2514.

α,δ-CYCLIC PEPTIDE BASED CAPSULES

As mentioned in the Introduction, in our group we recently developed α,γ-cyclic peptide-based capsules. For this purpose, the Fukuyama method for amine functionalization was followed.[260] This strategy consisted of using nitrobenzenesulfonamides (Ns-amides) as both a protecting and activating group for the introduction of a define functionality at the N-terminal end of the γ-residue. This group consists of an electron-poor aromatic sulfonamide with a nitro group at its *ortho* or *para* position. The acidity of the sulfonamide proton increases notably by inductive effect decreasing the pKa value under 15 units, considerably lower than those observed for amines, amides or carbamates. This facilitates its subtraction by mild basic conditions, friendly with other groups that might be sensitive to strong bases. After deprotonation of the sulfonamide, the resulting anion can be captured with a poorly sterically hindered electrophile generating the N-alkyl species. In this way, the use of electrophiles that includes a specific function would enable the anchoring of a molecular cap. Subsequent self-assembly of both peptide subunits directed by hydrogen bonding will led to the supramolecular capsules. For instance, the condensation reaction between two hydrazide motifs located on the alkylated face of a CP and an aldehyde function at the peripheral site of a porphyrin unit gave rise to a peptide-based supramolecular capsule that was able to recognize selectively different diamine ligands within the inner volume (Figure 80A).[261] A cyclic hexapeptide decorated with three *meta*-pyridyl moieties was shown to provide dimeric capsules capable to confine xenon with unexpected selectivity (Figure 80B).[122] The encapsulation of this element permitted its handling under open-air environment. Likewise, an *ortho*-pyridine-substituted cyclic hexapeptide was reported (Figure 80C).[146] These assemblies were proven as good ion transporters across lipid membranes.

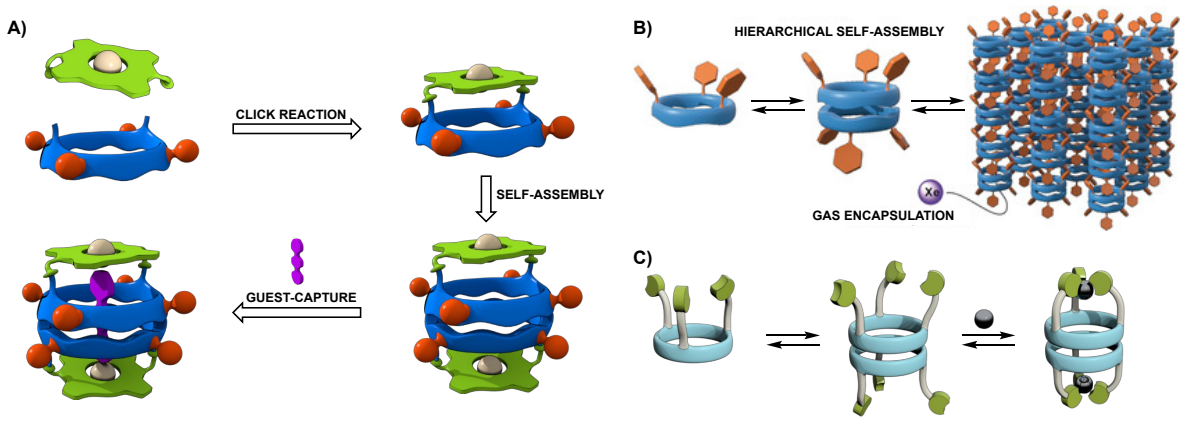


Figure 80. Cyclic peptide based-capsules: A) Click reaction between a cyclic peptide and a porphyrin molecule that act as a cover and those bearing B) *meta*- C) *orto*-pyridine motifs.

USC UNIVERSIDADE DE SANTIAGO DE COMPOSTELA

[260] a) T. Fukuyama, C.-K. Jow, M. Cheung, *Tetrahedron Lett*. **1995**, *36*, 6373 – 6374. **b)** T. Fukuyama, M. Cheung, C.-K. Jow, Y. Hidai, T. Kant, *Tetrahedron Lett*. **1997**, *38*, 5831 – 5834.

[261] H. L. Ozores, M. Amorín, J. R. Granja, *J. Am. Chem. Soc*. **2017**, *139*, 776 − 784.

DESIGN

As outlined in Chapter 2, the recognition capacity of a molecular receptor is determined by the nature and shape of the internal cavity. In some cases, it has been observed that the encapsulation process can be modulated introducing a motif that actively participate in this event by interacting with the guests to promote the reception of the substrates. Thus, it might be possible to increase the selectivity of certain compounds, to recognize hosts with low affinity for the cavity or to increase the association constants due to the additional stabilization effect provided by the directing group. We have demonstrated that dodecameric α,δ-cyclic peptide nanotubes have the ability to encapsulate C_{60} fullerene molecules within the internal cavity. We envisioned that it would be possible to fine-tune this capacity inserting a fullerene-recognizing group. For this purpose, we considered that subphthalocyanine (SubPc) units would be the most suitable candidate in relation to the dimensions and symmetry of the dodecameric peptides. SubPc are organic compounds with C_3 simmetry composed of a macrocyclic ring system with a 14 π-electron aromatic core arranged by three isoindole subunits that are bound together by three aza-bridges.[262] This heteroannulene composition adopts a non-planar cone-shaped conformation with the ability to accommodate a B(III) ion at its central binding core. This macromolecule exhibit very attractive electronic and physical properties. It is worth to highlight its electron-donating behavior which matched perfectly with the electron-accepting ability of carbon allotropes for the construction of molecular photovoltaics.[263] Therefore, a N-alkylated α,δ-cyclic peptide can be covered with a SubPc cap upon a click-like reaction leading to a supramolecular capsule with fullerene recognition capacity. Moreover, the capsules could be connected through the boron atom axial position in the presence of diamine ligands leading to electronic cyclic peptide nanowires. This system would show light-harvesting properties and might be useful for the construction of peptide-based organic photovoltaics (OPVs).

USC UNIVERSIDADE DE SANTIAGO DE COMPOSTELA

[262] For further structural information of SubPc see: C. G. Claessens, D. González-Rodríguez, M. S. Rodríguez-Morgade, A. Medina, T. Torres, *Chem. Rev*. **2014**, *114*, 2192 – 2277.

[263] For further information about SubPc's applications see: G. de la Torre, G. Bottari, T. Torres, *Adv. Energy Mater*. **2017**, *7*, 1601700.

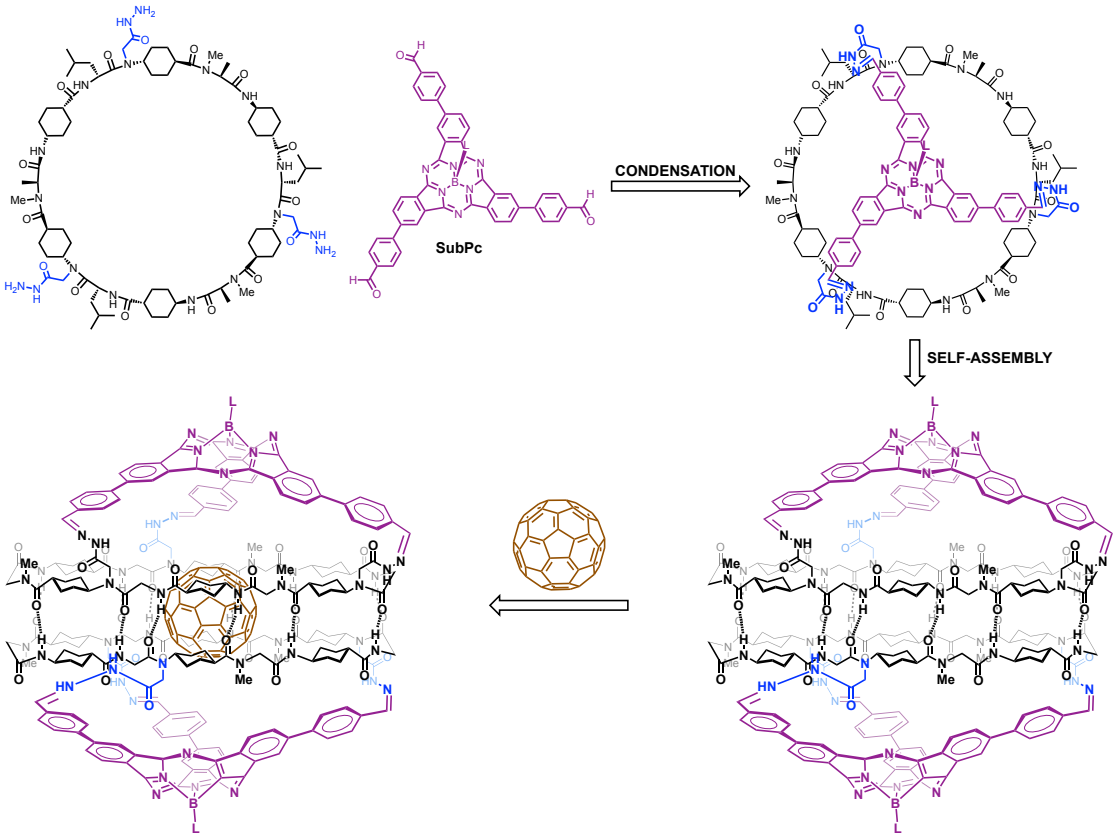


Figure 81. Representation of the proposed strategy for the formation of α,δ-cyclic peptide-based supramolecular capsules.

As mentioned earlier, SubPc presents a C_3 symmetry axis that match with α,δ-cyclic peptide dodecamer. Moreover, the distance between the tunable peripheral sites of the selected molecular cap match with the distance of the anchoring points of a dodecamer based on α,δ-CPs. For this reason, a 12-residues N-alkylated cyclic peptide was designed (Figure 81). Regarding the dimeric models used in Chapter 1, α-amino acids of the same chirality and those δ-Ach preceding them will be N-alkylated. Concerning the connection with the molecular cap, the condensation reaction of hydrazone formation seems to be the most suitable because it is a clean reaction and SubPC with three aldehyde groups can be easily synthesized. For this reason, those N-alkylated δ-Ach residues will be decorated with hydrazides groups. In contrast, α-amino acids of *L*-chirality will be N-methylated. Ala residues were chosen because of the simple N-methylation conditions. To promote the solubility in non-polar solvents, the other α-residues will be Leu. The target sequence of the supramolecular capsule-forming peptide is as follows: *c*-[^{2HNNH2Ac}*N*-δ-Ach-^{Me}*N*-*L*-Ala-δ-Ach-*D*-Leu-]$_3$.

COMPUTATIONAL STUDIES

To evaluate the viability of the proposed design, computational calculations were carried out. For this purpose, the geometry of the structures was optimized using the semiempirical

method PM7[264] employing the software Gaussian.[265] This level of optimization was necessary due to the large number of atoms that composed the supramolecular system. First, both subcomponents of the proposed capsule –α,δ-CP dimer and SubPC molecular cover– were modeled separately (). The distance between the aldehyde groups at the peripheral positions of the SubPc were close to the distance between the anchoring points with the peptide. Therefore, as we expected, the subunits have the appropriate geometry to be connected giving rise to the supramolecular capsule. Then, the stability of the system was assessed. It was observed that SubPc can be linked to the dimeric structure on the N-alkylated faces by a condensation reaction and the final architecture is completely stable. It is worth to mention that the resulting capsule has an internal volume big enough to accommodate up to three fullerene molecules.

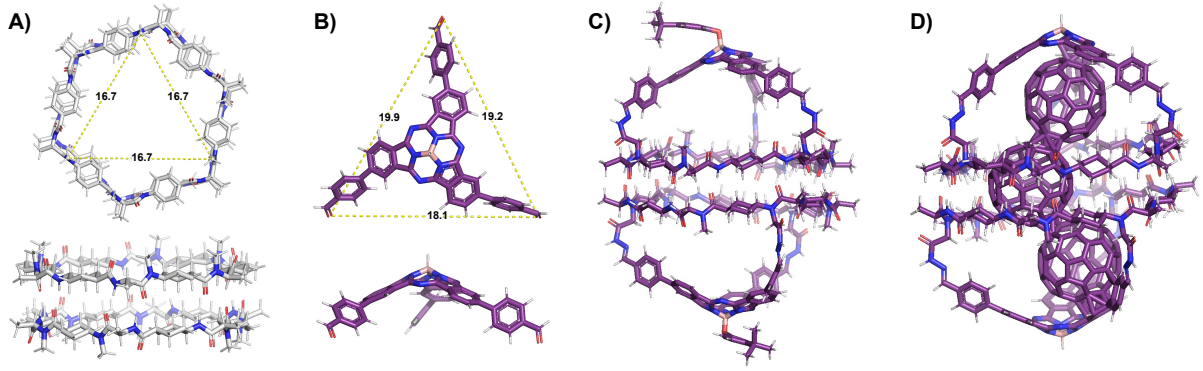


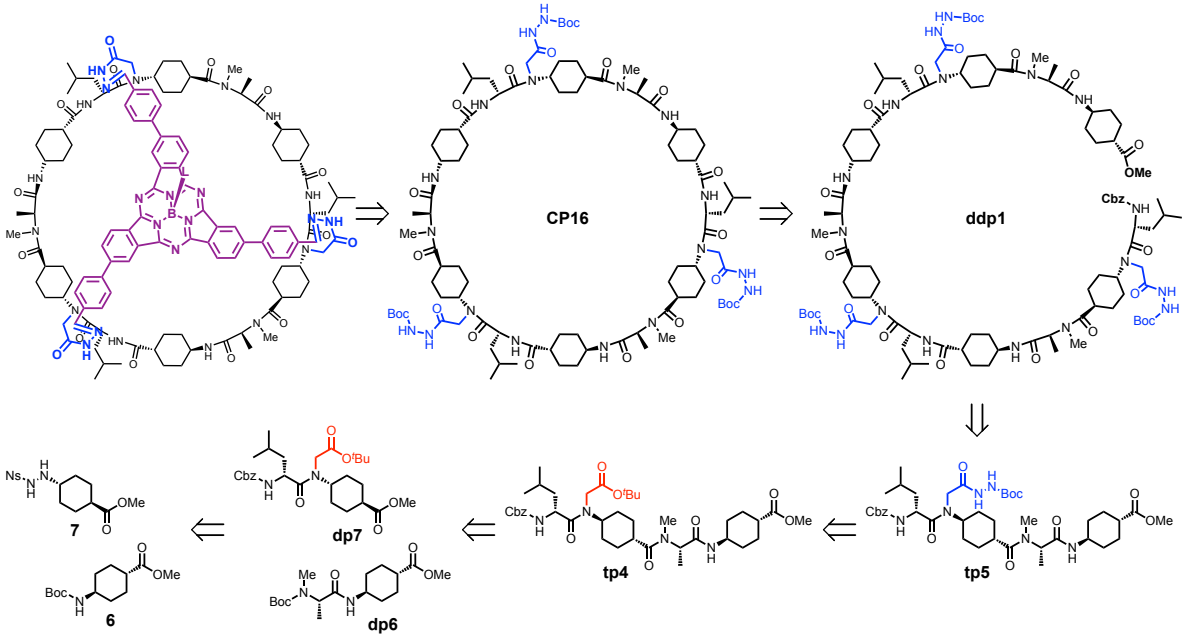
Figure 82. Optimized geometries at PM7 level of A) N-methylated α,δ-cyclic peptide dimer (on top, top-view with the corresponding distances between the anchoring points and bottom, side-view), B) SubPc motif decorated with aldehydes at its peripheral sites (on top, top-view with the corresponding distances between the aldehyde group and bottom, side-view) and C) α,δ-cyclic peptide capsule. D) Representation of a capsule with 3 fullerene molecules inside the inner volume.

1ST SYNTHETIC STRATEGY

Once settled the sequence of the capsule precursor cyclic peptide, the next step consisted of the definition of a synthetic strategy. Based on the dimeric CPs described above, we decided to employ a convergent synthesis in solution because the use of N-alkylated artificial amino acids required prior preparation. As already discussed, in-solution synthesis provides greater control over the necessary amino acid amounts and the alkyl groups also improves the solubility in organic solvents. Moreover, the peptide can be grown from a repetitive motif that will reduce the number of coupling step of less reactive secondary amines.

USC UNIVERSIDADE DE SANTIAGO DE COMPOSTELA

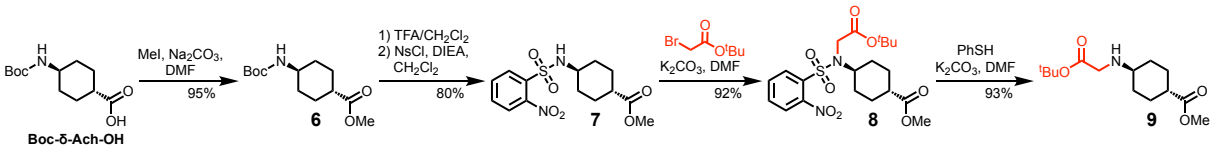
[264] J. J. P. Stewart, *J. Comput. Chem.* **1989**, *10*, 209 – 220.
[265] M. J. Frisch *et al*. *Gaussian, Inc. Wallingford CT*, **2016**.



Scheme 11. Retrosynthetic scheme for the preparation of the capsule forming cyclic peptide **CP16**.

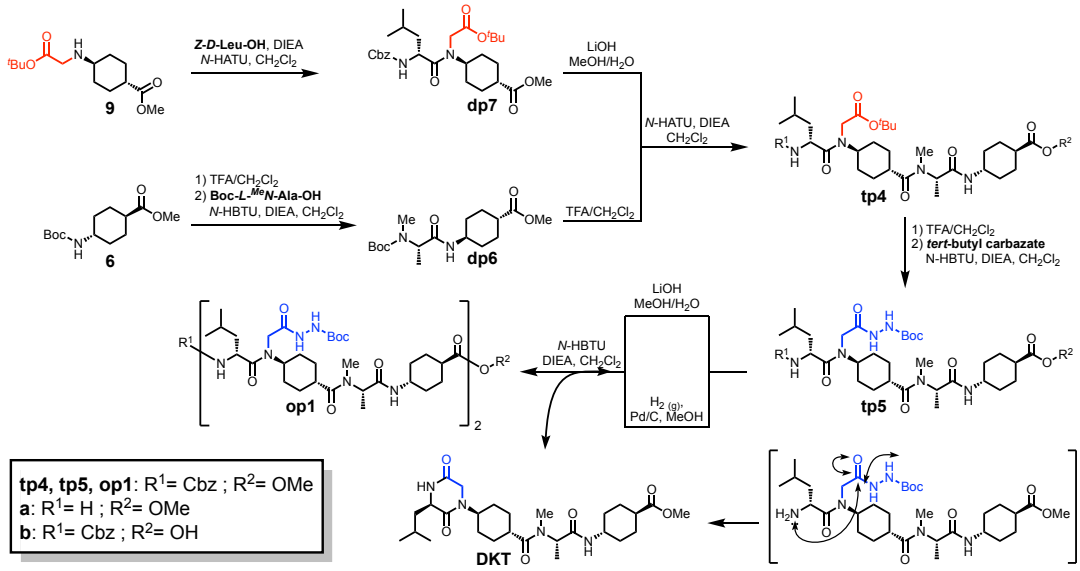
This peptide presents an additional functional group to attach the peptide to the molecular cap. At this respect, we considered that the choice of the protecting groups is a critical feature to obtain the desired CP. Furthermore, the introduction of the hydrazide group is a key synthetic step. As shown in the retrosynthetic analysis illustrated in Scheme 11, the designed cyclic peptide (**CP16**) would be cyclized from the linear dodecamer (**ddp1**) which would be prepared following a convergent synthetic process from the tetrapeptide **tp5**. At this point, the hydrazide motif would be introduced after a coupling reaction between the masked carboxylic acid on the amide nitrogen of the δ-Ach in **tp4** and the commercially available ***tert*-butyl carbazate**. The tetrapeptide **tp4** will be grown upon sequential deprotection/coupling steps from the corresponding amino acids **6** and **7**. In this synthesis we decided to use the benzyloxycarbonyl carbamate (*Z* or Cbz) and the methyl ester (OMe) protecting groups for the N- and C-terminal ends, respectively. Both groups are orthogonal and the deprotection conditions are simple and clean. An acid labile protecting group was selected for the N-substituent of the δ-residue. A *tert*-butyl ester for the carboxylic acid of **tp4** and *tert*-butoxylcarbonyl carbamate (Boc) for the hydrazide motif of **tp5**.

The synthetic process was started by preparing the N-functionalized δ-Ach. For this purpose, we employed the Fukuyama strategy (described above) for amine alkylation.[260] First, the **Boc-δ-Ach-OH** was protected at the C-terminal end as methyl ester by treatment with MeI in the presence of a base (Na_2CO_3). Then, the Boc group was removed in acidic medium and consecutively, the resulting ammonium salt was treated with 2-nitrobenzesulfonyl chloride in the presence of DIEA providing the fully protected amino acid **7**. This amino acid was dissolved in DMF and reacted with ***tert*-butyl bromoacetate** using K_2CO_3 as base to give the compound **8**. Finally, the Ns group was removed by treatment with thiophenol and K_2CO_3 affording the desired N-functionalized δ-residue in an overall yield of 65% for the four steps.



Scheme 12. Synthetic scheme for the preparation of the N-functionalized δ-Ach (**9**).

After the preparation of this essential building block, the next step was the synthesis of the desired intermediate tetrapeptide **tp5** (Scheme 13). The strategy used **Boc-δ-Ach-OMe** (**6**) as starting material that was reacted in a mixture of TFA/CH_2Cl_2 (1:1 v/v) and subsequently, coupled with **Boc-*^{Me}N-L*-Ala-OH** using *N*-HATU and DIEA to obtain **dp6**. On the other hand, compound **9** was coupled to **Cbz-*D*-Leu-OH** using *N*-HBTU as coupling agent and DIEA providing the corresponding dipeptide **dp7**. Both dipeptides were connected together. For that, **dp7** was dissolved in a mixture of MeOH/H_2O (3:1 v/v) and treated with LiOH giving rise to the carboxy-free derivative. Simultaneously, **dp6** was deprotected at its N-terminal end by treatment with a TFA/CH_2Cl_2 and the resulting ammonium salt was dissolved in dry CH_2Cl_2 and poured into a mixture of **dp7** carboxy-free derivative, *N*-HATU and DIEA in CH_2Cl_2 to afford **tp4**. At this point we decided to introduce the hydrazide group. For this, the *tert*-butyl ester was removed by stirring **tp4** in a mixture of TFA/CH_2Cl_2 (1:1, v/v) for 1 h. The resulting intermediate was treated with *N*-HBTU and DIEA, and then ***tert*-butyl carbazate** was added to give rise to the tetrapeptide with a protected hydrazide group (**tp5**).



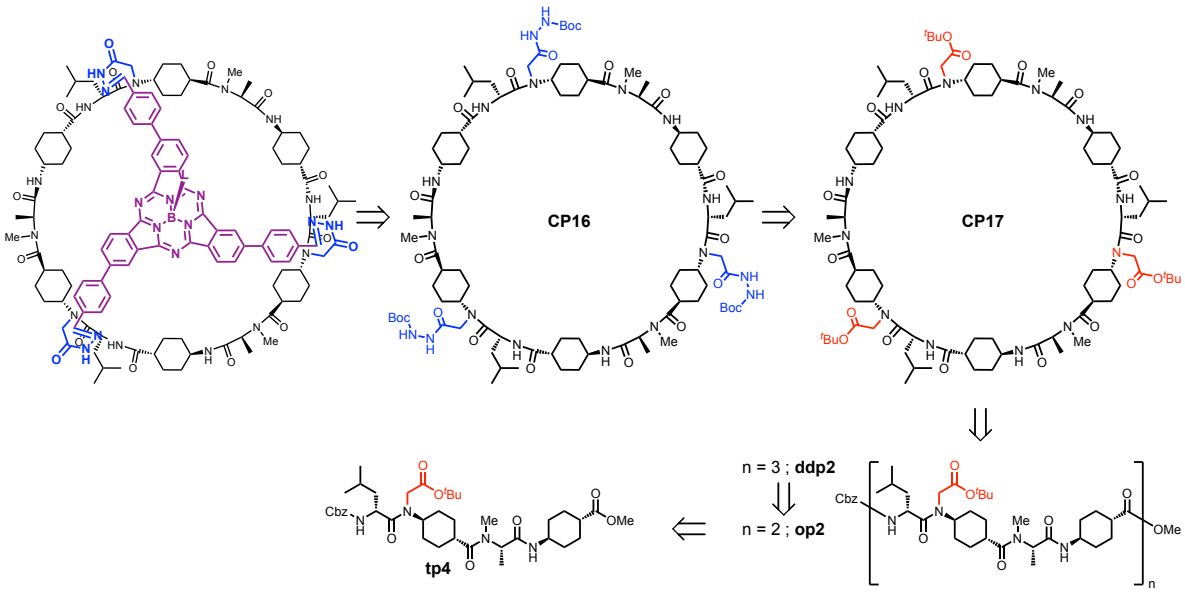
Scheme 13. Synthetic scheme for the preparation of **op1**. Below, the proposed mechanism of reaction of diketopiperazine by-product is detailed.

The target dodecamer would be grown from **tp5** by convergent synthesis using this tetramer as building block (Scheme 13). For this purpose, **tp5** was divided into three fractions. The first portion was deprotected at its N-terminal end through a palladium-catalyzed hydrogenolysis to provide **tp5a**. The second split was reacted with LiOH in a MeOH/H_2O mixture (3:1 v/v) to give rise to the tretapeptide with the free C-terminal end **tp5b**. The reaction of the resulting compounds in the presence of *N*-HBTU resulted in octapeptide **op1**, unfortunately in low yields (< 20%). MS analysis of the crude of the reaction revealed an ion

with a mass of 520 m/z signal that correspond with the product losing the *tert*-butyl carbazate motif. Based on this result, we identified this signal as a diketopiperazine (DKT) by-product. This product must be formed by an intramolecular addition/elimination reaction between the terminal free amine and the carbonyl function adjacent to the hydrazide group that act as the leaving group. This side reaction appears to proceed faster than the coupling process reducing drastically the yields. Since this problem would occur in the next stages of synthesis (dodecamer formation and cyclization), it was decided to explore other alternative routes for the preparation of the cyclic peptide.

2ND SYNTHETIC STRATEGY

Peptides are polyfunctional compounds susceptible to side reactions. For this reason, many efforts have been made to avoid such drawbacks. The choice of protecting groups is a key factor to preclude the formation of such undesired products.[266] In particular, the formation of diketopiperazines can be prevented using bulky protecting groups that disfavor intramolecular attack by steric hindrance.[267] It has been reported that the *tert*-butyl ester prevents diketopiperazine formation. Although the Boc group contains a *tert*-butyl group, the space between the carbonyl and this group may be large enough to allow the amine nucleophilic attack. In this context, we decided to prepare **CP16** from **CP17** which would be synthesized by a convergent peptide synthesis starting from already prepared **tp4** (Scheme 14). In this strategy, the hydrazide group would be incorporated at the end of the synthesis after the cyclization reaction.

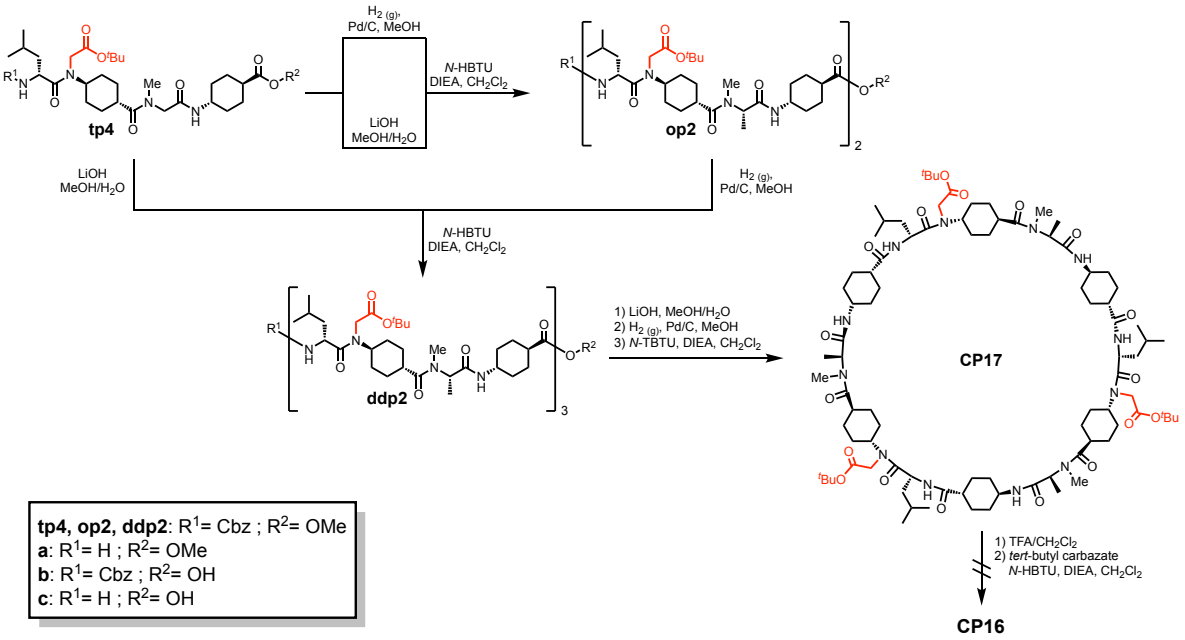


Scheme 14. Retrosynthetic scheme for the preparation of the cyclic peptide capsule precursor **CP16**.

Following the same procedure as the previous synthetic approach, the **tp4** was split into three fractions. One portion was treated with Pd/C in MeOH and reacted under hydrogen atmosphere providing the free terminal amine derivatie **tp4a**. On the other hand, the second

[266] A. I.-Llobet, M. Álvarez, F. Albericio, *Chem. Rev.* **2009**, *109*, 2455 – 2504.
[267] K. J. Jensen, J. Alsina, M. F. Songster, J. Vágner, F. Albericio, G. Barany, *J. Am. Chem. Soc.* **1998**, *120*, 5441 – 5452.

fraction was deprotected by treatment with LiOH yielding the free carboxylic acid (**tp4b**). The resulting compounds were couple using *N*-HBTU as coupling reagent in the presence of DIEA affording the desire octapeptide **op2** in good yields (55%). MS was used to elucidate the structure of this product because the NMR spectrum in non-polar solvents revealed a complex mixture of different conformations that did not allow a clear assignment of the proposed structure.



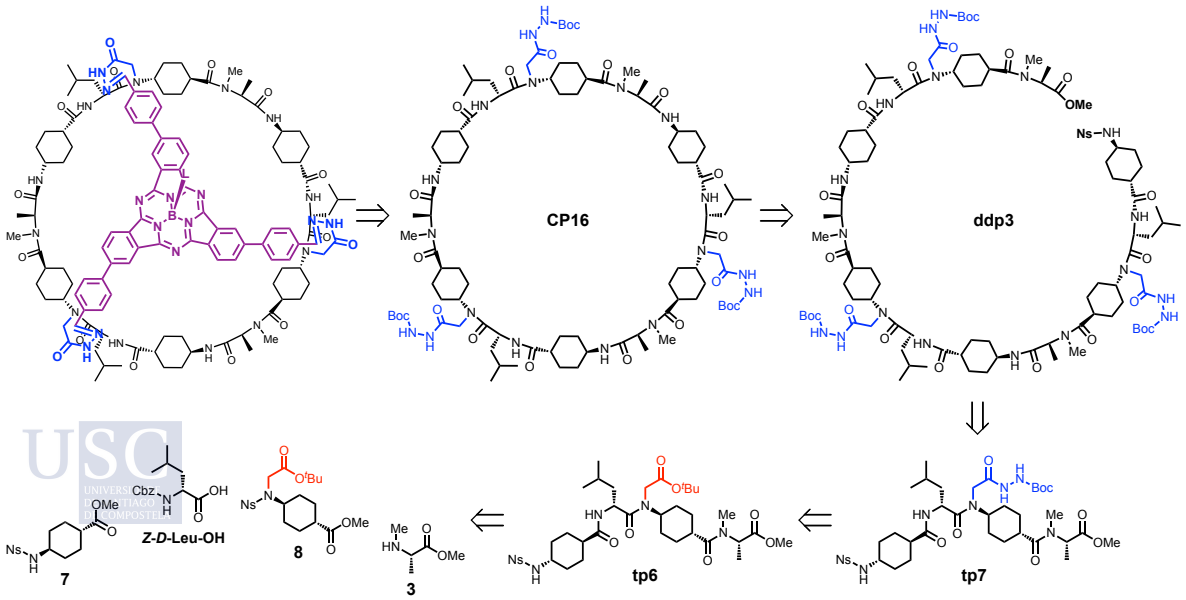
Scheme 15. Synthetic scheme for the preparation of capsule precursor cyclic peptide **CP16**.

We continued the synthesis with the preparation of **dd2**. For this purpose, palladium-catalyzed hydrogenation reaction of **op2** was used to remove the Cbz protecting group providing **op2a**. The resulting compound was reacted with the tetrapeptide carboxy-free derivative **tp4b** in a mixture of *N*-HBTU and DIEA in CH_2Cl_2. Under this conditions, the linear dodecamer **ddp2** was formed in good yields (57%). Again, the structure of this product was confirmed by MS. The next step was the macrocyclization reaction. To do this, the protecting groups at both terminal ends were removed. First, the methyl ester was hydrolyzed by treatment with LiOH and then, hydrogenolysis reaction led to the unprotected linear dodecamer **ddp2c**. Sequentially, the linear peptide was cyclized in high dilution conditions using *N*-TBTU as coupling reagent in the presence of DIEA providing cyclic peptide **CP17** in 32% yield. Now, this compound could be characterized by NMR. The simplicity derived from the C_3 symmetry permitted to elucidate the cyclic structure and the formation of the corresponding antiparallel supramolecular dimer as downfield chemical shft amide signals were detected. In order to prepare the capsule precursor peptide, the hydrazide motif has to be introduced at the acetyl groups attached at the CP skeleton. For that, **CP17** was treated with TFA/CH_2Cl_2. However, after 2 h of acid treatment, removal of the three *tert*-butyl groups was not observed. Unfortunately, longer reaction times led to the decomposition of the cyclic peptide making impossible the isolation of the unprotected cyclic peptide intermediate.

This synthetic strategy allowed to reach **CP17** confirming that the *tert*-butyl ester protecting group prevents diketopiperazine formation. In addition, it provided further evidence that the hydrazide motif can act as a leaving group favoring the intramolecular reaction. Although the deprotection conditions of ester removal at the last step of the synthesis could be optimized using a milder acid treatment for subsequent coupling with *tert*-butyl carbazate, it was decided to avoid the hydrazide incorporation at this stage. Therefore, we considered the evaluation of a different synthetic route.

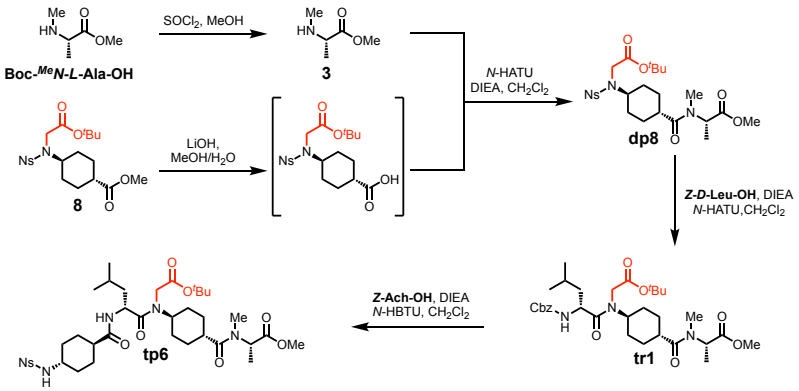
3RD SYNTHETIC STRATEGY

In previous synthetic approaches, the tetrameric building block was designed to provide a linear dodecamer that would enable to run the cyclization reaction from the primary amine of an α-amino acid. Another alternative to prevent the diketopiperazine formation side reaction would be redesigning the base tetrapeptide building block. Moving the acetyl derivative away from the second residue position would avoid the DKT formation reaction. Such strategy would allow to incorporate the hydrazide motif on the tetrameric building block facilitating the obtention of the cyclic peptide with the reactive group already attached to the final product. Therefore, we proposed a novel approach (showed in Scheme 16) in which the cyclic peptide would be prepared from the tetrapeptide **tp7**. In the novel strategy, the cyclization would take place between the carboxy group of a α-amino acid and the amine group of a δ-Ach residue. The compound **tp7** would be prepared through a coupling reaction between commercially available ***tert*-butyl carbazate** and the free carboxylic acid of **tp6** resulting from the hydrolysis of the *tert*-butyl ester. This precursor would be constructed by successive deprotection/coupling steps from the previously prepared amino acids. In this synthesis the 2-nitrobenzesulfonyl protecting group would be used during the growth of the cyclic peptide as we already had the compound **Ns-δ-Ach-OMe (7)** prepared in the lab. This group is stable under the synthetic conditions required during the construction of the target cyclic peptide.



Scheme 16. Novel retrosynthetic strategy for the preparation of cyclic peptide **CP16**.

The synthesis started with the esterification reaction of **H-*L*-^{Me}*N*-Ala-OH** by treatment with thionyl chloride providing the alanine methyl ester (**3**). The N-functionalized δ-Ach **8** was deprotected at its C-terminal using LiOH and the resulting carboxylic acid was coupled with **3** using *N*-HATU in the presence of DIEA. Under this conditions, dipeptide **dp8** was generated in 83% yield. The structure of this product was easily confirmed by NMR. The sulfonamide was removed with thiophenol in the presence of a base (K_2CO_3). The resulting product was purified by flash column chromatography to remove the sulfur by-products that might interfere in the following coupling reaction. After purification, ***Z-D*-Leu-OH** was coupled using *N*-HATU to afford tripeptide **trp1**. Unfortunately, the NMR did not provide full evidence of the tripeptide structure. In this case, as in previous peptide compounds, the tripeptide showed the characteristic behavior of different conformers in slow exchange at the NMR timescale. For this reason, MS was employed to complete the characterization of this product. The benzyloxycarbonyl masking motif was eliminated via palladium catalyzed hydrogenolysis. After filtration, the resulting material was coupled with the last residue. For this purpose, **Ns-δ-Ach-OMe** (**7**) was hydrolyzed by treatment with LiOH to give the carboxy-free derivative. The resulting product was preactivated by treatment with *N*-HBTU and DIEA in CH_2Cl_2 and then, the mixture was poured into solution of the previously deprotected tripeptide. Using this approach, **tp6** was obtained with an overall yield of 50%. NMR spectroscopy provided some structural information as certain characteristic signals could be identified, such as the aromatic signals of the nitrobenzenesulfonyl moiety and those attributed to the *tert*-butyl group on the δ-Ach. However, to fully elucidate the structure MS was necessary.



Scheme 17. Synthetic strategy for the preparation of **tp7**.

At this point, the incorporation of the hydrazide motif was studied. For this purpose, **tp6** was treated with a mixture of TFA/CH_2Cl_2 to remove the *tert*-butyl ester. The free carboxylic acid was then reacted with ***tert*-butyl carbazate** in the presence of a coupling agent. A screening of conditions to optimize the reaction yields was performed, the summary of these results is shown in Table 5. The use of *N*-HBTU or *N*-HATU with DIEA in CH_2Cl_2 as solvent provided **tp7** in poor yield. A carbodiimide coupling agent (EDC·HCl) in the presence of hydroxybenzotriazol as additive in CH_2Cl_2 gave rise to the desired product in moderate yield (55%). In order to improve these conditions, this reaction was also tested using DMF and MeCN as solvents. However, the reaction performance continued to be low. Treatment of the carboxylic acid with PyAOP and DIEA in CH_2Cl_2 resulted in **tp7** in very good yield (83%)

(Entry 6). Some changes in the NMR spectrum confirmed the formation of the desire product, such as the disappearance of the signal corresponding to the tert-butyl ester of **tp6** and the appearance of a new singlet characteristic of the Boc group. Moreover, novel signals related with the hydrazide protons were also detected. This reaction was scaled up without significant changes in yield.

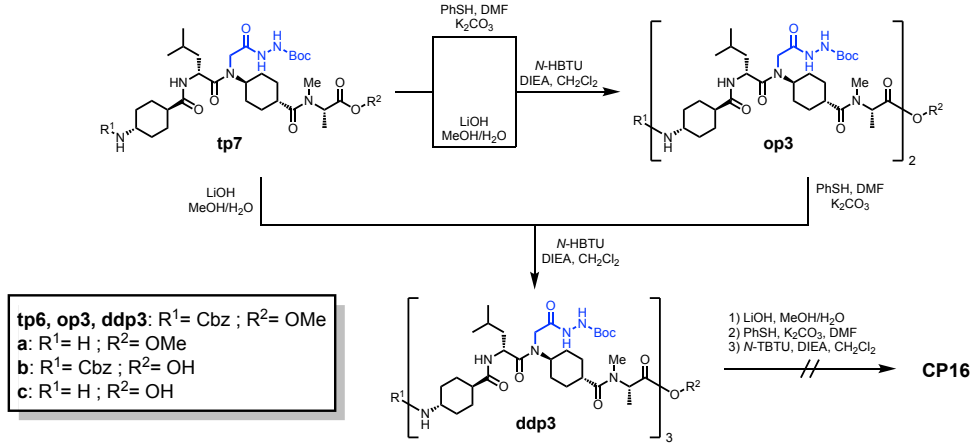


Entry	X: Coupling Reagent	Solvent	Reaction time (h)	Isolated Yield
1	*N*-HBTU	CH_2Cl_2	2	22%
2	*N*-HATU	CH_2Cl_2	2	30%
3	EDC·HCl	CH_2Cl_2	2	55%
4	EDC·HCl	DMF	2	58%
5	EDC·HCl	MeCN	2	22%
6	PyAOP	CH_2Cl_2	2	83%

Table 5. Optimization for the reaction of hydrazide introduction.

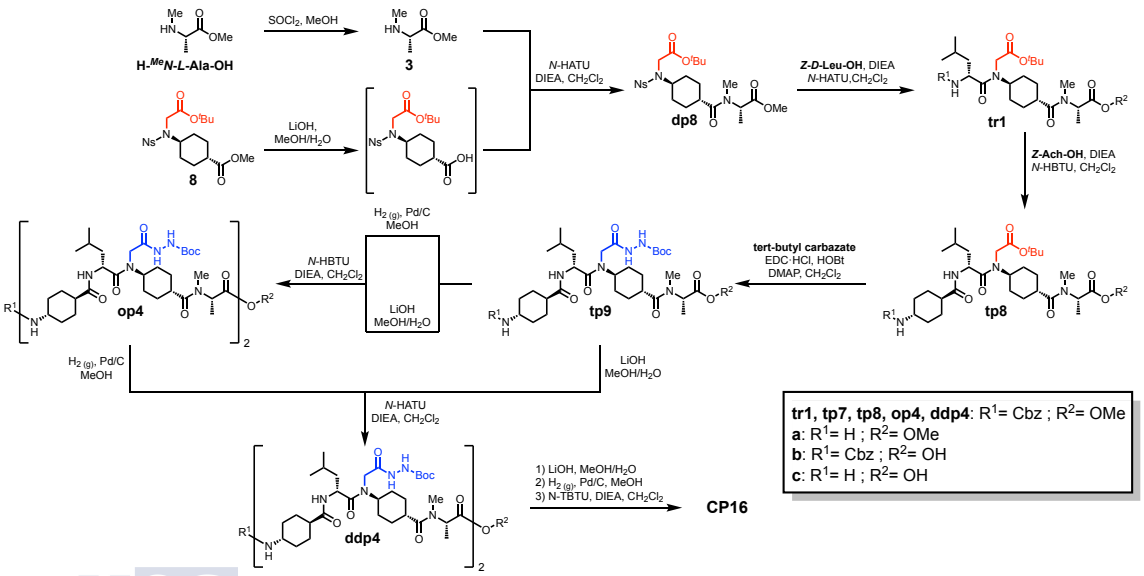
Once a considerable amount of the tetrapeptide was prepared, the linear peptide was growth following a similar procedure as previous synthesis attempts. Tetrapeptide **tp7** was divided into three portions. The first fraction was treated with thiophenol in the presence of K_2CO_3 in DMF to remove the sulfonamide. Then, H_2O was added to the reaction mixture. In this case, the thio-compound generated as by-product was eliminated by several washes of the resulting aqueous mixture with Et_2O. Finally, the aqueous solution was extracted with CH_2Cl_2 to provide the N-terminal unprotected tetrapeptide **tp7a**. On the other hand, the second fraction was deprotected at its C-terminal end by treatment with LiOH to provide **tp7b**. The resulting products were coupled using *N*-HBTU as reagent in the presence of DIEA to afford the octamer **op3** in good yields (66%). MS of the isolated compound confirmed the proposed structure. The next step involved the preparation of the linear dodecamer. For this purpose, the N- and C-terminal end protecting groups of **op3** and **tp7**, respectively, were removed and the unprotected peptides **op3a** and **tp7b** were reacted using a mixture of *N*-HBTU and DIEA in CH_2Cl_2. Under these conditions, the linear dodecamer **ddp3** was obtained in 50% yield. Again, this product was characterized by MS to confirm its structure. Finally, the cyclization of the linear dodecapeptide was carried out. To do that, the methyl ester was hydrolyzed by treatment with LiOH and subsequently, the sulfonamide was removed using standard condition to yield the linear unprotected peptide (**ddp3c**). Lastly, **ddp3c** was treated with *N*-TBTU under high dilution condition to promote its cyclization. Unfortunately, under these conditions the desired cyclic peptide was not detected. Careful analysis of deprotection and cyclization steps revealed

that half of the mass of the product was lost after the work-up of the nosyl group deprotection reaction. Moreover, the free peptide appears to be very insoluble in non-polar organic solvents. In view of these results, we considered to replace the protecting group on the N-terminal end of the tetrameric base building block.



Scheme 18. Synthetic strategy for the preparation of **CP16**.

In the previous synthetic attempt, a tedious work-up after the nosyl group deprotection step was required in order to remove the sulfur side products generated during the progress of the reaction. For this reason, we decided to use Cbz as protecting group at the N-terminal end because the catalytic hydrogenolysis necessary for the elimination of this group is cleaner and does not require laborious work-up in aqueous medium. Therefore, the loss of a large amount of product during this process would be minimized, specially at late-stage synthesis steps.



Scheme 19. Successful synthetic strategy for the obtention of the capsule forming cyclic peptide **CP16**.

For the preparation of the tetrameric building block base **tp9**, the same synthetic protocol described above was followed. In this case, **tr1a** was coupled with the commercially available **Cbz-δ-Ach-OH** to provide **tp8** in good yield (75%). The structure of this compound was confirmed by MS. For the introduction of the hydrazide motif, we found that the treatment of

tp8 with a weaker acid, such as formic acid, gave rise to the free carboxylic derivative in a cleaner manner. The reaction of the resulting compound with ***tert*-butyl carbazate** using EDC·HCl and HOBt as coupling agents led to **tp9** in 85% yield. In this case, the use of PyAOP yielded pyrrolidinic side products that were extremely difficult to separate from the product by flash column chromatography. This compound was again characterized by MS. Once this key intermediate was obtained, the linear dodecamer **ddp4** was grown. For this purpose, a series of consecutive deprotection and coupling reactions were performed using the standard conditions. The intermediate octamer **op4** obtained in x% yields and its structure was confirmed by MS. Once **ddp4** was obtained by coupling of the corresponding deprotected peptides **op1a** and **tp1b**, the peptide was cyclized. To do that, the C- and N-terminal ends were consecutively deprotected and then, the cyclization was run using *N*-TBTU under high dilution condition to facilitate the intramolecular reaction. To carry out this last reaction, DMF was added in order to enhace the solubility of the deprotected dodecamer **ddp4c** as it was shown to be slightly insoluble in dichloromethane. The synthesis was stopped at this stage because few product was obtained and purification conditions must be optimized before proceed with the condensation reaction that would provide the supramolecular capsules.

USC
UNIVERSIDADE
DE SANTIAGO
DE COMPOSTELA

USC
UNIVERSIDADE
DE SANTIAGO
DE COMPOSTELA

CONCLUSIONS

USC
UNIVERSIDADE
DE SANTIAGO
DE COMPOSTELA

USC
UNIVERSIDADE
DE SANTIAGO
DE COMPOSTELA

CONCLUSIONS

Throughout the lines of this PhD dissertation, we have elucidated the structural bases that govern the molecular self-assembly process of a new class of cyclic peptides (α,δ-CPs) that include a novel artificial residue (δ-Ach) that acts as a rigid elongator capable of modifying the internal properties of the resulting assembles.

First (Chapter 1), an exhaustive structural study to evaluate the supramolecular properties, differentiation between the parallel and antiparallel β-sheet structures, of this novel α,δ-CPs was carried out. The conducted experiments using cyclic peptide of different length revealed that dodecamers and hexadecamers self-assembled with high association constants, while octamers remained as monomers in non-polar solvents such as chloroform. In these studies, the relative stability of the possible parallel and antiparallel interactions was evaluated. Our results showed that in α,δ-CPs systems the parallel arrangement is more stable considering only the cyclic peptide backbone interactions. Computational studies using the same systems provided reasonable evidences that this tendency can be explained by the better packing of the axial hydrogens of cyclohexyl moieties, in contrast with the disfavored packing of the antiparallel stacking. An extension of these studies to α,γ-CPs showed that, contrary to initial assumptions, the parallel sheet is more stable when both peptide subunits share the same chirality. In addition, these experiments revealed new types of interactions not studied so far, in which the pairing peptides contained γ-amino acids of opposite chirality. The parallel interaction through the γ-face of this type of peptides was, therefore, evaluated and found to compete with the corresponding antiparallel homodimers with similar stability. Again, the higher stability of the parallel arrangement could be explained by the better packing of the axial hydrogens. It was also observed that this trend can be reversed by modulating the side chains interactions of the α-amino acids. The incorporation of amino acids with bulky side chains preferentially forms the antiparallel β-sheet. These results contrast with previous assumptions about α,γ-cyclic peptide-based systems and should be accounted for future designs of this type of cyclic peptides.

In the second Chapter of this manuscript, we used the information from the previous structural studies to prepare a nanotube-forming α,δ-CP. A dodecameric cyclic peptide that contain polar α-amino acids was shown to stack into tubular structures in aqueous solutions triggered by pH neutralization. The introduction of the δ-Ach derivatives into the cyclic peptide sequence provided nanotubes with internal hydrophobic properties due to the disposition of two methylene groups per cyclohexyl unit pointing into the inner cavity. The hydrophobic properties and the larger internal diameter of the resulting assemblies were efficiently implemented for the encapsulation of different non-polar macromolecules in biocompatible environments, such as fullerene C_{60} and Single-Walled Carbon Nanotubes (SWCNT). These findings led to new supramolecular polymers with tailored assembly properties that could be useful for the development of efficient drug delivery platforms. The new peptide hybrid

structures described in Chapter 2 would have potential applications as molecular electronic components.

Finally in the last chapter, we dealt with the construction of supramolecular capsules derived from self-assembled α,δ-CPs. Semiempirical computational calculations (PM7) revealed that a cyclic dodecamer bearing three chemical connectors pointing perpendicular to the peptide ring and a subphtalocyanine (SubPc) molecule would share the shape (C_3 symmetry) and size to form a new kind of supramolecular capsule. The resulting cage-like assemblies based on the α,δ-CPs/SubPc complex would have a large internal volume which could hold up to 3 C_{60}-fullerene molecules. For the construction of the capsule, several synthetic strategies for the preparation of precursor cyclic peptide were explored. In the first approach, the formation of diketopiperazine (DKT) was detected as capping by-product decreasing considerably the yield of the coupling steps. A new synthetic approach was proposed in which the acetyl hydrazide moiety of the Ach residue was relocated from the second position in the growing peptide chain to address the construction of the cyclic peptide scaffold avoiding DKT formation. For this, the position of the hydrazide group was shown to be a key feature for the viability of the synthesis. After searching for the most suitable protecting groups, we were able to prepare the desired cyclic peptide which would give rise to the desired supramolecular capsule. Future work will include the condensation reaction for the anchoring of the SubPc cap on the already synthetized cyclic peptide.

USC
UNIVERSIDADE
DE SANTIAGO
DE COMPOSTELA

EXPERIMENTAL SECTION

USC
UNIVERSIDADE
DE SANTIAGO
DE COMPOSTELA

USC
UNIVERSIDADE
DE SANTIAGO
DE COMPOSTELA

EXPERIMENTAL SECTION

GENERAL REMARKS

Commercially available reagents purchased from Acros Organics Ltd., Alfa Aesar, Bachem, Carbosynth, Fischer Scientific, Fluorochem Ltd., Iris Biotech, Sigma-Aldrich, TCI or GL Biochem (Shanghai) Ltd, China. They were used without further purification unless otherwise noted. Deuterated solvents were obtained from Aldrich or Deutero. Dichloromethane was distilled from calcium hydride immediately prior to their use. All solvents are HPLC or synthesis grade.

Analytical thin-layer chromatography was performed on E. Merck silica gel 60 F_{254} plates. In case of not been UV active (245/365 nm), the compounds were visualized by dipping the plate in revealing solutions: ninhydrin (2% in ethanol), Hanessian stain (200 mg $Ce(NH_4)_2(NO_3)_6$ + 9.6 g $Mo(NH_4)_2O_4$ + 11.2 mL H_2SO_4 + 200 mL H_2O), phosphomolybdic acid (3 g $H_3[P(Mo_3O_{10})_4]$ in 100 mL ethanol) or potassium permanganate (1.5 g $KMnO_4$ + 10 g K_2CO_3 + 1.25 mL aqueous solution NaOH (10%) + 200 mL H_2O), followed by heating. Silica gel flash chromatography was performed using E. Merck silica gel (type 60 SDS, 230-400 mesh). Solvent mixtures for chromatography are reported as v/v ratios. Normal phase HPLC purification was carried out on JASCO LC-4000 or Waters 2489 using a semipreparative Phenomenex Luna 5 µm silica 100 Å or SunFire Prep Silica OBD 5 µm columns with CH_2Cl_2/MeOH gradients between 100:0 and 85:15. Reverse phase HPLC purification was carried put on HITACHI D-7000 or Waters 2489 using a semipreparative Phenomenex Luna 5 µm C18 or preparative Agilent Eclipse XDB-C18 columns with H_2O MiliQ® (0.1% TFA)/MeCN (0.1% TFA) gradients between 100 and 5:95.

Supercritical Fluid Chromatography (SFC) analysis was executed on Jasco Series 4000 instrument using a Phenomenex Lux Cellulose-5 column.

Nuclear Magnetic Resonance spectra were recorded on Varian Inova 500, Bruker AVIII-500, Varian Mercury 300 or Varian VNMRS-300 spectrometers. Chemical shifts (δ) are given in parts per million (ppm) relative to *tetrakis*(trimethylsilyl)silane (δ= 0.22 ppm) or the deuterated solvent used to record the spectrum; the coupling constants (*J*) are reported in Hz. ^{1}H NMR splitting patterns are designated as singlet (s), doublet (d), triplet (t) or quartet (q). Splitting patterns that could not be easily interpreted are designated as multiplet (m) or broad (br). Carbon resonances were assigned using Distortionless Enhancement by Polarization Transfer (DEPT) spectra obtained with phase angles of 135º. ^{1}H NMR signals of peptides were identified from the corresponding 2D double-quantum-filled (COSY, TOCSY and/or NOESY and ROESY) spectra that were acquired at the indicated concentration and temperature. Mixing times ranging from 150 to 300 ms (for NOESY and ROESY) were not optimized.

Electrospray (ESI) low-resolution mass spectra were recorded on HPLC-MS Agilent 1100 series and Bruker BIOTOF II mass spectrometer instruments and are reported as

mass-per-charge ratio (*m/z*). Accurate mass determination (HRMS) using ESI-MS were performed on a Bruker FTMS APEXIII and Bruker microTOF spectrometers.

FTIR measurements were made on a JASCO FT/IR-400 placing the sample on a CaF_2 pellet or on a PerkinElmer FT-IR Spectrum Two ATR-FTIR casting the sample as a thin film directly over its diamond plate (neat).

UV/vis spectroscopy measurements were collected on a Cary 100 Bio (Varian) or Biochrom Libra S60 Double Beam UV/vis spectrophotometers using a Hellma analytics cuvette (1 cm path) at 20 ºC.

Circular dichroism measurements were recorded on a Jasco J-1100 CD Spectrometer equipped with a Jasco MCB-100 Mini Circulation Bath at 24 ºC using a 2 mm Hellma quartz cuvette.

Fluorescence spectroscopy assays were executed using a Cary Eclipse Fluorescence Spectrophotometer (Agilent) equipped with a temperature controller at 24 ºC.

Optical rotation ($[\alpha]_D$) measurements were carried out on a Jasco DIP-370 digital polarimeter. Sodium D line wavelength was used, and methanol HPLC grade was the solvent in all cases.

Non-contact mode Atomic Force Microscopy was conducted in ambient atmosphere at *rt* using NX-10 and XE-100 instruments fitted with ACTA 10M cantilevers (Park Systems Corporation). Scanning Electron Microscopy and Scanning Transmission Electron Microscopy images were taken on a Zeiss FESEM Ultra Plus operating at 3.0 and 20 kV, respectively. Samples were drop casted onto 300 mesh carbon type B film supported copper grids (Ted Pella Inc.) and stained with 2% aqueous solution of phosphotungstic acid or uranyl acetate.

FT-Raman scattering spectra were collected on a Bruker FT-Raman Ram II apparatus and a Nd:YAG laser source (λexc = 1064 nm), in a back-scattering configuration. The operating power for the exciting laser radiation was kept to 100 mW for SWCNT and CP-SWCNT samples or 1000 mW for peptide samples. Samples were analyzed as solutions or drop-casted films averaging 100 scans with 2 cm-1 of spectral resolution. Raman and ROA spectra were recorded simultaneously in a BioTools ChiralRAMAN© spectrometer from an aqueous solution of CP-SWCNT. Excitation wavelength at 532 nm was used as generated by a Nd:VO4 laser operating at 500 mW. Backscattering collection of the scattered radiation was used with a spectral resolution of 4 cm^{-1} and acquisition time of about 24 h.

USC UNIVERSIDADE DE SANTIAGO DE COMPOSTELA

SOLID PHASE SYNTHESIS

Fmoc Solid-Phase Peptide Synthesis (SPPS) was carried out according to the following protocol:

A solution of **Fmoc-*L*-Lys(Boc)-δ-Ach-OAll** (**dp4**) in a mixture of TFA/CH_2Cl_2 (1:1, v/v, 0.25 M) was stirred at *rt* for 20 min. Then, TFA was removed under reduced pressure and the resulting residue was dried under high vacuum. The residue was precipitated on chilled Et_2O to give **Fmoc-*L*-Lys-δ-Ach-OAll** (**dp5**) as a white solid. This compound was used for SPPS without further purification.

2-Chlorotrytil chloride resin (**2-CTC**, estimated loading: 0.5 mmol/g) was swollen in dry CH_2Cl_2 (3 mL) for 1 h and then, filtered off. A solution of **Fmoc-*L*-Lys-δ-Ach-OAll** (1.5 equiv) and DIEA (3 equiv) in dry CH_2Cl_2 was added over the swollen **2-CTC** resin in a peptide synthesis vessel and mechanically shaken for 2 h. Then, the suspension was filtered and washed with dry CH_2Cl_2 (3 x 2 mL) and Et_2O (3 x 2 mL). The resin was dried under high vacuum and resin loading was calculated by Fmoc group quantification.[198] For this, a weighed small portion of dried resin (*ca* 10 mg) was treated with piperidine/DMF mixture (1:4; 2 mL) for 30 min. An aliquot (20 μL) of this solution was diluted to 1 mL in DMF and the absorbance was recorded at 290 and 301 nm. The loading was calculated using the extinction coefficients for dibenzofulvene adducts reported in literature. The resin was capped with a mixture of CH_2Cl_2/MeOH/DIEA (8.5:1:0.5, 2 x 3 mL) and washed with CH_2Cl_2 (3 x 3 mL) and DMF (3 x 3 mL).

After this point, Fmoc group was removed by treatment with piperidine/DMF mixture (1:4, 3 mL) for 20 min. The resin was washed with DMF (6 x 3 mL) followed by amino acid coupling using the following conditions:

α-Aa: Fmoc-Aa-OH (3 equiv), *N*-HBTU (3 equiv) and DIEA (3 equiv). Time: 30 min.

δ-Aa: **Fmoc-δ-Ach-OH** (**5**, 2 equiv), *N*-HBTU (2 equiv) and DIEA (3 equiv). Time: 1 h.

The cycle was repeated until the last amino acid was coupled.

For allylic ester removal, the resin was washed with CH_2Cl_2 and treated with a mixture of $Pd(OAc)_2$ (0.25 equiv), PPh_3 (1.25 equiv), *N*-methylmorpholine (10 equiv) and Phenylsilane (10 equiv) in dry CH_2Cl_2 (3 mL). The suspension was mechanically shaken for 5 h. The resin was washed with CH_2Cl_2 (3 x 3 mL), DMF (3 x 3 mL), sodium diethyldithiocarbamate (0.5% w/v in DMF, 2 x 3 mL, 30 min), DIEA (10% v/v in DMF, 3 x 3 mL) and DMF (3 x 3 mL). The Fmoc protecting group was displaced by treatment with a mixture of piperidine/DMF (1:4, 3 mL) for 45 min. Then, the resin was washed with DMF (3 x 3 mL), DIEA solution in DMF (5% v/v, 3 x 3 mL), LiCl solution in DMF (0.8 M, 3 x 3 mL) and DMF (3 x 3 mL).

USC DE SANTIAGO DE COMPOSTELA

Finally, on-resin cyclization was performed reacting the resin with a mixture of *N*-TBTU (3 equiv) and DIEA (10 equiv) in DMF (3 mL). This process was repeated (3 x 1 h). After cyclization, the resin was washed with DMF (3 x 3 mL) and CH_2Cl_2, and the peptide was

cleaved from the resin by treatment with TFA cocktail (TFA/CH_2Cl_2/H_2O/TIS, 95:5:2.5:2.5, 3 mL) for 2 h. The solution was filtered, and the resin was washed with TFA (2 x 0.5 mL). The combined acidic extracts were concentrated under a flow of Ar to be then precipitated into cooled Et_2O (40 mL). The suspension was centrifuged 10 min at 3000 rpm and decanted. Et_2O (2 x 5 mL) was added to the precipitate, sonicated, centrifuged and decanted. The solid was dried under high vacuum and purified as stated.

USC
UNIVERSIDADE
DE SANTIAGO
DE COMPOSTELA

CHAPTER 1

SYNTHESIS AND CHARACTERIZATION

The synthesis and characterization of the following cyclic peptides and its intermediates has been already described.[183]

***c*-[(*D*-Tyr(Me)-^{Me}*N*-δ-Ach-^{Me}*N*-*L*-Ala-δ-Ach-)$_2$] (CP1)**

***c*-[(*D*-Tyr(Me)-^{Me}*N*-δ-Ach-^{Me}*N*-*L*-Ala-δ-Ach-)$_3$] (CP2)**

***c*-[(*D*-Leu-^{Me}*N*-δ-Ach-^{Me}*N*-*L*-Ala-δ-Ach-)$_4$] (CP3)**

***c*-[(*L*-Tyr(Bn)-^{Me}*N*-δ-Ach-^{Me}*N*-*D*-Ala-δAch-)$_2$] (CP4)**

***c*-[(*L*-Tyr(Bn)-^{Me}*N*-δ-Ach-^{Me}*N*-*D*-Ala-δAch-)$_3$] (C5)**

Boc-(*1R, 3S*)-γ-Ach-OH (1): A solution of **3-aminocyclohexanecarboxylic acid** (10.0 g, 69.8 mmol) in a mixture of 1,4-dioxane/H_2O (1:1, 140 mL) was treated with di-*tert*-butyl dicarbonate (18.3 g, 83.8 mmol) and DIEA (36 mL, 209 mmol). The mixture was stirred at *rt* for 3 h and then, 1,4-dioxane was removed under reduced pressure. The aqueous residue was acidified to pH 3 and extracted with CH_2Cl_2 (3 x 20 mL). The organic layer was dried over anhydrous $MgSO_4$, filtered and concentrated. The resulting oil was crystallized from a CH_2Cl_2/hexane mixture (2:1).

The racemic **Boc-(±)-γ-Ach-OH** (7.00 g, 28.8 mmol) enantiomerically resolved by crystallization from a $CHCl_3$/hexane mixture (3:1) in the presence of **(*R*)-(+)-1-phenylethylamine** (2.6 mL, 20.2 mmol). The crystalline precipitate was filtered, transferred to a separatory funnel and washed with aqueous solution of HCl (5%, 3 x 30 mL). The organic layer was dried over anhydrous $MgSO_4$, filtered and concentrated. The process was repeated 4 times increasing the amount of the quiral amine up to 1 equiv and decreasing the ratio of hexane affording 1.50 g of the enantiopure product as a white solid. The enantiomeric purity was determined by SFC analysis using a Lux Cellulose-5 [21%, t_R= 13.1 min (5% MeOH)].

^{1}H NMR (300 MHz, $CDCl_3$, δ) 4.48 (br, 1H, NH), 3.44 (br, 1H, Hγ Ach), 2.50 – 2.32 (m, 1H, Hα Ach), 2.32 – 2.18 (m, 1H), 2.04 – 1.89 (m, 2H), 1.92 – 1.78 (m, 1H), 1.43 (s, 9H, Boc), 1.37 – 1.14 (m, 3H), 1.05 (q, *J* = 11.1 Hz, 1H). **^{13}C NMR** (75 MHz, $CDCl_3$, δ) 180.3 (CO), 155.5 (CO), 79.7 (C), 49.1 (CH), 42.2 (CH), 35.5 (CH_2), 32.8 (CH_2), 28.5 (CH_3), 28.2 (CH_2), 24.3 (CH_2). **$[\alpha]_D$= -**48.4 (c= 0.99, MeOH). **MS (ESI)** [m/z, (%)]: 487.3 ($[2MH]^+$, 2), 266.1 ($[MNa]^+$, 22), 244.2 ($[MH]^+$, 31), 188.1 ($[MH\text{-}^t Bu]^+$, 100), 144.1 ($[MH\text{-Boc}]^+$, 42). **HRMS (ESI) calculated** for $C_{12}H_{22}NO_4$ ($[MH]^+$): 244.1543, **found**: 244.1548.

Boc-(*1S, 3R*)-γ-Ach-OH (1'): Compound **1'** was obtained following the experimental protocol described above for compound **1** starting from the same racemic mixture **Boc-(±)-γ-Ach-OH** (7.00 g, 28.8 mmol). The chiral resolution was done in the presence of **(*S*)-(-)-1-phenylethylamine** (2.6 mL, 20.2 mmol) to obtain 1.46 g of **1'** as a white solid. The enantiomeric purity was determined by SFC analysis using a Lux Cellulose-5 [21%, t_R= 11.5 min (5% MeOH)].

Th spectroscopic data matched those of its enantiomer **Boc-(*1R, 3S*)-γ-Ach-OH** (**1**). **MS (ESI)** [m/z, (%)]: 487.3 ($[2MH]^+$, 4), 266.1 ($[MNa]^+$, 18), 244.2 ($[MH]^+$, 40), 188.1 ($[MH-^tBu]^+$, 100), 144.1 ($[MH-Boc]^+$, 38). **HRMS (ESI) calculated** for $C_{12}H_{22}NO_4$ ($[MH]^+$): 244.1543, **found**: 244.1540. **$[\alpha]_D$=** -47.9 (c= 1.0, MeOH).

Boc-^{Me}*N*-*D*-Ala-OMe (2): A solution of **Boc-*D*-Ala-OH** (2.00 g, 10.6 mmol) in THF (53 mL) was cooled down to 0 ºC and treated with NaH (60% w/w, 1.27 g, 31.7 mmol). The heterogenous mixture was stirred for 30 min at 0 ºC. After this time, iodomethane (2.0 mL, 31.7 mmol) was added. The mixture was allowed to reach *rt* and stirred for 20 h. The reaction was quenched adding H_2O MiliQ and extracted with Et_2O (3 x 15 mL). The aqueous layer was acidified to pH 3 and extracted with CH_2Cl_2 (3 x 15 mL). The combined organic extracts were washed with aqueous solutions of NaCl (sat. 2 x 15 mL) and $Na_2S_2O_3$ (sat. 15 mL) dried over anhydrous $MgSO_4$, filtered and concentrated. The resulting white solid was dissolved in MeCN (53 mL) and treated with K_2CO_3 (2.93 g, 21.2 mmol) and iodomethane (2.0 mL, 31.8 mmol). The reaction mixture was stirred for 2 h. After this time, the solvent was removed under reduced pressure and H_2O MiliQ was added. The mixture was poured into a separatory funnel and extracted with Et_2O (3 x 15 mL). The organic layer was washed with aqueous solutions of NaCl (sat. 2 x 15 mL) and NH_4Cl (sat. 15 mL), dried over $MgSO_4$, filtered and concentrated. The crude was purified by flash column chromatography (20% EtOAc/hexane) to give 1.96 g of a colorless oil [85%, R_f = 0.42 (20% EtOAc/hexane)].

The spectroscopic data matched those already reported.

H-^{Me}*N*-*L*-Ala-OMe (3): Thionyl chloride (0.7 mL, 9.70 mmol) was added dropwise to a solution of ***N*-methyl-*L*-alanine** (500 mg, 4.85 mmol) in MeOH (10 mL) at 0 ºC. The reaction mixture was allowed to reach *rt* and stirred for 20 h and then, the solvent was removed in the rotatory evaporator. The resulting residue was precipitated with Et_2O and EtOH was added dropwise until the solid is completely solubilized. The mixture was left to crystallize in an ice-water bath and separated by filtration to yield 540 mg of compound **2** [95%, R_f = 0.21 (10% MeOH/CH_2Cl_2].

^{1}H NMR (300 MHz, CD_3OD, δ) 4.10 (q, *J* = 7.2 Hz, 1H, Hα), 3.86 (s, 3H, CO_2Me), 2.75 (s, 3H, NMe), 1.57 (d, *J* = 7.2 Hz, 3H, Me-Ala) **^{13}C NMR** (75 MHz, CD_3OD, δ) 170.9 (CO), 57.4 (CH), 53.9 (CH_3), 31.7 (CH_3), 14.6 (CH_3).

Boc-(*1R, 3S*)-γ-Ach-^{Me}*N*-*D*-Ala-OMe (dp1): A solution of **Boc-^{Me}*N*-*D*-Ala-OMe** (**2**, 447 mg, 2.06 mmol) in a mixture of TFA/CH_2Cl_2 (1:1, 2 mL) was stirred at *rt* for 15 min. Then, TFA was removed under reduced pressure and the resulting residue was dried under high vacuum. The resulting ammonium salt was dissolved in CH_2Cl_2 (2 mL) and treated with DIEA (0.9 mL, 2.50 mmol). This solution was added over a mixture of **Boc-(*1R, 3S*)-γ-Ach-OH** (**1**, 500 mg, 2.06 mmol), *N*-HATU (940 mg, 2.47 mmol) and DIEA (0.9 mL, 2.50 mmol) in CH_2Cl_2. The reaction mixture was stirred at *rt* for 18 h. Then, it was poured into a separatory funnel and washed with aqueous solutions of HCl (5%, 3 x 5 mL) and $NaHCO_3$ (sat. 3 x 5 mL). The organic layer was dried over anhydrous $MgSO_4$, filtered and concentrated. The crude was purified by

flash column chromatography (40-50% EtOAc/hexane) to give 567 mg of **dp1** as a white foam [81%, R_f = 0.62 (10% MeOH/CH_2Cl_2)].

^{1}H NMR (300 MHz, $CDCl_3$, δ) 5.16 (q, *J* = 7.3 Hz, 1H, Hα-Ala), 3.69 (s, 3H, CO_2Me), 3.55 – 3.38 (m, 1H, Hγ-Ach), 2.97 (s, 3H, NMe), 2.70 – 2.54 (m, 1H, Hα-Ach), 2.21 – 2.02 (m, 1H), 2.01 – 1.80 (m, 2H), 1.77 – 1.66 (m, 1H), 1.43 (s, 9H, Boc), 1.37 (d, *J* = 7.3 Hz, 3H, Me-Ala) **^{13}C NMR** (75 MHz, $CDCl_3$, δ) 175.4 (CO), 172.4 (CO), 155.5 (CO), 79.6 (C), 52.5 (CH), 52.3 (CH_3) , 49.4 (CH), 40.0 (CH), 35.7 (CH_2), 33.0 (CH_2), 31.7, 28.6 (CH_3), 28.2 (CH_2), 24.5 (CH_2), 14.6 (CH_3). **MS (ESI)** [m/z, (%)]: 707.4 ([2MNa]$^+$, 2), 365.2 ([MNa]$^+$, 32), 343.2 ([MH]$^+$, 18), 287.2 ([MH-^{t}Bu]$^+$, 7), 243.2 ([MH-Boc]$^+$, 100). **HRMS (ESI) calculated** for $C_{17}H_{31}N_2O_5$ ([MH]$^+$): 343.2227, **found**: 343.2237

Boc-(*1S, 3R*)-γ-Ach-^{Me}*N*-*L*-Ala-OMe (dp2): A solution of **Boc-(*1S, 3R*)-γ-Ach-OH** (**1'**, 350 mg, 1.44 mmol) in CH_2Cl_2 (7 mL) was treated with *N*-HATU (656 mg, 1.73 mmol) and DIEA (1.2 mL, 7.19 mmol). After 5 min, **H-^{Me}*N*-Ala-OMe** (**3**, 169 mg, 1.44 mmol) was added and the mixture was stirred at *rt* for 20 h. Then, it was poured into a separatory funnel and washed with aqueous solutions of HCl (5%, 3 x 5 mL) and $NaHCO_3$ (sat. 3 x 5 mL). The organic layer was dried over anhydrous $MgSO_4$, filtered and concentrated. The crude was purified by flash column chromatography on SiO_2 (40% EtOAc/hexane) to provide 443 mg of **dp2** as a white foam [90%, R_f = 0.62 (10% MeOH/CH_2Cl_2)].

The spectroscopic data matched those of its enantiomer **dp1**. **MS (ESI)** [m/z, (%)]: 707.4 ([2MNa]$^+$, 4), 365.2 ([MNa]$^+$, 28), 343.2 ([MH]$^+$, 21), 287.2 ([MH-^{t}Bu]$^+$, 8), 243.2 ([MH-Boc]$^+$, 100). **HRMS (ESI) calculated** for $C_{17}H_{31}N_2O_5$ ([MH]$^+$): 343.2227, **found**: 343.2232

Boc-(*1S, 3R*)-γ-Ach-^{Me}*N*-*L*-Val-OMe (dp3): A solution of **H-^{Me}*N*-*L*-Val-OH** (400 mg, 1.73 mmol) in MeOH (9 mL) was cooled down to 0 ºC and treated with $SOCl_2$ (0.3 mL, 3.46 mmol). The reaction mixture was left to reach *rt* and stirred under reflux conditions for 20 h. Then, the solvent was removed in the rotatory evaporator and the resulting residue was dried under high vacuum for 24 h providing the methyl ester protected amino acid which was used without further purification.

A solution of **Boc-(*1S, 3R*)-γ-Ach-OH** (**1'**, 372 mg, 1.53 mmol) in CH_2Cl_2 (6 mL) was treated with *N*-HATU (697 mg, 1.83 mmol) and DIEA (1.3 mL, 7.64 mmol). After 5 min, a solution of **H-^{Me}*N*-*L*-Val-OMe** in DMF (2 mL) was added. The reaction mixture was stirred at *rt* for 20 h. Then, the mixture was poured into a separatory funnel and washed with aqueous solutions of HCl (3 x 5 mL) and $NaHCO_3$ (3 x 5 mL). The organic layer was dried over $MgSO_4$, filtered and concentrated. Residual DMF was removed by azeotropic distillation in the presence of toluene. The crude was purified by flash column chromatography (0.25-1.5% MeOH/CH_2Cl_2) to afford 368 mg of **dp3** as a white foam [65% yield, R_f = 0.68 (10 % MeOH/CH_2Cl_2)].

USC
DE SANTIAGO
DE COMPOSTELA

^{1}H NMR (300 MHz, $CDCl_3$, δ) 4.91 (d, *J* = 10.5 Hz, 1H, Hα-Val), 4.47 – 4.41 (m, 1H, Hγ-Ach), 3.68 (s, 3H, CO_2Me), 3.50 – 3.44 (m, 1H, CH(CH_2)$_2$-Val), 2.70 – 2.57 (m, 1H, Hα-Ach), 2.29 – 2.11 (m, 1H), 2.03 – 1.60 (m, 6H), 1.43 (s, 9H, Boc), 0.99 (d, *J* = 6.6 Hz, 3H, CH(CH_2)$_2$), 0.82 (d, *J* = 6.8 Hz, 3H, CH(CH_2)$_2$) **MS (ESI)** [m/z, (%)]: 393.3 ([MNa]$^+$, 22), 371.3 ([MH]$^+$,

34), 315.2 ([MH-^{t}Bu]$^+$, 12), 271.2 ([MH-Boc]$^+$, 100). **HRMS (ESI) calculated** for $C_{19}H_{35}N_2O_5$ ([MH]$^+$): 371.2546, **found**: 371.2540

Boc-[(*1R, 3S*)-γ-Ach-^{Me}*N*-*D*-Ala]$_2$-OMe (tp1): A solution of **Boc-(*1R, 3S*)-γ-Ach-^{Me}*N*-*D*-Ala-OMe** (**dp1**, 200 mg, 0.584 mmol) in a mixture of MeOH/H_2O (3:1, 2.4 mL) was treated with LiOH (70.0 mg, 2.92 mmol). The reaction mixture was stirred at *rt* for 30 min. Then, organic solvent was removed in the rotatory evaporator. The aqueous residue was acidified to pH 3 and extracted with CH_2Cl_2 (3 x 3 mL). The combined organic extracts were dried over anhydrous $MgSO_4$, filtered and concentrated to afford the intermediate **dp1-OH** that was used without further purification.

A solution of **dp1** (200 mg, 0.584 mmol) in a mixture of TFA/CH_2Cl_2 (1:1, 1.2 mL) was stirred at rt for 15 min. Then, TFA was removed under reduced pressure and the resulting residue was dried under high vacuum. The product was dissolved in CH_2Cl_2 (1 mL), treated with DIEA (0.25 mL, 1.46 mmol) and added over a mixture of **dp1-OH**, *N*-HBTU (266 mg, 0.701 mmol) and DIEA (0.25 mL, 1,46 mmol) in CH_2Cl_2 (2 mL). The reaction mixture was stirred at *rt* for 1 h. Then, it was poured into a separatory funnel and washed with aqueous solutions of HCl (5%, 3 x 3 mL) and $NaHCO_3$ (sat. 3 x 3 mL). The organic layer was dried over anhydrous $MgSO_4$, filtered and concentrated. The crude was purified by flash column chromatography on SiO_2 (0.5-2% MeOH/CH_2Cl_2) providing 262 mg of **tp1** as a white foam [81%, R_f = 0.54 (10% MeOH/CH_2Cl_2)].

MS (ESI) [m/z, (%)]: 575.3 ([MNa]$^+$, 39), 553.4 ([MH]$^+$, 100), 453.3 ([MH-Boc]$^+$, 86). **HRMS (ESI) calculated** for $C_{28}H_{49}N_4O_7$ ([MH]$^+$): 553.3596, **found**: 553.3584.

Boc-[(*1S, 3R*)-γ-Ach-^{Me}*N*-*L*-Ala]$_2$-OMe (tp2): This tetrapeptide was synthesized following the experimental protocol described above for **tp1** starting from **Boc-(*1S, 3R*)-γ-Ach-^{Me}*N*-*L*-Ala-OMe** (**dp2**, 150 mg, 0.438 mmol) to obtain 205 mg of **tp2** as a white foam [84% yield, R_f = 0.54 (10% MeOH/CH_2Cl_2)].

MS (ESI) [m/z, (%)]: 575.3 ([MNa]$^+$, 39), 553.4 ([MH]$^+$, 100), 453.4 ([MH-Boc]$^+$, 93). **HRMS (ESI) calculated** for $C_{28}H_{49}N_4O_7$ ([MH]$^+$): 553.3596, **found**: 553.3597.

Boc-[(*1S, 3R*)-γ-Ach-^{Me}*N*-*L*-Val]$_2$-OMe (tp3): This tretrapeptide was synthesized following the experimental protocol described above for **tp1** starting from **Boc-(*1S, 3R*)-γ-Ach-^{Me}*N*-*L*-Val-OMe** (**dp3**, 100 mg, 0,270 mmol) to give 146 mg of **tp3** as a white foam [89%, R_f = 0.62 (10% MeOH/CH_2Cl_2)].

MS (ESI) [m/z, (%)]: 631.4 ([MNa]$^+$, 27), 609.4 ([MH]$^+$, 100), 509.3 ([MH-Boc]$^+$, 14). **HRMS (ESI) calculated** for $C_{32}H_{57}N_4O_7$ ([MH]$^+$): 609.4222, **found**: 609.4229.

Boc-[(*1R, 3S*)-γ-Ach-^{Me}*N*-*D*-Ala]$_3$-OMe (hp1): A solution of **Boc-(*1R, 3S*)-γ-Ach-^{Me}*N*-*D*-Ala-OMe** (**dp1**, 142 mg, 0.416 mmol) in a mixture of MeOH/H_2O (3:1, 2.1 mL) was treated with LiOH (50 mg, 2.08 mmol). The reaction mixture was stirred at *rt* for 30 min. Then, the organic solvent was removed in the rotatory evaporator. The aqueous residue was acidified to pH 3 and extracted with CH_2Cl_2 (3 x 3 mL). The combined organic extracts were dried over

anhydrous $MgSO_4$, filtered and concentrated to afford the intermediate **dp1-OH** that was used without further purification.

A solution of **Boc-[(*1R, 3S*)-γ-Ach-^{Me}*N-D*-Ala]$_2$-OMe** (**tp1**, 230 mg, 0.416 mmol) in a mixture of TFA/CH_2Cl_2 (1:1, 2 mL) was stirred at *rt* for 15 min. Then, TFA was removed under reduced pressure and the resulting residue was dried under high vacuum. The product was dissolved in CH_2Cl_2 (1 mL), treated with DIEA (0,15 mL, 0.900 mmol) and added over a mixture of **dp1-OH**, *N*-HBTU (165 mg, 0.434 mmol) and DIEA (0.16 mL, 0.910 mmol) in CH_2Cl_2 (3 mL). The reaction mixture was stirred at *rt* for 1 h. Then, it was poured into a separatory funnel and washed with aqueous solutions of HCl (5%, 3 x 3 mL) and $NaHCO_3$ (sat. 3 x 3 mL). The organic layer was dried over anhydrous $MgSO_4$, filtered and concentrated. The crude was purified by flash column chromatography on SiO_2 (2-4% MeOH/ CH_2Cl_2) providing 204 mg of **hp1** as a white solid [74%, R_f = 0.50 (5% MeOH/CH_2Cl_2)].

MS (ESI) [m/z, (%)]: 785.5 ([MNa]$^+$, 40), 763.5 ([MH]$^+$, 100), 663.4 ([MH-Boc]$^+$, 3). **HRMS (ESI) calculated** for $C_{39}H_{67}N_6O_9$ ([MH]$^+$): 763.4964, **found**: 763.4966.

Boc-[(*1S, 3R*)-γ-Ach-^{Me}*N-L*-Ala]$_3$-OMe (hp2): This hexapeptide was synthesized following the experimental protocol described above for **hp1** starting from **Boc-[(*1S, 3R*)-γ-Ach-^{Me}*N-L*-Ala]$_2$-OMe** (**tp2**, 145 mg, 0.262 mmol) and **Boc-(*1S, 3R*)-γ-Ach-^{Me}*N-L*-Ala-OMe** (**dp2**, 90.0 mg, 0.262 mmol) to afford 163 mg of **hp2** as a white solid [81% yield, R_f = 0.50 (5% MeOH/CH_2Cl_2)].

MS (ESI) [m/z, (%)]: 785.5 ([MNa]$^+$, 24), 763.5 ([MH]$^+$, 100), 663.4 ([MH-Boc]$^+$, 5). **HRMS (ESI) calculated** for $C_{39}H_{67}N_6O_9$ ([MH]$^+$): 763.4964, **found**: 763.4966.

Boc-[(*1S, 3R*)-γ-Ach-^{Me}*N-L*-Val]$_3$-OMe (hp3): This hexapeptide was synthesized following the same experimental protocol described above for **hp1** starting from **Boc-[(*1S, 3R*)-γ-Ach-^{Me}*N-L*-Val]$_2$-OMe** (**tp3**, 33.0 mg, 0.0540 mmol) and **Boc-(*1S, 3R*)-γ-Ach-^{Me}*N-L*-Val-OMe** (**dp3**, 20 mg, 0.0540 mmol) to afford 30 mg of **hp3** as a white solid [65% yield, R_f= 0.52 (5% MeOH/CH_2Cl_2)].

MS (ESI) [m/z, (%)]: 869.6 ([MNa]$^+$, 32), 847.6 ([MH]$^+$, 100), 747.5 ([MH-Boc]$^+$, 4). **HRMS (ESI) calculated** for $C_{45}H_{79}N_6O_9$ ([MH]$^+$): 847.5903, **found**: 847.5906.

***c*-{[(*1R, 3S*)-γ-Ach-^{Me}*N-D*-Ala-]$_3$} (CP6)**: A solution of **hp1** (100 mg, 0.131 mmol) in a mixture of MeOH/H_2O (3:1, 1.3 mL) was treated with LiOH (16 mg, 0.655 mmol). The reaction mixture was stirred at *rt* for 2 h. Then, the organic solvent was removed in the rotatory evaporator. The aqueous residue was acidified to pH 3 and extracted with CH_2Cl_2 (3 x 3 mL). The combined organic extracts were dried over anhydrous $MgSO_4$, filtered, concentrated and dried under high vacuum. The resulting white solid was dissolved in a mixture of TFA/CH_2Cl_2 (1:1, 1.4 mL) and stirred at *rt* for 30 min. Then, TFA was removed under reduced pressure. The resulting residue was dried under high vacuum, dissolved in CH_2Cl_2 (87 mL) and then, DIEA (0.11 mL, 0.655 mmol) and TBTU (50 mg, 0.157 mmol) were added. The reaction mixture was stirred at *rt* for 20 h and concentrated until around five times its initial volume. The mixture was transferred to a separatory funnel and washed with aqueous solutions of HCl (5%, 3 x

5 mL) and $NaHCO_3$ (sat. 3 x 5 mL). The organic layer was dried over $MgSO_4$, filtered and concentrated. The crude was purified by preparative normal phase HPLC to yield 20 mg of the desire **CP6** as a white solid [24% yield**,** t_R= 27 min (2-7% MeOH/CH_2Cl_2].

^{1}H NMR (500 MHz, $CDCl_3$, δ) 7.14 (s, 1H, NH), 5.21 (q, *J* = 7.2 Hz, 1H, Hα Ala), 3.82 – 3.70 (m, 1H, Hγ Ach), 3.04 (s, 3H, NMe), 2.70 – 2.62 (m, 1H, Hα Ach), 1.27 (d, *J* = 7.0 Hz, 3H, Me Ala) **^{13}C NMR** (126 MHz, $CDCl_3$, δ) 175.4 (CO), 170.4 (CO), 50.9 (CH), 47.4 (CH), 40.1 (CH), 35.0 (CH_2), 32.4 (CH_2), 30.6 (CH_3), 28.2 (CH_2), 24.3 (CH_2) 14.6 (CH_3). **MS (ESI)** [m/z, (%)]: 1262.8 ($[2MH]^+$, 8), 631.5 ($[MH]^+$, 50). **HRMS (ESI) calculated** for $C_{33}H_{55}N_6O_6$ ($[MH]^+$): 631.4178, **found**: 631.4182. **FTIR** (neat, cm^{-1}): ν = 3304 (amide A), 1669 (amide I_{II}), 1620 (amide I), 1529 (amide II).

***c*-{[*D*-Ala-^{Me}*N*-(*1R, 3S*)-γ-Ach-]$_3$} (CP7)**: This cyclic peptide was previously prepared following a similar protocol described above.[268]

^{1}H NMR ($CDCl_3$, 500 MHz, δ, ppm) 8.36 (d, *J* = 9.1 Hz, 1H), 5.18 (t, *J* = 7.9 Hz, 1H), 4.62–4.49 (m, 1H), 3.01 (s, 3H), 2.80 (bs, 1H). **^{13}C NMR** ($CDCl_3$, 75 MHz, δ, ppm) 175.1 (CO), 173.1 (CO), 51.6 (CH_3), 43.8 (CH), 43.2 (CH), 32.4 (CH_2), 29.8 (CH), 28.8 and 28.6 (CH_2), 24.9 (CH_2), 19.0 (CH_3). **MS (ESI)** [m/z, (%)]: 1262.8 ($[2MH]^+$, 6), 631.5 ($[MH]^+$, 40). **HRMS (ESI) calculated** for $C_{33}H_{55}N_6O_6$ ($[MH]^+$): 631.4178, **found**: 631.4176. **FTIR** (neat, cm^{-1}): ν = 3304 (amide A), 1669 (amide I_{II}), 1620 (amide I), 1529 (amide II).

***c*-{[(*1S, 3R*)-γ-Ach-^{Me}*N*-*L*-Ala-]$_3$} (CP8)**: This cyclic peptide was synthesized following the experimental protocol described above for **CP6** starting from **Boc-[(*1S, 3R*)-γ-Ach-^{Me}*N*-*L*-Ala]$_3$-OMe** (**hp2**, 100 mg, 0.131 mmol) to provide 20 mg of **CP8** as a white solid [24%, t_R= 27 min (2-7% MeOH/CH_2Cl_2)].

The spectroscopic data matched with those for its enantiomer **CP6**. **MS (ESI)** [m/z, (%)]: 1262.8 ($[2M+2H]^{2+}$, 5), 631.5 ($[MH]^+$, 43). **HRMS (ESI) calculated** for $C_{33}H_{55}N_6O_6$ ($[MH]^+$): 631.4178, **found**: 631.4172. **FTIR** (neat, cm^{-1}): ν = 3305 (amide A), 1672, 1614 (amide I), 1538 cm^{-1} (amide II_{II}).

***c*-{[(*1S, 3R*)-γ-Ach-^{Me}*N*-*L*-Val-]$_3$} (CP9)**: This peptide was synthesized following the experimental protocol described above for **CP8** starting from **Boc-[(*1S, 3R*)-γ-Ach-^{Me}*N*-*L*-Val]$_3$-OMe** (**hp3**, 30.0 mg, 0,0354 mmol) to give 3.5 mg of **CP10** a white solid [14%, t_R= 27.1 min (2-7% MeOH/CH_2Cl_2)].

^{1}H NMR (500 MHz, $CDCl_3$, δ) 7.93 (s, 1H, NH), 4.94 (br, 1H, Hα Val), 3.96 (br, 1H, Hγ Ach), 3.15 (s, 3H, NMe), 2.77 (br, 1H, Hα Ach), 2.32 – 2.20 (m, 1H, CH$(CH_2)_2$), 0.89 and 0.80 (d, *J* = 6.5 Hz, 3H, -CH(CH_2)$_2$). **^{13}C NMR** (126 MHz, $CDCl_3$, δ) 175.6 (CO), 169.7 (CO), 61.1 (CH), 47.2 (CH), 40.4 (CH), 35.4 (CH_2), 32.5 (CH_2), 31.1 (CH or CH_3), 28.2 (CH_2), 27.5 (CH

USC UNIVERSIDADE DE SANTIAGO DE COMPOSTELA

[268] A. Fuertes, *Nuevas Estrategias para el Transporte de Iones y la Encapsulación Selectiva de Ligandos Basadas en α,γ-Ciclopéptidos*. PhD. Dissertation, Universidade of Santiago de Compostela, Santiago de Compostela, **2019**.

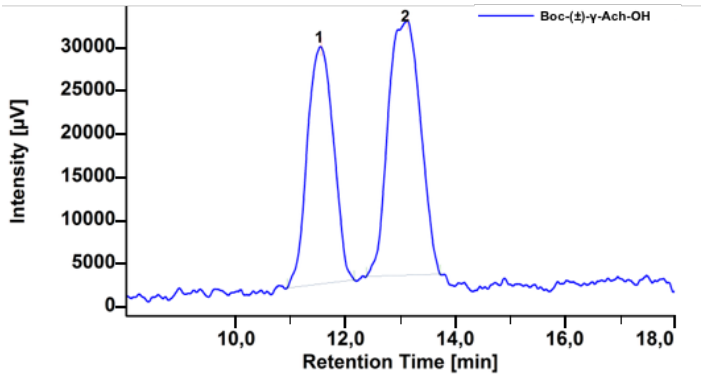
or CH_3), 24.7 (CH_2), 19.2 (CH_3), 18.7 (CH_3). **MS (ESI)** [m/z, (%)]: 1429.1 ($[2MH]^+$, 5), 714.5 ($[MH]^+$, 56). **HRMS (ESI) calculated** for $C_{39}H_{66}N_6O_6$ ($[MH]^+$): 714.5044, **found**: 714.5048.

USC
UNIVERSIDADE
DE SANTIAGO
DE COMPOSTELA

SUPERCRITICAL FLUID CHROMATOGRAPHY ANALYSIS

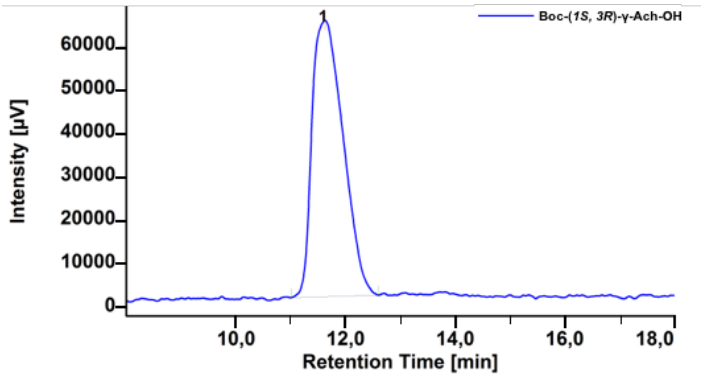
After the enantiomeric resolution, a solution of compound **1** or **1'** in MeOH (10 mg/mL, 1 mL) was analyzed by SFC using an isocratic method of 5% MeOH in supercritical CO_2 at 2 mL/min for 20 min with a Lux Cellulose-5 (T_{oven}= 40 ºC, 100 bar). The enantiomeric ratio was calculated comparing the areas of the peaks applying the following formula:

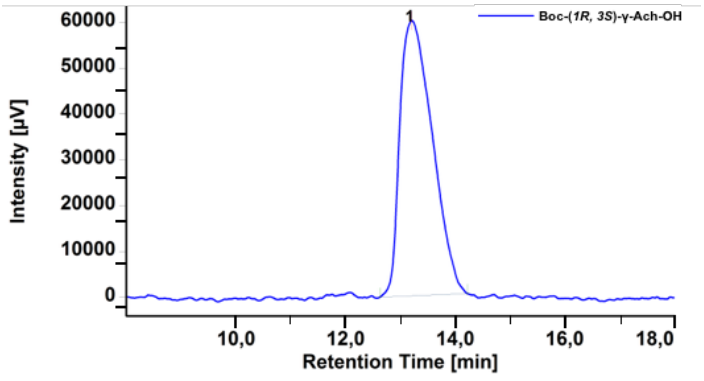
$$e.e = \frac{Area_L - Area_D}{Area_L + Area_D}$$



Peak Information

#	tR [min]	Area [µV·sec]	Height [µV]	Area%	Height%	Symmetry Factor
1	11,553	912030	27413	43,149	48,222	0,951
2	13,123	1201652	29434	56,851	51,778	0,925

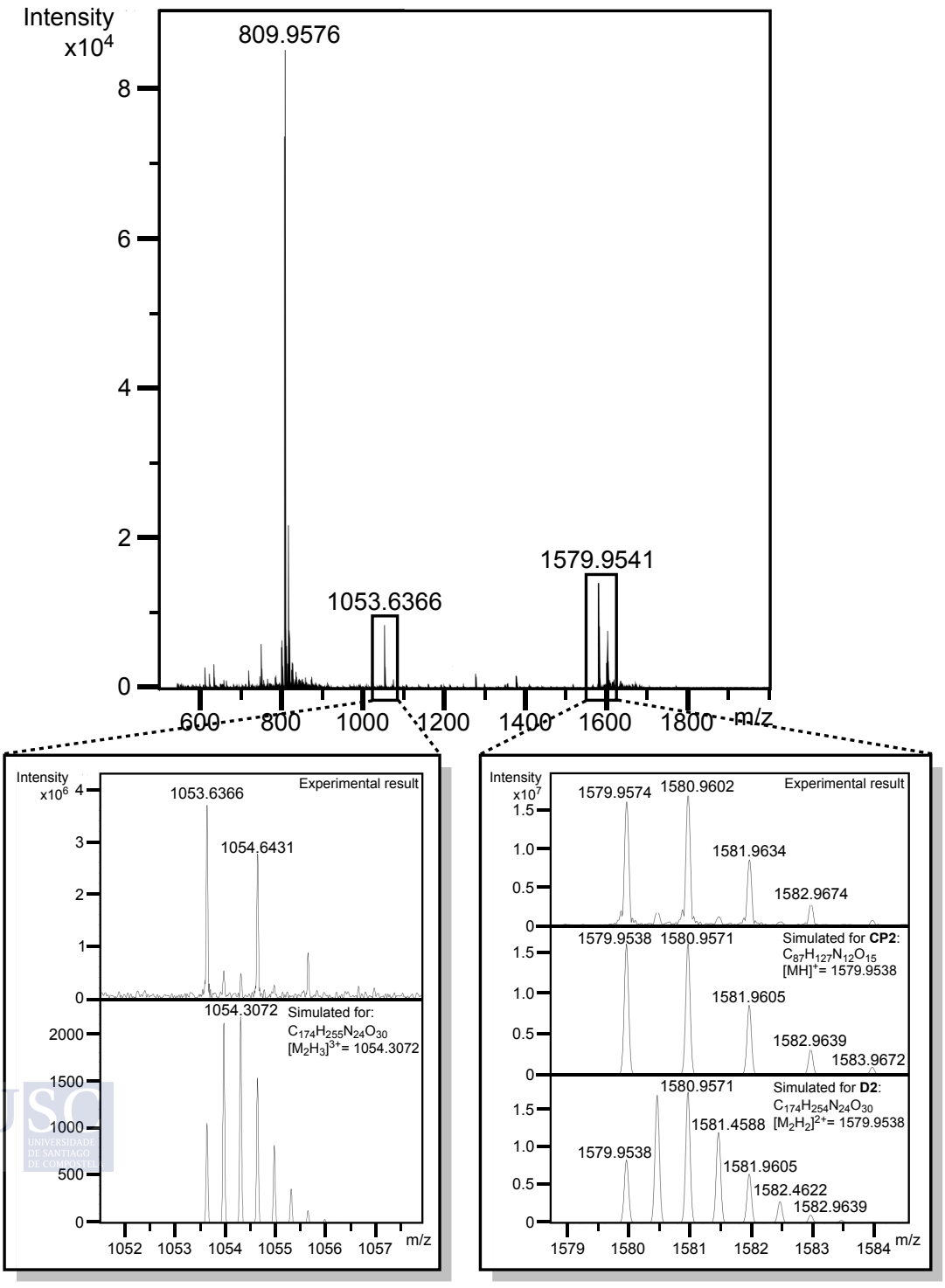




USC UNIVERSIDADE DE SANTIAGO DE COMPOSTELA

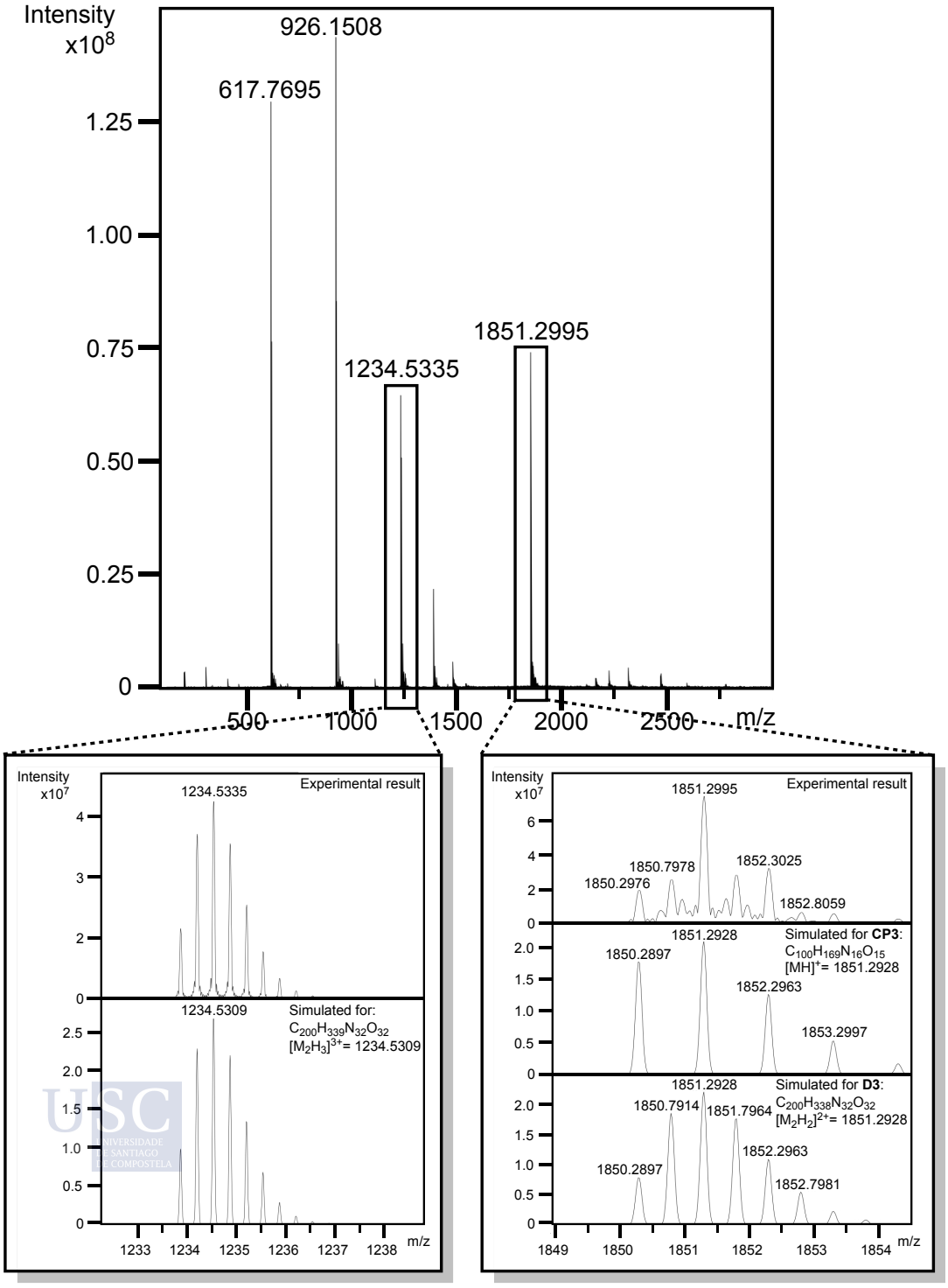
MASS SPECTROMETRY DIMER IDENTIFICATION:

D2a homodimer formation was identified by ESI-TOF mass spectrometry comparing the simulated isotropic distribution of the homodimer signals $[M_2H_2]^{2+}$ and $[M_3H_3]^{3+}$ with the experimental result. As the experimental spectrum matched with the simulated isotropic distribution, it was confirmed the formation of the corresponding antipararallel homodimeric structures.

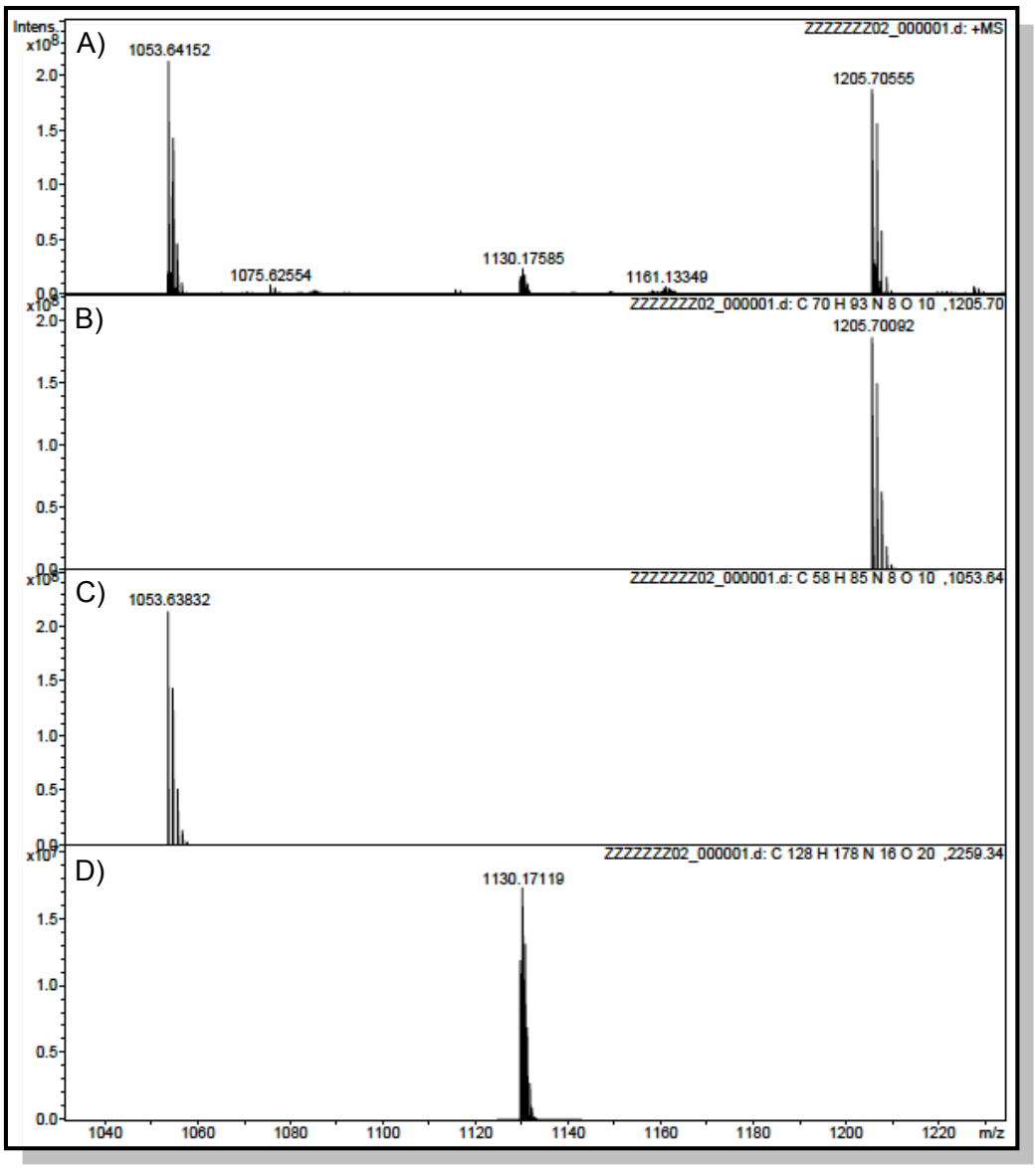


USC UNIVERSIDADE DE SANTIAGO DE COMPOSTELA

D3a homodimer formation was identified by ESI-TOF mass spectrometry comparing the simulated isotropic distribution of the homodimer signals $[M_2H_2]^{2+}$ and $[M_3H_3]^{3+}$ with the experimental result. As the experimental spectrum matched with the simulated isotropic distribution, it was confirmed the formation of the corresponding antipararallel homodimeric structures.

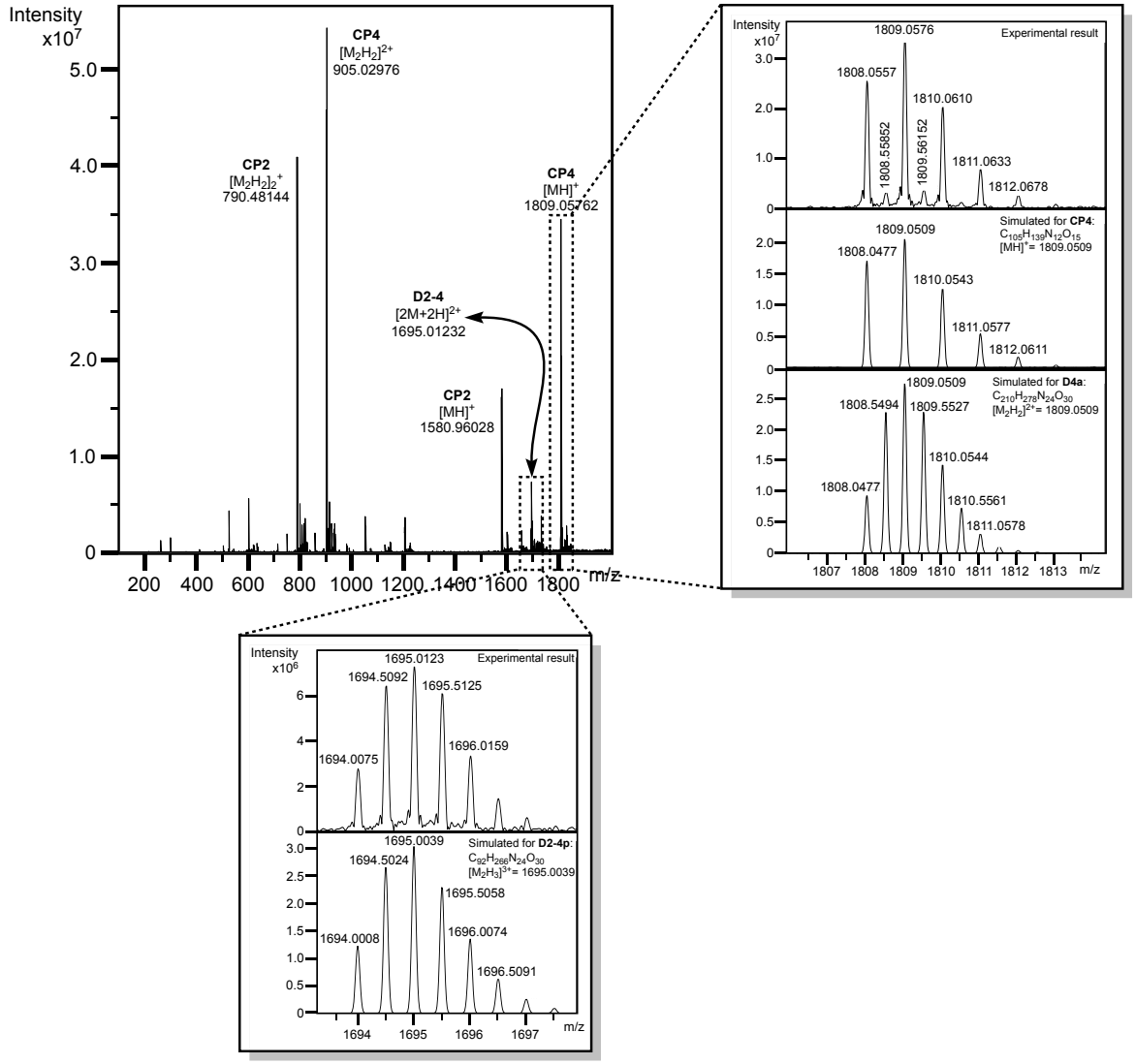


D1-5p heterodimer formation was identified by ESI-TOF mass spectrometry comparing the simulated isotropic distribution of $[M_2H_2]^{2+}$ signals with the experimental results. As the experimental spectrum matched with the simulated isotopic distribution, it was confirmed the presence of the parallel heterodimeric structures.



USC UNIVERSIDADE DE SANTIAGO DE COMPOSTELA

D2-4p heterodimer formation was identified by ESI-TOF mass spectrometry comparing the simulated isotropic distribution of $[M_2H_2]^{2+}$ signals with the experimental results. As the experimental spectrum matched with the simulated isotopic distribution, it was confirmed the presence of the parallel heterodimeric structures.

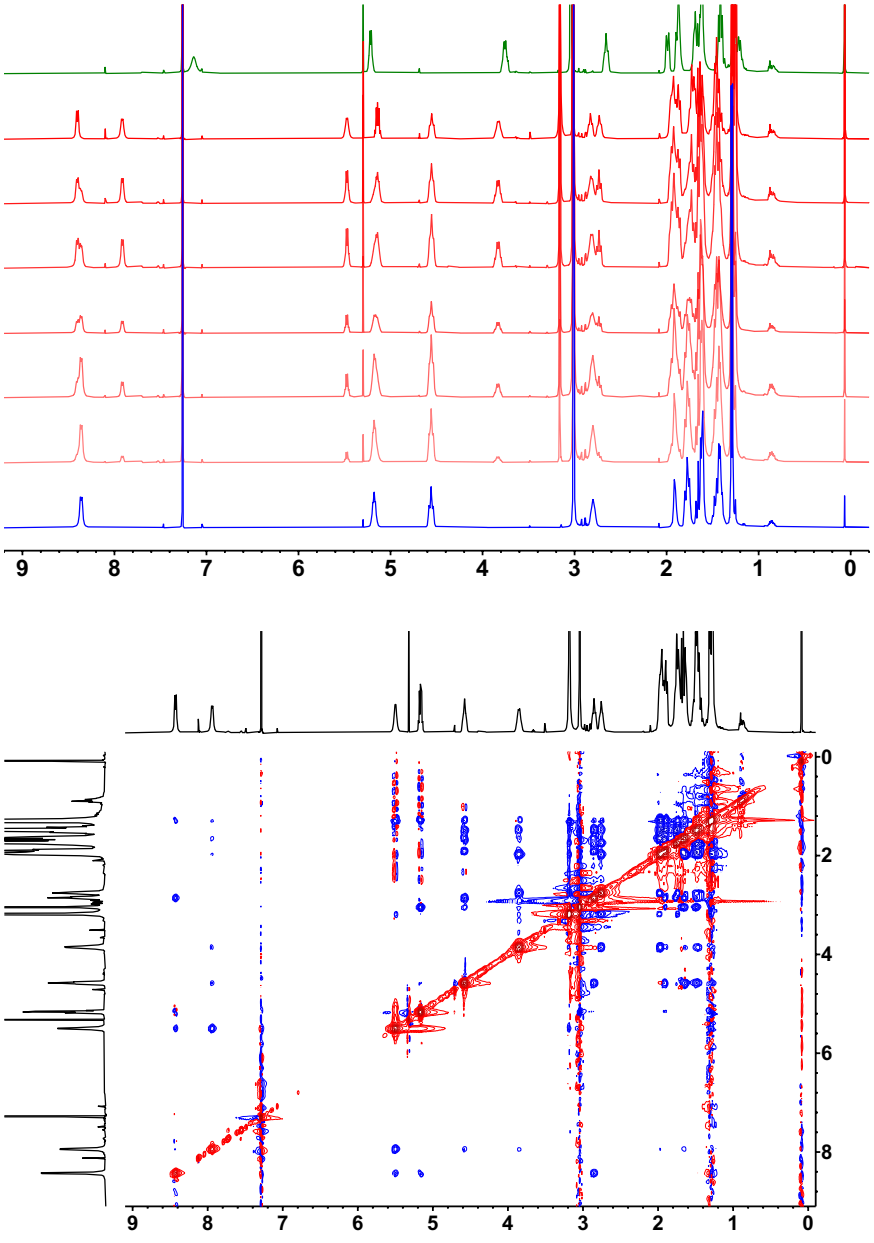


USC UNIVERSIDADE DE SANTIAGO DE COMPOSTELA

NMR Heterodimer Formation Studies

D6-7p:

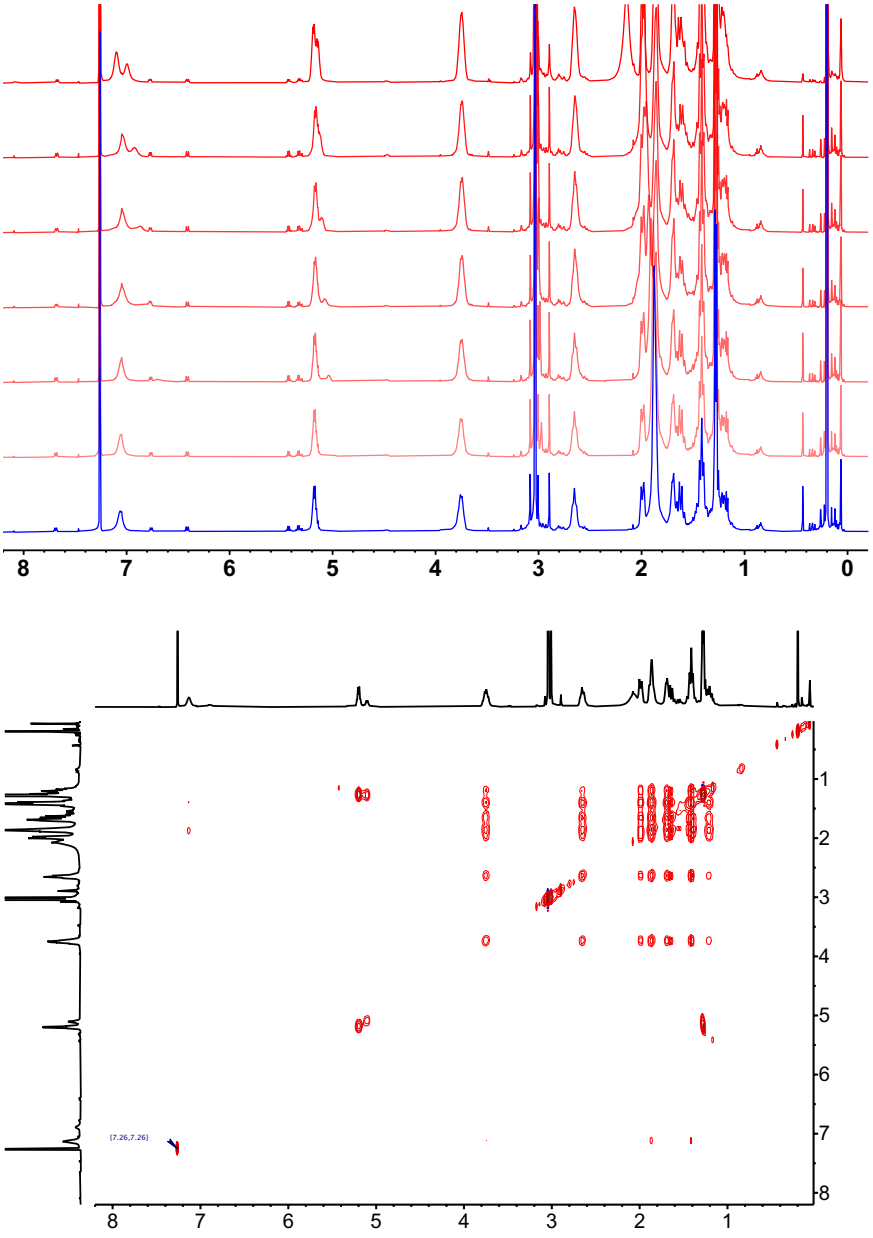
Small portions (20 µL, 0.2 equiv) of a deuterochloroform solution of **CP8** (27.3 mM, green spectrum) were added over a solution of **CP7** (5.1 mM, blue spectrum) until equimolarity was reached to form the heterodimer **D7-8p**. ROESY experiments (bottom) were carried out with the equimolar peptide mixture.



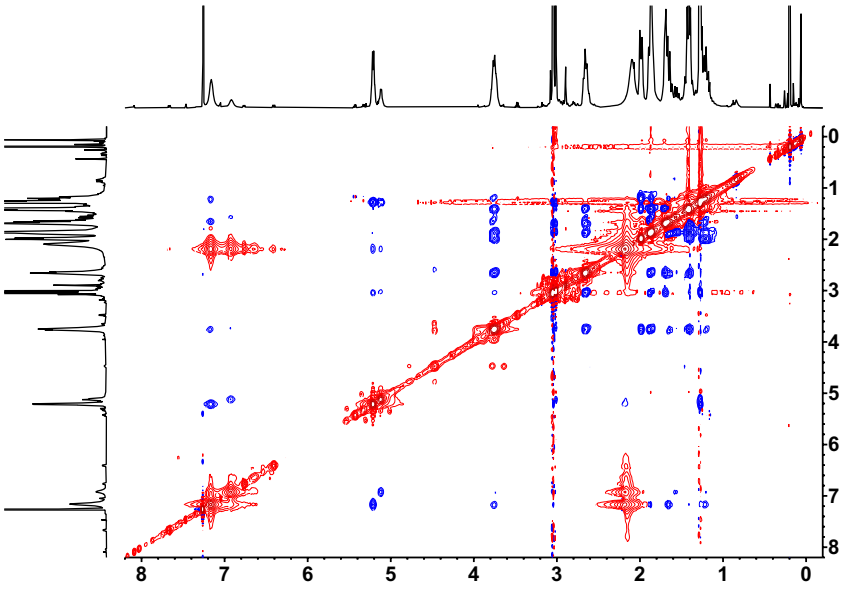
USC
UNIVERSIDADE DE SANTIAGO DE COMPOSTELA

D6-8p:

Small portions (20 µL, 0.2 equiv) of a deuterochloroform solution of **CP8** (30.0 mM, red top spectrum) were added over a solution of **CP6** (6.0 mM, blue spectrum) until equimolarity was reached to form the heterodimer **D6-8p**. 2D-NMR experiments (TOCSY and NOESY) were carried out with the equimolar peptide mixture to confirm the heterodimer formation.



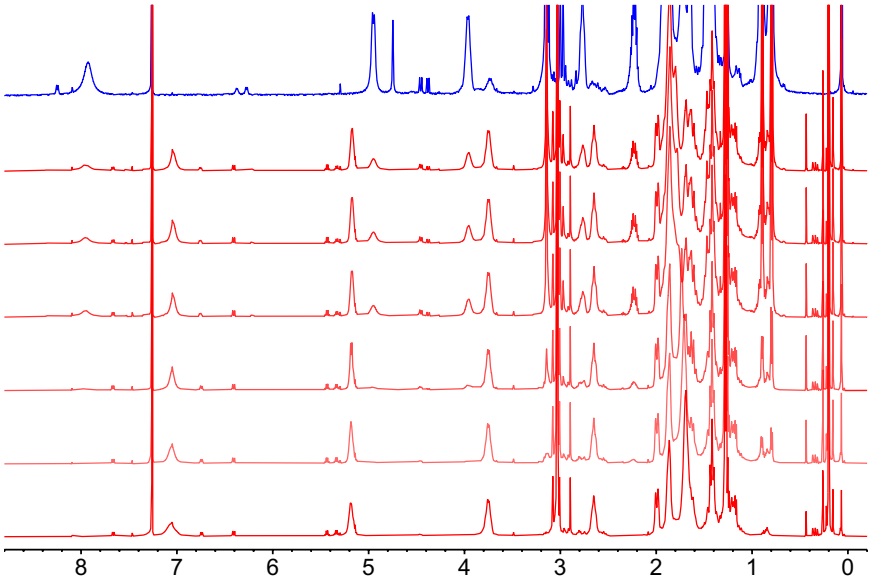
USC
UNIVERSIDADE DE SANTIAGO DE COMPOSTELA



USC
UNIVERSIDADE
DE SANTIAGO
DE COMPOSTELA

D6-9p:

Small portions (20 µL, 0.2 equiv) of a deuterochloroform solution of **CP9** (25.6 mM, blue spectrum) were added over a solution of **CP6** (8.5 mM, red bottom spectrum) until equimolarity was reached to form the heterodimer **D6-9p**.



USC
UNIVERSIDADE DE SANTIAGO DE COMPOSTELA

CHAPTER 2

SYNTHESIS AND CHARACTERIZATION

Boc-δ-Ach-OAll (4): A solution of **Boc-δ-Ach-OH** (1.0 g, 4.11 mmol) in CH_2Cl_2 (40 mL) was treated with EDC.HCl (1.58 g, 8.20 mmol), AllOH (0.8 mL, 12.3 mmol) and DMAP (100 mg, 0.820 mmol). The resulting mixture was stirred at *rt* for 2 h and then, it was poured into a separatory funnel and washed with aqueous solutions of HCl (5%, 3 x 20 mL) and $NaHCO_3$ (sat. 3x 20 mL). The organic layer was dried over $MgSO_4$, filtered and concentrated. The crude was purified by flash column chromatography on SiO_2 (0.5% MeOH/CH_2Cl_2) to obtain 1.04 g of **5** as a white solid [87%, R_f = 0.8 (5% MeOH/CH_2Cl_2)].

^{1}H NMR (300 MHz, $CDCl_3$, δ): 5.90 (ddt, *J* = 17.2, 10.4, 5.7 Hz, 1H, $CH_2CH{=}CH_2$), 5.30 (dq, *J* = 17.2 and 1.4 Hz, 1H, $CH_2CH{=}CH_2$), 5.22 (dq, *J* = 10.4 and 1.1 Hz, 1H, $CH_2CH{=}CH_2$), 4.56 (dt, *J* = 5.7 Hz and 1.4 Hz, 2H, $CH_2CH{=}CH_2$), 4.37 (br, 1H, NH), 3.41 (br, 1H, Hδ Ach), 2.25 (tt, *J* = 12.1 and 3.4 Hz, 1H, Hα Ach), 2.15 – 1.95 (m, 4H), 1.58 – 1.49 (m, 2H), 1.43 (s, 9H, Boc), 1.19 – 1.02 (m, 2H). **^{13}C NMR** ($CDCl_3$, 75 MHz, δ): 174.7 (C), 155.0 (C), 132.0 (CH), 117.7 (CH_2), 78.6 (C), 64.6 (CH_2), 48.7 (CH), 42.1 (CH), 32.1 (CH_2), 28.2 (CH_3), 27.6 (CH_2). **MS (ESI)** [m/z, (%)]: 306.2 ($[MNa]^+$, 100), 250.1 ($[MNa\text{-}^t Bu]^+$, 52). **HRMS (ESI) calculated** for $C_{15}H_{25}NNaO_4$ ($[MNa]^+$) 306.1678, **found**: 306.1677.

Fmoc-δ-Ach-OH (5): A solution of **Boc-δ-Ach-OH** (2.00 g, 8.22 mmol) in a mixture of TFA/CH_2Cl_2 (1:1, 8 mL) was stirred at *rt* for 20 min. Then, TFA was removed under reduced pressure and the resulting residue was dried under high vacuum. The resulting ammonium salt was dissolved in an aqueous solution of Na_2CO_3 (10% w/v, 40 mL) and then, 1,4-dioxane (20 mL) was added. The solution was cooled down to 0 ºC and treated with a solution of Fmoc-OSu (3.05 g, 9.04 mmol) in 1,4-dioxane (20 mL) using a dropping funnel. The heterogeneous mixture was stirred at *rt* for 18 h then, 1,4-dioxane was removed in the rotatory evaporator. The resulting aqueous residues was transferred into a separatory funnel, suspended in CH_2Cl_2 (20 mL) and decanted. The organic layer was concentrated in the rotatory evaporator and the resulting solid was filtered and washed with EtOAc (3 x 10 mL), hexane (3 x 10 mL) and Et_2O (3 x 10 mL) providing 2.18 g of **5** as a white solid [71%, R_f = 0.05 (10% MeOH/CH_2Cl_2].

^{1}H NMR (300 MHz, DMSO-*d6*, δ) 12.06 (s, 1H, $CO_2\underline{H}$), 7.88 (d, *J* = 7.5 Hz, 2H, Ar), 7.69 (d, *J* = 7.4 Hz, 2H, Ar), 7.45 – 7.29 (m, 4H, Ar), 7.24 (d, *J* = 7.9 Hz, 1H, NH), 4.32 – 4.17 (m, 3H, C$\underline{H}$ and C$\underline{H_2}$ Fmoc), 3.21 (br, 1H, Hδ Ach), 2.20 – 2.00 (m, 1H, Hα Ach), 1.97 – 1.71 (m, 4H), 1.42 – 1.02 (m, 3H). **^{13}C NMR** (75 MHz, DMSO-*d6*, δ) 176.8 (CO), 155.3 (CO), 143.9 (C), 140.7 (C), 139.4 (C), 137.4 (C), 128.9 (CH), 127.6 (CH), 27.3 (CH), 127.0 (CH), 125.1 (CH), 121.3 (CH), 120.0 (CH), 120.0 (CH), 65.1 (CH_2), 49.2 (CH), 46.8 (CH), 42.2 (CH), 31.7 (CH_2), 27.8 (CH_2).

USC DE SANTIAGO DE COMPOSTELA

Fmoc-*L*-Lys(Boc)-δ-Ach-OAll (dp4): A solution of **Boc-δ-Ach-OAll** (**5**, 450 mg, 1.58 mmol) in a mixture of TFA/CH_2Cl_2 (1:1, 3 mL) was stirred at *rt* for 15 min. Then, TFA was removed under reduced pressure and the resulting residue was dried under high vacuum. The resulting ammonium salt was dissolved in CH_2Cl_2 (2 mL) and treated with DIEA (0.7 mL, 3.95

mmol). This solution was added over a mixture of **Fmoc-*L*-Lys(Boc)-OH** (827 mg, 1.80 mmol), *N*-HATU (839 mg, 2.20 mmol) and DIEA (0.7 mL, 3.95 mmol) in CH_2Cl_2 (7 mL). The reaction mixture was stirred at *rt* for 1 h. Then, it was poured into a separatory funnel and washed with aqueous solutions of HCl (5%, 3 x 5 mL) and $NaHCO_3$ (sat. 3 x 5 mL). The organic layer was dried over anhydrous $MgSO_4$, filtered and concentrated. The crude was purified by flash column chromatography (1% MeOH/CH_2Cl_2) to give **dp4** as a white solid [94%, R_f = 0.4 (5% MeOH/CH_2Cl_2)].

^{1}H NMR (300 MHz, 2% CD_3OD/CD_2Cl_2, δ): 7.78 (d, *J* = 7.5, 2H, Ar), 7.61 (d, *J* = 7.4 Hz, 2H, Ar), 7.41 (t, *J* = 7.3 Hz, 2H, Ar), 7.32 (t, *J* = 7.5 Hz, 2H, Ar), 5.90 (ddt, *J* = 18.0, 10.4 and 5.5 Hz, 1H, $CH_2CH=CH_2$), 5.29 (dq, *J* = 18.0 and 1.3 Hz, 1H, $CH_2CH=CH_2$), 5.21 (dq, *J* = 10.4 and 1.3 Hz, 1H, $CH_2CH=CH_2$), 4.55 (dt, *J* = 5.5 and 1.3 Hz, 2H, $CH_2CH=CH_2$), 4.38 (d, *J* = 6.9 Hz, 2H, $\underline{CH_2}$-OFm), 4.22 (t, *J* = 6.8 Hz, 1H, $\underline{CH}$-OFm), 3.99 (s, 1H, Hα Lys), 3.66 (m, 1H, Hδ Ach), 3.05 (m, 2H), 2.25 (tt, *J* = 12.2, 3.4 Hz, 1H, Hα Ach), 2.06–1.81 (m, 6H), 1.65–1.43 (m, 6H), 1.41 (s, 9H, Boc), 1.36–1.07 (m, 2H). **^{13}C NMR** (75 MHz, 2% CD_3COD/CD_2Cl_2, δ): 175.6 (C), 171.9 (C), 157.0 (C), 144.5 (C), 141.8 (C), 133.0 (CH), 128.2 (CH), 127.6 (CH), 125.6 (CH), 120.5 (CH), 118.0 (CH_2), 79.6 (C), 67.3 (CH_2), 65.4 (CH_2), 55.3 (CH), 48.3 (CH), 47.7(CH), 42.9 (CH), 38.9 (CH), 32.8 (CH_2), 32.2 (CH_2), 32.1 (CH_2), 30.0 (CH_2), 28.6 (CH_3), 28.3 (CH_2), 23.0 (CH_2). **MS (ESI)** [m/z, (%)]: 656.3 ([MNa]$^+$, 100), 600.2 ([MNa-^{t}Bu]$^+$, 70), 407.3 ([MNa-Boc]$^+$, 35). **HRMS (ESI) calculated** for $C_{36}H_{47}N_3NaO_7$ ([MNa]$^+$): 656.3306, **found**: 656.3306.

***c*-[(*D*-Lys-δ-Ach-*L*-Leu-δ-Ach-*D*-Glu-δ-Ach-*L*-Glu-δ-Ach-*D*-Arg-δ-Ach-*L*-Lys-)] (CP10)**: This cyclic peptide was synthesized by Fmoc solid-phase peptide synthesis. The precipitate obtained suspended in chilled MeOH and sonicated for 5 min. Then, the suspension was centrifuged, and the supernatant was discarded. This process was repeated twice to obtain **CP10** as a white powder.

MS (MALDI) [m/z, (%)]: 1534.97103 ([MH]$^+$, 100). **HRMS (MALDI) calculated** for $C_{76}H_{128}N_{17}O_{16}$ ([MH]$^+$) 1534.97195, **found**: 1534.97103. **FTIR** (neat, cm^{-1}): ν = 3277 (amide A), 1674, 1620 (amide I), 1542 cm^{-1} (amide II_{II}).

***c*-[(*D*-His-δ-Ach-*L*-Leu-δ-Ach-*D*-His-δ-Ach-*L*-Glu-δ-Ach-*D*-Arg-δ-Ach-*L*-Lys-)] (CP11)**: This cyclic peptide was synthesized by Fmoc solid-phase peptide synthesis. The precipitated obtained was dissolved in H_2O MiliQ (0.1% v/v TFA) and purified by preparative RP-HPLC [H_2O (0.05% TFA + 0.05% HFIP)/CH_3CN (0.05% TFA + 0.05% HFIP) 100:0 (0→5 min), 100:0→88:12 (5→10 min), 88:12→78:22 (10→40 min)] using an Agilent Eclipse XDB-C18 to obtain 30 mg of **CP11** as a white powder [21%, t_R= 27.7 min].

^{1}H NMR (D_2O, 300 MHz, δ) 8.65 (s, 1H, Ar His), 8.14–7.93 (m, 5H, NH), 7.32 (s, 1H, Ar_{His}), 4.62–4.47 (m, 3H), 4.27–4.09 (m, 5H, $H\alpha_{\alpha\text{-aa}}$), 3.69–3.44 (m, 6H, $H\delta_{\delta\text{-Aca}}$), 3.27–3.05 (m, 6H, $H\delta_{Arg}$ and $H\beta_{His}$), 3.05–2.85 (m, 6H, $H\alpha_{\delta\text{-Aca}}$), 2.45 (t, *J* = 6.1 Hz, 2H, $H\varepsilon_{Lys}$), 2.37–2.17 (m, 6H, $H\gamma_{Glu}$), 2.03–1.79 (m, 20H), 1.59–1.38 (m, 14H), 1.37–1.13 (m, 11H), 0.91 (Overlapped doublets, *J* = 5.9 and 5.7 Hz, 6H, Me_{Leu}). **MS (ESI)** [m/z, (%)]: 926.2 ([MH]$^{2+}$, 100), 518.8 ([MH]$^{3+}$, 6). **HRMS (ESI) calculated** for $C_{77}H_{123}N_{20}O_{14}$ ([MH]$^+$): 1551.9524, **found**:

1551.9522. **FTIR** (neat, cm^{-1}): ν = 3270 (amide A), 1661, 1627 (amide I), 1537 cm^{-1} (amide II_{II}).

***c*-[(*L*-His-δ-Ach-*D*-Leu-δ-Ach-*L*-His-δ-Ach-*D*-Glu-δ-Ach-*L*-Arg-δ-Ach-*D*-Lys-)] (CP12)**: This cyclic peptide was synthesized by Fmoc solid-phase peptide synthesis. The precipitated obtained was dissolved in H_2O MiliQ (0.1% v/v TFA) and purified by preparative RP-HPLC [H_2O (0.05% TFA + 0.05% HFIP)/CH_3CN (0.05% TFA + 0.05% HFIP) 100:0 (0→5 min), 100:0→88:12 (5→10 min), 88:12→78:22 (10→40 min)] using an Agilent Eclipse XDB-C18 to obtain 25 mg of **CP12** as a white powder [24%, t_R= 27.7 min].

The spectroscopic data matched those for its enantiomer **CP12**. **MS (ESI)** [m/z, (%)]: 926.2 ($[MH]^{2+}$, 100), 518.8 ($[MH]^{3+}$, 12). **HRMS (ESI) calculated** for $C_{77}H_{123}N_{20}O_{14}$ ($[MH]^+$): 1551.9530, **found**: 1551.9522.

***c*-[(*D*-Ala-δ-Ach-*L*-His-δ-Ach-*D*-Leu-δ-Ach-*L*-His-δ-Ach-*D*-Ala-δ-Ach-*L*-Glu-δ-Ach-*D*-Arg-δ-Ach-*L*-Lys-)] (CP13)**: This cyclic peptide was synthesized by Fmoc solid-phase peptide synthesis. The precipitated obtained was suspended in chilled MeOH and sonicated for 5 min. Then, the suspension was centrifuged, and the supernatant was discarded. This process was repeated twice to obtain **CP15** as a white powder.

MS (MALDI) [m/z, (%)]: 1945.2 ($[MH]^+$, 40). **HRMS (MALDI) calculated** for $C_{97}H_{156}N_{24}O_{18}$ ($[MH]^+$) 1945.2030, **found**: 1945.2031. **FTIR** (neat, cm^{-1}): ν = ν = 3273 (amide A), 1665, 1631 (amide I), 1542 cm^{-1} (amide II_{II}).

***c*-[(*D*-Glu-δ-Ach-*L*-His-δ-Ach-*D*-Leu-δ-Ach-*L*-His-δ-Ach-*D*-Glu-δ-Ach-*L*-Glu-δ-Ach-*D*-Arg-δ-Ach-*L*-Lys-)] (CP14)**: This cyclic peptide was synthesized by Fmoc solid-phase peptide synthesis. The precipitated obtained was suspended in chilled MeOH and sonicated for 5 min. Then, the suspension was centrifuged, and the supernatant was discarded. This process was repeated twice to obtain **CP15** as a white powder.

MS (MALDI) [m/z, (%)]: 2061.2 ($[MH]^+$,73). **HRMS (MALDI) calculated** for $C_{101}H_{160}N_{24}O_{22}$ ($[MH]^+$) 2061.2140, **found**: 2061.2250. **FTIR** (neat, cm^{-1}): ν = 3271 (amide A), 1665, 1631 (amide I), 1538 cm^{-1} (amide II_{II}).

***c*-[(*D*-His-δ-Ach-*L*-His-δ-Ach-*D*-Leu-δ-Ach-*L*-His-δ-Ach-*D*-Leu-δ-Ach-*L*-His-δ-Ach-*D*-Arg-δ-Ach-*L*-Lys-)] (CP15)**: This cyclic peptide was synthesized by Fmoc solid-phase peptide synthesis. The precipitated obtained was suspended in chilled MeOH and sonicated for 5 min. Then, the suspension was centrifuged, and the supernatant was discarded. This process was repeated twice to obtain **CP16** as a white powder.

MS (MALDI) [m/z, (%)]: 2061.2 ($[MH]^+$, 100). **HRMS (MALDI) calculated** for $C_{104}H_{164}N_{28}O_{16}$ ($[MH]^+$) 2061.2724, **found**: 2061.2792. **FTIR** (neat, cm^{-1}): ν = 3272 (amide A), 1664, 1631 (amide I), 1540 cm^{-1} (amide II_{II}).

USC DE SANTIAGO DE COMPOSTELA

THIOFLAVIN T FLUORESCENCE EMISSION ASSAYS:

Fluorescence emission experiments were carried out using a Cary Eclipse Fluorescence Spectrophotometer (Agilent) with an excitation wavelength of 420 nm and recording the spectra between 440-650 nm with 5 nm slit. Emission spectra of a sample of ThT (1 mL, 20 μM) containing different volumes of a high-concentrated stock solution of cyclic peptide was recorded.

FULLERENE C_{60} SOLUBILIZATION IN THE PRESENCE OF CYCLIC PEPTIDE:

C_{60} fullerene (1 mg, Sigma Aldrich) was suspended in a 1 mM solution of **CP11** in MiliQ water at pH 8.1. pH was adjusted manually adding NaOH solution (0.1 M in MiliQ water). The suspension was sonicated for 40 min in a Branson 2800 Ultrasonic Cleaner. Then, it was submitted to 3 ultrasound cycles (3 min) in a Branson 450 SSE-1 tip horn ultrasonicator (20 cycles per min, 20% power) and sonicated another 40 min in the Branson 2800 Ultrasonic Cleaner. Finally, the suspension was centrifuged at 7500 rpm for 10 min and the supernatant was carefully decanted. UV/vis spectroscopy experiments were carried out to estimate the amount of dissolved fullerene.

PREPARATION OF SINGLE-WALLED CARBON NANOTUBES DISPERSIONS:

SWCNTs (1 mg, Sigma Aldrich, diameters) were suspended in a cyclic peptide solution in MiliQ water. The suspension was sonicated for 1 h in a Branson 2800 Ultrasonic Cleaner. Then, it was submitted to 3 ultrasound cycles (3 min) in a Branson 450 SSE-1 tip horn ultrasonicator (20 cycles per min, 20% power) and sonicated again 1 h in the Branson 2800 Ultrasonic Cleaner. Finally, the suspension was centrifuged at 14680 rpm (3 x 10 min) and the supernatant was carefully decanted. The suspensions were characterized by Raman spectroscopy as a film or in solution (macro).

ATOMIC FORCE MICROSCPY (AFM):

For AFM imaging, 20 μL of CP solution in were dropped onto freshly exfoliated mica disc (Ted Pella Inc. PELCO® Mica Discs, 9.9 mm Diameter) and after 1 min mica was dried under nitrogen flow.

SCANNING TRANSMISSION ELECTRON MICROSCOPY (STEM):

For STEM imaging a sample were drop casted in commercial microscopy grids (carbon type B film on 300 mesh cooper grid). After 10 min the sample excess was removed by placing the grid onto a filter paper and left to dry at room temperature overnight. The sample was stained with a 2% uranyl acetate solution or phosphotungstic acid by depositing a droplet onto the grid for 1 min. The excess was removed with filter paper and left to dry at room temperature for 1 h.

USC UNIVERSIDADE DE SANTIAGO DE COMPOSTELA

CHAPTER 3

SYNTHESIS AND CHARACTERIZATION

Boc-δ-Ach-OMe (6): A solution of *trans*-4-(*tert*-butoxycarbonyl)cyclohexanecarboxylic acid (2.00 g, 8.22 mmol) in DMF (27 mL) was treated with sodium carbonate (1.74 g, 16.4 mmol) and iodomethane (1.5 mL, 24.7 mmol). The reaction mixture was stirred for 2 h and then, H_2O was added and extracted with Et_2O (3 x 10 mL). The combined organic extracted were washed with aqueous solutions of $NaHCO_3$ (sat. 2 x 10 mL) and $Na_2S_2O_3$ (sat., 2x15 mL), dried over anhydrous $MgSO_4$, filtered and concentrated to afford the desired compound **6** as a white solid [1.86 g, 88%, R_f = 0.71 (40% EtOAC/hexane].

^{1}H NMR (500 MHz, $CDCl_3$, δ) 4.38 (s, 1H, NH), 3.65 (s, 3H, $CO_2\underline{Me}$), 3.47 (p, *J* = 6.8 Hz, 1H, H_δ-Ach), 3.39 (s, 1H), 2.21 (ddt, *J* = 13.1, 8.9, 4.2 Hz, 1H, H_α-Ach), 2.11–1.93 (m, 4H), 1.50 (q, *J* = 12.8 Hz, 1H), 1.42 (s, 9H, Boc), 1.20 (dd, *J* = 9.8, 4.2 Hz, 1H), 1.09 (q, *J* = 13.1 Hz, 2H). **^{13}C NMR** (126 MHz, $CDCl_3$, δ) 176.0 (CO), 155.3 (CO), 79.4 (C), 66.0 (CH_3), 51.7 (CH_2), 49.1 (CH_2), 42.5 (CH_2), 32.7 (CH), 28.5 (CH_2), 27.9 (CH), 15.4 (CH_2). **MS (ESI)** [m/z, (%)]: 280.2 ($[MNa]^+$, 15), 258.2 ($[MH]^+$, 2), 202.1 ($[MH\text{-}^t Bu]^+$, 100), 158.1 ($[MH\text{-Boc}]^+$, 9). **HRMS (ESI) calculated** for $C_{13}H_{24}NO_4$ ($[MH]^+$): 258.1700, **found**: 258.1701.

Ns-δ-Ach-OMe (7): A solution of **Boc-δ-Ach-OMe** (**6**, 2.00 g, 7.77 mmol) in a mixture of TFA/CH_2Cl_2 (1:1, 10 mL) was stirred a *rt* for 20 min. After this time, TFA was removed in the rotatory evaporator and the residue was dried under high vacuum. The resulting ammonium salt was dissolved in CH_2Cl_2 (30 mL) and treated with DIEA (5.3 mL, 31.1 mmol) then, 2-nitrobenzenesulfonyl chloride (2.06 g, 9.33 mmol) was added. The reaction mixture was stirred at *rt* for 20 h. It was transferred to a separatory funnel and washed with aqueous solution of HCl (10%, 3 x 15 mL). The organic layer was dried over anhydrous $MgSO_4$, filtered and concentrated. The crude was purified by flash column chromatography (40% EtOAc/hexane) to give 2.20g of **7** as a white solid (83%, R_f = 0.40 (40% EtOAC/hexane).

^{1}H NMR (500 MHz, $CDCl_3$, δ) 8.20 – 8.12 (m, 1H, Ar), 7.89 – 7.81 (m, 1H, Ar), 7.79 – 7.69 (m, 2H, Ar), 5.21 (d, *J* = 7.5 Hz, 1H, NH), 3.28 (tdt, *J* = 11.3, 7.6, 3.9 Hz, 1H, H_δ-Ach), 2.21 (tt, *J* = 12.0, 3.5 Hz, 1H, H_α-Ach), 2.00 – 1.89 (m, 4H), 1.51 – 1.39 (m, 3H). **^{13}C NMR** (126 MHz, $CDCl_3$, δ) 175.5 (CO), 148.0 (C), 135.1 (C), 133.6 (CH), 133.1 (CH), 130.8 (CH), 125.6 (CH), 53.2 (CH_3), 51.8 (CH), 41.8 (CH), 32.9 (CH_2), 27.7 (CH_2). **MS (ESI)** [m/z, (%)]: 360.1 ($[MNa]^+$, 38), 343.1 ($[MH]^+$, 17). **HRMS (ESI) calculated** for $C_{14}H_{19}N_2O_6S$ ($[MH]^+$): 343.0958, **found**: 343.0962.

Ns-δ-^{tBuOAc}Ach-OMe (8): A solution of **Ns-δ-Ach-OMe** (**7**, 2.00 g, 5.84 mmol) in DMF (29 mL) was treated with K_2CO_3 (1.61 g, 11.7 mmol) and *tert*-butyl bromoacetate (1.79 mL, 17.5 mmol). The reaction mixture was stirred at *rt* for 2 h and then, H_2O was added. The mixture was transferred to a separatory funnel and extracted with Et_2O (3 x 15 mL). The combined organic extracts were washed with aqueous solutions of $NaHCO_3$ (sat. 20 mL) and NaCl (sat. 20 mL), dried over anhydrous $MgSO_4$, filtered and concentrated. The crude was purified by

flash column chromatography (40% EtOAc/hexane) to provide **8** as a white solid [98%, R_f= 0.48 (40% EtOAC/hexane].

^{1}H NMR (300 MHz, $CDCl_3$, δ) 8.21 – 8.11 (m, 1H, Ar), 7.73 – 7.58 (m, 3H, Ar), 3.97 (s, 2H, C$\underline{H_2}CO_2{}^t$Bu), 3.73 (tt, *J* = 11.8, 3.8 Hz, 1H, Hδ Ach), 3.64 (s, 3H, $CO_2\underline{Me}$), 2.16 (tt, *J* = 12.2, 3.6 Hz, 1H, Hα Ach), 2.07 – 1.95 (m, 3H), 1.92 – 1.81 (m, 3H), 1.41 (s, 9H, $CH_2CO_2{}^t\underline{Bu}$) **^{13}C NMR** (75 MHz, $CDCl_3$, δ) 175.5 (CO), 168.9 (CO), 148.2 (C), 134.3 (C), 133.6 (CH), 131.8 (CH), 131.5 (CH), 124.3 (CH), 82.3 (C), 57.1 (CH), 51.8 (CH_3), 45.3 (CH_2), 42.1 (CH), 30.1 (CH_2), 28.4 (CH_2), 28.0 (CH_3). **MS (ESI)** [m/z, (%)]: 479.1 ($[MNa]^+$, 41), 457.2 ($[MH]^+$, 2), 401.1 ($[MH\text{-}{}^t Bu]^+$, 23). **HRMS (ESI) calculated** for $C_{20}H_{29}N_2O_8S$ ($[MH]^+$): 457.1639, **found**: 457.1623.

H-δ-^{tBuOAc}Ach-OMe (9): A solution of **Ns-δ-^{tBuOAc}Ach-OMe** (900 mg, 1.66 mmol) in DMF (8 mL) was treated with K_2CO_3 (689 mg, 4.99 mmol) and PhSH (0.7 mL, 6.65 mmol) successively. The reaction mixture was stirred at *rt* for 2 h and then, H_2O MiliQ was added. The mixture was transferred to a separatory funnel and extracted with CH_2Cl_2 (3 x 10mL). The combined organic extracts were dried over anhydrous $MgSO_4$, filtered and concentrated. Residual DMF was removed by azeotropic distillation in the presence of toluene. The crude was purified by flash column chromatography (% EtOAc/hexane) to give rise to **9** as a white foam [93%, Rf= (40% EtOAc/hexane].

Spectroscopic data

Boc-^{Me}*N*-Ala-δ-Ach-OMe (dp6): A solution of **Boc-δ-Ach-OMe** (**6**, 1.20 g, 4.65 mmol) in a mixture of TFA/CH_2Cl_2 (1:1, 5 mL) was stirred a *rt* for 20 min. After this time, TFA was removed in the rotatory evaporator and the residue was dried under high vacuum. The resulting ammonium salt was dissolved in CH_2Cl_2 (5 mL) and treated with DIEA (1.6 mL, 9.3 mmol). This solution was added over a mixture of **Boc-^{Me}*N*-Ala-OH** (950 mg, 4.65 mmol), *N*-HBTU (2.65 g, 6.98 mmol) and DIEA (1.6 mL, 9.3 mmol) in CH_2Cl_2 (18 mL). The reaction mixture was stirred at *rt* for 1 h. Then, it was poured into a separatory funnel and washed with aqueous solutions of HCl (5%, 3 x 5 mL) and $NaHCO_3$ (sat. 3 x 5 mL). The organic layer was dried over anhydrous $MgSO_4$, filtered and concentrated. The crude was purified by flash column chromatography (30-40% EtOAc/hexane) to give **dp6** as a white solid [73%, R_f = 0.54 (5% MeOH/CH_2Cl_2)].

MS (ESI) [m/z, (%)]: 707.4 ($[2MNa]^+$, 4), 365.2 ($[MNa]^+$, 32), 343.2 ($[MH]^+$, 46), 287.2 ($[MH\text{-}{}^t Bu]^+$, 12), 243.2 ($[MH\text{-Boc}]^+$, 100). **HRMS (ESI) calculated** for $C_{17}H_{31}N_2O_5$ ($[MH]^+$): 343.2227, **found**: 343.2230

Cbz-*D*-Leu-δ-^{tBuOAc}Ach-OMe (dp7): A solution of **Cbz-*D*-Leu-OH** (0.675 mg, 2.54 mmol) in CH_2Cl_2 (25 mL) was treated with *N*-HATU (1.45 g, 3.81 mmol) and DIEA (1.8 mL, 10.2 mmol) then, **H-δ-^{tBuOAc}Ach-OMe** (**9**, 690 mg, 2.54 mmol) was added. The reaction mixture was stirred at *rt* for 1 h. Then, it was poured into a separatory funnel and washed with aqueous solutions of HCl (5%, 3 x 5 mL) and $NaHCO_3$ (sat. 3 x 5 mL). The organic layer was dried over anhydrous $MgSO_4$, filtered and concentrated. The organic layer was dried over anhydrous $MgSO_4$, filtered and concentrated. The crude was purified by flash column

chromatography (30% EtOAc/hexane) to give **dp7** as a white solid [95%, R_f = 0.52 (5% MeOH/CH_2Cl_2)].

MS (ESI) [m/z, (%)]: 531.3 ([MNa]$^+$, 12), 519.3 ([MH]$^+$, 48), 463.2 ([MH-^{t}Bu]$^+$, 29). **HRMS (ESI) calculated** for $C_{28}H_{43}N_2O_7$ ([MH]$^+$): 519.3070, **found**: 519.3076.

Ns-δ-^{tBuOAc}Ach-^{Me}N-Ala-OMe (dp8): A solution of **Ns-δ-^{tBuOAc}Ach-OMe** (**8**, 1.04 g, 2.28 mmol) in a mixture of MeOH/H_2O (3:1, 11 mL) was treated with LiOH (328 mg, 13.7 mmol). The reaction mixture was stirred at *rt* for 1.5 h. Then, the organic solvent was removed in the rotatory evaporator. The aqueous residue was acidified to pH 3 and extracted with CH_2Cl_2 (3 x 10 mL). The combined organic extracts were dried over anhydrous $MgSO_4$, filtered and concentrated to afford **Ns-δ-^{tBuOAc}Ach-OH** that was used without further purification.

A solution of **Ns-δ-^{tBuOAc}Ach -OH** in CH_2Cl_2 (23 mL) was treated with *N*-HATU (1.04 g, 2.73 mmol) and DIEA (2 mL, 11.4 mmol), and then, **H-^{Me}N-Ala-OMe** (268 mg, 2.28 equiv) was added. The reaction mixture was stirred at *rt* for 20 h. Then, the mixture was poured into a separatory funnel and washed with aqueous solutions of HCl (3 x 15 mL) and $NaHCO_3$ (3 x 15 mL). The organic layer was dried over $MgSO_4$, filtered and concentrated. The crude was purified by flash column chromatography on SiO_2 (60% EtOAc/hexane) to afford 1.02 g of **dp6** as a white foam [83%, R_f= 0.76 (10% MeOH/CH_2Cl_2)].

^{1}H NMR (500 MHz, $CDCl_3$, δ) 8.22 – 8.15 (m, 1H, Ar), 7.71 – 7.66 (m, 2H, Ar), 7.66 – 7.61 (m, 1H, Ar), 5.17 (q, *J* = 7.3 Hz, 1H, Hα Ala), 3.99 (s, 2H, C<u>H$_2$</u>CO$_2$^{t}Bu), 3.76 – 3.69 (m, 1H, Hδ Ach), 3.68 (s, 3H, CO$_2$<u>Me</u>), 2.95 (s, 3H, N<u>Me</u>), 2.40 (tt, *J* = 11.8, 3.3 Hz, 1H, Hα Ach), 1.92 – 1.54 (m, 6H), 1.44 (s, 9H, CH$_2$CO$_2$^{t}<u>Bu</u>), 1.37 (d, *J* = 7.4 Hz, 3H, <u>Me</u> Ala) **^{13}C NMR** (126 MHz, $CDCl_3$, δ) 175.0 (CO), 172.2 (CO), 168.9 (CO), 147.8 (C), 134.0 (C), 133.4 (CH), 131.6 (CH), 131.4 (CH), 124.1 (CH), 82.1 (C), 57.0 (CH), 52.0 (CH_3), 45.3 (CH_2), 39.4 (CH_3), 31.3 (CH), 29.8 (CH_2), 29.8 (CH_2), 28.1 (CH_2), 28.0 (CH_2), 27.8 (CH_3), 14.3 (CH_3). **MS (ESI)** [m/z, (%)]: 564.2 ([MNa]$^+$, 16), 542.2 ([MH]$^+$, 35), 486.2 ([MH-^{t}Bu]$^+$, 40). **HRMS (ESI) calculated** for $C_{24}H_{36}N_3O_9S$ ([MH]$^+$): 542.2167, **found**: 542.2164.

H-δ-^{tBuOAc}Ach-^{Me}N-*D*-Ala-OMe (dp9): A solution of **Ns-δ-^{tBuOAc}Ach-^{Me}N-Ala-OMe** (900 mg, 1.66 mmol) in DMF (17 mL) was treated with K_2CO_3 (689 mg, 4.99 mmol) and PhSH (0.7 mL, 6.65 mmol) successively. The reaction mixture was stirred at *rt* for 2 h and then, H_2O MiliQ was added. The mixture was transferred to a separatory funnel and extracted with CH_2Cl_2 (3 x 10 mL). The combined organic extracts were dried over $MgSO_4$, filtered and concentrated. Residual DMF was removed by azeotropic distillation in the presence of toluene. The crude was purified by flash column chromatography on SiO_2 (60% EtOAc/hexane) to afford 580 mg of **dp9** as colorless oil [98%, R_f= 0.51 (10% MeOH/CH_2Cl_2)].

^{1}H NMR (300 MHz, $CDCl_3$, δ) 5.19 (q, *J* = 7.3 Hz, 1H, Hα Ala), 3.68 (s, 3H, CO$_2$<u>Me</u>), 3.33 (s, 2H, <u>CH$_2$</u>CO$_2$^{t}Bu), 2.96 (s, 3H, N<u>Me</u>), 2.54 – 2.39 (m, 2H, Hα + Hδ Ach), 2.10 – 1.50 (m, 6H), 1.45 (s, 9H, CH$_2$CO$_2$^{t}<u>Bu</u>), 1.37 (d, *J* = 7.4 Hz, 3H, Me Ala) **^{13}C NMR** (75 MHz, $CDCl_3$, δ) 176.0 (CO), 172.6 (CO), 171.8 (CO), 81.5 (C), 56.2 (CH), 52.2 (CH_3), 49.2 (CH_2), 40.5 (CH_3), 32.6 (CH_2), 31.5 (CH), 28.2 (CH_2), 27.7 (CH_2), 27.6 (CH_2), 14.6 (CH_3). **MS (ESI)**

[m/z, (%)]: 357.2 ([MH]$^+$, 49), 301.1 ([MH-^{t}Bu]$^+$, 90). **HRMS (ESI) calculated** for $C_{18}H_{33}N_2O_5$ ([MH]$^+$): 357.2384, **found**: 357.2389.

Cbz-*D*-Leu-δ-^{tBuOAc}Ach-^{Me}*N*-Ala-OMe (trp1): A solution of **Cbz-*D*-Leu-OH** (461 mg, 1.74 mmol) in CH_2Cl_2 (9 mL) was treated with *N*-HATU (794 mg, 2.09 mmol) and DIEA (1.5 mL, 8.70 mmol) and then, **H-δ-^{tBuOAc}Ach-^{Me}*N*-Ala-OMe** (**dp9**, 132 mg, 0.390 mmol) was added. The reaction mixture was stirred at *rt* for 20 h. Then, the mixture was poured into a separatory funnel and washed with aqueous solutions of HCl (3 x 5 mL) and $NaHCO_3$ (3 x 5 mL). The organic layer was dried over anhydrous $MgSO_4$, filtered and concentrated. The crude was purified by flash column chromatography on SiO_2 (1-2% MeOH/CH_2Cl_2) to afford 902 mg of **trp1** as a white solid [86%, R_f = 0.60 (10% MeOH/CH_2Cl_2)].

^{1}H NMR (300 MHz, $CDCl_3$, δ) 7.35 – 7.31 (m, 5H, CH_2Ph), 5H), 5.21 (q, *J* = 7.4 Hz, 1H, Hα Ala), 5.07 (s, 2H, CH_2Ph), 4.74 (t, *J* = 9.7 Hz, 1H, Hα Leu), 3.85 – 3.66 (m + s, 4H, CO_2Me + Hδ Ach), 2.98 (s, 2H, $CH_2CO_2{}^t$Bu), 2.83 (s, 3H, NMe), 2.11 – 1.54 (m, 8H), 1.43 (s, 9H, $CH_2CO_2{}^t$Bu), 1.39 (d, *J* = 7.1 Hz, 3H, Me Ala), 1.03 and 0.93 (d, *J* = 6.5 Hz, 3H, Me Leu). **MS (ESI)** [m/z, (%)]: 626.3 ([MNa]$^+$, 30), 604.4.2 ([MH]$^+$, 100), 548.3 ([MH-^{t}Bu]$^+$, 95). **HRMS (ESI) calculated** for $C_{32}H_{50}N_3O_8$ ([MH]$^+$): 604.3592, **found**: 604.3603.

Cbz-*D*-Leu-δ-^{tBuOAc}Ach-^{Me}*N*-Ala-δ-Ach-OMe (tp4): A solution of **Boc-^{Me}*N*-Ala-δ-Ach-OMe** (**dp6**, 132 g, 0.390 mmol) in a mixture of TFA/CH_2Cl_2 (1:1, 2 mL) was stirred a *rt* for 20 min. After this time, TFA was removed in the rotatory evaporator and the residue was dried under high vacuum to provide **H-^{Me}*N*-Ala-δ-Ach-OMe** that was used without further purification.

A solution of **Cbz-*D*-Leu-δ-^{tBuOAc}Ach-OMe** (**dp7**, 200 mg, 0.390 mmol) in a mixture of MeOH/H_2O (3:1, 2 mL) was treated with LiOH (43.2 mg, 1.93 mmol). The reaction mixture was stirred at *rt* for 1 h. Then, the organic solvent was removed in the rotatory evaporator. The aqueous residue was acidified to pH 3 and extracted with CH_2Cl_2 (3 x 5 mL). The combined organic extracts were dried over anhydrous $MgSO_4$, filtered and concentrated. The resulting carboxylic acid dissolved in CH_2Cl_2 (4 mL) and treated with *N*-HATU (220 mg, 0.580 mmol) and DIEA (0.2 mL, 1.16 mmol) then, **H-δ-^{tBuOAc}Ach-^{Me}*N*-Ala-δ-Ach-OMe** was added. The reaction mixture was stirred at *rt* for 1.5 h. Then, the mixture was poured into a separatory funnel and washed with aqueous solutions of HCl (3 x 5 mL) and $NaHCO_3$ (3 x 5 mL). The organic layer was dried over anhydrous $MgSO_4$, filtered and concentrated. The crude was purified by flash column chromatography on SiO_2 (1-3 % MeOH/CH_2Cl_2) to provide 207 mg of **tp4** as a white solid. [74%, R_f= 0.42 (5% MeOH/CH_2Cl_2)].

MS (ESI) [m/z, (%)]: 751.4 ([MNa]$^+$, 24), 729.4 ([MH]$^+$, 86), 673.4 ([MH-^{t}Bu]$^+$, 100). **HRMS (ESI) calculated** for $C_{39}H_{61}N_4O_9$ ([MH]$^+$): 729.4439, **found**: 729.4434.

Cbz-*D*-Leu-δ-^{BocNHNHAc}Ach-^{Me}*N*-Ala-δ-Ach-OMe (tp5): A solution of **Cbz-*D*-Leu-δ-^{tBuOAc}Ach-^{Me}*N*-Ala-δ-Ach-OMe** (**tp4**, 160 mg, 0.219 mmol) in a mixture of TFA/CH_2Cl_2 (1:1, 2 mL) was stirred a *rt* for 1.5 h. After this time, TFA was removed in the rotatory evaporator and the residue was dried under high vacuum. The resulting carboxylic acid was dissolved in CH_2Cl_2 (2 mL) and treated with *N*-HBTU (100 mg, 0.260 mmol) and DIEA (0.2 mL,

1.10 mmol) then, ***tert*-butyl carbazate** (29.0 mg, 0.220 mmol) was added. The reaction mixture was stirred at *rt* for 1.5 h. Then, the mixture was poured into a separatory funnel and washed with aqueous solutions of HCl (3 x 5 mL) and $NaHCO_3$ (3 x 5 mL). The organic layer was dried over anhydrous $MgSO_4$, filtered and concentrated. The crude was purified by flash column chromatography on SiO_2 (1-3 % MeOH/CH_2Cl_2) to provide 122 mg of **tp5** as a white solid. [71%, R_f= 0.38 (5% MeOH/CH_2Cl_2)].

MS (ESI) [m/z, (%)]: 809.4 ($[MNa]^+$, 12), 787.5 ($[MH]^+$, 100), 730.4 ($[MH\text{-}^t Bu]^+$, 46), 686.4 ($[MH\text{-Boc}]^+$,74). **HRMS (ESI) calculated** for $C_{40}H_{63}N_6O_{10}$ ($[MH]^+$): 787.4606, **found**: 787.4659.

Ns-δ-Ach-*D*-Leu-δ-^{tBuOAc}Ach-^{Me}*N*-Ala-OMe (tp6): A solution of **Cbz-*D*-Leu-δ-^{tBuOAc}Ach-^{Me}*N*-Ala-OMe** (**tr1**, 600 mg, 0.994 mmol) in MeOH (7 mL) was treated with Pd/C (159 mg, 0.149 mmol). The reaction mixture was stirred at *rt* for 1 h under H_2 atmosphere. Then, the heterogeneous mixture was filtered through celite®. The solvent was removed in the rotatory evaporator and the resulting residue was dried under high vacuum to yield the N-terminal deprotected intermediate **H-*D*-Leu-δ-^{tBuOAc}Ach-^{Me}*N*-Ala-OMe** that was used without further purification.

A solution of **Ns-δ-Ach-OMe** (**7**, 372 g, 1.09 mmol) in a mixture of MeOH/H_2O (3:1, 5 mL) was treated with LiOH (131 mg, 5.45 mmol). The reaction mixture was stirred at *rt* for 1 h. Then, the organic solvent was removed in the rotatory evaporator. The aqueous residue was acidified to pH 3 and extracted with CH_2Cl_2 (3 x 5 mL). The combined organic extracts were dried over anhydrous $MgSO_4$, filtered and concentrated. The resulting carboxylic acid was dissolved in CH_2Cl_2 (7 mL) and treated with *N*-HBTU (452 mg, 1.19 mmol) and DIEA (0.7 mL, 3.98 mmol) then, **H-*D*-Leu-δ-^{tBuOAc}Ach-^{Me}*N*-Ala-OMe** was added. The reaction mixture was stirred at *rt* for 1 h. Then, the mixture was poured into a separatory funnel and washed with aqueous solutions of HCl (3 x 5 mL) and $NaHCO_3$ (3 x 5 mL). The organic layer was dried over anhydrous $MgSO_4$, filtered and concentrated. The crude was purified by flash column chromatography on SiO_2 (1-3% MeOH/CH_2Cl_2) to provide 667 mg of **tp6** as a white solid. [86%, R_f= 0.44 (5% MeOH/CH_2Cl_2)].

MS (ESI) [m/z, (%)]: 802.4 ($[MNa]^+$, 7), 780.4 ($[MH]^+$, 100), 724.3 ($[MH\text{-}^t Bu]^+$, 14) **HRMS (ESI) calculated** for $C_{37}H_{58}N_5O_{11}S$ ($[MH]^+$): 780.3848, **found**: 780.3857.

Ns-δ-Ach-*D*-Leu-δ-^{BocNHNHAc}Ach-^{Me}*N*-Ala-OMe (tp7): A solution of **Cbz-*D*-Leu-δ-^{BocNHNHAc}Ach-^{Me}*N*-Ala-δ-Ach-OMe** (**tp4**) in a mixture of TFA/CH_2Cl_2 (1:1 v/v) was stirred a *rt* for 1 h. After this time, TFA was removed in the rotatory evaporator and the residue was dried under high vacuum. The resulting carboxylic acid was dissolved and treated with X (coupling reagent) and DIEA then, ***tert*-butyl carbazate** was added. The reaction mixture was stirred at *rt* for 2 h. Then, the mixture was poured into a separatory funnel and washed with aqueous solutions of HCl (3 x 5 mL) and $NaHCO_3$ (3 x 5 mL). The organic layer was dried over anhydrous $MgSO_4$, filtered and concentrated. The crude was purified by flash column chromatography on SiO_2 (2-3 % MeOH/CH_2Cl_2) to provide **tp7** as a white solid. [R_f= 0.41 (5% MeOH/CH_2Cl_2)].

ENTRY	X: COUPLING REAGENT	SOLVENT	ISOLATED YIELD
1	*N*-HBTU	CH_2Cl_2	22%
2	*N*-HATU	CH_2Cl_2	30%
3	EDC·HCl	CH_2Cl_2	55%
4	EDC·HCl	DMF	58%
5	EDC·HCl	MeCN	22%
6	PyAOP	CH_2Cl_2	83%

MS (ESI) [m/z, (%)]: 838.4 ([MH]$^+$, 33), 782.3 ([MH-^{t}Bu]$^+$, 20) **HRMS (ESI) calculated** for $C_{38}H_{60}N_7O_{12}S$ ([MH]$^+$): 838.4015, **found**: 838.4040.

Cbz-δ-Ach-*D*-Leu-δ-^{tBuOAc}Ach-^{Me}*N*-Ala-OMe (tp8): A solution of **Cbz-*D*-Leu-δ-^{tBuOAc}Ach-^{Me}*N*-Ala-OMe** (**tr1**, 900 mg, 1.49 mmol) in MeOH (15 mL) was treated with Pd/C (238 mg, 0.224 mmol). The reaction mixture was stirred at *rt* for 2 h under H_2 atmosphere. Then, the heterogeneous mixture was filtered through celite®. The solvent was removed in the rotatory evaporator and the resulting residue was dried under high vacuum to yield the N-terminal deprotected intermediate **H-*D*-Leu-δ-^{tBuOAc}Ach-^{Me}*N*-Ala-OMe** that was used without further purification.

A solution of **Cbz-δ-Ach-OH** (395 mg, 1.49 mmol) in CH_2Cl_2 (10 mL) was treated with *N*-HBTU (678 mg, 1.79 mmol) and DIEA (1.3 mL, 7.45 mmol) and then, **H-*D*-Leu-δ-^{tBuOAc}Ach-^{Me}*N*-Ala-OMe** was added. The reaction mixture was stirred at *rt* for 1 h. Then, the mixture was poured into a separatory funnel and washed with aqueous solutions of HCl (3 x 5 mL) and $NaHCO_3$ (3 x 5 mL). The organic layer was dried over $MgSO_4$, filtered and concentrated. The crude was purified by flash column chromatography on SiO_2 (1-3% MeOH/CH_2Cl_2) to afford 968 mg of **tp8** as a white solid [89%, R_f= 0.56 (10% MeOH/CH_2Cl_2)].

MS (ESI) [m/z, (%)]: 729.4. ([MH]$^+$, 100), 673.4 ([MH-^{t}Bu]$^+$, 48). **HRMS (ESI) calculated** for $C_{39}H_{61}N_4O_9$ ([MH]$^+$): 729.4439, **found**: 729.4428.

Cbz-δ-Ach-*D*-Leu-δ-^{BocNHNHAc}Ach-^{Me}*N*-Ala-OMe (tp9): A solution of **Cbz-δ-Ach-*D*-Leu-δ-^{tBuOAc}Ach-^{Me}*N*-Ala-OMe** (**tp4**, 150 mg, 0.206 mmol) in formic acid (2 mL) was stirred at *rt* for 24 h and then, H_2O MiliQ was added. The mixture was transferred to a separatory funnel and extracted with CH_2Cl_2 (3 x 5 mL). The combined organic extracts were dried over anhydrous $MgSO_4$, filtered and concentrated to give the intermediate **Cbz-δ-Ach-*D*-Leu-δ-^{HOAc}Ach-^{Me}*N*-Ala-OMe** that was used without further purification.

A solution of **Cbz-δ-Ach-*D*-Leu-δ-^{OHAc}Ach-^{Me}*N*-Ala-OMe** in CH_2Cl_2 (2 mL) was treated with EDC·HCl (78.6mg, 0.410 mmol), HOBt (111 mg, 0.820 mmol) and DMAP (75.2 mg, 0.246 mmol), and then, ***tert*-butyl carbazate** (32.5 mg, 0.246 mmol) was added. The reaction mixture was stirred at *rt* for 3 h. Then, the mixture was poured into a separatory funnel and washed with aqueous solutions of HCl (3 x 5 mL) and $NaHCO_3$ (3 x 5 mL). The organic layer

was dried over $MgSO_4$, filtered and concentrated. The crude was purified by flash column chromatography on SiO_2 (5% MeOH/CH_2Cl_2) to afford mg of **tp9** as a white solid [85%, R_f= 0.42 (10% MeOH/CH_2Cl_2)].

MS (ESI) [m/z, (%)]: 787.5 ([MH]$^+$, 64), 731.4 ([MH-^{t}Bu]$^+$, 18). **HRMS (ESI) calculated** for $C_{40}H_{63}N_6O_{10}$ ([MH]$^+$): 787.4606, **found**: 787.4612.

Cbz-(*D*-Leu-δ-^{BocNHNHAc}Ach-^{Me}*N*-Ala-δ-Ach)$_2$-OMe (op1): A solution of **Cbz-*D*-Leu-δ-^{BocNHNHAc}Ach-^{Me}*N*-Ala-δ-Ach-OMe** (**tp5**, 350 mg, 0.440 mmol) in MeOH (5 mL) was treated with Pd/C (72.7 mg, 0.0670 mmol). The reaction mixture was stirred at *rt* for 2 h under H_2 atmosphere. Then, the heterogeneous mixture was filtered through celite®. The solvent was removed in the rotatory evaporator and the resulting residue was dried under high vacuum to yield the intermediate **H-*D*-Leu-δ-^{BocNHNHAc}Ach-^{Me}*N*-Ala-δ-Ach-OMe** that was used without further purification.

A solution of **Cbz-*D*-Leu-δ-^{BocNHNHAc}Ach-^{Me}*N*-Ala-δ-Ach-OMe** (**tp5**, 350 mg, 0.440 mmol) in a mixture of MeOH/H_2O (3:1, 2.4 mL) was treated with LiOH (53.3 mg, 2.22 mmol). The reaction mixture was stirred at *rt* for 1 h. Then, the organic solvent was removed in the rotatory evaporator. The aqueous residue was acidified to pH 3 and extracted with CH_2Cl_2 (3 x 5 mL). The combined organic extracts were dried over anhydrous $MgSO_4$, filtered and concentrated. The resulting carboxylic acid was dissolved in CH_2Cl_2 (5 mL) and treated with *N*-HBTU (253 mg, 0.670 mmol) and DIEA (0.4 mL, 2.22 mmol) then, **H-*D*-Leu-δ-^{BocNHNHAc}Ach-^{Me}*N*-Ala-δ-Ach-OMe** was added. The reaction mixture was stirred at *rt* for 1 h. Then, the mixture was poured into a separatory funnel and washed with aqueous solutions of HCl (3 x 5 mL) and $NaHCO_3$ (3 x 5 mL). The organic layer was dried over anhydrous $MgSO_4$, filtered and concentrated. The crude was purified by flash column chromatography on SiO_2 (2-6% MeOH/CH_2Cl_2) to provide 88 mg of **op1** as a white solid. [14%, R_f= 0.51 (5% MeOH/CH_2Cl_2)].

MS (ESI) [m/z, (%)]: 1445.8 ([MNa]$^+$, 54), 1423.8 ([MH]$^+$, 82), 1323.8 ([MH-Boc]$^+$, 100), 1223.7 ([MH-2xBoc]$^+$, 62) **HRMS (ESI) calculated** for $C_{71}H_{115}N_{12}O_{18}$ ([MH]$^+$): 1423.8452, **found**: 1423.8444.

Cbz-(*D*-Leu-δ-^{tBuOAc}Ach-^{Me}*N*-Ala-δ-Ach)$_2$-OMe (op2): A solution of **Cbz-*D*-Leu-δ-^{tBuOAc}Ach-^{Me}*N*-Ala-δ-Ach-OMe** (**tp4**, 412 mg, 0.570 mmol) in MeOH (2 mL) was treated with Pd/C (61.6 mg, 0.0570 mmol). The reaction mixture was stirred at *rt* for 2 h under H_2 atmosphere. Then, the heterogeneous mixture was filtered through celite®. The solvent was removed in the rotatory evaporator and the resulting residue was dried under high vacuum to yield the intermediate **H-*D*-Leu-δ-^{tBuOAc}Ach-^{Me}*N*-Ala-δ-Ach-OMe** that was used without further purification.

A solution of **Cbz-*D*-Leu-δ-^{tBuOAc}Ach-^{Me}*N*-Ala-δ-Ach-OMe** (**tp5**, 412 mg, 0.570 mmol) in a mixture of MeOH/H_2O (3:1, 2 mL) was treated with LiOH (67.7 mg, x mmol). The reaction mixture was stirred at *rt* for 1 h. Then, the organic solvent was removed in the rotatory evaporator. The aqueous residue was acidified to pH 3 and extracted with CH_2Cl_2 (3 x 5 mL). The combined organic extracts were dried over anhydrous $MgSO_4$, filtered and concentrated.

The resulting carboxylic acid was dissolved in CH_2Cl_2 (6 mL) and treated with *N*-HBTU (321 mg, 0.850 mmol) and DIEA (0.5 mL, 2.83 mmol) then, **H-*D*-Leu-δ-^{tBuOAc}Ach-^{Me}*N*-Ala-δ-Ach-OMe** was added. The reaction mixture was stirred at *rt* for 1 h. Then, the mixture was poured into a separatory funnel and washed with aqueous solutions of HCl (3 x 5 mL) and $NaHCO_3$ (3 x 5 mL). The organic layer was dried over anhydrous $MgSO_4$, filtered and concentrated. The crude was purified by flash column chromatography on SiO_2 (2-5% MeOH/CH_2Cl_2) to provide 405 mg of **op2** as a white solid. [55%, R_f= 0.38 (5% MeOH/CH_2Cl_2)].

MS (ESI) [m/z, (%)]: 1329.8 ([MNa]$^+$, 34), 1307.8 ([MH]$^+$, 84), 1251.8 ([MH-^{t}Bu]$^+$, 100), 1195.7 ([MH-2xBoc]$^+$, 47) **HRMS (ESI) calculated** for $C_{69}H_{111}N_8O_{16}$ ([MH]$^+$): 1307.8118, **found**: 1307.8110.

Ns-(δ-Ach-*D*-Leu-δ-^{BocNHNHAc}Ach-^{Me}*N*-Ala)$_2$-OMe (op3): A solution of **Ns-δ-Ach-*D*-Leu-δ-^{BocNHNHAc}Ach-^{Me}*N*-Ala-OMe** (**tp7**, 50 mg, 0.0597 mmol) in DMF (2.5 mL) was treated with K_2CO_3 (24.7 mg, 0.179 mmol) and PhSH (0.03 mL, 0.298 mmol) successively. The reaction mixture was stirred at *rt* for 2 h and then, H_2O MiliQ was added. The mixture was transferred to a separatory funnel and extracted with Et_2O (3x 5 mL) and CH_2Cl_2 (3 x 5 mL). The chlorinated layer was dried over anhydrous $MgSO_4$, filtered and concentrated to provide **H-δ-Ach-*D*-Leu-δ-^{BocNHNHAc}Ach-^{Me}*N*-Ala-OMe** that was used without further purification.

A solution of **Ns-δ-Ach-*D*-Leu-δ-^{BocNHNHAc}Ach-^{Me}*N*-Ala-OMe** (**tp7**, 50 mg, 0.0597 mmol) in a mixture of MeOH/H_2O (3:1, 2.4 mL) was treated with LiOH (7.1 mg, 0.298 mmol). The reaction mixture was stirred at *rt* for 2 h. Then, the organic solvent was removed in the rotatory evaporator. The aqueous residue was acidified to pH 3 and extracted with CH_2Cl_2 (3 x 5 mL). The combined organic extracts were dried over anhydrous $MgSO_4$, filtered and concentrated. The resulting carboxylic acid was dissolved in CH_2Cl_2 (3 mL) and treated with *N*-HBTU (27.2 mg, 0.0716 mmol) and DIEA (0.04 mL, 0.239 mmol) then, **H-δ-Ach-*D*-Leu-δ-^{BocNHNHAc}Ach-^{Me}*N*-Ala-OMe** was added. The reaction mixture was stirred at *rt* for 1.5 h. Then, the mixture was poured into a separatory funnel and washed with aqueous solutions of HCl (3 x 5 mL) and $NaHCO_3$ (3 x 5 mL). The organic layer was dried over anhydrous $MgSO_4$, filtered and concentrated. The crude was purified by flash column chromatography on SiO_2 (3-6 % MeOH/CH_2Cl_2) to provide 50 mg of **op3** as a white solid. [57%, R_f= 0.51 (5% MeOH/CH_2Cl_2)].

MS (ESI) [m/z, (%)]: 2917.6 ([2MH]$^+$, 3), 1480.8 ([MNa]$^+$, 52), 1458.8 ([MH]$^+$, 93), 1402.7 ([MH-^{t}Bu]$^+$, 12), 1358.7 ([MH-Boc]$^+$, 100), **HRMS (ESI) calculated** for $C_{69}H_{112}N_{13}O_{19}S$, ([MH]$^+$): 1458.7913, **found**: 1458.7873.

Cbz-(δ-Ach-*D*-Leu-δ-^{BocNHNHAc}Ach-^{Me}*N*-Ala)$_2$-OMe (op4): A solution of **Cbz-δ-Ach-*D*-Leu-δ-^{BocNHNHAc}Ach-^{Me}*N*-Ala-OMe** (50 mg, 0.0635 mmol) in MeOH (2 mL) was treated with Pd/C (14 mg, 0.0127 mmol). The reaction mixture was stirred at *rt* for 3 h under H_2 atmosphere. Then, the heterogeneous mixture was filtered through celite®. The solvent was removed in the rotatory evaporator and the resulting residue was dried under high vacuum to yield the

intermediate **H-δ-Ach-*D*-Leu-δ-^{BocNHNHAc}Ach-^{Me}*N*-Ala-OMe** that was used without further purification.

A solution of **Cbz-δ-Ach-*D*-Leu-δ-^{BocNHNHAc}Ach-^{Me}*N*-Ala-OMe** (50 mg, 0.0635 mmol) in a mixture of MeOH/H_2O (3:1, 2 mL) was treated with LiOH (15 mg, 0.635 mmol). The reaction mixture was stirred at *rt* for 3 h. Then, the organic solvent was removed in the rotatory evaporator. The aqueous residue was acidified to pH 3 and extracted with CH_2Cl_2 (3 x 5 mL). The combined organic extracts were dried over $MgSO_4$, filtered and concentrated to afford **Cbz-δ-Ach-*D*-Leu-δ-^{BocNHNHAc}Ach-^{Me}*N*-Ala-OH** that was used without further purification.

A solution of **Cbz-δ-Ach-*D*-Leu-δ-^{BocNHNHAc}Ach-^{Me}*N*-Ala-OH** in CH_2Cl_2 (3 mL) was treated with *N*-HBTU (28.9 mg, mmol) and DIEA (50 µL, 0.254 mmol), and then, **H-δ-Ach-*D*-Leu-δ-^{BocNHNHAc}Ach-^{Me}*N*-Ala-OMe** was added. The reaction mixture was stirred at *rt* for 15 h. Then, the mixture was poured into a separatory funnel and washed with aqueous solutions of HCl (3 x 5mL) and $NaHCO_3$ (3 x 5 mL). The organic layer was dried over $MgSO_4$, filtered and concentrated. The crude was purified by flash column chromatography on SiO_2 (2-7% MeOH/CH_2Cl_2) to afford 57 mg of **op1** as a white solid [64%, R_f= 0.48 (10% MeOH/CH_2Cl_2)].

MS (ESI) [m/z, (%)]: 1429.8 ($[MNa]^+$, 73), 1407.9 ($[MH]^+$, 82), 1307.8 ($[MH\text{-}Boc]^+$, 100), 1207.8 ($[MH\text{-}2xBoc]^+$, 82.1) **HRMS (ESI) calculated** for $C_{71}H_{115}N_{12}O_{17}$ ($[MH]^+$): 1407.8498, **found**: 1407.8504.

Cbz-(*D*-Leu-δ-^{tBuOAc}Ach-^{Me}*N*-Ala-δ-Ach)$_3$-OMe (ddp2): A solution of **Cbz-(*D*-Leu-δ-^{tBuOAc}Ach-^{Me}*N*-Ala-δ-Ach)$_2$-OMe** (**op2**, 405 mg, 0.310 mmol) in MeOH (3 mL) was treated with Pd/C (34.2 mg, 0.0310 mmol). The reaction mixture was stirred at *rt* for 3 h under H_2 atmosphere. Then, the heterogeneous mixture was filtered through celite®. The solvent was removed in the rotatory evaporator and the resulting residue was dried under high vacuum to yield the intermediate **H-(*D*-Leu-δ-^{tBuOAc}Ach-^{Me}*N*-Ala-δ-Ach)$_2$-OMe** that was used without further purification.

A solution of **Cbz-*D*-Leu-δ-^{tBuOAc}Ach-^{Me}*N*-Ala-δ-Ach-OMe** (**tp4**, 228 mg, 0.310 mmol) in a mixture of MeOH/H_2O (3:1, 3 mL) was treated with LiOH (37.5 mg, 1,57 mmol). The reaction mixture was stirred at *rt* for 2 h. Then, the organic solvent was removed in the rotatory evaporator. The aqueous residue was acidified to pH 3 and extracted with CH_2Cl_2 (3 x 5 mL). The combined organic extracts were dried over anhydrous $MgSO_4$, filtered and concentrated. The resulting carboxylic acid was dissolved in CH_2Cl_2 (3 mL) and treated with *N*-HBTU (178 mg, 0.470 mmol) and DIEA (0.3 mL, 1.57 mmol) then, **H-(*D*-Leu-δ-^{tBuOAc}Ach-^{Me}*N*-Ala-δ-Ach)$_2$-OMe** was added. The reaction mixture was stirred at *rt* for 1 h. Then, the mixture was poured into a separatory funnel and washed with aqueous solutions of HCl (3 x5 mL) and $NaHCO_3$ (3 x 5 mL). The organic layer was dried over anhydrous $MgSO_4$, filtered and concentrated. The crude was purified by flash column chromatography on SiO_2 (3-6% MeOH/CH_2Cl_2) to provide 0.332 mg of **ddp2** as a white solid. [57%, R_f= 0.35 (5% MeOH/CH_2Cl_2)].

MS (ESI) [m/z, (%)]: 1876.3 ([MNa]$^+$, 42), 1854.2 ([MH]$^+$, 100), 1798.1 ([MH-^{t}Bu]$^+$, 62) 1742.1 ([MH-2^{t}Bu]$^+$, 18), 1686.0 ([MH-3^{t}Bu]$^+$, 9). **HRMS (ESI) calculated** for $C_{99}H_{161}N_{12}O_{21}$ ([MH]$^+$): 1854.1899, **found**: 1854.1888.

Ns-(δ-Ach-*D*-Leu-δ-^{BocNHNHAc}Ach-^{Me}*N*-Ala)$_3$-OMe (ddp3): A solution of **Ns-(δ-Ach-*D*-Leu-δ-^{BocNHNHAc}Ach-^{Me}*N*-Ala)$_2$-OMe** (**op3**, 50.0 mg, 0.0343 mmol) in DMF (1.5 mL) was treated with K_2CO_3 (14.2 mg, 0.103 mmol) and PhSH (0.02 mL, 0.171 mmol) successively. The reaction mixture was stirred at *rt* for 2 h and then, H_2O MiliQ was added. The mixture was transferred to a separatory funnel and extracted with Et_2O (3x 5 mL) and CH_2Cl_2 (3 x 5 mL). The chlorinated layer was dried over anhydrous $MgSO_4$, filtered and concentrated to provide **H-(δ-Ach-*D*-Leu-δ-^{BocNHNHAc}Ach-^{Me}*N*-Ala)$_3$-OMe** that was used without further purification.

A solution of **Ns-δ-Ach-*D*-Leu-δ-^{BocNHNHAc}Ach-^{Me}*N*-Ala-OMe** (**tp7**, 28.7 mg, 0.0343 mmol) in a mixture of MeOH/H_2O (3:1, 1.5 mL) was treated with LiOH (4.1 mg, 0.171 mmol). The reaction mixture was stirred at *rt* for 1.5 h. Then, the organic solvent was removed in the rotatory evaporator. The aqueous residue was acidified to pH 3 and extracted with CH_2Cl_2 (3 x 5 mL). The combined organic extracts were dried over anhydrous $MgSO_4$, filtered and concentrated. The resulting carboxylic acid was dissolved in CH_2Cl_2 (1.5 mL) and treated with *N*-HBTU (15.6 mg, 0.0411 mmol) and DIEA (0.03 mL, 0.137 mmol) then, **H-(δ-Ach-*D*-Leu-δ-^{BocNHNHAc}Ach-^{Me}*N*-Ala)$_3$-OMe** was added. The reaction mixture was stirred at *rt* for 1 h. Then, the mixture was poured into a separatory funnel and washed with aqueous solutions of HCl (3 x 5 mL) and $NaHCO_3$ (3 x 5 mL). The organic layer was dried over anhydrous $MgSO_4$, filtered and concentrated. The crude was purified by flash column chromatography on SiO_2 (3-7 % MeOH/CH_2Cl_2) to provide 30.6 mg of **ddp3** as a white solid. [86%, R_f= 0.36 (5% MeOH/CH_2Cl_2)].

MS (ESI) [m/z, (%)]: 2101.1 ([MNa]$^+$, 55), 2080.3 ([MH]$^+$, 100), 1979.1 ([MH-Boc]$^+$, 62) 1879.1 ([MH-2Boc]$^+$, 21), 1779.0 ([MH-3Boc]$^+$, 9). **HRMS (ESI) calculated** for $C_{100}H_{164}N_{19}O_{26}S$ ([MH]$^+$): 2079.1810, **found**: 2079.1795.

Cbz-(δ-Ach-*D*-Leu-δ-^{BocNHNHAc}Ach-^{Me}*N*-Ala)$_3$-OMe (ddp4): A solution of **Cbz-(δ-Ach-*D*-Leu-δ-^{BocNHNHAc}Ach-^{Me}*N*-Ala)$_2$-OMe** (48 mg, 0.0341 mmol) in MeOH (1 mL) was treated with Pd/C (7.2 mg, 0.00682 mmol). The reaction mixture was stirred at *rt* for 4 h under H_2 atmosphere. Then, the heterogeneous mixture was filtered through celite®. The solvent was removed in the rotatory evaporator and the resulting residue was dried under high vacuum to yield the intermediate **H-(δ-Ach-*D*-Leu-δ-^{BocNHNHAc}Ach-^{Me}*N*-Ala)$_2$-OMe** that was used without further purification.

A solution of **Cbz-δ-Ach-*D*-Leu-δ-^{BocNHNHAc}Ach-^{Me}*N*-Ala-OMe** (27 mg, 0.0341 mmol) in a mixture of MeOH/H_2O (3:1, 1.5 mL) was treated with LiOH (8 mg, 0.341 mmol). The reaction mixture was stirred at *rt* for 3 h. Then, the organic solvent was removed in the rotatory evaporator. The aqueous residue was acidified to pH 3 and extracted with CH_2Cl_2 (3 x 5 mL). The combined organic extracts were dried over $MgSO_4$, filtered and concentrated to afford **Cbz-δ-Ach-*D*-Leu-δ-^{BocNHNHAc}Ach-^{Me}*N*-Ala-OH** as a white solid that was used without further purification.

USC UNIVERSIDADE DE SANTIAGO

A solution of **Cbz-δ-Ach-*D*-Leu-δ-^{BocNHNHAc}Ach-^{Me}*N*-Ala-OH** in CH_2Cl_2 (1 mL) was treated with *N*-HBTU (15.5 mg, 0.0409 mmol) and DIEA (25 μL, 0.136 mmol), and then, **H-(δ-Ach-*D*-Leu-δ-^{BocNHNHAc}Ach-^{Me}*N*-Ala)$_2$-OMe** was added. The reaction mixture was stirred at *rt* for 14 h. Then, the mixture was poured into a separatory funnel and washed with aqueous solutions of HCl (3 x 5 mL) and $NaHCO_3$ (3 x 5 mL). The organic layer was dried over $MgSO_4$, filtered and concentrated. The crude was purified by flash column chromatography on SiO_2 (% MeOH/CH_2Cl_2) to afford mg of **ddp4** as a white solid [4-10%, R_f= 0.44 (10% MeOH/CH_2Cl_2)].

MS (ESI) [m/z, (%)]: 2050.2 ([MNa]$^+$, 64), 2028.2 ([MH]$^+$, 50), 1928.2 ([MH-Boc]$^+$, 34) 1897.2 ([MH-BocNHNH]$^+$, 10). **HRMS (ESI) calculated** for $C_{102}H_{167}N_{18}O_{24}$ ([MH]$^+$): 2028.2395, **found**: 2028.2390.

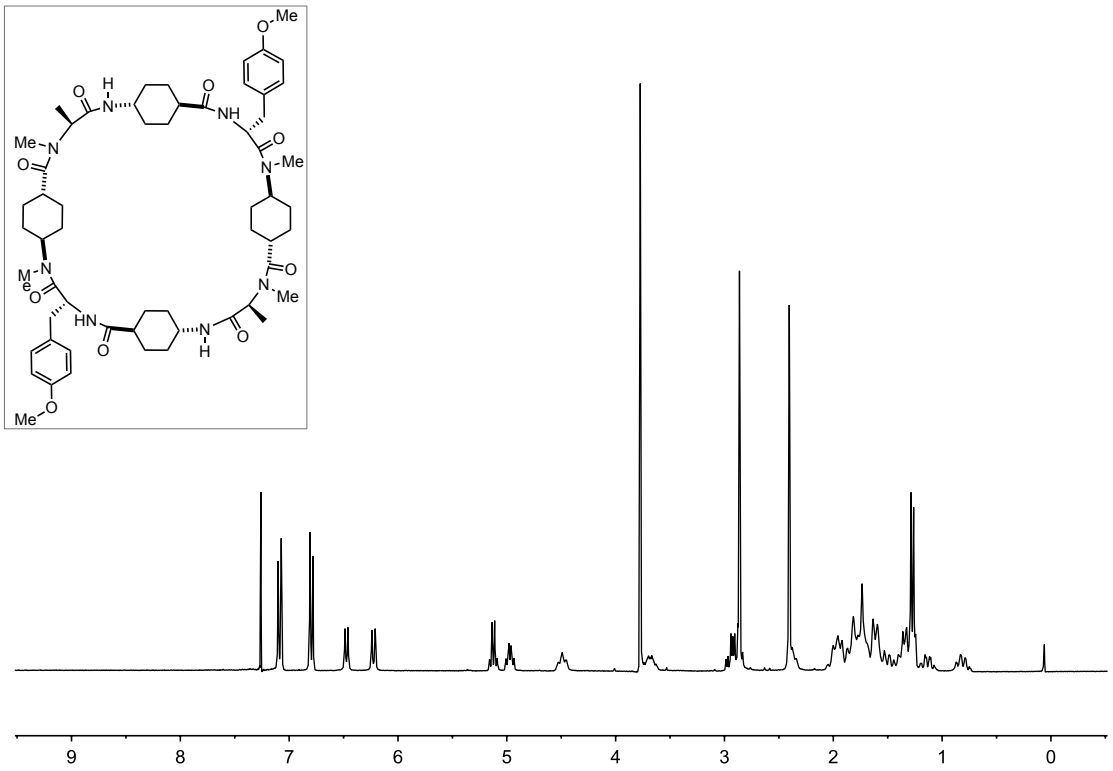
USC
UNIVERSIDADE DE SANTIAGO DE COMPOSTELA

USC
UNIVERSIDADE
DE SANTIAGO
DE COMPOSTELA

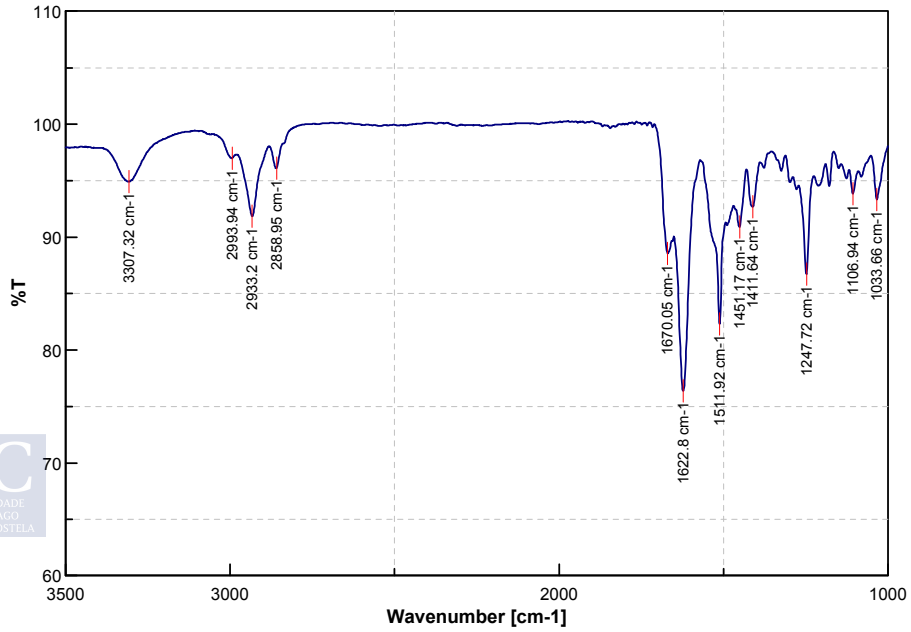
SELECTED SPECTRA

c-[(*D*-Tyr(Me)-^{Me}*N*-δ-Ach-^{Me}*N*-*L*-Ala-δ-Ach-)$_2$] (CP1)

^{1}H NMR ($CDCl_3$, 300 MHz, 298 K)



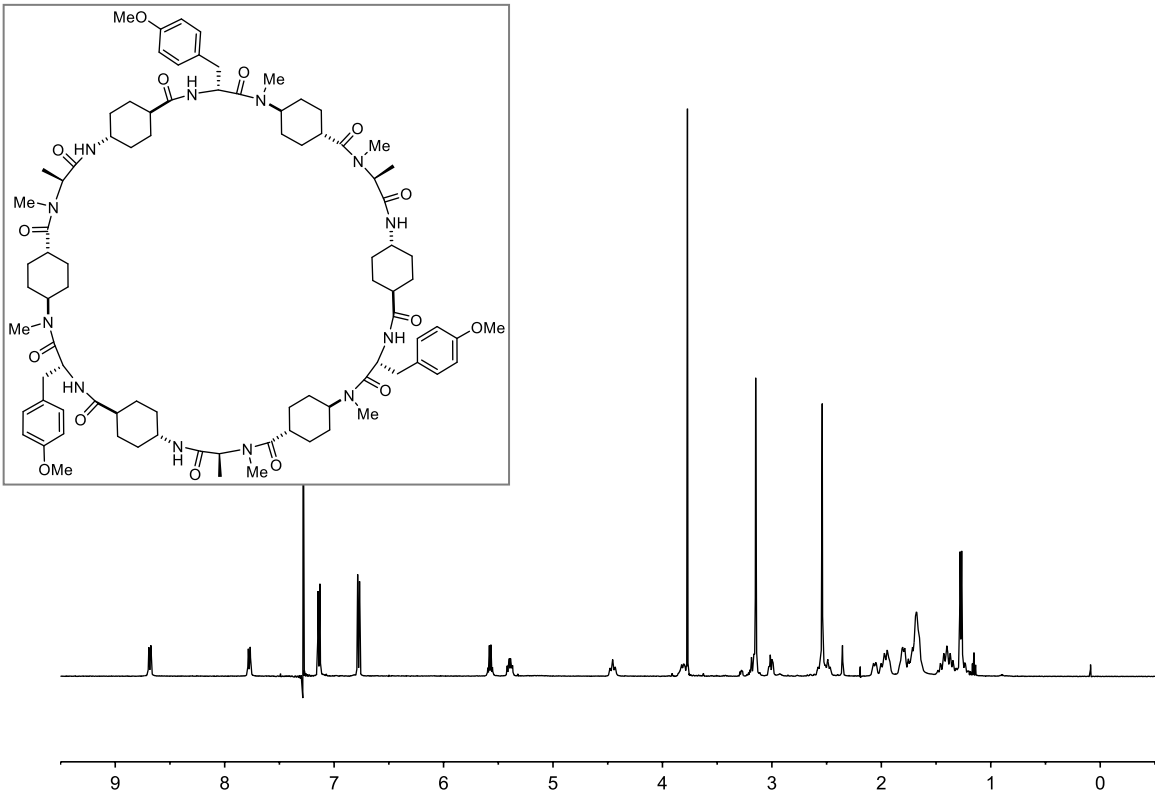
FT-IR ($CHCl_3$, 298 K).



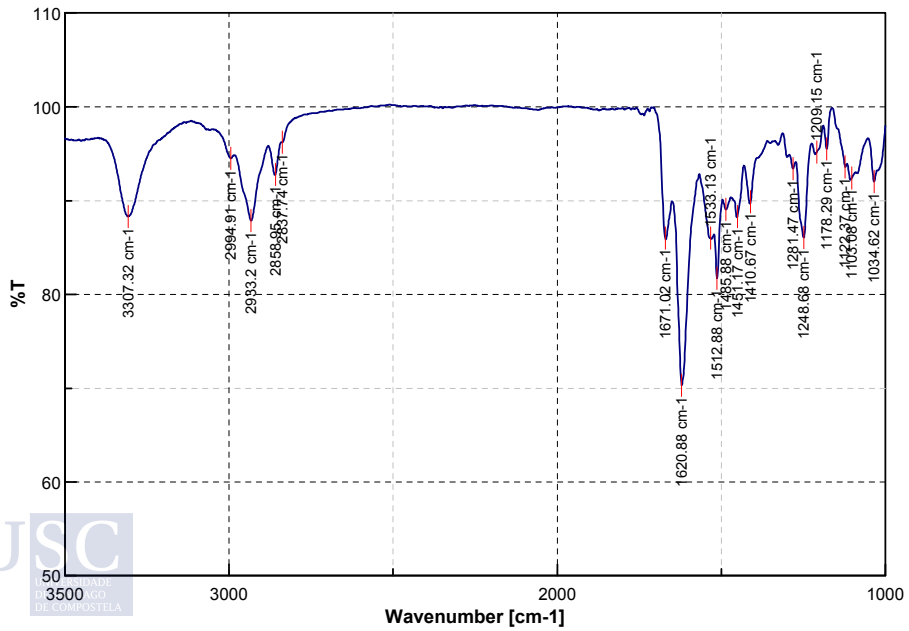
USC UNIVERSIDADE DE SANTIAGO DE COMPOSTELA

c-[(*D*-Tyr(Me)-^{Me}*N*-δ-Ach-^{Me}*N*-*L*-Ala-δ-Ach-)$_3$] (CP2)

^{1}H NMR ($CDCl_3$, 500 MHz, 298 K)

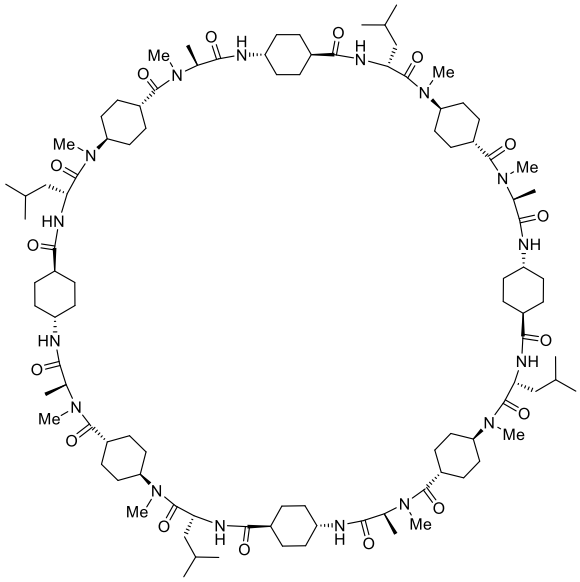


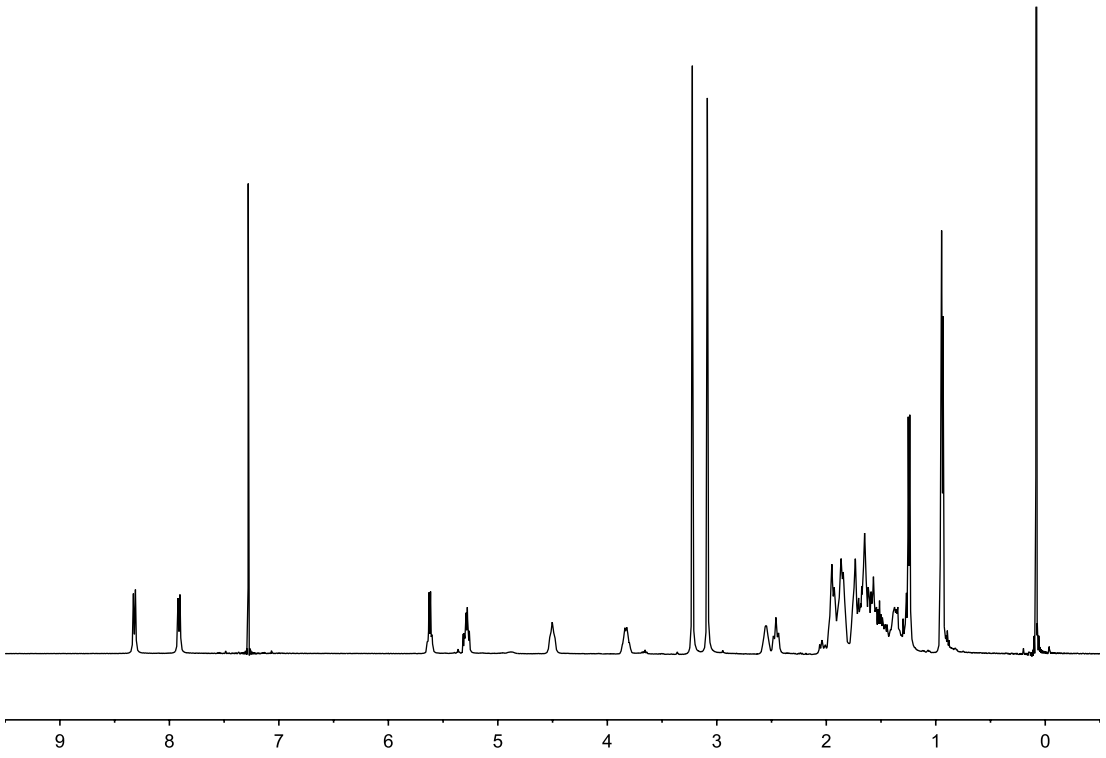
FT-IR ($CHCl_3$, 298 K)



***c*-[(*D*-Leu-^{Me}*N*-δ-Ach-^{Me}*N*-*L*-Ala-δ-Ach-)$_4$] (CP3)**

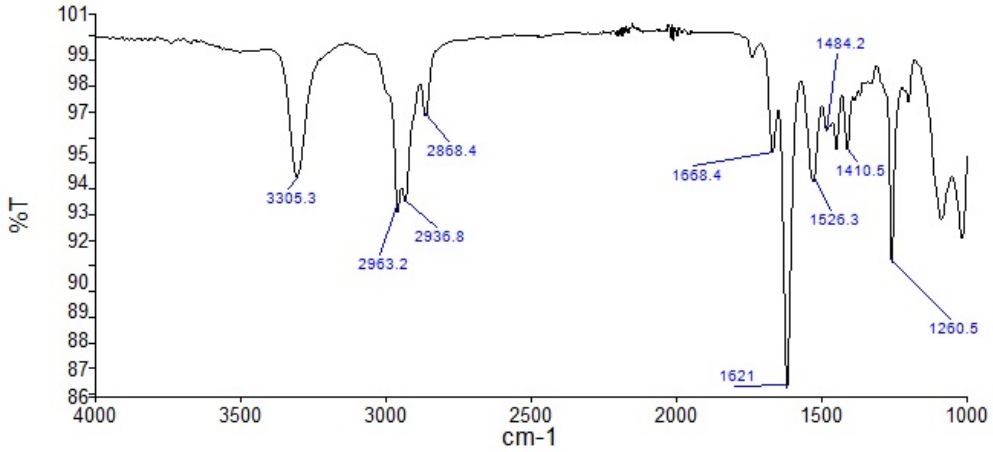
^{1}H NMR ($CDCl_3$, 500 MHz, 298 K)





USC
UNIVERSIDADE DE SANTIAGO DE COMPOSTELA

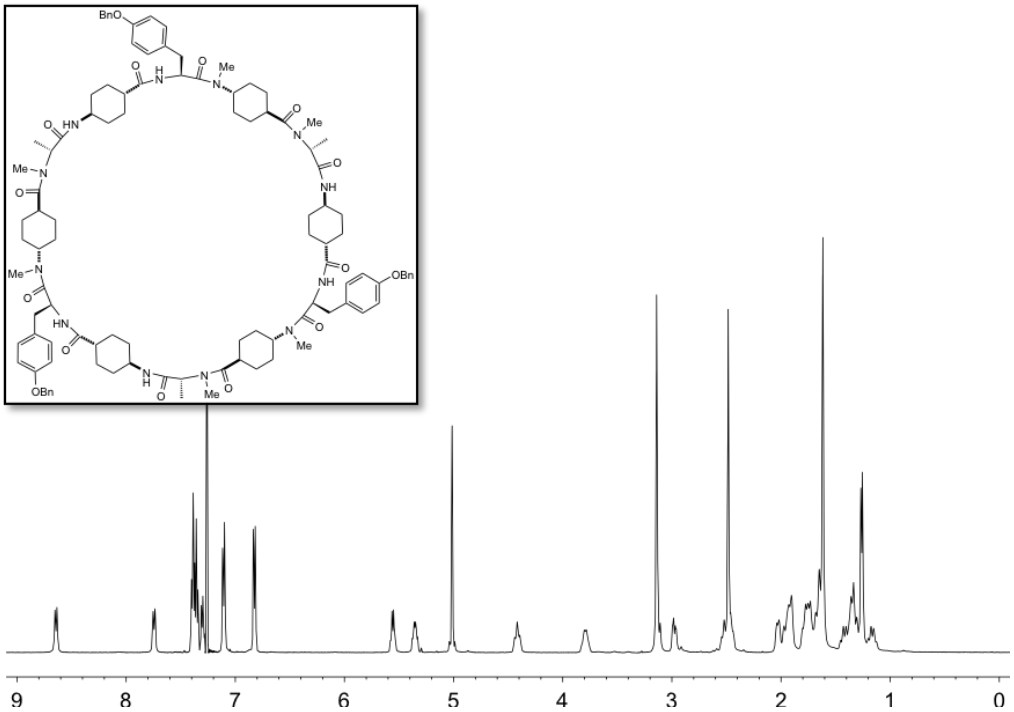
FT-IR ($CHCl_3$, 298 K)



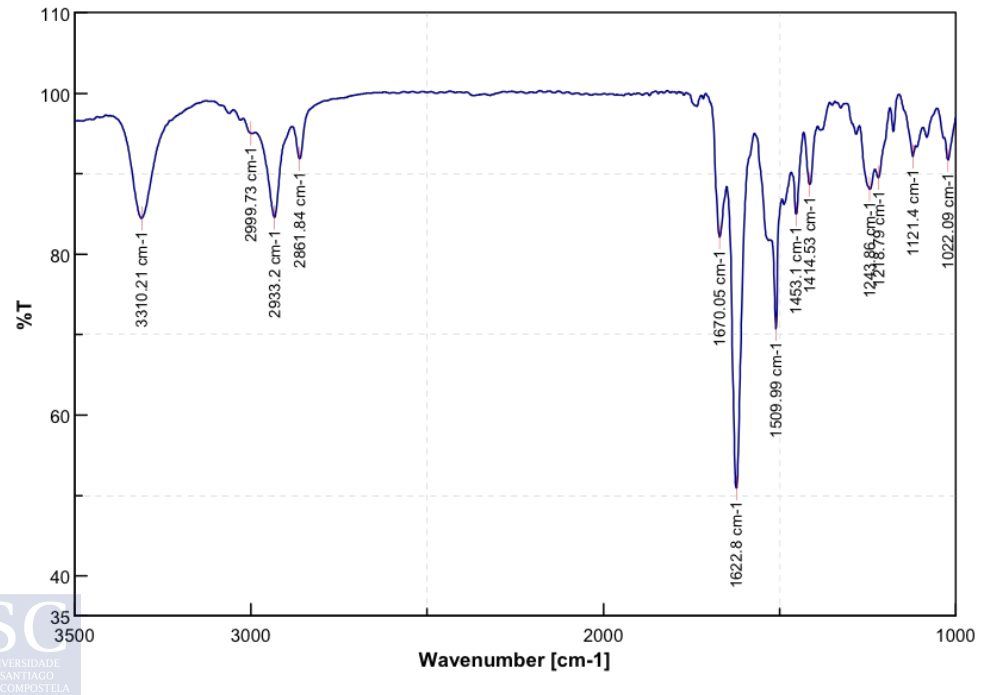
USC UNIVERSIDADE DE SANTIAGO DE COMPOSTELA

***c*-{[*L*-Tyr(Bn)-^{Me}*N*-δ-Ach-*D*-Ala-δ-Ach-]$_3$} (CP4):**

^{1}H RMN [$CDCl_3$, 500 MHz, δ, ppm]



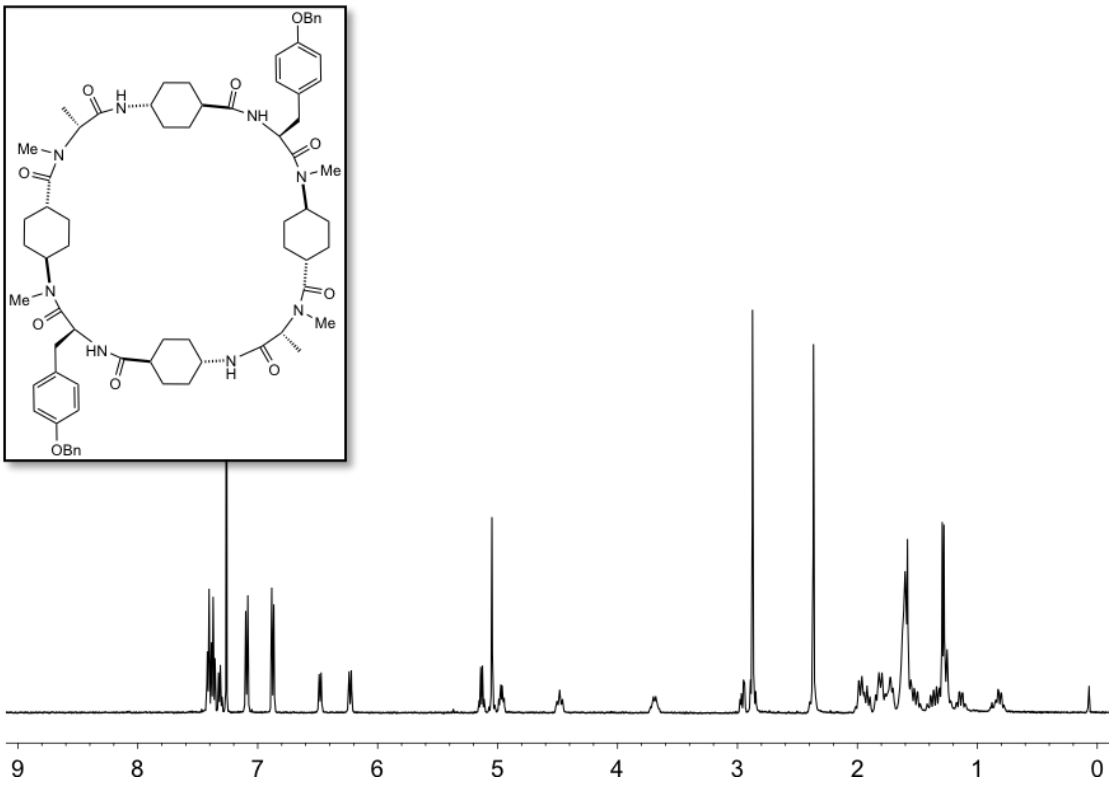
FTIR (CaF_2 pellet, 298 K, cm^{-1})



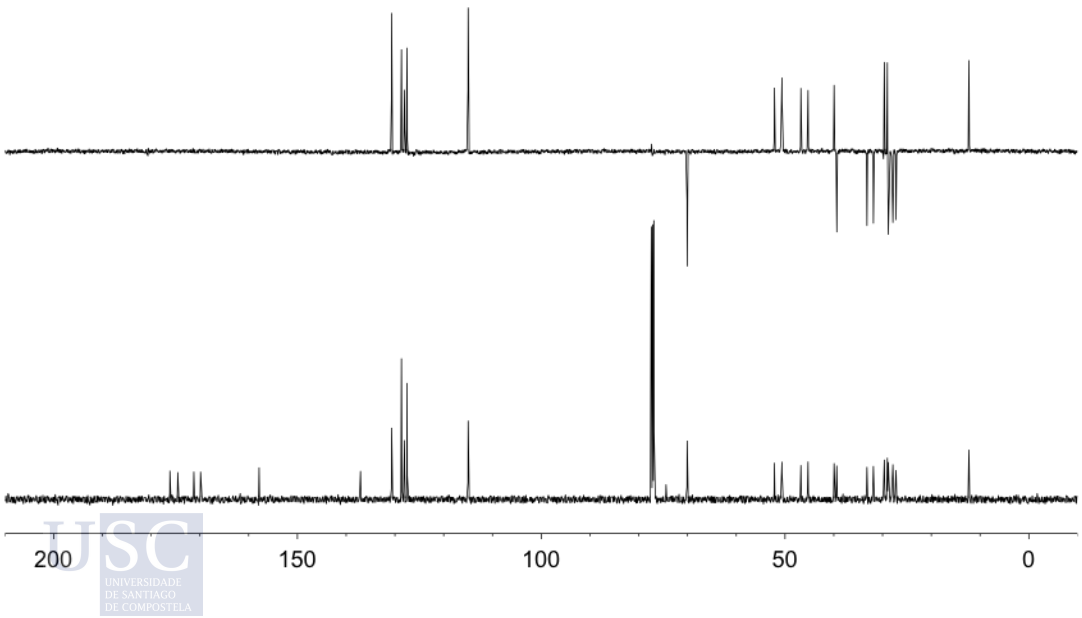
USC UNIVERSIDADE DE SANTIAGO DE COMPOSTELA

***c*-{[*L*-Tyr(Bn)-^{Me}*N*-δ-Ach-*D*-Ala-δ-Ach-]$_2$} (CP5):**

^{1}H RMN [$CDCl_3$, 500 MHz, δ, ppm]

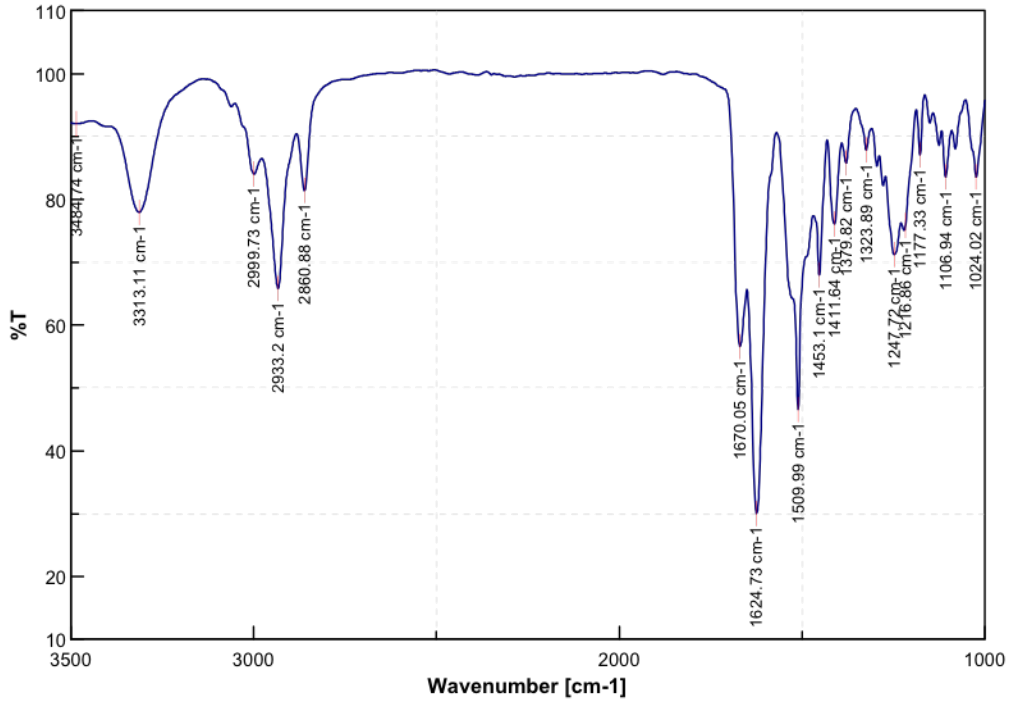


^{13}C RMN [$CDCl_3$, 75 MHz, δ, ppm]



USC
UNIVERSIDADE
DE SANTIAGO
DE COMPOSTELA

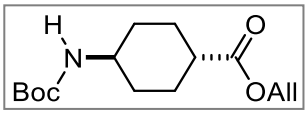
FTIR (CaF_2 pellet, 298 K)

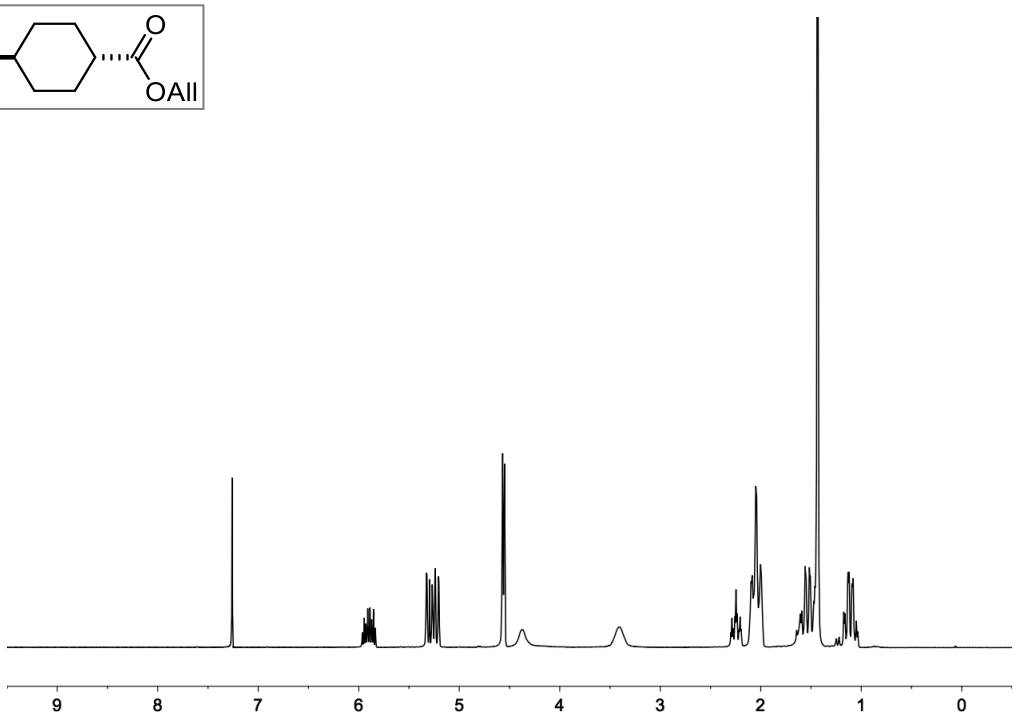


USC
UNIVERSIDADE DE SANTIAGO DE COMPOSTELA

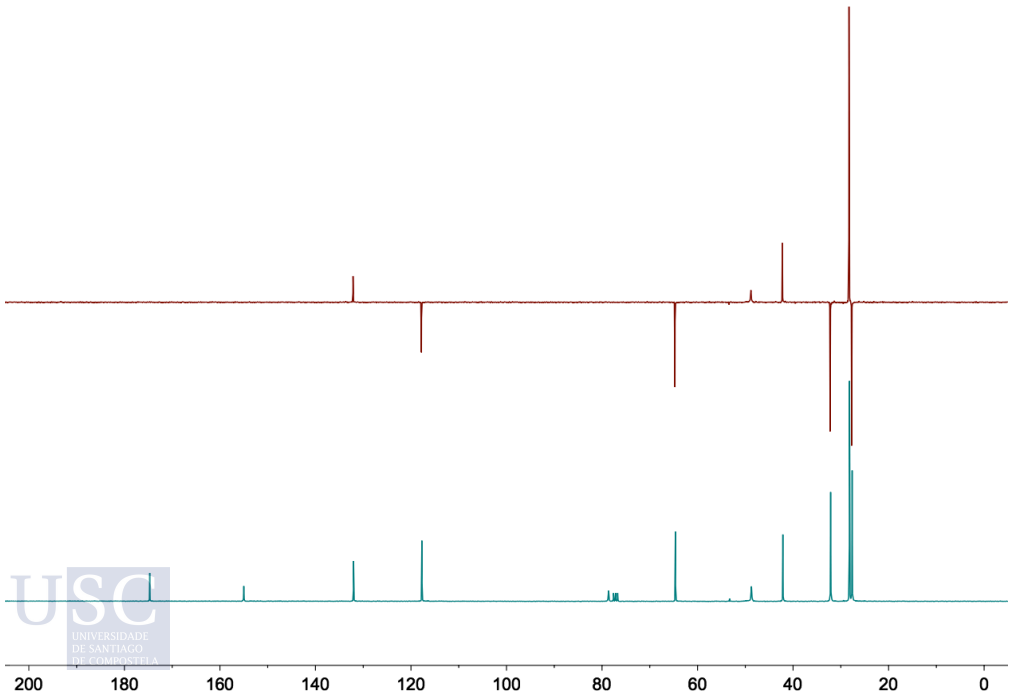
Boc-δ-Ach-OAll

^{1}H NMR ($CDCl_3$, 300 MHz, 298 K)





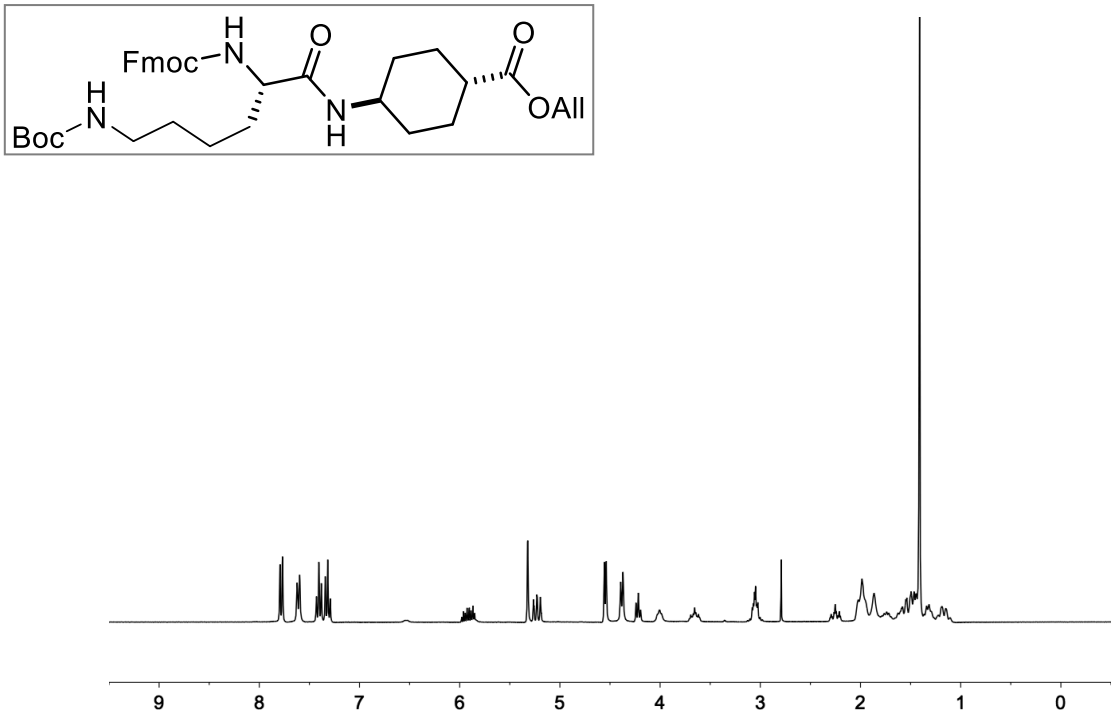
^{13}C NMR and DEPT ($CDCl_3$, 63 MHz, 298 K)



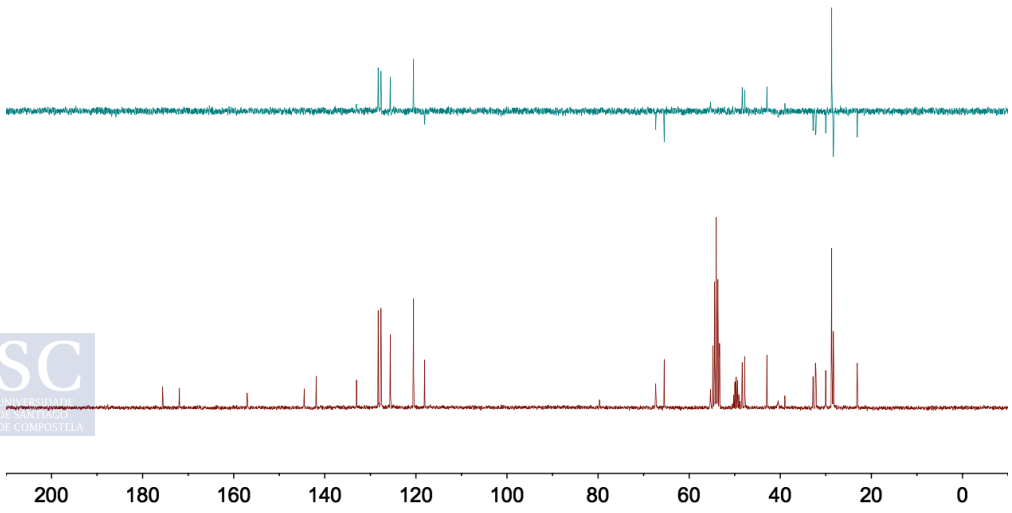
USC
UNIVERSIDADE DE SANTIAGO DE COMPOSTELA

Fmoc-*L*-Lys(Boc)-δ-Ach-OAll (Dp4)

^{1}H NMR (2% $CD_3OD/CCl2D_2$, 300 MHz, 298 K)



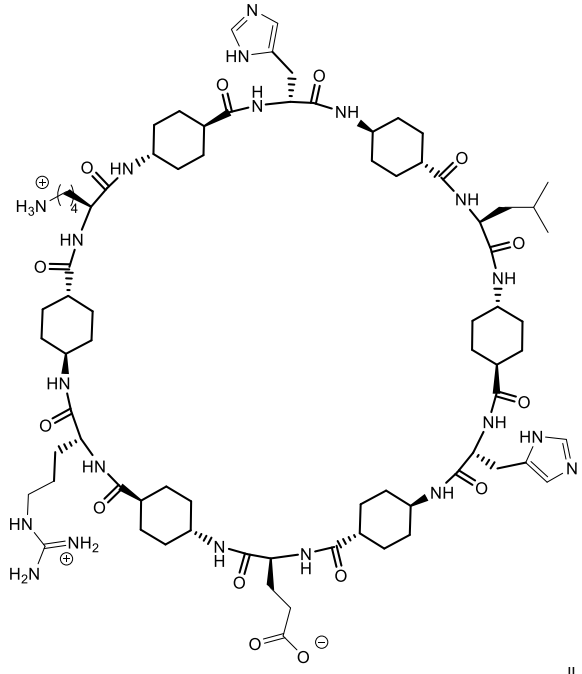
^{13}C NMR and DEPT (2% $CD_3OD/CCl2D_2$, 63 MHz, 298 K)

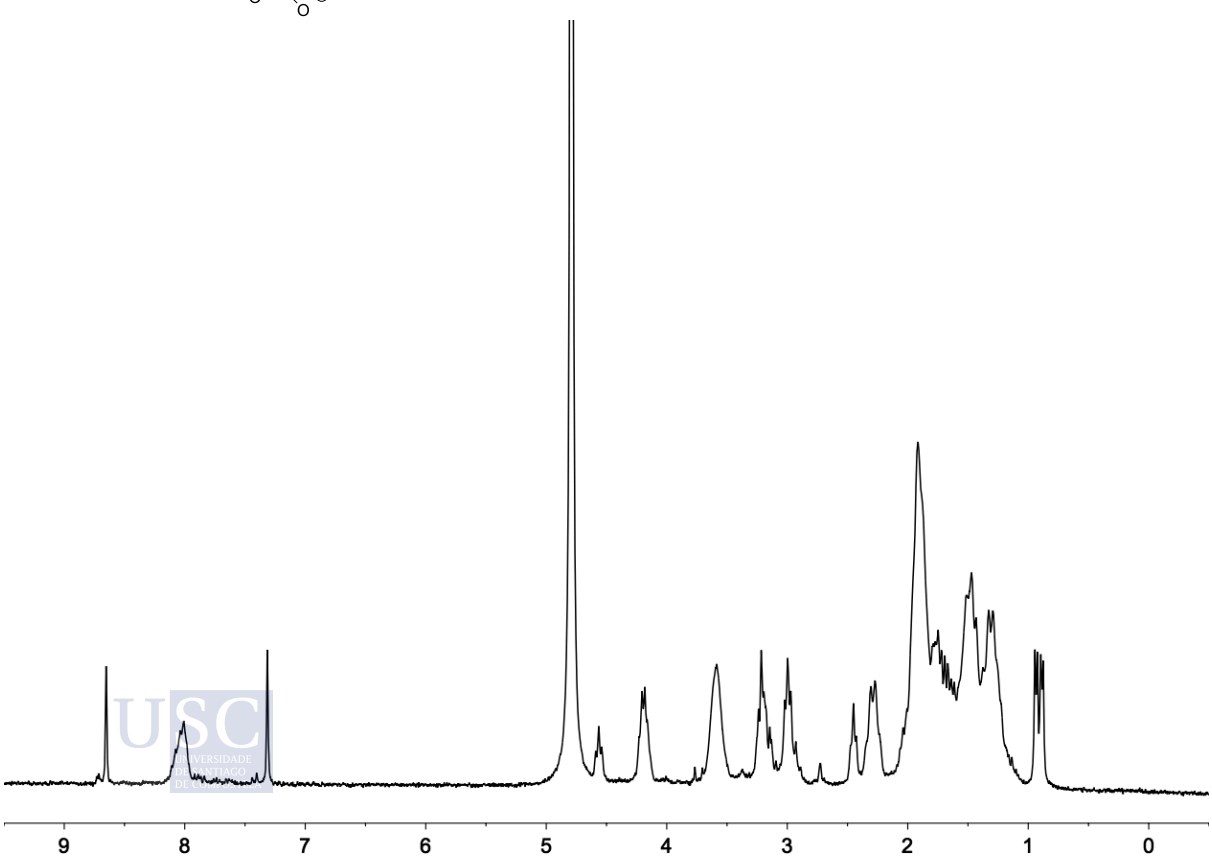


USC UNIVERSIDADE DE SANTIAGO DE COMPOSTELA

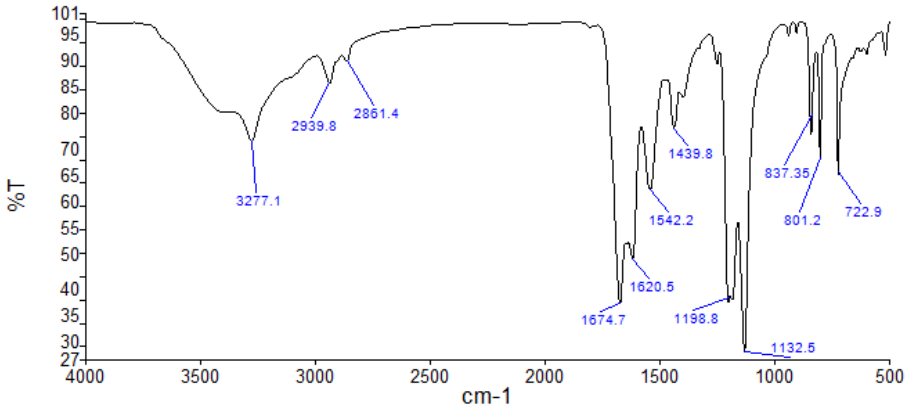
***c*-[*D*-His-δ-Ach-*L*-Leu-δ-Ach-*D*-His-δ-Ach-*L*-Glu(tBu)-δ-Ach-*D*-Arg(Pbf)-δ-Ach-*L*-Lys-δ-Ach-] (CP11)**

^{1}H NMR (D_2O, 300 MHz, 298 K)





FT-IR (H_2O, 298 K)



USC
UNIVERSIDADE DE SANTIAGO DE COMPOSTELA

USC
UNIVERSIDADE
DE SANTIAGO
DE COMPOSTELA

LIST OF PUBLICATIONS

Title	New self-assembling peptide nanotubes of large diameter using δ-amino acids
Authors	Alejandro Lamas, Arcadio Guerra, Manuel Amorín, Juan Ramón Granja
Year	2018
Journal	Chemical Science
Volume and pages	9, 8228–8233
Impact Factor	9.825
PhD student contribution	Synthesis and study the supramolecular and encapsulation properties of nanotube forming cyclic peptides

New self-assembling peptide nanotubes of large diameter using δ-amino acids†

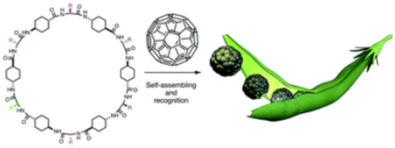
Check for updates

Alejandro Lamas,[a] Arcadio Guerra,[a] Manuel Amorín *[a] and Juan R. Granja *[a]

Author affiliations

Abstract

Here we show that 4-aminocyclohexanecarboxylic acid is a rigid stretcher building block for the preparation of cyclic peptides that self-assemble to form peptide nanotubes with large diameter and hydrophobic pores. The hydrophobic properties of the resulting nanotubes provided by the two methylene groups per δ-residue allow the encapsulation of C_{60} moieties forming a new type of bionanopeapod structure.



A. Lamas, A. Guerra, M. Amorín and J. R. Granja, *Chem. Sci.*, 2018, **9**, 8228 **DOI:** 10.1039/C8SC02276C

This article is licensed under a Creative Commons Attribution-NonCommercial 3.0 Unported Licence. **You can use material from this article in other publications, without requesting further permission** from the RSC, provided that the correct acknowledgement is given and it is not used for commercial purposes.

To request permission **to reproduce material from this article in a commercial publication**, please go to the Copyright Clearance Center request page.

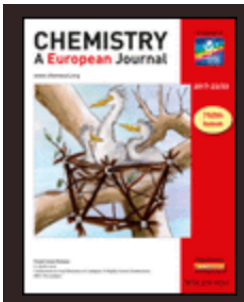
If you are **an author contributing to an RSC publication, you do not need to request permission** provided correct acknowledgement is given.

If you are **the author of this article, you do not need to request permission to reproduce figures and diagrams** provided correct acknowledgement is given. If you want to reproduce the whole article in a third-party commercial publication (excluding your thesis/dissertation for which permission is not required) please go to the Copyright Clearance Center request page.

Read more about how to correctly acknowledge RSC content.

USC UNIVERSIDADE DE SANTIAGO DE COMPOSTELA

Title	Parallel versus antiparallel β-sheet structure in cyclic peptide hybrids containing γ- or δ-amino acids
Authors	Martín Calvelo, Alejandro Lamas, Arcadio Guerra, Manuel Amorín, Rebeca García Fandiño, Juan Ramón Granja
Year	2020
Journal	Chemistry – A European Journal
Volume and pages	26, 5846–5858
Impact Factor	5.236
PhD student contribution	Synthesis and study of the self-assembly process of different cyclic peptides



Thank you for your order!

Dear Mr. Alejandro Lamas,

Thank you for placing your order through Copyright Clearance Center's RightsLink® service.

Order Summary

Licensee:	Universidade de Santiago de Compostela
Order Date:	Feb 17, 2022
Order Number:	5251540066311
Publication:	Chemistry - A European Journal
Title:	Parallel Versus Antiparallel β-Sheet Structure in Cyclic Peptide Hybrids Containing γ- or δ-Cyclic Amino Acids
Type of Use:	Dissertation/Thesis
Order Total:	0.00 EUR

View or print complete details of your order and the publisher's terms and conditions.

Sincerely,

Copyright Clearance Center





Cyclic peptides have the ability to provide supramolecular tubular structures through stacking of the peptide subunits. This self-assembly capability makes them an attractive platform for the construction of complex structures with programmable dimensions. The peptide nature of the resulting systems converts them into suitable candidates for the development of novel nanobiomaterials. In this PhD Thesis, a novel class of cyclic peptides that incorporates cyclic non-natural amino acids are introduced. Their supramolecular properties as well as their ability to encapsulate different hydrophobic substances were explored. Finally, the introduction of a molecular cap was proposed with the aim of obtaining peptide-based molecular containers with improved encapsulation properties.